UNIVERSITY OF CALIFORNIA

Los Angeles

Reprogramming T Cells to Interrogate Intracellular Disease Signatures

A dissertation submitted in partial satisfaction of the requirements for the degree

Doctor of Philosophy in Chemical Engineering

by

Patrick Ho

2019

ABSTRACT OF THE DISSERTATION

Reprogramming T Cells to Interrogate Intracellular Disease Signatures

by

Patrick Ho

Doctor of Philosophy in Chemical Engineering

University of California, Los Angeles, 2019

Professor Yvonne Y. Chen, Chair

Adoptive T-cell therapy—an emerging paradigm in which tumor-targeting T cells serve as living therapeutic modalities administered to cancer patients—has demonstrated remarkable curative potential in patients with relapsing B-cell malignancies, but clinical translation has not been extended to the vast majority of diseases. In particular, the lack of tumor-exclusive surface-bound antigens presents a fundamental challenge to conventional targeting approaches involving surface receptor engineering, due to an inherent risk for 'on-target, off-tumor' toxicities. To expand the pool of candidate disease signatures for adoptive T-cell therapy, we devised a strategy to reprogram T cells to interrogate target cells for intracellular antigen expression prior to enacting cytolytic programs. Specifically, we genetically replaced the endogenous and constitutively cytotoxic granzyme B (GrB) payload with a GrB-based switch, termed Cytoplasmic Oncoprotein VErifier and Response Trigger (COVERT), which remains inactive until encounter with an intracellular disease signature. In this manner, the COVERT system complements surface receptor technologies to enable AND-gate Boolean logic computation for spatiotemporally segregated input signals, first at the target-cell surface, and then from within the target cell. Here, we report the design of a small ubiquitin-like modifier protein (SUMO)-GrB fusion that is

specifically activated by the intracellular tumor-associated protease, SENP1, to selectively initiate apoptosis. We systematically optimized the T-cell genome-editing workflow to facilitate the efficient manufacture of primary human $CD8^+$ T cells that express SUMO-GrB and a chimeric antigen receptor (CAR) instead of wild-type GrB and the endogenous T-cell receptor, respectively. We also provide the first demonstration of selective T-cell lytic function in response to intracellular antigen expression. Finally, we explore the design of allosterically regulated COVERT switches by nanobody domain insertion, with the aim of developing a modular architecture that supports the rapid optimization of switch behavior for any intracellular disease biomarker. As medical strategies continue to shift toward precision medicine, the COVERT platform represents a potentially transformative technology that can enhance the safety of adoptive T-cell therapy to enable implementation as a front-line treatment option for a broader range of diseases.

The dissertation of Patrick Ho is approved.

Donald Barry Kohn

Yi Tang

Michael Alan Teitell

Yvonne Y. Chen, Committee Chair

University of California, Los Angeles

2019

TABLE OF CONTENTS

List of Figures

List of Supplementary Figures and Texts

Acknowledgements

Although the ink on the ensuing pages depict the culmination of an arduous journey, the same ink also paints a vision that has yet to be realized. It is my hope that my colleagues and I have carved a strong foothold that shortens the distance toward finally reaching that dream.

First and foremost, I must thank my graduate advisor, Prof. Yvonne Chen, who courageously accepted an unproven student such as myself into her brand-new lab, and then worked tirelessly to ensure that her risky decision would prove to be a rewarding one (at least for me). Over the past several years, she has simultaneously been my harshest critic and my most steadfast supporter, and I appreciate her sincerity, even if we had our fair share of ideological disagreements regarding research pursuits. I have no doubt that I owe more to Yvonne for my technical development and ongoing personal growth than I presently realize. Her unwavering resolve to seeing her students succeed will be the legacy she imparts upon the generations of young scientists fortunate enough to train, directly or indirectly, under her patient guidance.

Life in the Chen lab has evolved a great deal since the day I first set foot in our once Wi-Fi–less and windowless cave in the sky, but I am fortunate that one aspect has remained constant throughout—the camaraderie of dear friends and lab mates, without whom I would not have found enough borrowed strength to trek this far. I am especially grateful for the Chen lab's *de facto* first post doc, ZeNan Chang, who embraced his role as a guide despite not having the same luxury himself, as well as my year mates, Eugenia Zah and Meng-Yin Lin, perhaps the only people in the world who fully understood the rigors of navigating the ever-changing tide of responsibilities and expectations that accompanied us through the Chen lab's initial years. Beyond instilling the extraordinary work ethic and resilience the fledgling Chen lab has already become renowned for, their individual fingerprints have been imprinted throughout my graduate experience. Whether it be ZeNan's graceful handling of every situation, Eugenia's methodical approach through unending assignments, or Meng-Yin's steely determination in the face of bitter disappointments,

I will leave the Chen lab having learned valuable lessons in simply taking the ups and downs this life has to offer.

This is not to say that I successfully mastered the application of those lessons during my time as a graduate student. It is for this reason that I am particularly thankful for the entire COVERT team—Chris Ede, Cliff Boldridge, Laurence Chen, and Andrew Hou—not only for their numerous intellectual and experimental contributions, but also for lending a patient ear to my frustrated rants, as well as for entertaining many long discussions wrought with my unpolished ideas. Although it is not easy to part before I consider my task done, it is comforting to know that it is Andrew and Laurence who are being entrusted with taking up the COVERT banner. That same banner might never have been raised without the brave and spirited efforts of Luke Riggan, Kiki Kong, Sabah Rahman, Jaimie Chen, Andy Alag, and Vinya Bhuvan, a veteran corps of PhD rotation and undergraduate students resourceful enough to survive my attempts at mentorship and still support my endeavors to think *inside* the box.

Even the most disciplined army can only march so far on empty stomachs, and I thank Ximin Chen, Tasha Lin, and the aforementioned lab members, as well as Brenda Huang, Lemuel Soh, Carly Bond, Alec Jaeger, Tony Wu, Harry Tong, and Wes Tamanaha for maintaining a steady supply of snacks, both in the office and on our numerous adventures. Graduate school would have been far less enjoyable without our many feasts, sometimes to celebrate weddings or holidays, but more oftentimes just because. I will fondly remember battling wizarding sloths, and our annual encounters with zombies, as well as repeatedly narrowly surviving the wintry conditions at Grand Canyon, Yosemite, Bryce Canyon, and Zion National Parks, and nearly losing our way in the desert at Joshua Tree National Park. I will also forever be grateful for the enduring friendship of Kevin Shen, Richard Chui, Michael Cheng, and the rest of the 401 ballin' crew, along with Ed & Lulu Kung, each of whom have shown me a depth of grace I can never repay.

Apart from the support of close friends, my graduate school experience has been made smoother by the goodwill displayed by alumni and newer members of the Chen lab—including

Mickey Lorenzini, Josh Bengayan, Chris Walthers, Eunwoo Nam, and Stan Gosliner—and of the neighboring Segura, Liao, and Tang labs. Although their individual names and contributions are far too many to list, I would undoubtedly have spent many more long nights in Boelter Hall if not for their generosity in pointing me toward new experimental techniques, sharing back-ordered reagents, and unlocking physical doors to essential instruments.

I thank Gregor Adams and the rest of the Kite Pharma R&D team for affording me the opportunity to gain invaluable perspective concerning the clinical translation of novel T-cell engineering technologies within an industrial setting. The advice of Caroline Kuo, along with the sharing of AAV6 packaging vectors and protocols by Prof. David Schaffer, were instrumental toward the development of optimized protocols used in this work. I must also thank my committee members, Prof. Yi Tang, Prof. Donald Kohn, and Prof. Michael Teitell, as well as Prof. Tatiana Segura, Prof. Antoni Ribas, Prof. James Liao, Prof. Jane Chang, and Anjie Zhen, for spending time to provide insights on my research, and to prepare me for my intended career path.

Lastly, while graduate school has at times felt akin to running an undisciplined marathon, simply being able to start the race is already a testament to the unconditional love and support of my family. Mom and Dad, thank you for teaching me to dream, and for always providing me with the opportunities to work toward those dreams. Although this may not have been the career path you imagined for me, my imagination only exists because of your perpetual sacrifice and encouragement. Finally, to my beloved sisters, Sherry and Theresa, your perseverance and empathy have always been an inspiration to hope for that which cannot be seen.

This work was supported by grants from the National Institutes of Health (NIH) and the National Science Foundation (NSF) awarded to Yvonne Y. Chen, as well as a predoctoral training grant from the NIH-funded Biotechnology Training in Biomedical Sciences and Engineering Program.

Excerpts from Chapter 1, including Fig 1.1-1.3. were adapted from two previously published works: (1) Ho, P. and Chen, Y.Y. “Synthetic Biology in Immunotherapy.” *Synthetic Biology*, edited by Christina Smolke, vol. 8, Wiley-VCH, 2018, pp. 349-372, and (2) Ho, P. and Chen, Y.Y. (2017) Mammalian synthetic biology in the age of genome editing and personalized medicine. *Curr. Opin. Chem. Biol.*, **40**, 57–64

Data in Chapters 2 and 3 were published in an Open Access article: Ho, P., Ede, C., & Chen, Y.Y. Modularly Constructed Synthetic Granzyme B Molecule Enables Interrogation of Intracellular Proteases for Targeted Cytotoxicity. *ACS Synth. Biol.*, **6** (8), 1484–1495.

VITA

EDUCATION

Dec. 2012	Northwestern University, Evanston, IL M.S., Biotechnology
Jun. 2011	University of California–Los Angeles, Los Angeles, CA B.S., Chemical Engineering

RESEARCH EXPERIENCE

Sep. 2013 – Present	Laboratory of Prof. Yvonne Chen, University of California–Los Angeles Reprogramming T Cells to Interrogate Intracellular Disease Signatures • Engineering granzyme B switches to regulate T-cell lytic function • Genome editing of primary human T cells
Sep. – Dec. 2016	Internship (supervised by Dr. Gregor Adams), Kite Pharma, Inc. • Assay development for off-tumor toxicity of candidate CAR constructs • Evaluation of CAR-T cell function
Feb. – Aug. 2013	Laboratory of Prof. Ian Wheeldon, University of California–Riverside Lipid Droplet Scaffolds for Metabolic Engineering in Yeast • Lipid droplet scaffolding of metabolic enzymes in yeast • Synthetic peptide design and validation of lipid droplet localization
Dec. 2011 – Dec. 2012	Laboratories of Profs. Keith Tyo & Josh Leonard, Northwestern University Developing a Yeast-based Diagnostic for Resource-poor Settings • Development of low-cost, cell-based disease diagnostics • Vector design to facilitate modular cloning of receptor constructs

AWARDS

2018	UCLA Dissertation Year Fellowship
2018	AAI Young Investigator Oral Presentation Prize, ImmunologyLA 2018
2018	Keystone Symposia Scholarship
2017	Best Presentation Prize, UCLA CBE 4th-year Symposium
2015 – 2017	NIH T32 Biotechnology Training Grant

PATENTS

Chen, Y.Y. & **Ho, P.** Cytotoxic molecules responsive to intracellular ligands for selective T cell mediated killing. US62/091,937. PCT/US2015/065623 (2015).

PUBLICATIONS

1. **Ho, P.** and Chen, Y.Y. "Synthetic Biology in Immunotherapy." *Synthetic Biology*, edited by Christina Smolke, vol. 8, Wiley-VCH, 2018, pp. 349–372.
2. **Ho, P.** and Chen, Y.Y. (2017) Mammalian synthetic biology in the age of genome editing and personalized medicine. *Curr. Opin. Chem. Biol.*, **40**, 57–64.
3. **Ho, P.**, Ede, C., and Chen, Y.Y. (2017) Modularly Constructed Synthetic Granzyme B Molecule Enables Interrogation of Intracellular Proteases for Targeted Cytotoxicity. *ACS Synth. Biol.*, **6** (8), 1484–1495.

PRESENTATIONS & POSTERS (*Presenter)

1. **Ho, P.***, Ede, C., & Chen, Y.Y. COVERT T Cells: Engineering T cells to Interrogate Intracellular Antigens. (*Oral Presentation*). UCLA I3T Seminar Series: Research In Progress, 10/09/2018.
2. **Ho, P.***, Ede, C., & Chen, Y.Y. COVERT T Cells: Engineering T Cells to Interrogate Intracellular Antigens. (*Oral Presentation*). ImmunologyLA 2018, 06/15/2018.

3. **Ho, P.***, Ede, C., & Chen, Y.Y. COVERT T Cells: Engineering T Cells to Interrogate Intracellular Antigens. (*Oral Presentation*). Mammalian Synthetic Biology Workshop 5.0, 05/05/2018.
4. **Ho, P.***, Ede, C., & Chen, Y.Y. COVERT T Cells: Engineering T Cells to Interrogate Intracellular Antigens. (*Oral Presentation*). Keystone Symposia, Emerging Cellular Therapies: T Cells and Beyond, 02/12/2018.
5. **Ho, P.***, Ede, C., & Chen, Y.Y. COVERT T Cells: Engineering T Cells to Interrogate Intracellular Antigens. (*Poster*). Keystone Symposia, Emerging Cellular Therapies: T Cells and Beyond, 02/12/2018.
6. **Ho, P.***, Ede, C., & Chen, Y.Y. COVERT Cancer Therapeutics: Engineering T Cells to Target the Untargetable. (*Oral Presentation*). UCLA-NIH Biotechnology Symposium 2017, 07/14/2017.
7. **Ho, P.***, Ede, C., & Chen, Y.Y. COVERT Cancer Therapeutics: Engineering T Cells to Target the Untargetable. (*Oral Presentation*). UCLA CBE 4th-year Symposium, 05/19/2017.
8. **Ho, P.***, Ede, C., & Chen, Y.Y. Designing Targeted Therapeutics to Interrogate Intracellular Tumor Antigens. (*Oral Presentation*). ACS 253rd National Meeting, 04/04/2017.
9. **Ho, P.*** & Chen, Y.Y. COVERT Cancer Therapeutics: Engineering T Cells to Interrogate Intracellular Tumor Antigens. (*Oral Presentation*). UCLA-NIH Biotechnology Symposium 2016, 06/02/2016.
10. **Ho, P.*** & Chen, Y.Y. COVERT Cancer Therapeutics: Engineering T Cells to Interrogate Intracellular Tumor Antigens. (*Oral Presentation*). AIChE 2015 Annual Meeting, 11/12/2015.
11. **Ho, P.**, Lin, J.L.*, & Wheeldon, I. Engineering Lipid Droplet Targeting Domains in S. Cerevisiae. (*Poster*). AIChE 2013 Annual Meeting, 11/06/2013.

TEACHING EXPERIENCE

Teaching Assistant, University of California–Los Angeles

Spring 2018	CHE 103 Separation Processes
Winter 2015	CHE 104DL Molecular Biotechnology Laboratory
Spring 2014	CHE 104DL Molecular Biotechnology Laboratory

MENTORING EXPERIENCE

Student Research Mentor, University of California–Los Angeles

	<u>Graduate Students</u>
Sep. – Dec. 2017	Luke Riggan (UCLA Molecular Biology, *PhD rotation*)
Jan. – Jul. 2015	William Clifford Boldridge (UCLA Chemistry & Biochemistry, *PhD rotation*)
	<u>Undergraduate Students</u>
Sep. 2017 – Present	Anya Alag (UCLA Microbiology, Immunology, & Molecular Genetics)
Jun. 2017 – Present	Jaimie Chen (UCLA Chemical & Biomolecular Engineering)
Sep. 2016 – Present	Sabah Rahman (UCLA Chemical & Biomolecular Engineering)
Jun. 2018 – Sep. 2018	Vinya Bhuvan (UCLA Chemical & Biomolecular Engineering, *NSF REU*)
Mar. 2016 – Mar. 2018	Lingqi Kong (UCLA Chemistry & Biochemistry)
Jan. – Mar. 2015	George Wang (UCLA Bioengineering)
	<u>High School Students</u>
Jun. – Aug. 2017	Ali Vakilimafakheri (High Tech Los Angeles, *HSSRP*)
Sep. 2014 – May 2015	David Olin (Wildwood High School)

Chapter 1. Cellular Immunotherapy and the Future of Modern Medicine

Partially adapted, with permissions from (1) Ho, P. and Chen, Y.Y. "Synthetic Biology in Immunotherapy." *Synthetic Biology*, edited by Christina Smolke, vol. 8, Wiley-VCH, 2018, pp. 349-372., and (2) Ho, P. and Chen, Y.Y. (2017) Mammalian synthetic biology in the age of genome editing and personalized medicine. *Curr. Opin. Chem. Biol.*, **40**, 57–64.

Adoptive T-cell therapy is an emerging paradigm in which living T cells from the adaptive immune system are targeted against tumor cells to serve as the therapeutic modalities administered to cancer patients[1–3]. This approach toward redirecting the immune response to attack cells bearing tumor-associated surface antigens has yielded unprecedented anti-tumor efficacy in patients with relapsing B-cell malignancies, prompting the recent US Food and Drug Administration (FDA)-approval of the first gene-modified cell therapies[4,5]. However, the clinical translation of adoptive T-cell therapy has yet to be extended to the vast majority of diseases, primarily due to the frequent risk for 'on-target, off-tumor' toxicities that result from misidentification of normal cells expressing the target surface-bound antigen at low, basal levels[3,6–10]. In lieu of tumor-exclusive surface markers, we propose to reprogram T cells to interrogate target cells for the expression of well-characterized intracellular disease signatures prior to enacting cytolytic programs, thereby expanding the pool of candidate antigens that can be targeted by adoptive T-cell therapy. Specifically, this thesis focuses on the design and implementation of granzyme B (GrB)-based cytotoxic switch payload proteins, termed Cytoplasmic Oncoprotein VErifier and Response Trigger (COVERT) molecules, which can be delivered by T cells to trigger target-cell apoptosis specifically upon encounter with an intracellular target antigen. By engineering T cells to sense and respond to previously inaccessible

biomarkers, we aim to enhance the safety and targeting precision of rationally designed therapeutics, addressing challenges that have permeated medical strategy since the dawn of modern medicine.

As the germ theory of disease achieved prominence in the late 19th century, a confluence of public health policies and biomedical innovations quickly reshaped the medical landscape[11]. In particular, Paul Ehrlich expanded upon the experimental findings of Louis Pasteur and Robert Koch to popularize his 'magic bullet' concept of targeted therapy, in which therapeutic agents are designed to selectively damage pathogenic microbes[12]. After screening hundreds of organoarsenic compounds for anti-syphilis activity, the quest for 'magic bullets' eventually yielded the discovery of the first chemotherapeutic, Salvarsan, and successfully laid the blueprint for modern pharmaceutical research[13]. Once the availability of antibiotics and viral vaccines had outpaced the threat of infectious epidemics, the focus of targeted therapy turned to confront an emerging frontier of genetic diseases, with products of gene dysfunction replacing foreign pathogens as the molecular targets for therapeutic intervention. By the 1980s, the introduction of recombinant DNA technology enabled the generation of genetically engineered biologics—e.g., monoclonal antibodies and recombinant proteins such as trastuzumab (Herceptin) and etanercept (Enbrel)—to complement chemically synthesized small-molecule inhibitors such as imatinib (Gleevec) in the modern pharmaceutical arsenal[14–17].

Despite significant advancements in medical technology over the past several decades, a myriad of autoimmune disorders and cancers remain incurable by conventional treatment strategies involving surgery, radiotherapy, or chemotherapy. For example, glioblastomas are not surgically resectable, and as with pancreatic cancer diagnoses, portend just a 7% overall five-year median survival rate[18]. Unlike foreign pathogens, tumors frequently resemble healthy tissues at the cell surface, and can further evade pharmaceutical detection through genetic hypermutation or via localization to physiological niches that are impenetrable by small molecules or antibody therapeutics[19]. Additionally, the pharmacokinetics of administered drugs are subject to

idiosyncratic parameters such that optimal dosages require empirical determination on a patient-specific basis[20]. Together, these challenges limit the safety and efficacy of chemically derived compounds and protein-based therapeutics. In contrast to static therapeutic modalities, live cells are motile, adaptive, and possess the capacity for self-renewal, enabling cell-based 'living therapies' to process complex arrays of physiological signals and dynamically tune sustained responses according to the disease burden in real-time. Cell-based immunotherapies aim to harness the unique intercommunicative and memory-forming nature of immune cells to tailor and establish long-term therapeutic responses. In particular, adoptive T-cell therapy has emerged as a promising alternative to traditional treatment options due to the precise antigen-recognition and immunological homing capabilities of patient-derived T lymphocytes.

Adoptive T-cell Therapy: Promise and Unrealized Potential

Adoptive T-cell therapy is a novel cancer treatment paradigm in which autologous T cells with tumor-targeting specificity are expanded *ex vivo* prior to re-infusion into a patient[21–23] (Figure 1.1). T cells normally identify target cells via T-cell receptors (TCRs), which bind to cognate antigen peptides presented in the context of major histocompatibility complexes (MHCs) on the target-cell surface and activate effector responses, including proliferation, cytokine secretion, and cytotoxic payload delivery. Naturally occurring tumor-infiltrating lymphocytes (TILs) can be directly isolated from biopsied tissues to yield polyclonal populations of tumor-reactive T cells without *a priori* knowledge of antigen-specificity[24,25]. While this strategy has proven moderately effective for treating melanomas, the low relative abundance of TILs in less-immunogenic cancers limits the scope of TIL transfer[21]. As an alternative approach, the targeting specificity of peripheral T cells can be redirected through the introduction of synthetic TCRs. In particular, chimeric antigen receptors (CARs) are modular fusion proteins that tether an antibody-derived extracellular ligand-binding domain to intracellular costimulatory and T-cell activation domains, enabling genetically

modified T cells to sense and respond to surface-bound antigens in the absence of peptide-MHC presentation[26].

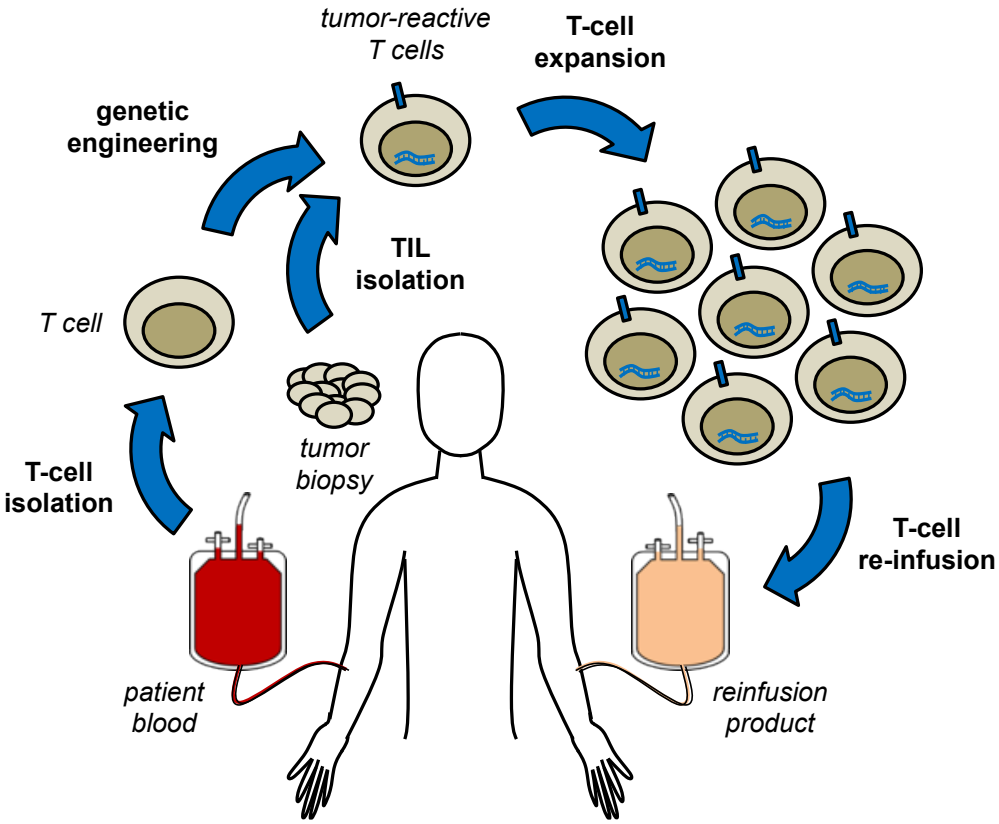

Figure 1.1. Schematic of adoptive T-cell therapy. T cells are isolated from the peripheral blood of cancer patients and genetically engineered to express tumor-targeting TCRs or CARs that re-direct T-cell effector functions against molecularly defined diseased cell populations. Alternatively, TILs can be directly isolated from tumor biopsies to yield polyclonal populations of tumor-reactive T cells without knowledge of antigen-specificity *a priori*. The tumor-targeting T-cell population is then expanded *ex vivo* to obtain a clinical dose of T cells that can be re-administered into patients to mediate potent anti-tumor activities.

Although recent FDA approvals for tisagenlecleucel (Kymriah®) and axicabtagene ciloleucel (Yescarta™) highlight the clinical successes of CD19 CAR-T cell therapies in the treatment of select B-cell lymphomas, several obstacles currently limit the application of adoptive T-cell therapy as a front-line cancer treatment option for the vast majority of cancers[27–30]. Tumor-targeting T cells are frequently rendered anergic in the tumor microenvironment of solid

malignancies, which is wrought with inhibitory metabolites, cytokines, and checkpoint ligands, and further fortified by an immunosuppresive network of tumor-associated macrophages (TAMs) and regulatory T cells (Tregs)[31,32]. However, efforts to 'armor' T cells and counteract TAM- and Treg-mediated immunosuppression through the constitutive secretion of immunostimulatory cytokines have resulted in systemic toxicities[33,34]. More generally, immune hyperactivation induced by T-cell effector function can trigger severe cytokine release syndrome (CRS), a condition that can quickly turn fatal if the immune response is not promptly attenuated[35,36]. The unpredictable development and severity of CRS in patients also allude to the aforementioned 'on-target, off-tumor' consequences of unintended T-cell activation by normal cells. While TCRs and CARs allow T cells to engage target antigens with exquisite specificity, the surface presentation of candidate target antigens is rarely tumor-exclusive, and receptor cross-reactivities can result in the destruction of healthy tissues, directly contributing to patient fatalities[9,10]. Collectively, these challenges reveal the fine margins between therapeutic safety and efficacy, underscoring the urgent need for technologies that offer increasingly precise control over T-cell functions.

Mammalian Genome-editing Tools: Progress and Therapeutic Prospects

Synthetic biology is an interdisciplinary field founded on the application of engineering principles to biology, with primary aims to advance the mechanistic understanding and programmability of living systems. While foundational studies largely revolved around the construction of transcriptional circuits in prokaryotes, the inception of powerful genome-editing and protein-engineering tools has propelled the design of sophisticated mammalian systems with far-reaching implications for health and medicine. Perhaps the most influential driver of recent toolkit expansion, the clustered regularly interspaced short palindromic repeats (CRISPR)/CRISPR-associated protein 9 (Cas9) system was originally discovered as an adaptive RNA-guided, DNA-cleaving mechanism that confers bacterial immunity against viral infections[37,38]. In the native context, CRISPR RNA (crRNA) sequences are derived from invading

viral genomes and form tripartite ribonucleoprotein (RNP) complexes with trans-activating crRNA (tracrRNA) and Cas9 protein to direct nuclease activity against viral DNA via Watson–Crick base pairing[39–41]. Unlike prior genome-editing tools including zinc-finger nucleases (ZFNs) and transcription activator-like effector nucleases (TALENs), which rely on strings of context-specific DNA-binding protein domains, sequence-specific DNA-targeting moieties can be generated for CRISPR/Cas9 by simply appending customized crRNA sequences with tracrRNA. Thus, the modularity of single guide RNA (sgRNA) design allows protein-DNA interactions to be defined with unprecedented accessibility and scalability[42,43].

The endogenous nuclease activity of Cas9 protein readily lends CRISPR/Cas9 technology to mammalian genome-editing applications by generating a precise double-stranded break (DSB) three base pairs from the 3' end of the guiding crRNA sequence[44]. Due to the error-prone nature of DSB repair mechanisms in mammalian cells, CRISPR-targeted loci typically exhibit a high frequency of frame-shift insertions and deletions (indels), providing a robust method to knock out undesired gene expression[45]. For example, one strategy to overcome immunosuppression in the tumor microenvironment involves disabling the expression of checkpoint receptors, including programmed death receptor 1 (PD-1) and cytotoxic T-lymphocyte–associated antigen 4 (CTLA-4), thereby preventing the downregulation of effector functions by cognate ligands presented on tumor-cell surfaces[46]. In the context of the COVERT strategy, it is also essential to remove constitutively cytotoxic payloads that do not contribute to lytic selectivity.

Alternatively, homology-directed repair (HDR) templates can be simultaneously co-delivered with CRISPR/Cas9 components to mediate site-specific integrations, replacements, or modifications with genetic elements encoding user-defined functions[47]. These genome-editing techniques are already being incorporated into efforts to develop allogeneic T-cell products by knocking out the endogenous TCR and other cell-surface molecules involved in transplant rejection or graft-versus-host disease (GvHD)[48]. Several groups have expanded on this approach by site-specifically integrating a CAR into the TCR alpha chain constant region (TRAC) locus,

simultaneously disrupting endogenous TCR expression and redirecting engineered T cells against a defined tumor-associated antigen[49,50]. A recent study by Eyquem *et al.* offered additional support for this strategy by suggesting that CD19 CAR integration specifically into the TRAC locus may enhance *in vivo* T-cell persistence and function resulting from increased temporal regulation and uniformity of CAR expression levels across the engineered T-cell population[49].

In addition to modifying chromosomal makeup, the ease and predictability of sgRNA design has inspired the development of high-throughput, genome-wide screening platforms involving multiplexed, barcoded sgRNA libraries[51,52]. For example, phenotypic screens of CRISPR/Cas9-treated cell populations have elucidated complex gene networks and epigenetic landscapes in somatic cell reprogramming and immune cell activation[53,54]. Catalytically inert Cas9 mutants have also been engineered to serve as the DNA-binding domain of transcriptional activators (CRISPRa) and inhibitors (CRISPRi), enabling temporal and reversible control over genetic perturbations[55]. Bolstered by increasingly efficient bioinformatics algorithms, these foundational techniques are poised to illuminate novel genetic interactions and guide next-generation therapeutic design.

Beyond decoding natural cellular programs, a central tenet of synthetic biology is the ability to rewire cellular devices to respond to novel environmental inputs with robust functional outputs. Toward this end, the Chen lab systematically evaluated a panel of minimal promoters and transcriptional regulatory elements in mammalian cell lines to inform the construction of a synthetic promoter that enables human T cells to induce CAR expression specifically under hypoxic conditions[56]. Aided by an expanding repository of biological sensors and actuators, mammalian whole-cell devices have also demonstrated closed-loop control over hepatocyte growth factor secretion during liver failure[57], insulin release in response to hyperglycemia[58], and suppression of thyroid-stimulating hormone receptor in Graves' disease[59]. Despite operating in

distinct disease contexts, each of these cell-based control systems share similar design features, emphasizing modularity as a hallmark of synthetic biology design.

Chimeric Antigen Receptors: Building on Modular Design Principles

Modular design principles have also fueled the rapid ascent of cell-based immunotherapy, most prominently through the re-targeting of patient-derived T cells with genetically engineered CARs. Although CARs are designed to mimic TCRs in function, the synthetic and endogenous receptors share little in structural similarity. Mature TCRs of conventional helper T cells (T_h) and cytotoxic T lymphocytes (CTLs) consist of heterodimers between TCRα and TCRβ chains, and further associate with an assortment of CD3 chains (i.e., CD3γ, CD3δ, CD3ε, and CD3ζ) to form a signaling complex at the T-cell surface[60]. Recognition of cognate peptide-MHC complexes presented on the target-cell surface also requires simultaneous engagement of the CD4 or CD8 co-receptor in T_h cells and CTLs, respectively[61,62]. Once the target cell has been identified, immunoreceptor tyrosine activating motifs (ITAMs) on the clustered CD3 chains are phosphorylated to trigger T-cell activation and effector functions[63].

Unlike TCRs, CARs are single-chain receptors, and mediate target-cell recognition to trigger T-cell activation in the absence of CD4 and CD8 co-receptor–binding. Instead of probing peptide-MHC complexes, CARs rely on an antibody-derived single-chain variable fragment (scFv) to recognize unique epitopes on surface-bound antigens[64,65]. In first-generation CAR designs, an N-terminal scFv is followed by an extracellular spacer, a transmembrane domain, and the ITAM-rich intracellular portion of the CD3ζ chain[66] (Figure 1.2). Second- and third-generation CARs further incorporate T-cell costimulatory domains, most commonly CD28 and/or CD137 (4-1BB), to provide additional signals that enhance or sustain T-cell responses[67]. Thus, the modularity of CAR design provides a means to tune both the specificity of targeted antigen input and the magnitude of the T-cell activation output.

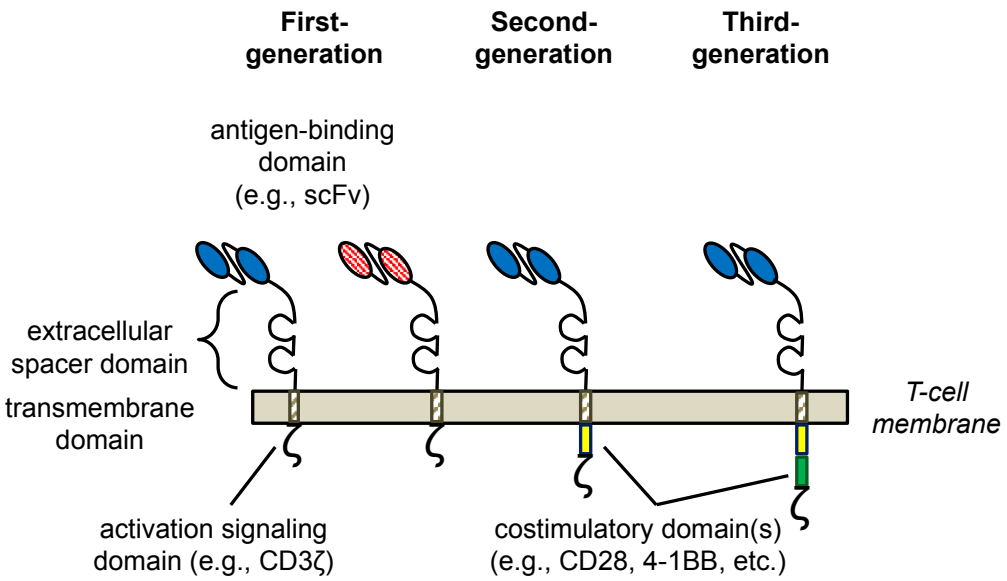

Figure 1.2. Schematic of CAR components and modular receptor design. First-generation CARs consist of an antibody-derived scFv antigen-binding domain, an extracellular spacer, a transmembrane domain, and the intracellular portion of the CD3ζ chain, which contain ITAMs that become phosphorylated upon CAR–antigen binding and trigger T-cell activation. New CARs can be generated to target distinct antigens by simply exchanging the scFv with an alternative scFv or ligand-binding domain for the antigen of interest. Beyond changing the antigen specificity, the dynamics of receptor binding and signaling can be fine-tuned by altering the scFv binding affinity or the structural properties of the extracellular spacer and transmembrane domains. Second- and third-generation CARs contain one or two additional costimulatory domains, respectively. These costimulatory domains are most commonly derived from the intracellular signaling domains of CD28 or 4-1BB and provide secondary signaling to support robust T-cell activation.

While CARs can successfully redirect T-cell functions against any number of surface-bound antigens in principle, surface-antigen expression is seldom restricted to diseased cells, and receptor-mediated misidentification of normal cells has resulted in unintended damage to healthy tissues[64,68–70]. Notably, the pan–B-cell marker CD19 is expressed by all B cells during normal development, and all patients that respond to CD19 CAR-T cell therapy develop sustained B-cell aplasia following adoptive T-cell transfer[29]. This ‘on-target, off-tumor’ toxicity is also manifest in other dose-limiting conditions that include severe skin rashes or life-threatening colitis when T cells are engineered to target melen-A (MART1) in melanomas[71], or carcinoembryonic antigen (CEA) in colorectal carcinomas[72], respectively. Although the aforementioned toxicities are

often clinically manageable, autologous transfers of T cells targeting commonly hyped cancer antigens such as human epidermal receptor growth factor 2 (HER2)[9] or melanoma-associated antigen 3 (MAGE-A3)[10] have resulted in unanticipated receptor cross-reactivities against vital cardiac or neurologic tissues, directly contributing to patient fatalities. In each instance, pre-clinical models failed to reveal warning signs of potential on-target, off-tumor toxicities, highlighting the challenge of developing safe receptor-based therapeutics for human patients. As a result of these clinical failures, there is now a growing consensus that the lack of suitable candidate target antigens is the primary obstacle for cancer immunotherapy[73,74].

Multi-input Receptor Systems: Encoding Boolean Logic Computation

In response to the pressing need to improve the precision of engineered T-cell responses, several groups have explored the design of multi-input receptor systems that enable T cells to sense and respond to combinations of surface-bound antigens. Much like digital processors, these synthetic receptor platforms aim to execute Boolean logic in order to determine the appropriate functional output for an integrated array of signal inputs.

OR-gate Logic

One of the most successful demonstrations of multi-input processing in human T cells has been the development of bispecific CARs to address the CD19 antigen-downregulation routinely characterized by relapsed malignancies following CD19 CAR-T cell therapy[75,76]. Bispecific CARs display a tandem of scFvs, each individually able to bind a cognate antigen present on the target-cell surface, thereby triggering T-cell activation in response to either or both target antigens (Figure 1.3a). This OR-gate strategy was applied by the Chen lab to yield an optimized CD20-CD19 bispecific CAR that enables T cells to sustain anti-tumor responses against heterogenous B-cell populations in an *in vivo* model of CD19 escape, and additional pairs of antigen targets are now under evaluation across multiple clinical trials (NCT03614858 and NCT03241940).

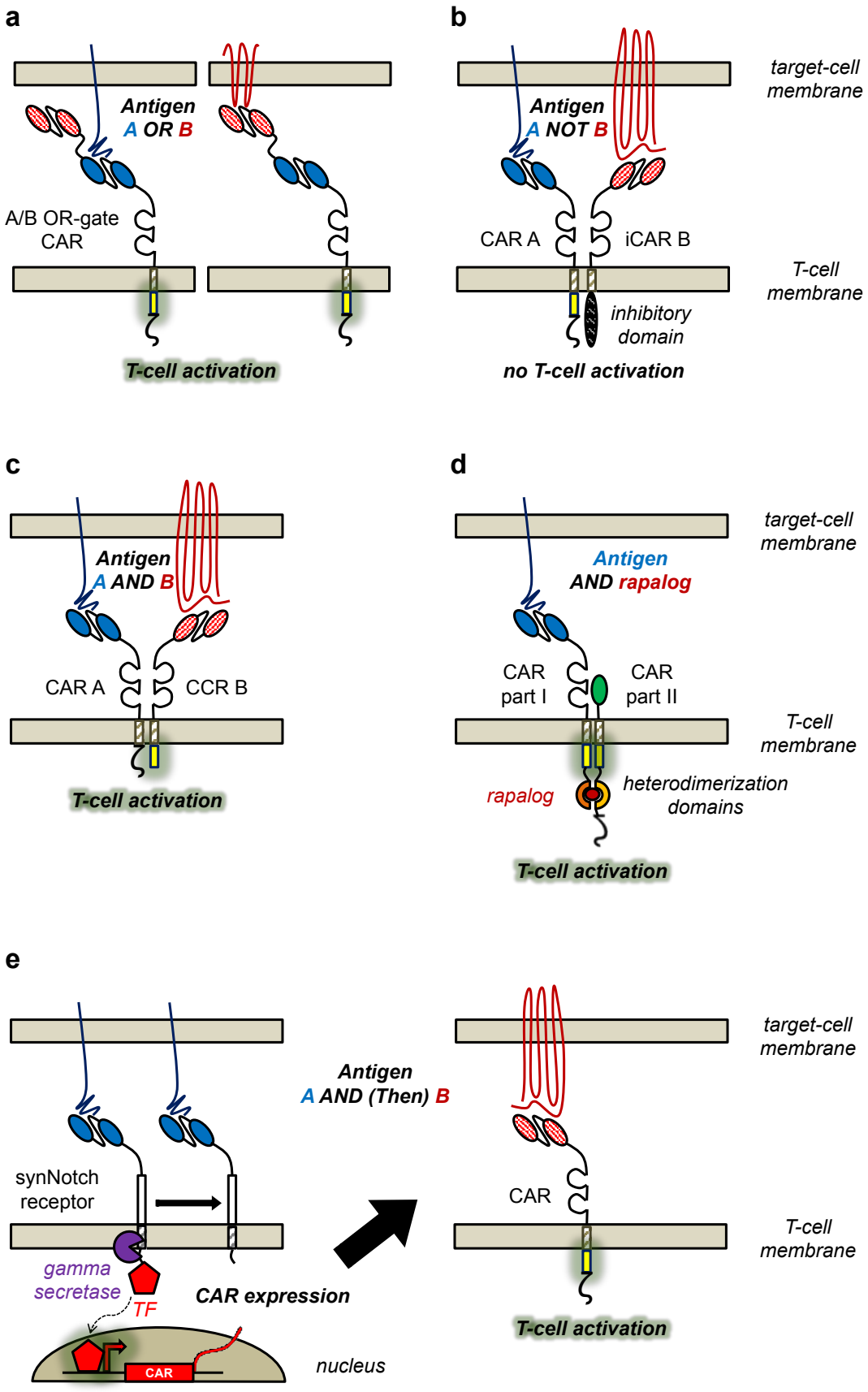
a
Antigen
A OR B
A/B OR-gate
CAR
T-cell activation
b
target-cell
membrane
Antigen
A NOT B
CAR A
iCAR B
T-cell
membrane
inhibitory
domain
no T-cell activation
c
Antigen
A AND B
CAR A
CCR B
T-cell activation
d
target-cell
membrane
Antigen
AND rapalog
CAR
part I
CAR
part II
T-cell
membrane
rapalog
heterodimerization
domains
T-cell activation
e
target-cell
membrane
Antigen
A AND (Then) B
synNotch
receptor
gamma
secretase
TF
CAR expression
CAR
T-cell
membrane
T-cell activation
CAR
nucleus

Figure 1.3. Multi-input receptor systems enable T cells to compute Boolean logic. **(a)** Bispecific OR-gate CARs contain two scFvs fused in tandem, with each scFv independently targeting a distinct antigen, and thus trigger T-cell activation in response to either antigen. **(b)** Inhibitory CARs (iCARs) utilize the inhibitory intracellular domain of checkpoint receptors instead of the ITAM-containing domain of CD3ζ to suppress T-cell activation in response to the target antigen. When paired with a normal activating CAR, iCARs enable AND-NOT–gate logic computation. **(c)** Chimeric costimulatory receptors (CCRs) lack CD3ζ and therefore cannot trigger T-cell activation independently. However, CCR activation provides crucial costimulatory signaling to sustain T-cell activation triggered by a paired CAR in AND-gate fashion. **(d)** Split-CARs heterodimerize in response to rapalog, allowing AND-gated T-cell activation in response to a single tumor antigen in combination with the pharmaceutical input. **(e)** SynNotch receptors release a transcription factor upon recognition of a target antigen, triggering the expression of a CAR targeting a different antigen, thus generating an AND-gate system that requires a priming signal prior to arming T cells with a functional CAR.

AND-NOT–gate Logic

While the broadened antigen-recognition of bispecific CARs has proven beneficial toward preventing tumor antigen-escape, alternative CAR architectures have focused on selectively restraining the T-cell response to improve the specificity of tumor-targeting. One such design by Fedorov *et al.* replaced the CD3ζ domain of a prostate-specific membrane antigen (PSMA)-targeting CAR with inhibitory signaling domains derived from checkpoint receptors such as PD-1 or CTLA-4 to generate inhibitory CARs (iCARs) that prevent T-cell activation in the presence of PSMA[77] (Figure 1.3b). When paired with a second-generation CD19 CAR, the PSMA iCARs supported AND-NOT–gate behavior by suppressing T-cell effector functions against CD19 and PSMA dual-positive target cells[77].

AND-gate Logic

In native interactions between T cells and antigen-presenting cells (APCs), this balancing act between activating and inhibitory signals is also influenced by secondary signals termed co-stimulation, which are necessary to prime maximal T-cell proliferation, interleukin-2 (IL-2) production, and effector differentiation[78]. Conversely, stimulation of the TCR in the absence of co-stimulation drives T-cell anergy, resulting in immune tolerance of host tissues. Taking advantage of this natural host-protective mechanism, Kloss *et al.* devised an AND-gated dual-receptor

system to specifically target tumor cells expressing both PSMA and prostate stem cell antigen (PSCA) by dividing the CAR signaling domains between a PSMA-targeting chimeric costimulatory receptor (CCR) containing both CD28 and 4-1BB but lacking CD3ζ, and a first-generation PSCA CAR devoid of costimulatory domains[79] (Figure 1.3c.). In the absence of PSMA, T-cell responses against $PSCA^+$ target cells were successfully dampened, although a substantial amount of trial-and-error was required to balance the signaling strength of both receptors.

To modulate the re-constitution of activating and costimulatory signals more robustly, researchers have also engineered a CD19 CCR that carries a C-terminal fusion to FK506 binding protein (FKBP), a chemically induced heterodimerization partner of the FKBP-rapamycin binding (FRB) domain[80] (Figure 1.3d). A separate FRB–CD3ζ fusion is tethered to the cell membrane as part of a truncated receptor lacking an extracellular ligand-recognition domain, forming a fully functional CAR only upon pharmaceutical addition of a rapamycin analog (rapalog) that induces heterodimerization of the FKBP and FRB domains. Another recently developed AND-gate strategy minimized off-tumor T-cell activation by repressing CAR expression entirely, until encounter with a target priming antigen. This system revolves around a synthetic Notch (synNotch) receptor, which exposes a juxtamembrane cleavage sequence to the endogenous intramembrane protease, gamma-secretase, upon ligand binding[81,82] (Figure 1.3e). Proteolysis of the synNotch receptor then releases the intracellular transcription activator domain to the nucleus to drive the expression of a CAR that recognizes a separate antigen. By pairing a green fluorescent protein (GFP)-targeted synNotch receptor with a CD19 CAR, T cells were able to eradicate tumors expressing both GFP and CD19, but not CD19 alone[82].

Thinking *Inside* the Box: Interrogating Intracellular Disease Signatures

Although innovative multi-input receptor-based systems, including those described above, have successfully rewired T cells to sense and respond to combinations of antigens, each of these architectures retain a heavy reliance upon the existing repertoire of candidate markers expressed

at the target-cell surface. In contrast to extracellular biomarkers, the expression profiles of intracellular oncoproteins and tumor suppressors are well-characterized molecular determinants of disease[83–86], representing an underexplored basis for engineered tumor-targeting specificity in adoptive T-cell therapy. Therefore, in lieu of truly tumor-exclusive surface-bound antigens, we set out to engineer T cells that can interrogate target cells for intracellular antigen expression prior to triggering cytotoxicity.

A primary mechanism for T-cell lytic function is the targeted release of cytotoxic effector proteins from lytic granules in response to receptor-mediated target-cell identification[87,88]. Since these cytotoxic payloads, particularly GrB and perforin (Pfn), constitutively trigger target-cell apoptosis[89–91], the selectivity of T-cell lytic function normally hinges on the exclusivity of surface-antigen expression (Figure 1.4a). As an alternative to traditional receptor-engineering approaches, our strategy is to directly reprogram T-cell–mediated cytotoxicity by replacing the endogenous cytotoxic payload with a GrB-based, intracellular-antigen–responsive COVERT switch (Figure 1.4b). The COVERT switch is still degranulated from T cells upon target-cell recognition but remains inactive in the absence of the intracellular disease biomarker, thereby sparing normal cells of the usual ‘lethal hit’. However, COVERT encounter with the intracellular tumor antigen within the target cell activates GrB activity and initiates the natural cytotoxic cascade (Figure 1.4c). In this manner, the COVERT system complements surface-receptor technologies to equip T cells with AND-gate logic computation for spatiotemporally segregated signal inputs, first at the target-cell surface, and then from within the target cell.

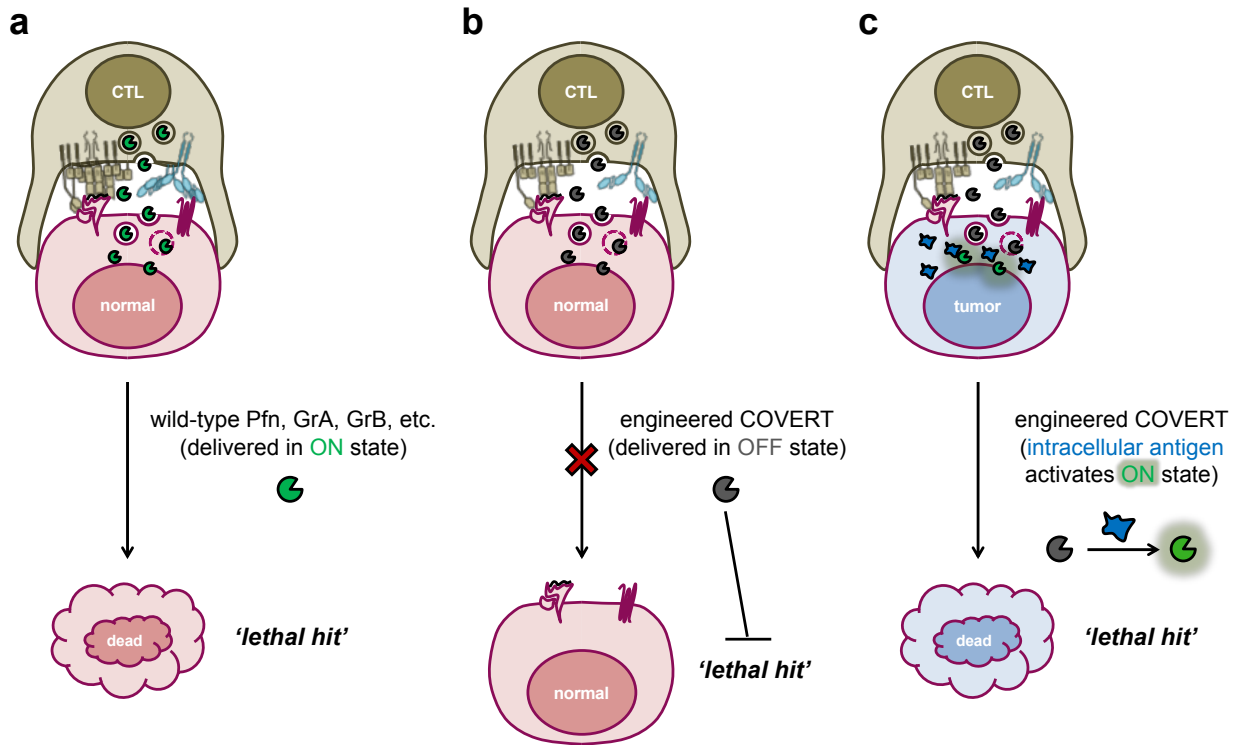

Figure 1.4. Schematic of COVERT interrogation of intracellular disease signatures. **(a)** CTLs degranulate constitutively active cytotoxic payloads, including perforin (Pfn), granzyme A (GrA), and granzyme B (GrB) upon surface-antigen recognition, resulting in the delivery of a 'lethal hit' to misidentified normal cells that express the target surface antigen. **(b)** Replacement of wild-type GrB with a COVERT switch protects normal cells from the usual 'lethal hit' by remaining inactive in the absence of an intracellular target antigen. **(c)** COVERT encounter with the target intracellular antigen (dark blue) within tumor cells initiates GrB activation to selectively trigger apoptosis in diseased cells.

The remaining chapters of this thesis describe the theoretical considerations and experimental groundwork involved in 're-imagining' T-cell–mediated cytotoxicity to selectively lyse target cells on the basis of intracellular target-antigen expression. Chapter 2 briefly reviews the cytotoxic mechanisms and payloads naturally available to T cells and highlights the properties that qualify GrB to serve as a T-cell–compatible chassis for an engineered cytotoxic switch. In Chapter 3, we proceed to apply the modular design principles of synthetic biology to develop a protease-responsive GrB-based switch architecture, and demonstrate the selective lytic potential of a small ubiquitin-like modifier (SUMO)-GrB fusion against human cells that overexpress the tumor-associated protease sentrin-specific protease 1 (SENP1). Since COVERT-mediated

regulation of lytic function requires the disruption of endogenous cytotoxic payloads, Chapter 4 focuses on the optimization of T-cell manufacturing workflows to enable efficient knock out of wild-type GrB and simultaneous introduction of SUMO-GrB expression into CAR-T cells. Finally, in Chapter 5, we share our broader vision and initial steps toward developing a versatile platform that enables the rapid design and optimization of COVERT molecules for compositionally and mechanistically diverse disease signatures. By complementing already robust surface-receptor technologies, the COVERT platform is poised to significantly expand the pool of disease signatures that can be targeted by adoptive T-cell therapy. Within the past several decades, the completion of the Human Genome Project and parallel advances in sequencing technology have enabled high-throughput analyses of cancer omics data[92–94]. As increasingly comprehensive patient data sets become available through the recently launched Precision Medicine Initiative, we anticipate the eventual realization of the COVERT vision, thus bridging the gap between omics-driven biomarker discovery and the development of safer, next-generation T-cell therapies for a broader range of diseases.

REFERENCES

1. Gross, G., Waks, T. & Eshhar, Z. Expression of immunoglobulin-T-cell receptor chimeric molecules as functional receptors with antibody-type specificity. *Proc. Natl. Acad. Sci. U. S. A.* **86,** 10024–8 (1989).
2. Porter, D. L., Levine, B. L., Kalos, M., Bagg, A. & June, C. H. Chimeric antigen receptor-modified T cells in chronic lymphoid leukemia. *N. Engl. J. Med.* **365,** 725–33 (2011).
3. Kalos, M. *et al.* T cells with chimeric antigen receptors have potent antitumor effects and can establish memory in patients with advanced leukemia. *Sci. Transl. Med.* **3,** 95ra73 (2011).
4. Abid, M. B. The revving up of CARs. *Gene Ther.* **25,** 162–162 (2018).
5. Jain, M. D., Bachmeier, C. A., Phuoc, V. H. & Chavez, J. C. Axicabtagene ciloleucel (KTE-C19), an anti-CD19 CAR T therapy for the treatment of relapsed/refractory aggressive B-cell non-Hodgkin's lymphoma. *Ther. Clin. Risk Manag.* **14,** 1007–1017 (2018).
6. Stauss, H. J. & Morris, E. C. Immunotherapy with gene-modified T cells: limiting side effects provides new challenges. *Gene Ther.* **20,** 1029–32 (2013).
7. Parkhurst, M. R. *et al.* T cells targeting carcinoembryonic antigen can mediate regression of metastatic colorectal cancer but induce severe transient colitis. *Mol. Ther.* **19,** 620–6 (2011).
8. Lamers, C. H. *et al.* Treatment of metastatic renal cell carcinoma with CAIX CAR-engineered T cells: clinical evaluation and management of on-target toxicity. *Mol. Ther.* **21,** 904–12 (2013).
9. Linette, G. P. *et al.* Cardiovascular toxicity and titin cross-reactivity of affinity-enhanced T cells in myeloma and melanoma. *Blood* **122,** 863–71 (2013).
10. Morgan, R. A. *et al.* Cancer Regression and Neurological Toxicity Following Anti-MAGE-A3 TCR Gene Therapy. *J. Immunother.* **36,** 133–151 (2013).

11. Gelpi, A. & Tucker, J. D. The magic bullet hits many targets: Salvarsan's impact on UK health systems, 1909-1943. *Sex. Transm. Infect.* **91,** 69–70 (2015).

12. Strebhardt, K. & Ullrich, A. Paul Ehrlich's magic bullet concept: 100 years of progress. *Nat. Rev. Cancer* **8,** 473–480 (2008).

13. Bosch, F. & Rosich, L. The contributions of Paul Ehrlich to pharmacology: a tribute on the occasion of the centenary of his Nobel Prize. *Pharmacology* **82,** 171–9 (2008).

14. Adams, G. P. & Weiner, L. M. Monoclonal antibody therapy of cancer. *Nat. Biotechnol.* **23,** 1147–1157 (2005).

15. Hudis, C. A. Trastuzumab — Mechanism of Action and Use in Clinical Practice. *N. Engl. J. Med.* **357,** 39–51 (2007).

16. Haraoui, B. & Bykerk, V. Etanercept in the treatment of rheumatoid arthritis. *Ther. Clin. Risk Manag.* **3,** 99–105 (2007).

17. Iqbal, N. & Iqbal, N. Imatinib: a breakthrough of targeted therapy in cancer. *Chemother. Res. Pract.* **2014,** 357027 (2014).

18. American Cancer Society. *Cancer Facts & Figures 2018*. (American Cancer Society, 2018).

19. Bovenberg, M. S. S., Degeling, M. H. & Tannous, B. A. Advances in stem cell therapy against gliomas. *Trends Mol. Med.* **19,** 281–291 (2013).

20. Bartelink, I. H. *et al.* Tumor Drug Penetration Measurements Could Be the Neglected Piece of the Personalized Cancer Treatment Puzzle. *Clin. Pharmacol. Ther.* (2018).

21. Johnson, L. A. & June, C. H. Driving gene-engineered T cell immunotherapy of cancer Introduction: fantastic voyage. *Cell Res.* **27,** 38–58 (2017).

22. Chakravarti, D. & Wong, W. W. Synthetic biology in cell-based cancer immunotherapy. *Trends Biotechnol.* **33,** 449–461 (2015).

23. Humphries, C. Adoptive cell therapy: Honing that killer instinct. *Nature* **504,** S13-5 (2013).

24. Kvistborg, P. *et al.* TIL therapy broadens the tumor-reactive CD8(+) T cell compartment in

melanoma patients. *Oncoimmunology* **1,** 409–418 (2012).

25. Robbins, P. F. *et al.* Mining exomic sequencing data to identify mutated antigens recognized by adoptively transferred tumor-reactive T cells. *Nat. Med.* **19,** 747–52 (2013).
26. Eshhar, Z., Waks, T., Gross, G. & Schindler, D. G. Specific activation and targeting of cytotoxic lymphocytes through chimeric single chains consisting of antibody-binding domains and the gamma or zeta subunits of the immunoglobulin and T-cell receptors. *Proc. Natl. Acad. Sci. U. S. A.* **90,** 720–4 (1993).
27. Kochenderfer, J. N. *et al.* Chemotherapy-Refractory Diffuse Large B-Cell Lymphoma and Indolent B-Cell Malignancies Can Be Effectively Treated With Autologous T Cells Expressing an Anti-CD19 Chimeric Antigen Receptor. *J Clin Oncol* **33,** 540–549 (2015).
28. Davila, M. L. *et al.* Efficacy and Toxicity Management of 19-28z CAR T Cell Therapy in B Cell Acute Lymphoblastic Leukemia. *Sci. Transl. Med.* **6,** 224ra225 (2014).
29. Maude, S. L. *et al.* Chimeric Antigen Receptor T Cells for Sustained Remissions in Leukemia. *N. Engl. J. Med.* **371,** 1507–1517 (2014).
30. Wang, X. *et al.* Phase 1 studies of central memory–derived CD19 CAR T–cell therapy following autologous HSCT in patients with B-cell NHL. *Blood* **127,** 2980–2990 (2016).
31. Berraondo, P., Umansky, V. & Melero, I. Changing the tumor microenvironment: New strategies for immunotherapy. *Cancer Res.* **72,** 5159–5164 (2012).
32. Wang, D. *et al.* Targeting EZH2 Reprograms Intratumoral Regulatory T Cells to Enhance Cancer Immunity. *Cell Rep.* **23,** 3262–3274 (2018).
33. Zhang, L. *et al.* Tumor-Infiltrating Lymphocytes Genetically Engineered with an Inducible Gene Encoding Interleukin-12 for the Immunotherapy of Metastatic Melanoma. *Clin. Cancer Res.* **21,** 2278–2288 (2015).
34. Kerkar, S. P. *et al.* Tumor-specific CD8+ T cells expressing interleukin-12 eradicate established cancers in lymphodepleted hosts. *Cancer Res.* **70,** 6725–34 (2010).
35. Giavridis, T. *et al.* CAR T cell–induced cytokine release syndrome is mediated by

macrophages and abated by IL-1 blockade. *Nat. Med.* **24,** 731–738 (2018).

36. Norelli, M. *et al.* Monocyte-derived IL-1 and IL-6 are differentially required for cytokine-release syndrome and neurotoxicity due to CAR T cells. *Nat. Med.* **24,** 739–748 (2018).
37. Zhang, F., Wen, Y. & Guo, X. CRISPR/Cas9 for genome editing: progress, implications and challenges. *Hum. Mol. Genet.* **23,** R40–R46 (2014).
38. Hsu, P. D., Lander, E. S. & Zhang, F. Development and applications of CRISPR-Cas9 for genome engineering. *Cell* **157,** 1262–78 (2014).
39. Kim, S., Kim, D., Cho, S. W., Kim, J.-S. J. & Kim, J.-S. J. Highly efficient RNA-guided genome editing in human cells via delivery of purified Cas9 ribonucleoproteins. *Genome Res.* **24,** 1012–9 (2014).
40. Ran, F. A. *et al.* In vivo genome editing using Staphylococcus aureus Cas9. *Nature* **520,** 186–91 (2015).
41. Jinek, M. *et al. A Programmable Dual-RNA-Guided DNA Endonuclease in Adaptive Bacterial Immunity*.
42. Dominguez, A. A., Lim, W. A. & Qi, L. S. Beyond editing: repurposing CRISPR-Cas9 for precision genome regulation and interrogation. *Nat. Rev. Mol. Cell Biol.* **17,** 5–15 (2016).
43. Kiani, S. *et al.* Cas9 gRNA engineering for genome editing, activation and repression. *Nat. Methods* **12,** 1051–1054 (2015).
44. Pyzocha, N. K., Ran, F. A., Hsu, P. D. & Zhang, F. RNA-guided genome editing of mammalian cells. *Methods Mol. Biol.* **1114,** 269–77 (2014).
45. Su, S. *et al.* CRISPR-Cas9 mediated efficient PD-1 disruption on human primary T cells from cancer patients. *Sci. Rep.* **6,** 20070 (2016).
46. Rupp, L. J. *et al.* CRISPR/Cas9-mediated PD-1 disruption enhances anti-tumor efficacy of human chimeric antigen receptor T cells. *Sci. Rep.* **7,** 737 (2017).
47. Schumann, K. *et al.* Generation of knock-in primary human T cells using Cas9 ribonucleoproteins. *Proc. Natl. Acad. Sci.* **112,** 201512503 (2015).

48. Poirot, L. *et al.* Multiplex genome edited T-cell manufacturing platform for 'off-the-shelf' adoptive T-cell immunotherapies. *Cancer Res.* **75,** 3853–3864 (2015).

49. Eyquem, J. *et al.* Targeting a CAR to the TRAC locus with CRISPR/Cas9 enhances tumour rejection. *Nature* **543,** 113–117 (2017).

50. MacLeod, D. T. *et al.* Integration of a CD19 CAR into the TCR Alpha Chain Locus Streamlines Production of Allogeneic Gene-Edited CAR T Cells. *Mol. Ther.* **25,** 949–961 (2017).

51. Stockman, V. B. *et al.* A High-Throughput Strategy for Dissecting Mammalian Genetic Interactions. *PLoS One* **11,** e0167617 (2016).

52. Wong, A. S. L. *et al.* Multiplexed barcoded CRISPR-Cas9 screening enabled by CombiGEM. *Proc. Natl. Acad. Sci. U. S. A.* **113,** 2544–9 (2016).

53. Toh, C.-X. D. *et al.* RNAi Reveals Phase-Specific Global Regulators of Human Somatic Cell Reprogramming. *Cell Rep.* **15,** 2597–2607 (2016).

54. Singer, M. *et al.* A Distinct Gene Module for Dysfunction Uncoupled from Activation in Tumor-Infiltrating T Cells. *Cell* **166,** 1500–1511.e9 (2016).

55. Zalatan, J. G. *et al.* Engineering Complex Synthetic Transcriptional Programs with CRISPR RNA Scaffolds. *Cell* **160,** 339–350 (2015).

56. Ede, C., Chen, X., Lin, M.-Y. & Chen, Y. Y. Quantitative Analyses of Core Promoters Enable Precise Engineering of Regulated Gene Expression in Mammalian Cells. *ACS Synth. Biol.* **5,** 395–404 (2016).

57. Bai, P. *et al.* A synthetic biology-based device prevents liver injury in mice. *J. Hepatol.* **65,** 84–94 (2016).

58. Xie, M. *et al.* β-cell-mimetic designer cells provide closed-loop glycemic control. *Science (80-.).* **354,** 1296–1301 (2016).

59. Saxena, P., Charpin-El Hamri, G., Folcher, M., Zulewski, H. & Fussenegger, M. Synthetic gene network restoring endogenous pituitary–thyroid feedback control in experimental

Graves' disease. *Proc. Natl. Acad. Sci.* **113,** 1244–1249 (2016).

60. Birnbaum, M. E. *et al.* Molecular architecture of the αβ T cell receptor-CD3 complex. *Proc. Natl. Acad. Sci. U. S. A.* **111,** 17576–81 (2014).

61. Artyomov, M. N., Lis, M., Devadas, S., Davis, M. M. & Chakraborty, A. K. CD4 and CD8 binding to MHC molecules primarily acts to enhance Lck delivery. *Proc. Natl. Acad. Sci. U. S. A.* **107,** 16916–21 (2010).

62. Viola, A. *et al.* Quantitative contribution of CD4 and CD8 to T cell antigen receptor serial triggering. *J. Exp. Med.* **186,** 1775–9 (1997).

63. Bettini, M. L. *et al.* Cutting Edge: CD3 ITAM Diversity Is Required for Optimal TCR Signaling and Thymocyte Development. *J. Immunol.* **199,** 1555–1560 (2017).

64. Jensen, M. C. & Riddell, S. R. Design and implementation of adoptive therapy with chimeric antigen receptor-modified T cells. *Immunol. Rev.* **257,** 127–44 (2014).

65. Love, P. E. & Hayes, S. M. ITAM-mediated signaling by the T-cell antigen receptor. *Cold Spring Harb. Perspect. Biol.* **2,** a002485 (2010).

66. Sadelain, M., Brentjens, R. & Rivière, I. The promise and potential pitfalls of chimeric antigen receptors. *Curr. Opin. Immunol.* **21,** 215–23 (2009).

67. Lim, W. A. & June, C. H. The Principles of Engineering Immune Cells to Treat Cancer. *Cell* **168,** 724–740 (2017).

68. Gargett, T. & Brown, M. P. The inducible caspase-9 suicide gene system as a 'safety switch' to limit on-target, off-tumor toxicities of chimeric antigen receptor T cells. *Front. Pharmacol.* **5,** 235 (2014).

69. Fedorov, V. D., Sadelain, M. & Kloss, C. C. Novel approaches to enhance the specificity and safety of engineered T cells. *Cancer J.* **20,** 160–5

70. Kalos, M. & June, C. H. Adoptive T cell transfer for cancer immunotherapy in the era of synthetic biology. *Immunity* **39,** 49–60 (2013).

71. Johnson, L. A. *et al.* Gene therapy with human and mouse T-cell receptors mediates

cancer regression and targets normal tissues expressing cognate antigen. *Blood* **114,** 535–46 (2009).

72. Morgan, R. A. *et al.* Case report of a serious adverse event following the administration of T cells transduced with a chimeric antigen receptor recognizing ERBB2. *Mol. Ther.* **18,** 843–51 (2010).

73. Rosenberg, S. A. Finding suitable targets is the major obstacle to cancer gene therapy. *Cancer Gene Ther.* **21,** 45–7 (2014).

74. Hinrichs, C. S. & Restifo, N. P. Reassessing target antigens for adoptive T-cell therapy. *Nat. Biotechnol.* **31,** 999–1008 (2013).

75. Zah, E., Lin, M.-Y., Silva-Benedict, A., Jensen, M. C. & Chen, Y. Y. T cells expressing CD19/CD20 bi-specific chimeric antigen receptors prevent antigen escape by malignant B cells. *Cancer Immunol. Res.* **4,** 498–508 (2016).

76. Zah, E., Lin, M.-Y., Silva-Benedict, A., Jensen, M. C. & Chen, Y. Y. ADDENDUM: T Cells Expressing CD19/CD20 Bispecific Chimeric Antigen Receptors Prevent Antigen Escape by Malignant B Cells. *Cancer Immunol. Res.* **4,** 639–641 (2016).

77. Fedorov, V. D., Themeli, M. & Sadelain, M. PD-1- and CTLA-4-based inhibitory chimeric antigen receptors (iCARs) divert off-target immunotherapy responses. *Sci. Transl. Med.* **5,** 215ra172 (2013).

78. Long, A. H. *et al.* 4-1BB costimulation ameliorates T cell exhaustion induced by tonic signaling of chimeric antigen receptors. *Nat. Med.* **21,** 581–590 (2015).

79. Kloss, C. C., Condomines, M., Cartellieri, M., Bachmann, M. & Sadelain, M. Combinatorial antigen recognition with balanced signaling promotes selective tumor eradication by engineered T cells. *Nat. Biotechnol.* **31,** 71–5 (2013).

80. Wu, C.-Y., Roybal, K. T., Puchner, E. M., Onuffer, J. & Lim, W. A. Remote control of therapeutic T cells through a small molecule-gated chimeric receptor. *Science* **350,** aab4077 (2015).

81. Morsut, L. *et al.* Engineering Customized Cell Sensing and Response Behaviors Using Synthetic Notch Receptors. *Cell* **164,** 780–791 (2016).

82. Roybal, K. T. *et al.* Precision Tumor Recognition by T Cells With Combinatorial Antigen-Sensing Circuits. *Cell* **164,** 770–779 (2016).

83. Davies, H. *et al.* Mutations of the BRAF gene in human cancer. *Nature* **417,** 949–54 (2002).

84. Kranenburg, O. The KRAS oncogene: past, present, and future. *Biochim. Biophys. Acta* **1756,** 81–2 (2005).

85. Dang, C. V. MYC on the path to cancer. *Cell* **149,** 22–35 (2012).

86. Harris, C. C. *Structure and Function of the p53 Tumor Suppressor Gene: Clues for Rational Cancer Therapeutic Strategies*. *J Natl Cancer Inst* **88,** (1996).

87. Lieberman, J. The ABCs of granule-mediated cytotoxicity: new weapons in the arsenal. *Nat. Rev. Immunol.* **3,** 361–70 (2003).

88. Raja, S. M., Metkar, S. S. & Froelich, C. J. Cytotoxic granule-mediated apoptosis: unraveling the complex mechanism. *Curr. Opin. Immunol.* **15,** 528–32 (2003).

89. Smyth, M. J. & Trapani, J. A. Granzymes: exogenous proteinases that induce target cell apoptosis. *Immunol. Today* **16,** 202–6 (1995).

90. Cullen, S. P., Brunet, M. & Martin, S. J. Granzymes in cancer and immunity. *Cell Death Differ.* **17,** 616–23 (2010).

91. Chowdhury, D. & Lieberman, J. Death by a thousand cuts: granzyme pathways of programmed cell death. *Annu. Rev. Immunol.* **26,** 389–420 (2008).

92. Vucic, E. A. *et al.* Translating cancer 'omics' to improved outcomes. *Genome Res.* **22,** 188–95 (2012).

93. Shibata, T. Current and future molecular profiling of cancer by next-generation sequencing. *Jpn. J. Clin. Oncol.* (2015).

94. Kwon, M.-S. *et al.* Integrative analysis of multi-omics data for identifying multi-markers for

diagnosing pancreatic cancer. *BMC Genomics* **16 Suppl 9,** S4 (2015).

Chapter 2. Evaluating Granzyme B as the Molecular Chassis for a T-cell–compatible Cytotoxic Switch

Partially adapted, with permission from Ho, P., Ede, C., & Chen, Y.Y. Modularly Constructed Synthetic Granzyme B Molecule Enables Interrogation of Intracellular Proteases for Targeted Cytotoxicity. *ACS Synth. Biol.*, **6** (8), 1484–1495.

ABSTRACT

Although the autologous transfer of T cells targeting the pan–B-cell marker CD19 has demonstrated remarkable curative potential in patients with relapsed B-cell malignancies, the lack of tumor-exclusive candidate target antigens currently limits the application of adoptive T-cell therapy for the vast majority of diseases. In particular, the selectivity of T-cell lytic function is normally defined via receptor-mediated interactions at the cell surface, which initiate potent cytotoxic effector programs against targeted cells. Since endogenous cytotoxic payloads are constitutively active when deployed, the recognition of surface-bound antigens is sufficient to trigger target-cell apoptosis. We propose to expand the antigen-recognition capabilities of engineered T cells by developing a cytotoxic switch payload, termed Cytoplasmic Oncoprotein VErifier and Response Trigger (COVERT), which is delivered in response to receptor-mediated target-cell recognition, but remains inactive until encounter with an intracellular disease signature within the target cell. Here, we specifically evaluate the suitability of granzyme B (GrB) to serve as a molecular chassis for COVERT switch design by verifying the safe packaging and trafficking of recombinant GrB in T-cell lytic granules, as well as delivery into target cells. We also provide evidence that human GrB is a major contributor to T-cell–mediated cytotoxicity, and further

demonstrate that the disruption of endogenous GrB expression is sufficient to abrogate efficient T-cell lytic activity without significant impact on non-cytotoxic effector functions.

INTRODUCTION

Adoptive T-cell therapy is a novel cancer treatment paradigm that aims to harness the precise antigen-specificity and long-term memory of the adaptive immune response by administering tumor-reactive T cells to eradicate diseased cell populations[1,2]. Although T cells with engineered specificity for the pan–B-cell marker CD19 have achieved complete and durable responses in patients with relapsed B-cell malignancies[3–6], several fundamental limitations prevent the widespread implementation of adoptive T-cell therapy as a front-line cancer treatment option[7,8]. In particular, T-cell lytic selectivity is normally defined by antigen-specific surface receptors, which activate potent cytotoxic effector programs in response to surface-bound antigens. Unfortunately, the current repertoire of accessible target antigens primarily consists of surface markers that are rarely tumor-exclusive, and low, basal expression of the targeted antigen by normal cells can elicit the destruction of healthy tissues[9–13]. In contrast, several intracellular oncoproteins are well-established molecular signatures of disease and constitute an underexplored pool of candidate antigens for targeting T-cell lytic function[14–16].

As the primary effectors of adaptive immunity, cytotoxic T lymphocytes (CTLs) are armed with a powerful arsenal of apoptosis-inducing payloads, each with distinct mechanisms and sites of action. Death receptor ligands, including CD95L (FasL) and other members of the tumor necrosis factor (TNF) family (i.e., TNF-α and TNF-β), bind to cognate death receptors on the target-cell surface to trigger death domain-mediated recruitment and activation of initiator caspase-8[17]. Meanwhile, lytic granule serine proteases (i.e., granzymes) and perforin (Pfn) are degranulated into the immunological synapse upon antigen-specific receptor cross-linking, with subsequent Pfn oligomerization and transmembrane pore formation facilitating granzyme uptake

and eventual endosomal escape into the target-cell cytoplasm[18–20]. Once released into the cytosol, granzymes proceed to cleave a variety of substrates involved in multiple caspase-dependent and caspase-independent apoptotic pathways[21,22]. Thus, while wild-type granzymes are constitutively active and therefore do not contribute to lytic selectivity, the natural mode of Pfn-mediated granzyme delivery presents an intriguing engineering opportunity for the development of a synthetic payload that can probe intracellular antigen expression. Specifically, we rationalized that granzymes could serve as the molecular chasses upon which to design cytotoxic switches, termed Cytoplasmic Oncoprotein VErifier and Response Trigger (COVERT), which require activation by intracellular disease signatures prior to initiating apoptosis-inducing cytotoxic cascades.

Since the effectiveness of a synthetic cytotoxic switch device hinges on its ability to induce target-cell apoptosis in the ON-state, we rationalized that a suitable chassis should naturally exhibit strong cytolytic potential. Among the five human granzymes, granzyme A (GrA) and granzyme B (GrB) are the most well-characterized, and believed to contribute the most to T-cell–mediated cytotoxicity[23,24]. However, to our knowledge, reports of human granzyme deficiency are absent from the medical record, and as a result, our cumulative understanding of granzyme biology has been heavily influenced by granzyme-knockout murine models. For example, both $GrA^{-/-}$ and $GrB^{-/-}$ single-knockout but not $GrA^{-/-}$ $GrB^{-/-}$ dual-knockout mice have been shown to resist tumor and viral challenges, a finding often used to support the position that GrA and GrB serve critical but redundant roles in T-cell–mediated cytotoxicity[25–27]. Despite this, careful biochemical studies have clearly demonstrated that purified GrA and GrB cleave distinct classes of substrates and trigger target-cell apoptosis on differing time scales[28,29]. In particular, GrB uniquely possesses Asp-ase activity, a feature that enables direct cleavage and activation of several rapidly acting pro-apoptotic factors including caspase-3 and the mitochondrial protein Bid[30]. In contrast, the primary cleavage targets for GrA, such as the endoplasmic reticulum-

associated SET complex, induce single-stranded DNA damage, eventually resulting in target-cell death[31].

Recently, other research groups have speculated that discrepancies between murine and human granzyme biology may also limit the extrapolation of experimental results from mouse models toward elucidating human granzyme function[29]. First, there are nine murine granzyme family members, as opposed to five in humans, with several murine granzyme loci carrying traces of gene duplication from GrB[32]. Perhaps due to this interspecies difference in granzyme evolutionary history, recent characterization studies have revealed divergence in substrate preferences between murine and human granzyme orthologues[29,30]. Moreover, studies have shown target-cell susceptibility to human GrB at EC_{50} levels a full order-of-magnitude lower than those for murine GrB, while human GrA must be supplied at higher-than-physiological concentrations to elicit the same cytotoxic response. Direct comparisons of cytotoxic potential further indicate that the apparent redundancy of GrA and GrB observed in mouse models may not accurately reflect the balance of cytotoxic contributions by GrA and GrB in human CTLs. While the available evidence does not discount the cytotoxic functions of human GrA or alternative apoptosis-inducing effector molecules and mechanisms, the robust and well-established cytotoxic potential of human GrB appears well-suited for the development of a COVERT switch payload.

The ability to regulate T-cell lytic selectivity in response to intracellular disease signatures would substantially expand the pool of candidate biomarkers that can be targeted by adoptive T-cell therapy. As outlined in Chapter 1, strategies to redirect T-cell targeting specificity have traditionally focused on the design of chimeric antigen receptors (CARs) and other synthetic surface-receptor systems, thereby restricting target selection to extracellular epitopes expressed on the target-cell surface. While endogenous T-cell receptors (TCRs) naturally mediate recognition of antigen peptides derived from intracellular proteins, surface-presentation requires peptide loading into the antigen-binding grooves of major histocompatibility complex (MHC) molecules, a process that is frequently dysregulated in diseased cells[33,34]. Furthermore, standard

receptor-engineering techniques do not apply to the identification of tumor-reactive TCRs, as the diversity and specificity of endogenous TCRs stem from random genetic recombination events that are not conducive to rational design[35]. As an alternative to receptor-based targeting, we propose to directly reprogram the cytotoxic payloads deployed by T cells to interrogate intracellular signals prior to triggering apoptosis. Here, we specifically evaluate the suitability of human GrB to serve as the molecular chassis for an engineered T-cell–compatible cytotoxic switch. In particular, we focus on the storage safety, delivery efficiency, and cytolytic potential that formulate essential design criteria for COVERT switch development.

METHODS

DNA Constructs. DNA was chemically synthesized as oligonucleotides or gBlocks by Integrated DNA Technologies (Coralville, IA) and assembled using standard molecular cloning techniques. Unless otherwise indicated, all constructs were cloned into the epHIV7 lentiviral expression vector[36], although expression was induced by transient DNA transfection in the absence of viral packaging. The QPY variant of human GrB was used in this study, and the S183A mutant was generated by introducing a TCT to GCC codon mutation via isothermal DNA assembly. The CD19 CAR was constructed as previously reported[37], and fused to GrB-mCherry via a 2A peptide using isothermal DNA assembly. The MSCV-IRES-EGFP retroviral vector and pHIT60 and RD114 retroviral packaging vectors were generous gifts from Dr. Steven Feldman (National Cancer Institute). EF1α-CD19 CAR-T2A-GrB-mCherry was downstream of the 5' LTR in the MSCV vector via isothermal DNA assembly, and a woodchuck hepatitis virus posttranscriptional regulatory element (WPRE) was subsequently inserted at the ClaI site by restriction-ligation cloning.

Cell Lines. HEK293T and Jurkat E6 cells were obtained from ATCC (Manassas, VA) in 2011. ATCC verified the identity of each purchased cell line by short tandem repeat analysis prior to

shipment. Raji cells and TM-LCLs were generous gifts from Dr. Michael C. Jensen (Seattle Children's Research Institute); the cell line was originally obtained from ATCC in 2003 and was authenticated again by short tandem repeat profiling at the University of Arizona Genetics Core in 2015. OKT3$^+$ TM-LCLs were a kind gift from Dr. Christine Brown (City of Hope). Cells were cultured in DMEM (HEK293T) or RPMI-1640 (Jurkat, Raji, and TM-LCL) supplemented with 10% heat-inactivated FBS (HI-FBS). All mammalian cell cultures were maintained at 37°C and 5% CO_2.

Primary Human T-cell Isolation and culture. Primary human CD8$^+$ T cells were isolated from healthy donor blood samples obtained from the UCLA Blood & Platelet Center using the RosetteSep CD8$^+$ Human T-cell Enrichment Cocktail (Stemcell Technologies, Vancouver, Canada), according to the manufacturer's protocol. Freshly isolated T cells were seeded at 1 x 10^6 cells/mL in T-cell media (RPMI-1640 supplemented with 10% HI-FBS), and stimulated with anti-CD3/CD28 Dynabeads (Life Technologies, Carlsbad, CA) at 1:1 cell:bead ratio. Cultures were supplemented with 50 U/mL IL-2 (Life Technologies) and 1 ng/mL IL-15 (Peprotech, Rocky Hill, NJ) every 48 hours.

Cell Transfection. HEK293T cells were seeded at 2.5 x 10^4 cells/0.25 mL/well in 48-well plates, 24 hours prior to transfection with 250 ng plasmid DNA and 15 nmol linear polyethylenimine (PEI, 25 kDa). For co-transfection experiments, plasmids were mixed at 1:1 mass ratio. The resulting DNA mixture totaling 250 ng was complexed with PEI, incubated at room temperature for 15 min, and then applied to seeded HEK293T cells. Jurkat T cells (5 x 10^6) were resuspended in 100 µL of Amaxa Cell Line Nucleofector™ V Solution (Lonza, Walkersville, MD) and electroporated with 5 µg plasmid DNA using Program X-001 of the Nucleofector™ 2b Device (Lonza), according to the manufacturer's protocol.

CRISPR/Cas9 RNP Nucleofection. Chemically synthesized sgRNAs (Synthego, Menlo Park, CA) were ordered with 2'-O-methyl analogs and 3' phosphorothioate internucleotide linkages at the 3 bases on both 5' and 3' ends for GrB sgRNA#9 (G*C*C*AGGGCAGACAUGCAGUG). Each sgRNA was resuspended to 100 µM in nuclease-free Tris-HCl pH 8.0 and aliquoted for storage at -20°C upon arrival. 3 µL of thawed sgRNA was diluted with 4.5 µL of nuclease-free H_2O in a 0.65 mL microfuge tube, while 5 µL of thawed in-house purified SpCas9 protein (10 mg/mL) was diluted with 2.5 µL of Cas9 storage buffer in a separate microfuge tube. CRISPR/Cas9 RNP complexes were assembled by adding diluted Cas9 to diluted sgRNA at 1:1 sgRNA:Cas9 ratio over a period of ~30 seconds, while swirling gently. Complexing reactions were allowed to incubate at room temperature for at least 10 minutes prior to nucleofection. 5×10^6 primary human $CD8^+$ T cells were washed 3 times with PBS (no FBS) via centrifugation at 100 *x g* for 10 min prior to resuspension in 100 µL of Ingenio® electroporation solution (Mirus Bio LLC, Madison, WI) and electroporated with the entire 300 pmol RNP complexing mixture using Program T-017 of the Nucleofector™ 2b Device (Lonza), according to the manufacturer's protocol. Nucleofected cells were allowed to incubate at room temperature within the nucleofection cuvette for 10 minutes prior to transfer into complete T-cell media supplemented with 50 U/mL IL-2 (Life Technologies) and 1 ng/mL IL-15 (Peprotech).

Ac-IEPD-pNA Activity Assay. Lysates were prepared by incubating cells in lysis buffer (150 mM NaCl, 20 mM Tris pH7.2, 1% (v/v) Triton-X) on ice for 45 min, and clarified of nuclear debris by centrifugation at 20,000 *x g* for 10 min. The protein concentration of the supernatant was determined via Bradford assay (Bio-Rad, Hercules, CA). 10 µg of primary human $CD8^+$ T-cell lysate, corresponding to 1.25×10^5 cells was pre-incubated with z-AAD-CMK (EMD Millipore, Burlington, MA) or DMSO at 2x the indicated concentrations in 50 µL of lysis buffer for 1 hour at room temperature to allow GrB inhibition to reach equilibrium. Samples were then diluted with 50 µL of assay buffer (50 mM HEPES pH 7.5, 10% (w/v) sucrose, 0.05% (w/v) CHAPS, 5 mM DTT)

containing 200 μM Ac-IEPD-pNA substrate (Enzo Life Sciences, Farmingdale, NY), as described by Ewen et al.[38]. Absorbance at 405 nm was measured every minute for 4 hours on an EONC microplate reader (BioTek, Winooski, VT). Activity was calculated by using the LINEST function in Excel to determine the line of best fit for the initial rate (dOD_{405}/min) by the least squares method.

Flow Cytometry. For GrB cytotoxicity experiments, transiently transfected HEK293T cells were harvested for analysis at 24 hours post-transfection. Culture media containing any dislodged cells were collected in centrifuge tubes before adherent cells were trypsinized and subsequently collected into the same tubes. The cells were washed twice with PBS prior to staining with 7-AAD (Life Technologies), according to manufacturer's protocols. For GrB-mCherry delivery experiments, primary human T cells expressing CD19 CAR and GrB-mCherry were co-cultured with 20,000 Raji cells at 3:1 effector:target ratio for 45 min. Co-cultures were then suspended by rigorous pipetting and stained with CD8-VioGreen (clone BW135/80; Miltenyi Biotec, San Diego, CA) and CD19-VioBlue (clone LT19; Miltenyi Biotec) prior to data acquisition on a MACSQuant VYB flow cytometer (Miltenyi Biotec). For intracellular staining experiments, cells were fixed with 1.5% formaldehyde in T-cell media for 15 min prior to permeabilization with ice-cold methanol for 30 min. Cells were subsequently stained with antibodies for GrB (clone GB11; Biolegend, San Diego, CA) or an isotype control (clone MOPC-21; Biolegend). Compensation and data analysis were performed using FlowJo Data Analysis software (TreeStar, Ashland, OR).

Live-cell Confocal Microscopy. Raji target cells were resuspended to 3 x 10^4 cells/50 μL in imaging media (RPMI-1640 without Phenol Red and L-glutamine supplemented with 10% HI-FBS and 20 mM HEPES) and seeded into 48-well glass plates (MatTek, Ashland, MA) to settle for 15 min. For T-cell activation experiments, Jurkat T cells were pre-loaded with calcium indicator by incubation with 1 μM Fluo-4 (Life Technologies) in imaging media containing 0.02% (w/v) Pluronic

F127 (Sigma-Aldrich) at room temperature for 20 min. Cells were then washed extensively to remove excess dye and resuspended in fresh imaging media. Jurkat cells expressing CD19 CAR and GrB-mCherry were resuspended to 2x 10^4 cells/25 µL and added to each well immediately prior to imaging with a C2+ confocal microscope (Nikon, Melville, NY).

Retrovirus Production and Retroviral Transduction. HEK293T cells were seeded at 6.5 x 10^6 cells/10 mL/dish in 10-cm tissue-culture dishes and culture medium was replaced with fresh DMEM plus 10% HI-FBS immediately before transfection with 3.8 µg retroviral construct, 3.8 µg pHIT60, and 2.4 µg RD114 using linear PEI. Sixteen hours post-transfection, cells were washed with 10 mL of phosphate buffered saline (PBS) and cultured in DMEM plus 10% HI-FBS, 20 mM HEPES, and 10 mM sodium butyrate for 8 hours before media change to DMEM plus 10% HI-FBS and 20 mM HEPES (no sodium butyrate). Viral supernatants were harvested on each of the two subsequent days post-media change, and filtered through a 0.45-µm low–protein-binding filter immediately prior to transduction of primary human T cells. At 48 and 72 hours post-isolation, T cells (1 x 10^6) were transduced with 1.8 mL of fresh retroviral supernatant supplemented with 5 µg/mL polybrene (Sigma-Aldrich, St. Louis, MO) via spinfection at 800 *x g* for 90 min at 32°C. Immediately following each spinfection, 1.8 mL of transduction supernatant was replaced with 1.8 mL of fresh T-cell media.

TIDE Analysis. Genomic DNA was harvested via the Qiagen DNeasy Blood & Tissue kit, according to manufacturer's instructions. Oligos flanking the CRISPR/Cas9 cut site were used to PCR amplify a ~900 bp fragment for Sanger sequencing (Retrogen, San Diego, CA). Chromatograms were subsequently uploaded to the TIDE calculator web tool (www.tide.deskgen.com) for % indel analysis with the following parameters: left boundary, 200; decomposition window, 300-500; indel size range, 50.

Flow-based Lysis Assay. OKT3$^+$ TM-LCLs were pre-labeled with 1 μM carboxyfluorescein succinimidyl ester (CFSE, Life Technologies), according to manufacturer's instructions, while primary human CD8$^+$ T cells were pre-treated with z-AAD-CMK or DMSO at 2x the indicated concentrations for 1 hour at room temperature. CFSE-labeled OKT3$^+$ TM-LCLs were seeded at 5 x 10^3 cells/well in a 96-well U-bottom plate and co-incubated with primary human CD8$^+$ T cells at 1:1, 5:1, or 25:1 E:T ratio in RPMI-1640 without Phenol Red. After 4 hours, the number of surviving CFSE-labeled target cells was quantified via data acquisition a MACSQuant VYB flow cytometer (Miltenyi Biotec). Compensation and data analysis were performed using FlowJo Data Analysis software. % specific lysis was calculated as $100 \times \frac{(\text{surviving target cells in experimental sample})}{(\text{surviving target cells in target–only controls})}$.

Cytotoxicity Assay. OKT3$^+$ or parental TM-LCLs were seeded at 1 x 10^4 cells/well in a 96-well V-bottom plate and co-incubated with CRISPR/Cas9 RNP-treated or mock primary human CD8$^+$ T cells at 1:1, 3:1, or 10:1 E:T ratio in RPMI without Phenol Red. After 4 hours, supernatant was harvested and lactate dehydrogenase (LDH) release was quantified via the CytoTox96 NonRadioactive Cytotoxicity Assay kit (Promega, Madison, WI), according to manufacturer's instructions. Absorbance at 590 nm was measured on an EONC microplate reader (BioTek), and % cytotoxicity was calculated as $\%\ \text{cytotoxicity} = 100 \times \frac{(\text{experimental} - \text{effector spontaneous} - \text{target spontaneous})}{(\text{target maximum} - \text{target spontaneous})}$, where the spontaneous and maximum LDH release were determined from effector–only or target–only samples, and samples treated with kit lysis buffer, respectively.

Repeated Antigen Challenge Assay. OKT3$^+$ or parental TM-LCLs previously engineered to stably express an EGFP-firefly luciferase (ffluc) fusion protein were seeded at 1 x 10^5 cells/well in a 48-well plate and co-incubated with CRISPR/Cas9 RNP-treated or mock primary human CD8$^+$ T cells at 1:1 E:T ratio in complete T-cell media. Media color and culture density were routinely evaluated, and if necessary, half-media changes were performed to mitigate nutrient inhibition.

Every 48 hours, 50 µL was harvested from resuspended samples to quantify the number of surviving EGFP$^+$ target cells and EGFP$^-$ T cells. Following sample harvest, 1 x 10^5 fresh target cells were added to each culture. In the event of substantial T-cell expansion, cultures were re-seeded at 1 x 10^5 T cells/well, and the dilution ratio was factored into the analysis for total cell counts at each subsequent time point. Target-cell fold-survival and T-cell fold-expansion are normalized to the number of cells seeded at the time of the 1st challenge.

T-cell proliferation assay. CRISPR/Cas9 RNP-treated or mock primary human CD8$^+$ T cells were pre-labeled with 5 µM of CellTrace Violet (CTV, Life Technologies), according to manufacturer's instructions. EGFP-ffluc$^+$ OKT3$^+$ or EGFP-ffluc$^+$ parental TM-LCLs were seeded at 5 x 10^4 cells/well in a 96-well U-bottom plate and co-incubated with CTV-labeled primary human CD8$^+$ T cells at 1:1 E:T ratio in complete T-cell media. Samples were resuspended to quantify CTV dilution in EGFP$^-$ T cells via flow cytometry at 3 and 5 days, with data acquisition on a MACSQuant VYB flow cytometer (Miltenyi Biotec). Compensation and data analysis were performed using FlowJo Data Analysis software (TreeStar, Ashland, OR). The MFI CTV for each sample was normalized to the initial MFI CTV of each T-cell sample on Day 0.

ELISA. OKT3$^+$ or parental TM-LCLs were seeded at 1 x 10^4 cells/well in a 96-well U-bottom plate and co-incubated with CRISPR/Cas9 RNP-treated or mock primary human CD8$^+$ T cells at 1:1, E:T ratio in complete T-cell media. At 24 hours, 150 µL of supernatant (out of 200 µL culture volume) was harvested into a separate 96-well U-bottom plate and spun at 300 x g for 2 min. 125 µL of supernatant was subsequently transferred to a new 96-well U-bottom plate and sealed with parafilm for storage at -80°C prior to sample analysis with Human IL-2 and human IFN-γ ELISA MAX^{TM} Deluxe kits (Biolegend) according to manufacturer's instructions. Absorbance at 450 nm and 570 nm were measured on an EONC microplate reader (BioTek), and the concentration of

secreted cytokine was determined according to the standard curve generated from cytokine standards provided in the kit.

Statistics. Statistical significance was determined via two-tailed, homoscedastic Student's *t*-test with a *p*-value cutoff of 5E-2.

RESULTS

Engineered GrB-based molecules are mechanistically compatible with lytic granule storage and delivery

Wild-type GrB is a highly versatile cytotoxic effector protein that rapidly triggers apoptosis by initiating multiple caspase-dependent and caspase-independent cytolytic cascades. Therefore, as is the case for endogenous GrB, an important COVERT design consideration is the strict requirement to avert cytotoxic activity within host T cells. The native GrB pre-pro leader sequence encodes localization signals and autoinhibitory mechanisms that work in concert to restrain GrB activity from the time of protein expression to the time of lytic granule release. First, the pre-sequence directs translocation to the endoplasmic reticulum, where its removal releases the pro-GrB zymogen to continue trafficking through the secretory pathway. Upon packaging into T-cell lytic granules, the inactivating pro-peptide is then cleaved off by dipeptidyl peptidase I (CatC), thus freeing the new N-terminal Ile16 residue to form an interior salt bridge with Asp226 and stabilize the substrate-binding cleft in its mature conformation. We first verified that the endogenous Gly-Glu pro-peptide would prevent premature activation of recombinant GrB-based molecules by transfecting HEK293T cells to transiently express either recombinant full-length GrB or a mature GrB construct lacking the inhibitory pro-peptide (Δpro-GrB) (Figure 2.1a). Since HEK293T cells lack lytic granules, GrB expression is not sequestered within specialized storage compartments and transfected cells are subject to the effects of cytoplasmic GrB exposure. GrB

activity was detected in lysates harvested from cells expressing Δpro-GrB, but not full-length GrB, as determined by cleavage of a chromogenic Ac-IEPD-pNA tetrapeptide substrate (Figure 2.1b). As anticipated, HEK293T cells transfected to express Δpro-GrB suffered a significant loss of viability relative to samples expressing full-length GrB (Figure 2.1c), demonstrating the protective function of the Gly-Glu pro-peptide. Interestingly, exchange of the GrB pre-sequence with the murine IgG,κ pre-sequence, which directs protein secretion out of the cell, resulted in similar levels of cytotoxicity (IgG,κ s.s.-Δpro-GrB in Figure 2.S1, Supplementary Information), indicating that transient exposure may be sufficient to initiate apoptosis.

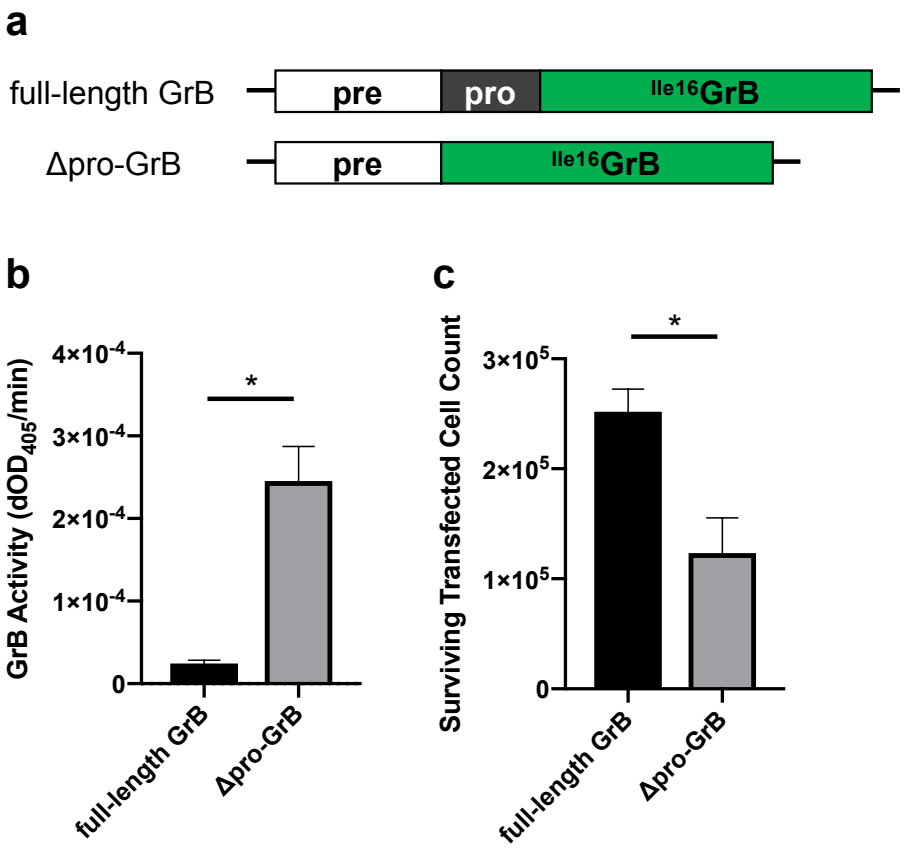

Figure 2.1. The GrB pro-peptide inhibits GrB activity and prevents premature activation in transiently transfected HEK293T human cells. (a) Full-length GrB and Δpro-GrB DNA constructs are shown with pre and pro leader sequences annotated. Cleavage of the pre-peptide from the Δpro-GrB construct is sufficient to expose a new N-terminal Ile16 residue, which enables GrB to undergo a conformational change that results in GrB activation. (b) Lysates were harvested from

HEK293T cells transiently transfected to express full-length GrB and Δpro-GrB, and GrB activities against an Ac-IEPD-pNA substrate were quantified by the rate of increase in absorbance at 405 nm. (c) Transiently transfected HEK293T cells were trypsinized and stained with a 7-aminoactinomycin D (7-AAD) viability dye prior to counting the number of surviving cells via flow cytometry. All values indicate the mean of triplicate samples and error bars represent ±1 s.d. *p < 5E-2.

Since lytic granules are T-cell– and NK-cell–specific secretory organelles, we were unable to verify proper packaging of recombinant GrB in HEK293T cells. To confirm that the GrB pre-pro leader sequence would allow engineered GrB-based molecules to interface with endogenous packaging mechanisms, recombinant full-length GrB was fused to a fluorescent mCherry tag via a short peptide linker and transiently expressed in human Jurkat T cells. Confocal microscopy images revealed a punctate distribution of GrB-mCherry throughout the cytoplasm, a pattern consistent with granular sequestration (Figure 2.2a). To further verify that packaged COVERT switches would be efficiently trafficked in response to antigen stimulation, we nucleofected Jurkat T cells to co-express a CD19 CAR and the GrB-mCherry fusion, and subsequently co-incubated the Jurkat cells with Raji target cells that naturally express CD19 antigen. Time-lapse images show that GrB-mCherry is initially present in dispersed lytic granules within the Jurkat cell prior to target-cell contact, and that the granules rapidly traffic to the immunological synapse following target-cell conjugation (Figure 2.2b). In a subsequent experiment, Jurkat T cells expressing CD19 CAR and GrB-mCherry were pre-loaded with the calcium indicator Fluo-4, and activated Jurkat cells, identified by Fluo-4 signals, exhibited high levels of sustained GrB-mCherry polarization consistent with lytic granule release[39] (Figure 2.2c). These images demonstrate that recombinant GrB-based molecules can be engineered to interface with the same storage compartments and trafficking mechanisms that human T cells utilize to deploy wild-type GrB.

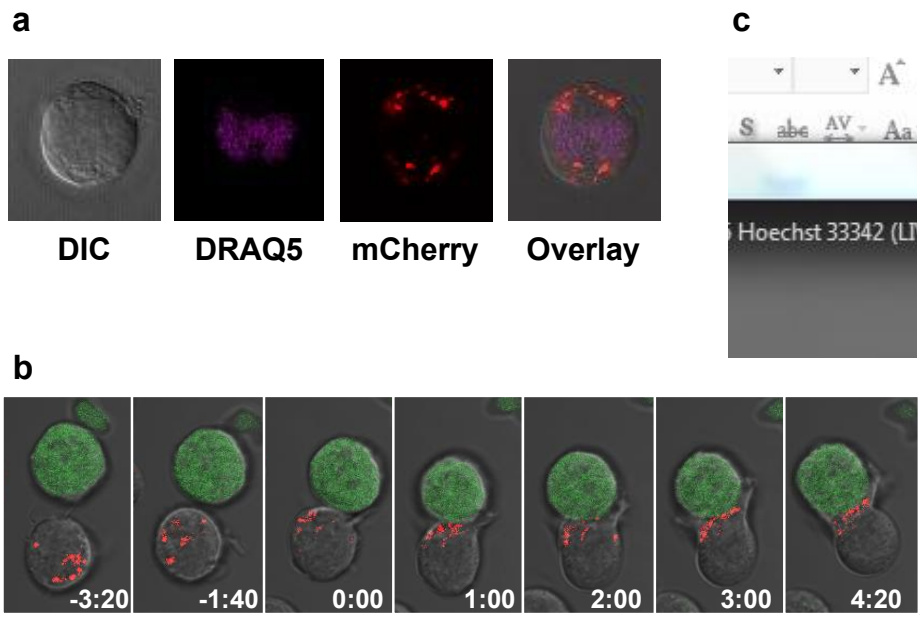

Figure 2.2. Engineered GrB-mCherry molecules are efficiently expressed, packaged into lytic granules, and trafficked to the immunological synapse by human T cells. (a) Jurkat T cells nucleofected to express a GrB-mCherry fusion (red) and stained with the nuclear dye DRAQ5 (purple) display a punctate and cytoplasmic distribution of GrB-mCherry, consistent with the packaging and storage of wild-type GrB in lytic granules. (b) Time-lapse confocal microscopy of Jurkat T cells co-expressing a CD19 CAR and GrB-mCherry (red) reveals rapid movement of GrB-mCherry to the immunological synapse upon encounter with Raji target cells (green) that naturally expresses CD19. Time signatures indicate minutes:seconds, with 0:00 set to the time of initial cell-cell contact. (c) Jurkat T cells co-expressing CD19 CAR and GrB-mCherry (red) were pre-loaded with the calcium indicator Fluo-4 and co-incubated with CD19+ Raji cells pre-labeled by Hoechst 33342 staining (blue). Fluo-4 signal (green) indicates T-cell activation triggered by target-cell engagement, which was accompanied by rapid and sustained GrB-mCherry polarization to the immunological synapse in preparation for directional release toward the target cell.

However, despite clear visuals of granule trafficking to the immunological synapse, no GrB-mCherry signal was detected within target cells by confocal microscopy, possibly because the absence of Pfn expression by Jurkat T cells precluded efficient delivery of lytic granule contents into target cells. In contrast to Jurkat T cells, activated human $CD8^+$ T cells naturally express ample amounts of Pfn, which is degranulated alongside GrB, and facilitates GrB entry into the target-cell cytoplasm[40]. To verify the transfer of recombinant GrB-based molecules from T cells into target cells, we first transduced primary human $CD8^+$ T cells with a retroviral construct encoding a CD19 CAR and GrB-mCherry. The transduced cells were then co-incubated with

CD19^{+} Raji target cells and analyzed by flow cytometry. We observed a significant increase in the percentage of CD19^{+}/mCherry^{+} target cells (Figure 2.3a,b), as well as a concurrent reduction in the mCherry MFI of the T cells following co-incubation (Figure 2.3c,d), indicating successful GrB-mCherry release by T cells and uptake by target cells. Together, these results confirm the ability of T cells to produce, package, and deliver engineered GrB-based molecules, and demonstrate the mechanistic compatibility of the proposed COVERT platform with existing surface-receptor technologies for adoptive T-cell therapy.

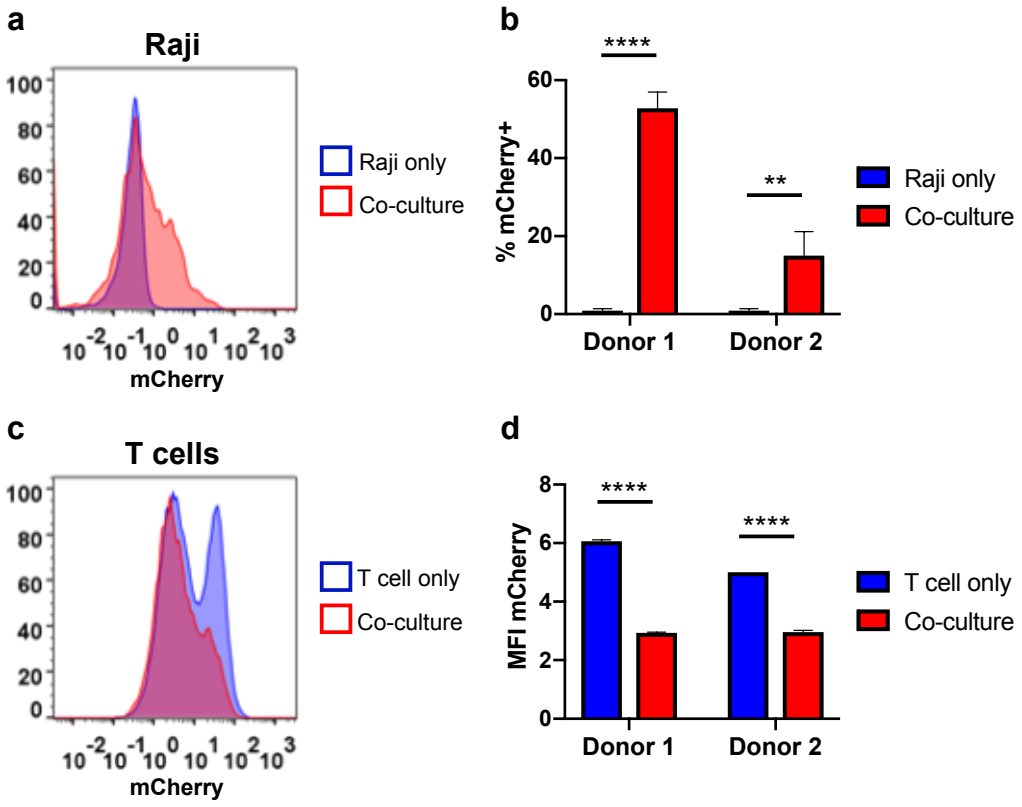

Figure 2.3. CD19 CAR-T cells successfully delivered engineered GrB-mCherry molecules into CD19-expressing Raji target cells. Primary human CD8+ T cells from two healthy donors were retrovirally transduced to co-express a CD19 CAR and GrB-mCherry, and then co-incubated with CD19+ Raji at 3:1 effector:target ratio. Prior to resuspension and analysis via flow cytometry, samples were stained for CD8 and CD19 to distinguish singlet T cells and target cells from T-cell/target-cell conjugates. (a) GrB-mCherry uptake was detected in CD19+/CD8- gated Raji target cells following co-incubation with CD19 CAR-T cells. (b) % mCherry+ of co-cultured Raji cells was calculated by Overton histogram subtraction, with Raji cells cultured in the absence of T cells serving as the reference. (c,d) Degranulation of GrB-mCherry was reflected in a decrease

in median mCherry intensity in CD8+/CD19- gated T cells following co-incubation with Raji target cells. Representative data from one of two primary human T-cell donors are shown. T-cell–only samples were assayed in duplicate and error bars represent the range. All other values indicate the mean of triplicate samples and error bars represent ±1 s.d. ** p < 5E-3; **** p < 5E-5.

GrB activity is strongly correlated with the lytic potential of human CTLs

In addition to safe storage in T cells and efficient delivery into target cells, COVERT switches must be sufficiently cytotoxic in the ON-state to trigger target-cell apoptosis. Although mature GrB is a potent toxin when artificially overexpressed by HEK293T cells, GrB is only one of several effector protein payloads deployed by CTLs to mediate target-cell lysis. To investigate the relative cytotoxic contribution of wild-type human GrB to T-cell–mediated cytotoxicity, we evaluated the lytic activity of primary human $CD8^+$ T cells in the presence or absence of the cell-permeable, GrB-specific suicide-inhibitor, z-Ala-Ala-Asp-chloromethylketone (z-AAD-CMK) (Figure 2.4a). Since peripheral human CTLs isolated from healthy donor blood are polyclonal in TCR expression and antigen-specificity, we co-incubated the T cells with TM-LCL tumor cells previously engineered to express surface-bound OKT3, an anti-CD3 protein that enables T-cell recognition via any endogenous TCR complex. As expected, target-cell survival was reduced at all tested effector:target (E:T) ratios in the absence of the GrB inhibitor (Figure 2.4b). However, pre-treatment of the CTLs with 300 μM z-AAD-CMK resulted in complete inhibition of target-cell lysis at 1:1 E:T ratio in a 4-hour lysis assay, indicating that suppression of GrB activity is sufficient to dramatically inhibit T-cell–mediated cytotoxicity. Target-cell lysis was gradually restored at higher E:T ratios, possibly due the dilution of available z-AAD-CMK molecules across an increased number of T cells. To verify that the inhibition of target-cell lysis resulted from the loss of GrB activity, we harvested lysates from activated primary human $CD8^+$ T cells and quantified the GrB activity remaining after a 1-hour co-incubation with increasing concentrations of z-AAD-CMK (Figure 2.4c). At 10 μg of input lysate, corresponding to the number of T cells co-incubated in the lysis assay at 25:1 E:T ratio, 300 μM of z-AAD-CMK resulted in a 44.7% reduction in GrB activity (Figure 2.4c). Yet, despite inhibition of nearly half of the GrB activity available for mediating

cytotoxicity against target cells, the substantial recovery of lytic potential at 25:1 E:T ratio suggests that near-complete disruption of endogenous GrB may be necessary to allow for COVERT regulation over T-cell–mediated cytotoxicity (Figure 2.4b).

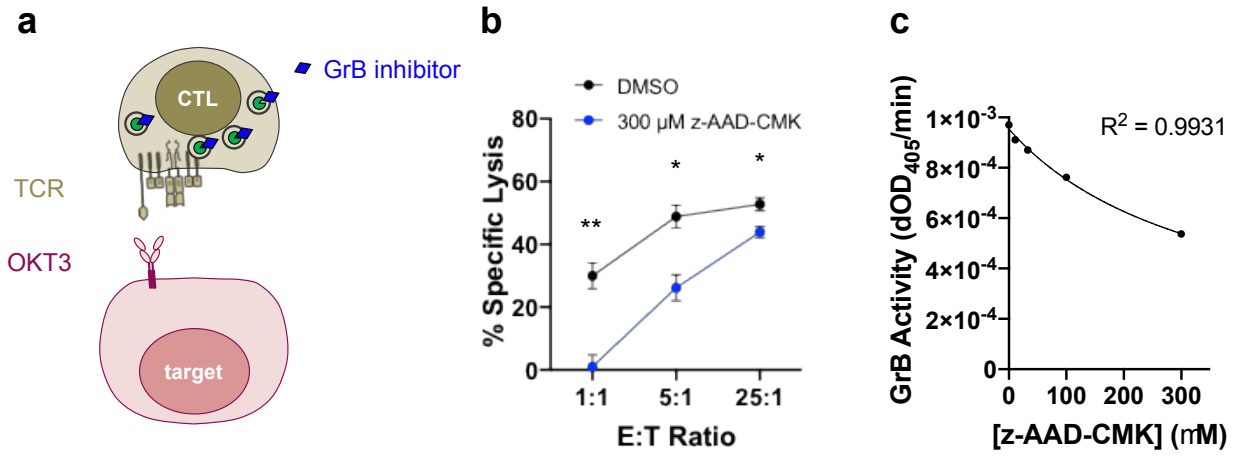

Figure 2.4. Chemical inhibition of GrB activity dramatically reduces human CTL-mediated lysis of OKT3-expressing TM-LCL target cells. (a) CTLs target OKT3$^+$ TM-LCLs via CD3 chains in endogenous TCR complexes. Addition of cell-permeable z-AAD-CMK inhibits GrB activity by irreversibly binding to the GrB active site. (b) The % specific lysis of CFSE dye-labeled OKT3$^+$ TM-LCLs was quantified via flow cytometry following a 4-hour co-incubation with primary human CD8$^+$ T cells pre-treated with 300 μM z-AAD-CMK or DMSO as a negative control. E:T ratios were adjusted by scaling up the T-cell input for a fixed number of 5 x 10^3 target cells. (c) Lysates were harvested from 1.25 x 10^5 activated primary human CD8$^+$ T cells and co-incubated with z-AAD-CMK over a range of inhibitor concentrations for 1 hour to allow GrB inhibition to reach equilibrium. The remaining GrB activity was quantified by the rate of increase in absorbance at 405 nm upon addition of the Ac-IEPD-pNA chromogenic substrate. A non-linear regression curve was fit to the data, and extrapolation indicates an IC_{50} of 348.7 μM z-AAD-CMK. Representative data from one of three primary human T-cell donors are shown. All plotted data points indicate the mean of triplicate samples and error bars represent ±1 s.d. *p < 5E-2; **p < 5E-3.

GrB knockout is sufficient to significantly disrupt the lytic potential of human CTLs

Having validated the central role of endogenous human GrB in T-cell–mediated cytotoxicity, we rationalized that the disruption of wild-type GrB expression alone could potentially sufficiently reduce the lytic potential of CTLs to allow COVERT switches to regulate target-cell lysis. Therefore, we nucleofected primary human CD8$^+$ T cells with CRISPR/Cas9 ribonucleoprotein (RNP) complexes targeting exon 4 of the GrB locus. While it is often preferable

to direct nuclease activity against target sequences in earlier exons, a high degree of DNA sequence homology between endogenous human GrB and other human genes prohibited the design of efficient sgRNAs that target earlier coding regions of the GrB locus. However, the selected cleavage site in exon 4 splits the Ser195 residue encoded in exon 5 from the rest of the catalytic triad, effectively abolishing GrB activity (Figure 2.5a). The efficiency of indel generation in nucleofected CTL samples was approximated via Tracking of Indels by DEcomposition (TIDE) analysis[41], with frame-shifting mutations observed at 80-85% of endogenous GrB loci 4 days following RNP treatment (Figure 2.5b). Seeing as GrB-deficient human T cells have not been described in the medical record, these GrB RNP-treated cells afforded us the first known opportunity to assess whether GrB expression may directly or indirectly impact human T-cell viability or proliferation. Through two weeks in *in vitro* culture, no proliferative defects were observed in CTLs treated with GrB-targeted CRISPR/Cas9 RNPs, and the percentage of GrB loci featuring indels remained unchanged, indicating that GrB expression is not essential for T-cell survival (Figure 2.5b).

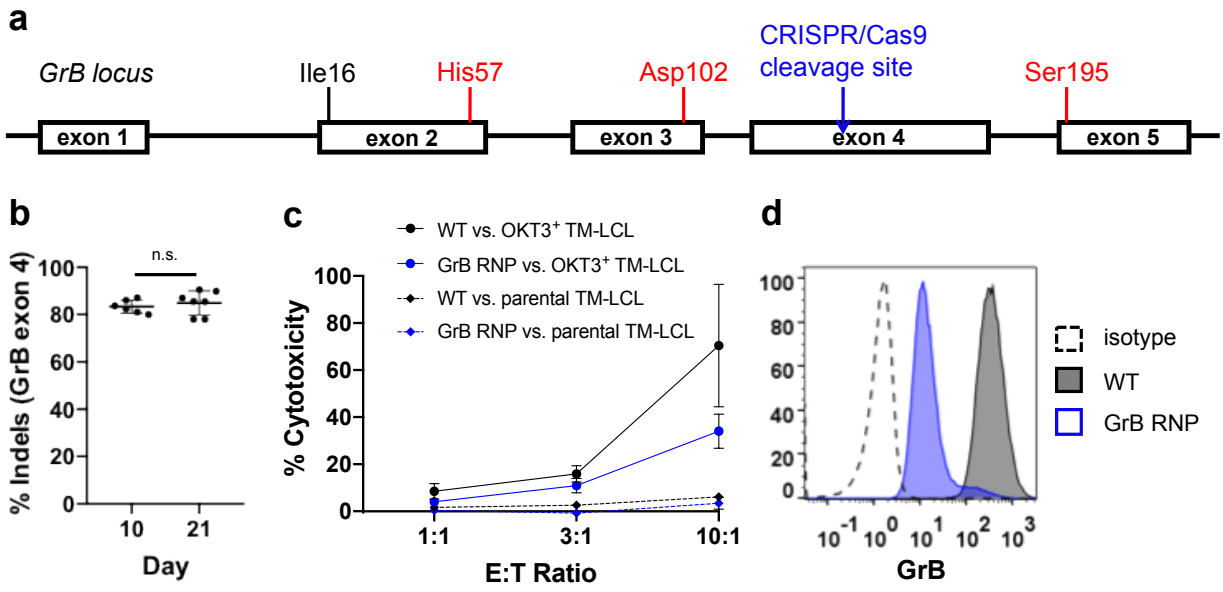

Figure 2.5. Targeted genetic disruption of endogenous GrB expression does not significantly reduce T-cell–mediated cytotoxicity nor intracellular GrB protein levels. (a,b) The human GrB locus consists of 5 exons, with the residues forming the catalytic triad (red) split among exons 2, 3, and 5. A CRISPR/Cas9 sgRNA targeting exon 4 induced frame-shifting indels at 80-85% of GrB loci in genomic DNA samples harvested from RNP-nucleofected primary human CD8 T cells. Each plotted data point in (b) represents the % indels at the GrB locus for a different primary human T-cell donor. Genomic DNA samples were harvested on Day 10 and Day 21, 7 and 18 days post-RNP nucleofection, respectively. (c) GrB RNP-treated T cells were co-incubated with OKT3-expressing TM-LCLs or "off-target" parental TM-LCLs at 1:1, 3:1, and 10:1 E:T ratio for 4 hours prior to harvesting supernatants for quantification of lactate dehydrogenase (LDH) release from membrane-compromised cells via the Promega CytoTox96® cytotoxicity assay. The % cytotoxicity was calculated from the absorbance at 490 nm using the formula: % cytotoxicity = $100 \times \frac{(\text{experimental} - \text{effector spontaneous} - \text{target spontaneous})}{(\text{target maximum} - \text{target spontaneous})}$. Each plotted data point indicates the mean of triplicate samples and error bars represent ±1 s.d. (d) Intracellular GrB protein levels of GrB RNP-treated and untreated WT primary human $CD8^+$ T cells were assessed via immunofluorescence flow cytometry on Day 10, 7 days following RNP treatment.

Since the chemical inhibition of GrB was sufficient to completely abrogate target-cell lysis at low E:T ratios, we anticipated that GrB knockout CTLs would exhibit a similar inability to lyse OKT3-expressing TM-LCL target cells. Surprisingly, RNP-treated primary human $CD8^+$ T cells retained strong lytic potential during a 4-hour cytotoxicity assay, despite the high percentage of indels at GrB loci (Figure 2.5c). Furthermore, nearly the entire RNP-treated T-cell population remained GrB^+ by immunofluorescent intracellular staining (Figure 2.5d). Although initially puzzling, we rationalized that unlike cell-surface proteins, wild-type GrB is stored in long-lived lytic granules, and therefore, proteins sequestered within the lytic granule compartment may not undergo a rapid rate of turnover. As a result, even though CRISPR/Cas9-mediated knockout disables further GrB production, any GrB mRNA and protein already present prior to RNP delivery could contribute to a pre-existing stockpile of GrB (Figure 2.6a). Indeed, GrB expression is very strongly upregulated during the three days of CD3/CD28 stimulation required to activate T cells for efficient RNP nucleofection, and even in untreated, wild-type CTLs, GrB protein levels remain elevated for several days after the stimulus has been removed (Figure 2.6b).

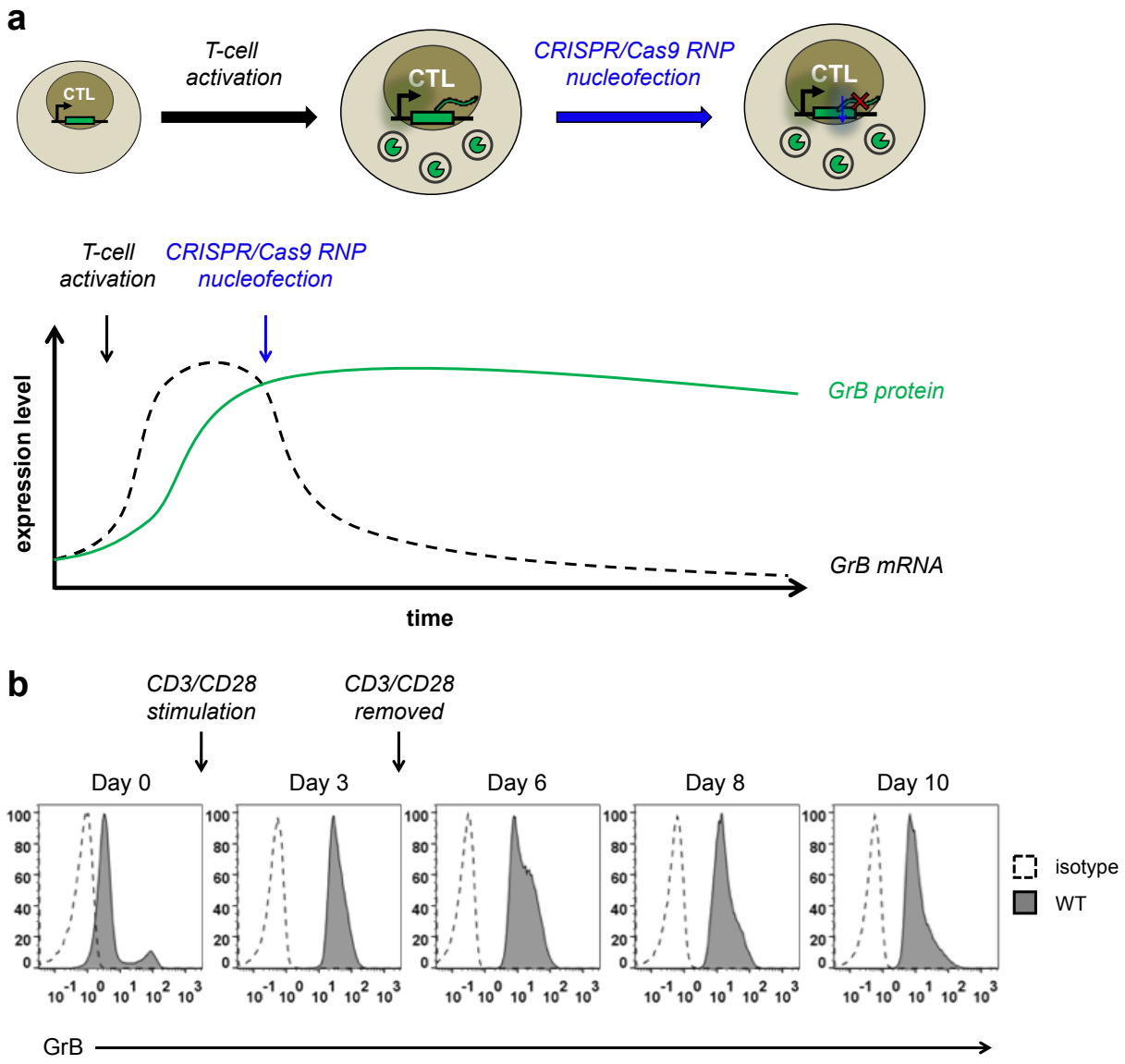

Figure 2.6. Intracellular GrB protein levels remain high in the absence of fresh protein production. (a) Schematic illustrating the observed CTL phenotype in response to CRISPR/Cas9 RNP-mediated disruption of the GrB locus. T-cell activation triggers rapid upregulation of GrB mRNA transcript (dashed black line) and protein (solid green line) levels. Since wild-type GrB is stably stored within the lytic granule compartment, the natural rate of GrB protein turnover may be relatively slow, and although the delivery of GrB-targeting CRISPR/Cas9 RNPs can quickly attenuate the future production of GrB-encoding mRNA transcripts, genetic disruption of the GrB locus does not impact the already translated GrB protein sequestered within T-cell lytic granules. (b) Freshly isolated primary human $CD8^+$ T cells were activated with Dynabeads® Human T-activator CD3/CD28 at 1:1 cell:bead ratio. After 72 hours, the CD3/CD28 stimulus was removed and intracellular GrB expression was assessed every 2-3 days. Intracellular immunofluorescence staining revealed a very gradually receding level of GrB protein expression despite the absence of subsequent antigen stimulation. Flow cytometry histograms show the GrB expression profile from different representative primary human T-cell donors at each time point.

We reasoned that there are two ways for the eventual depletion of pre-existing GrB stores to occur: (1) cell division, thereby diluting the GrB content between two daughter cells, and (2) degranulation. Since T-cell proliferation and lytic granule secretion are both triggered by antigen-stimulation, we set up an extended co-incubation between GrB RNP-treated primary human $CD8^+$ T cells and OKT3-expressing TM-LCLs, and subsequently challenged the T cells with fresh target cells every two days (Figure 2.7a). Following the expected initial target-cell lysis during the first challenge, the GrB RNP-treated T cells rapidly lost the ability to control tumor outgrowth (Figure 2.7b), strongly suggesting that the depletion of and inability to replenish GrB stores is sufficient to significantly disrupt the lytic potential of human CTLs. Importantly, untreated wild-type T cells continued to efficiently clear co-cultured $OKT3^+$ target cells through 4 rounds of target-cell addition and maintained a high level of GrB expression (Figure 2.7c). In contrast, GrB expression was noticeably absent from RNP-treated T cells by the end of the fourth challenge (Figure 2.7c), an observation that further supports the critical importance of human GrB to T-cell mediated cytotoxicity. Interestingly, other slower-acting cytotoxic payloads and mechanisms failed to compensate for the loss of GrB, despite the prolonged interaction between T cells and target cells. Although the lengthy duration of antigen exposure may raise concerns regarding an increased risk of T-cell exhaustion, the RNP-treated T cells also continued to expand at a similar rate to wild-type T cells throughout four repeat target-cell challenges (Figure 2.7d), consistent with the earlier observation that GrB knockout does not appear to convey a substantial growth disadvantage.

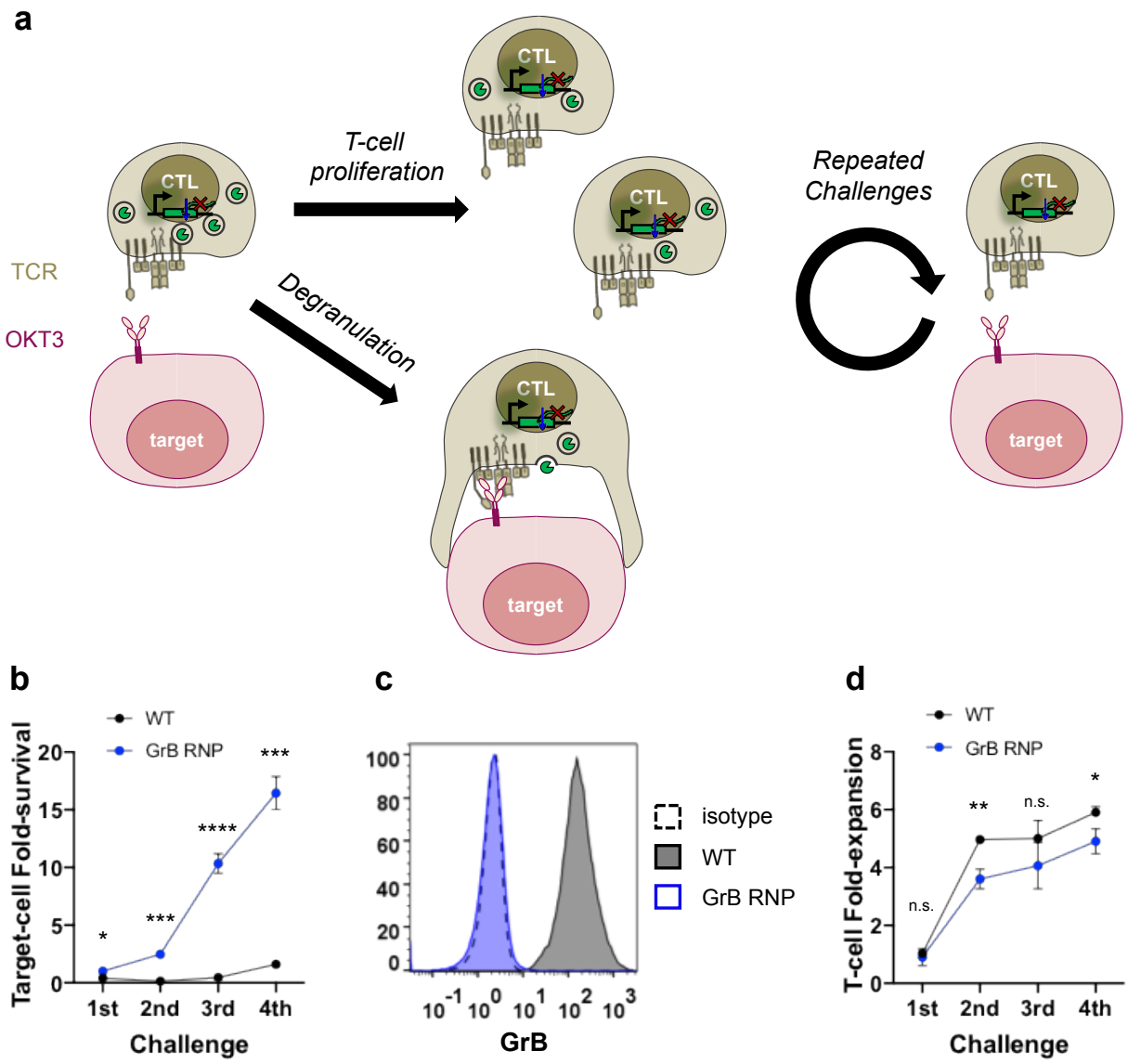

Figure 2.7. Repeated antigen stimulation depletes the pre-existing intracellular GrB stockpiles and cytolytic potential of GrB RNP-treated CTLs. (a) Repeated challenges by target cell addition results in the eventual depletion of intracellular GrB from GrB RNP-treated primary human $CD8^+$ T cells due to the degranulation of pre-existing lytic granule stores, as well as dilution between daughter cells during activation-induced proliferation. (b) Target-cell survival was quantified by flow cytometry every 2 days prior to re-challenge with fresh $OKT3^+$ target cells. (c) Intracellular GrB protein levels were evaluated 2 days following the 4^{th} challenge by immunofluorescence flow cytometry. (d) T-cell expansion was tracked via flow cytometry every 2 days prior to re-challenge with fresh $OKT3^+$ target cells. Representative data from one of two primary human T-cell donors are shown. All plotted data points indicate the mean of triplicate samples and error bars represent ±1 s.d. *p < 5E-2; **p < 5E-3, ***p < 5E-4; ****p < 5E-5.

GrB knockout does not hinder non-cytotoxic T-cell effector functions

Antigen stimulation signals peripheral CTLs to rapidly transition from a naïve phenotype to an activated cell state, initiating an entire suite of T-cell programs that include T-cell proliferation, inflammatory cytokine production, cytotoxic payload armament, and effector differentiation. Since the abilities of activated T cells to clonally replicate and secrete immunostimulatory cytokines are crucial elements for a robust immune response, it is important to verify that the loss of GrB expression does not directly hinder these non-cytotoxic effector functions. To evaluate the proliferative capacity of GrB knockout CTLs, we dye-labeled RNP-treated or mock-nucleofected primary human $CD8^+$ T cells with CellTrace Violet (CTV) and co-incubated the T cells with either $OKT3^+$ TM-LCLs or off-target, wild-type TM-LCLs. Recognition of OKT3 by the endogenous TCR stimulates T-cell division, resulting in an approximately even distribution of CTV between daughter cells. In this manner, the CTV signal intensity remaining within each cell corresponds to the number of generations between that cell and its ancestral parent. While minimal CTV dilution was observed in T-cell populations challenged with off-target cells, OKT3 stimulation induced strong T-cell division by both RNP-treated and wild-type T cells (Figure 2.8a,b), demonstrating that GrB knockout T cells can survive and continue to proliferate through several cell generations. In accordance with retaining strong proliferative potential, RNP-treated T cells secreted the T-cell proliferation-inducing cytokine IL-2, as well as immunostimulatory IFN-γ, at levels similar to wild-type T cells still expressing endogenous GrB (Figure 2.8c,d).

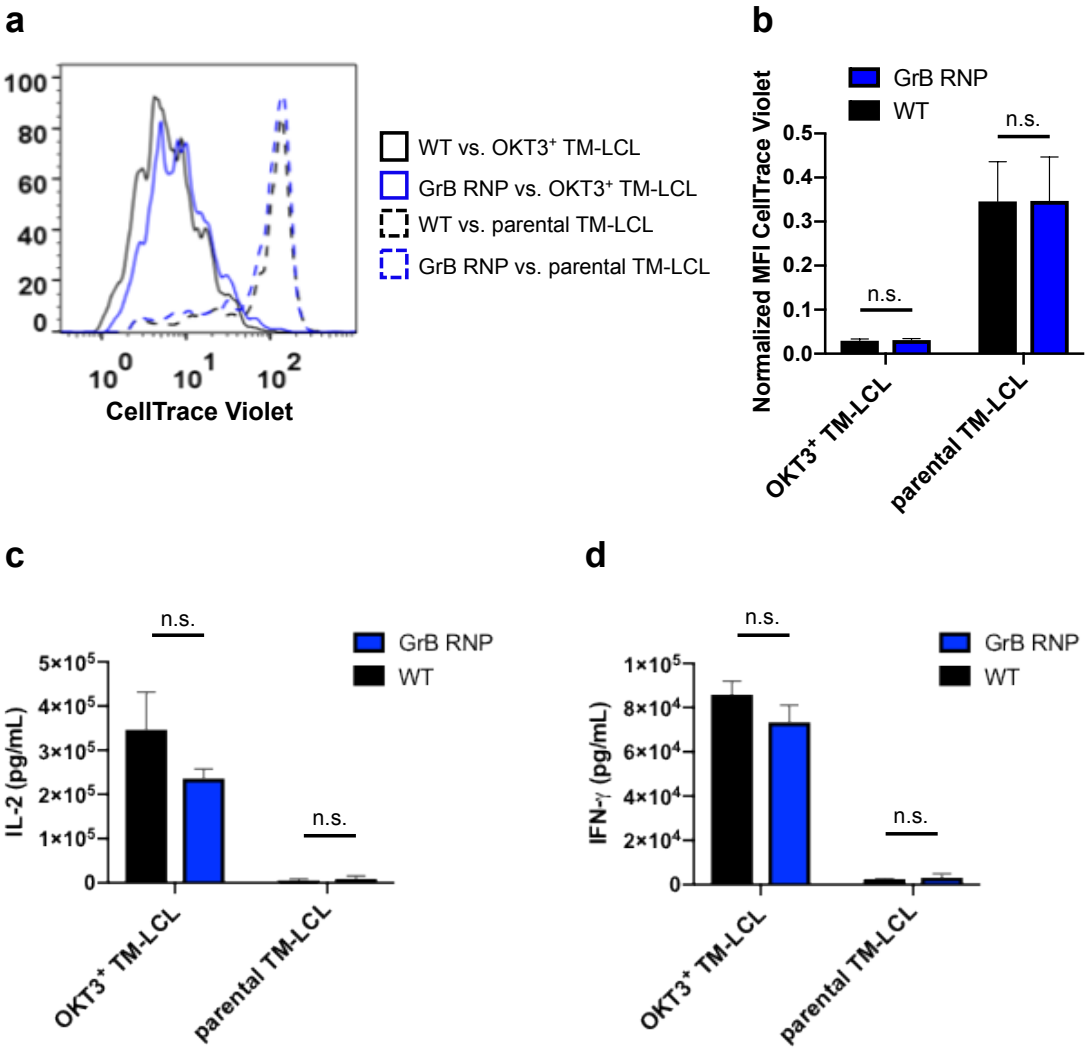

Figure 2.8. GrB RNP-treated primary human CD8$^+$ T cells retain non-cytotoxic effector functions. (a) CellTrace Violet (CTV) dye-labeled GrB RNP-treated or WT primary human CD8$^+$ T cells were co-incubated with OKT3$^+$ or parental TM-LCL target cells and T-cell proliferation was evaluated after 5 days via flow cytometry. Cell division results in the distribution of CTV between daughter cells, resulting in diminished CTV signals. (b) MFI CTV quantification of the results in (a). (c,d) IL-2 and IFN-γ secretion by WT or GrB RNP-treated primary human CD8$^+$ T cells in response to antigen stimulation by OKT3$^+$ target cells were measured by sandwich ELISA. Background cytokine secretion was determined by co-incubating T cells with off-target parental TM-LCL target cells. Representative data from one of three primary human T-cell donors are shown. All plotted data points indicate the mean of triplicate samples and error bars represent ±1 s.d.

DISCUSSION

The frequent occurrence of 'on-target, off-tumor' toxicities resulting from misidentification of healthy tissues presents a fundamental limitation to the widespread implementation of adoptive T-cell therapy. In particular, receptor-mediated recognition of surface-bound antigens directs the delivery of potent cytolytic effector protein payloads across the immunological synapse from CTLs into target cells. Since these cytotoxic payloads are constitutively active, target-cell identification is carried out entirely by interactions at the cell surface. In lieu of tumor-exclusive surface markers, we devised a strategy to engineer synthetic protein switches, termed COVERT molecules, that can interrogate target cells for intracellular disease signatures prior to unleashing cytotoxicity. However, the cytotoxic mechanisms available to CTLs are diverse in mode and location of action, and the selection of a molecular chassis for COVERT switch development requires the careful consideration of key design parameters including (1) safe storage within T cells, (2) efficient delivery into the target-cell cytoplasm, and (3) the ability to induce target-cell apoptosis in the ON-state. In this study, we evaluated the biological properties and cytotoxic contribution of human GrB to T-cell–mediated cytotoxicity to determine whether human GrB is a suitable molecular chassis upon which to design disease-targeting COVERT molecules.

We demonstrated that the retention of the endogenous GrB pro-peptide effectively inhibits pre-mature GrB activation in ectopically transfected human cell lines, even without GrB sequestration into T-cell lytic granules. Recombinant human GrB constructs were also safely packaged into lytic granules upon expression by human Jurkat T cells, as well as primary human T cells, and efficiently trafficked to the immunological synapse in response to antigen stimulation. Similar to endogenous GrB, the ability of recombinant, fluorescently tagged GrB molecules to gain entry into the target-cell cytoplasm was dependent on the concurrent degranulation of Pfn, further validating our ability to engineer GrB-based payloads that can robustly interface with host storage, trafficking, and delivery mechanisms naturally provided by the T cell.

The vast majority of our knowledge of GrB function has been heavily influenced by studies involving murine models. Although these foundational studies have been instrumental toward elucidating the broad role of GrB in CTL-mediated target-cell lysis, several genetic and biochemical differences in granzyme expression and function may preclude accurate extrapolation of findings with mouse T cells to human systems. Using a GrB-specific suicide inhibitor, we demonstrated that chemical inhibition of human GrB is sufficient to abrogate efficient target-cell lysis at low E:T ratios. In the same vein, dilution of the cell-permeable inhibitor across an increased number of effector T cells resulted in a sharp recovery of T-cell lytic potential, indicating that GrB is an extremely potent cytolytic effector. Since the successful implementation of COVERT regulation over T-cell–mediated cytotoxicity strictly requires the disablement of constitutively apoptosis-inducing payloads, our finding strongly suggests GrB expression would need to be knocked out from COVERT T cells.

However, due to the lack of reported GrB deficiency in human patients, it was previously unknown if human GrB may provide essential signal(s) for T-cell survival. We successfully knocked out GrB expression from primary human CTLs via CRISPR/Cas9 RNP nucleofection and developed a method to deplete any remaining intracellular GrB protein that was expressed prior to genetic disruption of the GrB locus. Primary human CTLs rapidly lost the ability to control target-cell outgrowth following GrB depletion, providing further evidence that human GrB may play a more central role in CTL-mediated cytotoxicity relative to its murine homolog. Furthermore, GrB RNP-treated T cells did not exhibit substantial defects in T-cell proliferation nor immunostimulatory cytokine secretion, indicating that genetic replacement of endogenous GrB with engineered COVERT payloads may serve as a viable strategy toward developing T-cell therapies that can selectively target cells on the basis of intracellular biomarker expression.

While the work presented in this chapter focused on the evaluation of human GrB as a molecular chassis for COVERT switch design, our observations also provide opportunities for foundational studies on human T-cell function. For example, we presented the first demonstration

of successful GrB knockout from human CTLs. Our GrB knockout model and the ability to apply CRISPR/Cas9 technology to knock out additional cytotoxic payloads individually or in combination may facilitate in-depth characterization of cytotoxic mechanisms or human granzyme biology, particularly the functional importance of lesser understood orphan granzymes. As greater clarity over the individual contributions of the CTL cytotoxic arsenal is achieved, we envision the robust engineering of COVERT-T cells to become a transformative step toward the design of adoptive T-cell therapies for a broader range of diseases.

ACKNOWLEDGEMENTS

The work described in this chapter was supported by the National Institutes of Health (5DP5OD012133; grant to YYC) and the National Science Foundation (1553767; grant to YYC). PH was supported by the Biotechnology Training in Biomedical Sciences and Engineering Program funded by the National Institutes of Health. We also thank Christopher Ede for optimizing the retroviral vectors used to generate the GrB-mCherry–expressing primary human T cells in the GrB trafficking and delivery studies, and Anya (Andy) Alag for performing the ELISA experiments.

REFERENCES

1. Porter, D. L., Levine, B. L., Kalos, M., Bagg, A. & June, C. H. Chimeric antigen receptor-modified T cells in chronic lymphoid leukemia. *N. Engl. J. Med.* **365,** 725–33 (2011).
2. Kalos, M. *et al.* T cells with chimeric antigen receptors have potent antitumor effects and can establish memory in patients with advanced leukemia. *Sci. Transl. Med.* **3,** 95ra73 (2011).
3. Kochenderfer, J. N. *et al.* Chemotherapy-Refractory Diffuse Large B-Cell Lymphoma and Indolent B-Cell Malignancies Can Be Effectively Treated With Autologous T Cells Expressing an Anti-CD19 Chimeric Antigen Receptor. *J Clin Oncol* **33,** 540–549 (2015).
4. Davila, M. L. *et al.* Efficacy and Toxicity Management of 19-28z CAR T Cell Therapy in B Cell Acute Lymphoblastic Leukemia. *Sci. Transl. Med.* **6,** 224ra225 (2014).
5. Maude, S. L. *et al.* Chimeric Antigen Receptor T Cells for Sustained Remissions in Leukemia. *N. Engl. J. Med.* **371,** 1507–1517 (2014).
6. Wang, X. *et al.* Phase 1 studies of central memory–derived CD19 CAR T–cell therapy following autologous HSCT in patients with B-cell NHL. *Blood* **127,** 2980–2990 (2016).
7. Sadelain, M., Brentjens, R. & Rivière, I. The basic principles of chimeric antigen receptor design. *Cancer Discov.* **3,** 388–98 (2013).
8. Kalos, M. & June, C. H. Adoptive T Cell Transfer for Cancer Immunotherapy in the Era of Synthetic Biology. *Immunity* **39,** 49–60 (2013).
9. Hinrichs, C. S. & Restifo, N. P. Reassessing target antigens for adoptive T-cell therapy. *Nat. Biotechnol.* **31,** 999–1008 (2013).
10. Rosenberg, S. A. Finding suitable targets is the major obstacle to cancer gene therapy. *Cancer Gene Ther.* **21,** 45–7 (2014).
11. Parkhurst, M. R. *et al.* T cells targeting carcinoembryonic antigen can mediate regression of metastatic colorectal cancer but induce severe transient colitis. *Mol. Ther.* **19,** 620–6 (2011).

12. Morgan, R. A. *et al.* Case report of a serious adverse event following the administration of T cells transduced with a chimeric antigen receptor recognizing ERBB2. *Mol. Ther.* **18,** 843–51 (2010).

13. Linette, G. P. *et al.* Cardiovascular toxicity and titin cross-reactivity of affinity-enhanced T cells in myeloma and melanoma. *Blood* **122,** 863–71 (2013).

14. Davies, H. *et al.* Mutations of the BRAF gene in human cancer. *Nature* **417,** 949–54 (2002).

15. Kranenburg, O. The KRAS oncogene: past, present, and future. *Biochim. Biophys. Acta* **1756,** 81–2 (2005).

16. Dang, C. V. MYC on the path to cancer. *Cell* **149,** 22–35 (2012).

17. Walczak, H. Death receptor-ligand systems in cancer, cell death, and inflammation. *Cold Spring Harb. Perspect. Biol.* **5,** a008698 (2013).

18. Trapani, J. A. & Smyth, M. J. Functional significance of the perforin/granzyme cell death pathway. *Nat. Rev. Immunol.* **2,** 735–47 (2002).

19. Froelich, C. J. *et al.* New Paradigm for Lymphocyte Granule-mediated Cytotoxicity. Target Cells Bind and Internalize Granzyme B, but an Endosomolytic Agent is Necessary for Cytosolic Delivery and Subsequent Apoptosis. *J. Biol. Chem.* **271,** 29073–29079 (1996).

20. Voskoboinik, I., Whisstock, J. C. & Trapani, J. A. Perforin and granzymes: function, dysfunction and human pathology. *Nat. Rev. Immunol.* **15,** 388–400 (2015).

21. Barry, M. *et al.* Granzyme B short-circuits the need for caspase 8 activity during granule-mediated cytotoxic T-lymphocyte killing by directly cleaving Bid. *Mol. Cell. Biol.* **20,** 3781–94 (2000).

22. Pinkoski, M. J., Heibein, J. A., Barry, M. & Bleackley, R. C. Nuclear translocation of granzyme B in target cell apoptosis. *Cell Death Differ.* **7,** 17–24 (2000).

23. Trapani, J. A. Granzymes: a family of lymphocyte granule serine proteases. *Genome*

Biol. **2,** REVIEWS3014 (2001).

24. Chowdhury, D. & Lieberman, J. Death by a thousand cuts: granzyme pathways of programmed cell death. *Annu. Rev. Immunol.* **26,** 389–420 (2008).
25. Simon, M. M. *et al.* In vitro- and ex vivo-derived cytolytic leukocytes from granzyme A x B double knockout mice are defective in granule-mediated apoptosis but not lysis of target cells. *J. Exp. Med.* **186,** 1781–6 (1997).
26. Ebnet, K. *et al.* Granzyme A-deficient mice retain potent cell-mediated cytotoxicity. *EMBO J.* **14,** 4230–9 (1995).
27. Heusel, J. W., Wesselschmidt, R. L., Shresta, S., Russell, J. H. & Ley, T. J. Cytotoxic lymphocytes require granzyme B for the rapid induction of DNA fragmentation and apoptosis in allogeneic target cells. *Cell* **76,** 977–87 (1994).
28. Mahrus, S. & Craik, C. S. Selective chemical functional probes of granzymes A and B reveal granzyme B is a major effector of natural killer cell-mediated lysis of target cells. *Chem. Biol.* **12,** 567–77 (2005).
29. Kaiserman, D. *et al.* The major human and mouse granzymes are structurally and functionally divergent. *J. Cell Biol.* **175,** 619–30 (2006).
30. Casciola-Rosen, L. *et al.* Mouse and human granzyme B have distinct tetrapeptide specificities and abilities to recruit the bid pathway. *J. Biol. Chem.* **282,** 4545–52 (2007).
31. Lieberman, J. Granzyme A activates another way to die. *Immunol. Rev.* **235,** 93–104 (2010).
32. Pham, C. T., MacIvor, D. M., Hug, B. A., Heusel, J. W. & Ley, T. J. Long-range disruption of gene expression by a selectable marker cassette. *Proc. Natl. Acad. Sci. U. S. A.* **93,** 13090–5 (1996).
33. Khanna, R. Tumour surveillance: missing peptides and MHC molecules. *Immunol. Cell Biol.* **76,** 20–6 (1998).
34. Bubeník, J. MHC class I down-regulation: tumour escape from immune surveillance? *Int.*

J. Oncol. **25,** 487–91 (2004).

35. Charles A Janeway, J., Travers, P., Walport, M. & Shlomchik, M. J. T-cell receptor gene rearrangement. (2001).

36. Yam, P. *et al.* Design of HIV Vectors for Efficient Gene Delivery into Human Hematopoietic Cells. *Mol. Ther.* **5,** 479–484 (2002).

37. Zah, E., Lin, M.-Y., Silva-Benedict, A., Jensen, M. C. & Chen, Y. Y. T cells expressing CD19/CD20 bi-specific chimeric antigen receptors prevent antigen escape by malignant B cells. *Cancer Immunol. Res.* **4,** 498–508 (2016).

38. Ewen, C. *et al.* A novel cytotoxicity assay to evaluate antigen-specific CTL responses using a colorimetric substrate for Granzyme B. *J. Immunol. Methods* **276,** 89–101 (2003).

39. Dustin, M. L. & Long, E. O. Cytotoxic immunological synapses. *Immunol. Rev.* **235,** 24–34 (2010).

40. Voskoboinik, I., Dunstone, M. A., Baran, K., Whisstock, J. C. & Trapani, J. A. Perforin: structure, function, and role in human immunopathology. *Immunol. Rev.* **235,** 35–54 (2010).

41. Brinkman, E. K., Chen, T., Amendola, M. & van Steensel, B. Easy quantitative assessment of genome editing by sequence trace decomposition. *Nucleic Acids Res.* **42,** e168–e168 (2014).

SUPPLEMENTARY INFORMATION

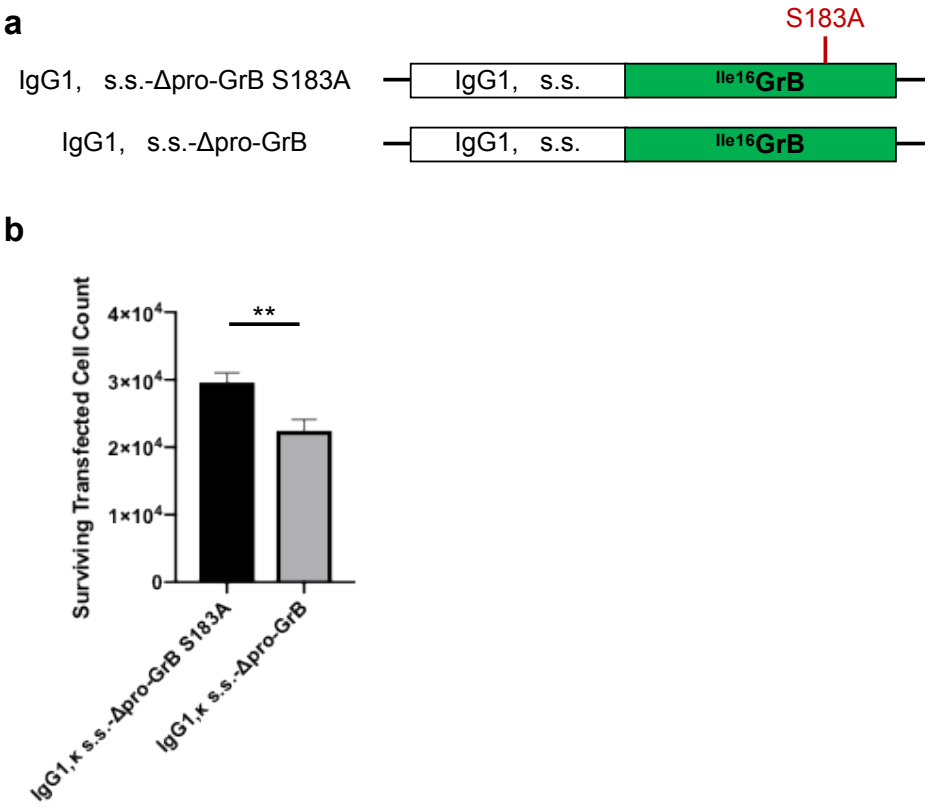

Figure 2.S1. A secreted version of mature GrB triggers cytotoxicity in transiently transfected HEK293T cells. (a) Replacement of the GrB pre-sequence with a murine IgG1,κ signal sequence results in secretion of mature GrB. A Ser183Ala mutation disrupts the catalytic triad, yielding a completely inert construct as a non-cytotoxic control. (c) Transiently transfected HEK293T cells were trypsinized and stained with a 7-aminoactinomycin D (7-AAD) viability dye prior to counting the number of surviving cells via flow cytometry. All values indicate the mean of triplicate samples and error bars represent ±1 s.d. ***p* < 5E-3.

Chapter 3. Interrogating Intracellular Protease Activities with Cleavage-dependent Granzyme B Switches

Adapted with permission from Ho, P., Ede, C., & Chen, Y.Y. Modularly Constructed Synthetic Granzyme B Molecule Enables Interrogation of Intracellular Proteases for Targeted Cytotoxicity. *ACS Synth. Biol.*, **6** (8), 1484 – 1495.

ABSTRACT

Targeted therapies promise to increase the safety and efficacy of treatments against diseases ranging from cancer to viral infections. However, the vast majority of targeted therapeutics relies on the recognition of extracellular biomarkers, which are rarely restricted to diseased cells and are thus prone to severe and sometimes-fatal off-target toxicities. In contrast, intracellular antigens present a diverse yet underutilized repertoire of disease markers. Here, we report a protein-based therapeutic platform—termed Cytoplasmic Oncoprotein VErifier and Response Trigger (COVERT)—which enables the interrogation of intracellular proteases to trigger targeted cytotoxicity. COVERT molecules consist of the cytotoxic protein granzyme B (GrB) fused to an inhibitory N-terminal peptide, which can be removed by researcher-specified proteases to activate GrB function. We demonstrate that fusion of a small ubiquitin-like modifier 1 (SUMO1) protein to GrB yields a SUMO-GrB molecule that is specifically activated by the cancer-associated sentrin-specific protease 1 (SENP1). SUMO-GrB selectively triggers apoptotic phenotypes in HEK293T cells that overexpress SENP1, and it is highly sensitive to different SENP1 levels across cell lines. We further demonstrate the rational design of additional COVERT molecules responsive to enterokinase (EK) and tobacco etch virus protease (TEVp), highlighting

the COVERT platform's modularity and adaptability to diverse protease targets. Our findings set the foundation for future intracellular-antigen–responsive therapeutics that can complement surface-targeted therapies.

INTRODUCTION

Precision medicine is an emerging cancer therapy paradigm that utilizes patient-specific genetic information to identify disease-specific molecular targets for therapeutic intervention[1,2]. Unlike conventional, indiscriminately toxic treatments, targeted therapies recognize aberrantly expressed biomarkers to operate against molecularly defined, diseased cell populations. There has been a long-standing interest in developing anti-tumor "magic bullets" by coupling tumor-targeting moieties to potent cytotoxic molecules[3]. In particular, monoclonal antibodies bind to unique epitopes with high specificity and are frequently conjugated to small-molecule chemotherapeutics, either through direct chemical linkage in antibody-drug conjugates or by surface presentation on drug-delivery vehicles[4]. Alternatively, non-selective toxins can be designed to function as prodrugs that activate upon cleavage by tumor-secreted proteases, thereby confining toxicity to cells in the local microenvironment[5]. While mechanistically diverse, these "smart drugs" share a heavy reliance on the recognition of extracellular signals to achieve specific targeting, even though surface-marker expression and soluble-factor secretion are rarely restricted to tumor cells. Consequently, dose-limiting, off-tumor toxicities are often manifest in therapies directed against extracellular antigen targets[6–8].

Despite the lack of tumor-exclusive extracellular biomarkers, contemporary tumor-targeting strategies continue to rely on the recognition of surface-bound antigens. This design focus has persisted through the advent of adoptive T-cell therapy, in which T cells are redirected to attack target cells via engineered receptor-antigen interactions on the cell surface[9]. Notably, T cells expressing chimeric antigen receptors (CARs) specific for the pan–B-cell marker CD19 have

demonstrated robust clinical efficacy in patients with relapsed B-cell malignancies[10–13]. However, due to natural CD19 expression on non-malignant B cells, sustained B-cell aplasia inevitably accompanies tumor eradication in responding patients[10–13]. Although B-cell aplasia is a clinically manageable condition, T cells engineered to target other tumor-associated antigens such as carcinoembryonic antigen (CEA) and HER2 have triggered severe dose-limiting or fatal toxicities in response to expression of the targeted molecules on normal tissue[14,15]. Therefore, the lack of disease-exclusive surface targets presents a recurrent critical barrier to clinical practice.

Meanwhile, the completion of the Human Genome Project and parallel advances in sequencing technology have enabled high-throughput, high-resolution analyses of cancer omics data, revealing a plethora of unexploited, intracellular disease signatures[16–18]. While native T-cell receptors (TCRs) naturally recognize short, antigen peptides derived from intracellular proteins, peptide surface-presentation must occur in the context of major histocompatibility complex (MHC) molecules, which are frequently downregulated during disease transformation[19]. Yet, in stark contrast to the multitude of innovative therapeutic modalities that target extracellular antigens, therapies responsive to intracellular antigens remain few and underdeveloped. Small-molecule drugs can permeate cell membranes to inhibit intracellular enzymes, but they generally display limited surface area and depend on hydrophobic contact for target binding, making them prone to non-specific interactions[20,21]. We hypothesize that the vast structural and biochemical diversity of proteins can be harnessed to achieve fine-tuned ligand specificity, allowing protein-based therapeutics to react to distinct physiological stimuli. Here, we report a novel protein-based therapeutic platform, termed Cytoplasmic Oncoprotein VErifier and Response Trigger (COVERT), which enables interrogation of intracellular tumor antigens—in particular, proteases—with the use of conditionally active granzyme B (GrB) molecules.

GrB is the initiator of multiple pro-apoptotic pathways and serves as the principle cytotoxic molecule deployed by T cells and natural killer (NK) cells to eliminate target cells[22,23]. Endogenous GrB is produced as a zymogen bearing an N-terminal Gly-Glu dipeptide that prevents the

formation of a functional catalytic triad[24]. Upon packaging into lytic granules inside the immune cell, GrB is processed by the dipeptidyl peptidase cathepsin C (CatC), which cleaves off GrB's Gly-Glu dipeptide and frees the newly N-terminal Ile16 residue to insert into the interior of the molecule and form a salt bridge with Asp194. The resulting conformational change enables the simultaneous generation of an oxyanion hole and maturation of the active-site S1 pocket[25,26]. Since endogenous GrB is activated prior to its release from the lytic granules of T cells and NK cells, it indiscriminately kills any target cell it enters and does not independently ascertain the identity of the target cell. Instead, target-cell identification is established exclusively at the cell surface via receptor-antigen interactions, whose specificities are subject to the limitations outlined above. Given its cytotoxic potential, GrB has been the subject of numerous attempts to engineer targeted therapeutics[27,28]. The vast majority of these designs consist of C-terminal fusions to binding domains that recognize surface-bound receptors or antigens. As a result, the specificity and therapeutic application of these engineered GrB molecules remain limited by the lack of disease-specific extracellular markers.

We hypothesized that engineering GrB to be a conditionally active molecule that is delivered into target cells in a dormant form but becomes activated after detecting a confirmatory, disease-identifying signal inside the target cell could significantly increase the specificity and safety profile of cell-based immunotherapy. We designed COVERT molecules to achieve this sense-and-respond function by fusing GrB to an N-terminal inhibitory peptide, which can be selectively removed by a cognate protease to activate GrB's catalytic function. As initial proof of concept, we focused on intracellular proteases as input signals to activate the engineered GrB. Intracellular proteases exert precise control over cellular signaling processes by rapidly enabling or inhibiting the biological activity of cleaved protein substrates, and they play essential roles in post-translational modification processes[29]. For example, sentrin-specific proteases (SENPs) work in concert with small ubiquitin-like modifier (SUMO) ligases to dynamically regulate the covalent attachment and detachment of SUMO-peptide modifications to protein substrates, and

this interplay is responsible for fine-tuning the structure, activity, and subcellular localization of the substrate proteins[30,31]. Dysregulation of the intricate balance between post-translational–modification states is frequently implicated in tumorigenesis, making intracellular proteases compelling disease targets[32,33]. In particular, SENP1 has been shown to be upregulated in a variety of tumors, including prostate, pancreatic, and oncocytic thyroid cancers[34–36].

Here, we report the development of synthetic COVERT molecules that can be produced, packaged, trafficked, and delivered by human T cells in the same manner as endogenous GrB, but which require the presence of specific proteases such as SENP1 inside target cells for their activation. We demonstrate that fusion of a SUMO1 peptide to the N-terminus of GrB yields a COVERT molecule that is specifically activated by the presence of SENP1. We further demonstrate that the modular COVERT architecture can accommodate a variety of different N-terminal fusion partners recognized by different proteases, and we confirm dose-responsive induction of GrB activity for each version of COVERT molecules tested. Finally, as a step toward engineering tumor-targeting T cells with high specificity and low off-tumor toxicity, we demonstrate that T-cell–compatible GrB-based switches can selectively mediate cytotoxicity in SENP1-overexpressing target cells.

METHODS

Cell Lines. HEK293T, MCF7, Jurkat E6, and H9 cells were obtained from ATCC (Manassas, VA) in 2011, and RWPE-1 and PC-3 were obtained from ATCC in 2014. ATCC verified the identity of each purchased cell line by short tandem repeat analysis prior to shipment. Raji cells were a generous gift from Dr. Michael C. Jensen (Seattle Children's Research Institute); the cell line was originally obtained from ATCC in 2003 and was authenticated again by short tandem repeat profiling at the University of Arizona Genetics Core in 2015. RWPE-1 cells were cultured in Keratinocyte serum-free medium (K-SFM) supplemented with 0.05 mg/mL bovine pituitary extract

(BPE) and 5 ng/mL recombinant human epidermal growth factor (rhEGF), purchased from Life Technologies (Grand Island, NY). Other cell lines were cultured in F-12K (PC-3), DMEM (HEK293T and MCF7), or RPMI-1640 (Jurkat, H9, and Raji) supplemented with 10% heat-inactivated FBS (HI-FBS). All mammalian cell cultures were maintained at 37°C and 5% CO_2.

DNA Constructs. DNA was chemically synthesized as oligonucleotides or gBlocks by Integrated DNA Technologies (Coralville, IA) and assembled using standard molecular cloning techniques. Unless otherwise indicated, all constructs were cloned into the epHIV7 lentiviral expression vector[37], although expression was induced by transient DNA transfection in the absence of viral packaging. The QPY variant of human GrB was used in this study, and the S183A mutant was generated by introducing a TCT to GCC codon mutation via isothermal DNA assembly. The DNA sequences for the three COVERT molecules and associated GrB control constructs are included in Text S1, Supporting Information. pFLAG-SENP1 was obtained from Addgene (plasmid 17357), and the SENP1 gene was subsequently cloned as a T2A fusion to TagBFP or mCherry. The TEVp gene was constructed from gBlocks.

Cell Transfection. HEK293T cells were seeded at 2.5 x 10^4 cells/0.25 mL/well in 48-well plates, 24 hours prior to transfection with 250 ng plasmid DNA and 15 nmol linear polyethylenimine (PEI, 25 kDa). For co-transfection experiments, plasmids were mixed at 1:1 mass ratio. The resulting DNA mixture totaling 250 ng was complexed with PEI, incubated at room temperature for 15 min, and then applied to seeded HEK293T cells. Jurkat T cells (5 x 10^6) were resuspended in 100 µL of Amaxa Cell Line Nucleofector™ V Solution (Lonza, Walkersville, MD) and electroporated with 5 µg plasmid DNA using Program X-001 of the Nucleofector™ 2b Device (Lonza), according to the manufacturer's protocol.

Ni^{2+}-affinity Protein Purification. HEK293T cells were seeded at 15 x 10^6 cells/25 mL/flask in T-150 flasks and transfected via the linear PEI method. Culture media were changed to serum-free DMEM 16 hours post-transfection, and supernatants were harvested at 48 and 72 hours post-media change. Supernatants from different collection times were pooled, and His-tagged proteins were batch-bound to Ni-NTA resin (Life Technologies) in binding buffer (500 mM NaCl, 20 mM Tris, pH 8.0) for 1 hour prior to being washed three times with binding buffer supplemented with 20 mM imidazole (Fisher Scientific, Hampton, NH), and then eluted with binding buffer supplemented with 500 mM imidazole through a chromatography column. Eluted proteins were buffer-exchanged into storage buffer (50 nM NaCl, 20 mM Tris pH7.4, 10% glycerol) by successive concentration and resuspension steps in Amicon centrifugal columns (10 kDa; EMD Millipore, Billierica, MA) following manufacturer's recommendations. Purified proteins were then aliquoted and frozen at -20°C.

Western Blot. Lysates were prepared by incubating cells in lysis buffer (150 mM NaCl, 20 mM Tris pH7.2, 1% (v/v) Triton-X) on ice for 45 min, and clarified of nuclear debris by centrifugation at 20,000 *x g* for 10 min. The protein concentration of the supernatant was determined via Bradford assay (Bio-Rad, Hercules, CA). For the SUMO-GrB cleavage assay, 30 µg of mock or SENP1-overexpressing HEK293T lysate was co-incubated with 2.5 pmol of purified SUMO-GrB for 2 hours at 37°C. Protein samples were resolved on 4-12% bis-tris SDS-PAGE gels, blotted onto nitrocellulose membranes, and probed with antibodies for GrB (clone 2C5; Santa Cruz Biotech, Dallas, TX) or SENP1 (clone C12; Santa Cruz Biotech), followed by staining with an anti-mouse secondary antibody conjugated to horseradish peroxidase (HRP; Jackson ImmunoResearch, West Grove, PA). Blots were visualized using SuperSignal West Pico Chemiluminescent Substrate (Thermo Scientific).

Ac-IEPD-pNA Activity Assay. SUMO-GrB was activated by co-incubating 30 µg of target cell lysate with 2.5 pmol of purified SUMO-GrB in 50 µL of lysis buffer for 30 min at 37°C. Samples were then diluted with 50 µL of assay buffer (50 mM HEPES pH 7.5, 10% (w/v) sucrose, 0.05% (w/v) CHAPS, 5 mM DTT) containing 200 µM Ac-IEPD-pNA substrate (Enzo Life Sciences, Farmingdale, NY), as described by Ewen et al.[39]. Purified EK (New England Biolabs, Ipswich, MA) and purified TEVp (prepared in-house) were added at the indicated concentrations to 2.5 pmol of DDDDK-GrB and ENLYFQ-GrB, respectively. Absorbance at 405 nm was measured every minute for 4 hours on an EONC microplate reader (BioTek, Winooski, VT). Activity was calculated by using the LINEST function in Excel to determine the line of best fit for the initial rate (dOD_{405}/min) by the least squares method.

Flow Cytometry. For cytotoxicity experiments, transiently transfected HEK293T cells were harvested for analysis at 24 hours (SUMO-GrB) or 48 hours (ENLYFQ-GrB) post-transfection. Culture media containing any dislodged cells were collected in centrifuge tubes before adherent cells were trypsinized and subsequently collected into the same tubes. The cells were washed twice with PBS prior to staining with 7-AAD (Life Technologies), DRAQ7 (eBioscience, San Diego, CA), or Annexin V-FITC (BioLegend, San Diego, CA), according to manufacturer's protocols. For GrB-mCherry delivery experiments, primary human T cells expressing CD19 CAR and GrB-mCherry were co-cultured with 20,000 Raji cells at 3:1 effector:target ratio for 45 min. Co-cultures were then suspended by rigorous pipetting and stained with CD8-VioGreen (clone BW135/80; Miltenyi Biotec, San Diego, CA) and CD19-VioBlue (clone LT19; Miltenyi Biotec) prior to data acquisition on a MACSQuant VYB flow cytometer (Miltenyi Biotec). Compensation and data analysis were performed using FlowJo Data Analysis software (TreeStar, Ashland, OR).

Statistics. Statistical significance was determined via two-tailed, homoscedastic Student's *t*-test with a *p*-value cutoff of 5E-3.

RESULTS

Engineering protease-responsive GrB switches

Similar to most trypsin-like serine proteases, GrB activation is strictly dependent on the generation of a free N-terminal Ile16 residue, which initiates the conformational change that creates an oxyanion hole and enables substrate access to the S1 pocket of the enzyme[26] (Figure 3.1a). Taking advantage of this sequence and structural requirement, we developed a protease-responsive COVERT architecture by engineering synthetic GrB zymogens that are only activated upon the removal of inhibitory N-terminal residues by specific proteases, with SENP1 being the protease of interest in our first demonstration (Figure 3.1b). SENP1 naturally removes SUMO1 modifications from substrate proteins by cleaving the SUMO1 peptide after Gly97[40]. By replacing the Gly-Glu dipeptide of wild-type GrB with the first 97 residues of zzSUMO1, we generate SUMO-GrB molecules that remain an inactive zymogen inside the lytic granule since they can no longer be cleaved by CatC to reveal an N-terminal Ile16. Instead, only an encounter with SENP1 can result in proper cleavage between Gly97 of the SUMO1 peptide and Ile16 of GrB, thereby triggering GrB activation.

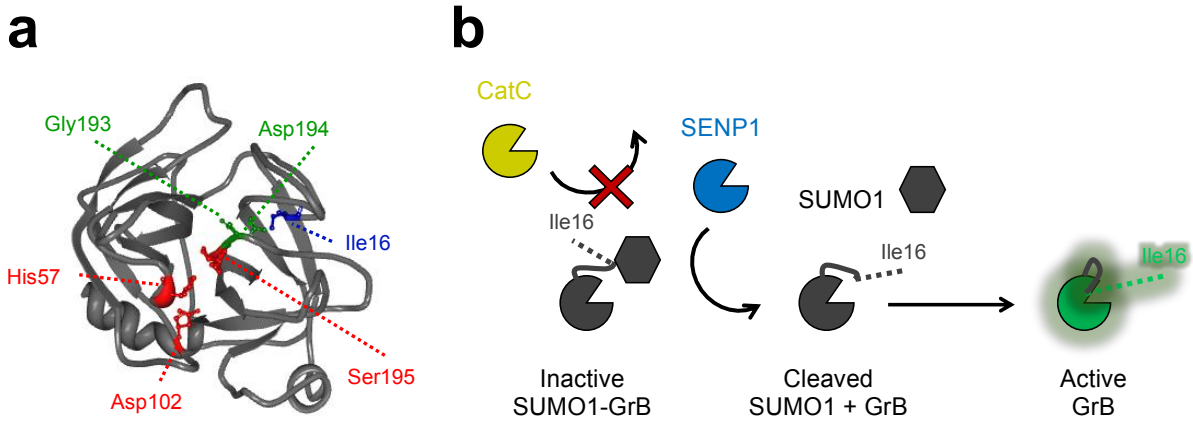

Figure 3.1. N-terminal fusion of SUMO1 to mature GrB yields a SENP1-activated zymogen. (a) Crystal structure of mature GrB (PDB #1IAU) shows the requisite salt bridge interaction between the N-terminal Ile16 (blue) and Asp194 (green), which forms the oxyanion hole between the

nitrogen atoms of Gly193, Asp194, and Ser195, and activates the catalytic triad of His57, Asp102, and Ser195 (red). (b) Replacement of the wild-type GrB pro-peptide with SUMO1 renders SUMO-GrB inactive as a synthetic zymogen that cannot be properly processed by cathepsin C (CatC). Encounter with SENP1 and removal of SUMO1 generates a free Ile16 N-terminus, which enables SUMO-GrB to undergo the conformational change necessary to achieve an active state.

We first confirmed that SUMO-GrB can be properly expressed by human cells and processed by SENP1 into mature GrB. A secreted, His-tagged version of SUMO-GrB was purified from the supernatant of transiently transfected HEK293T cells (which do not endogenously express GrB), and western blot verified that SUMO-GrB is specifically and efficiently cleaved upon co-incubation with lysate taken from SENP1-overexpressing cells (Figure 3.2a). Human GrB is 32 kDa when glycosylated[41], and genetic fusion with the SUMO1 peptide results in expression of full-length SUMO-GrB as a 43-kDa protein. Western blot stained with an anti-GrB antibody indicated that a 32-kDa fragment was released in the presence of SENP1, consistent with the expected processing of SUMO-GrB into mature GrB (Figure 3.2a).

To quantify the functional activation of SUMO-GrB, we utilized an N-acetyl-Ile-Glu-Pro-Asp-paranitroanilide (Ac-IEPD-pNA) tetrapeptide substrate, which releases a chromogenic paranitroaniline group upon cleavage by GrB. Purified SUMO-GrB was co-incubated with SENP1-transfected or mock-transfected HEK293T lysates, and the rate of Ac-IEPD-pNA substrate cleavage by GrB was measured as absorbance at 405 nm over time (Figure 3.2b). SUMO-GrB was nearly catalytically inert in the complete absence of SENP1, confirming the inhibitory nature of an N-terminal fusion architecture. Basal SENP1 levels in HEK293T induced statistically significant but limited activation of SUMO-GrB. In comparison, SENP1 overexpression resulted in a sizable and significant increase in SUMO-GrB's enzymatic activity (Figure 3.2b). (Western blots indicated that HEK293T cells transfected with SENP1-encoding plasmids expressed 1.8X to 3.2X more SENP1 compared to untransfected HEK293T cells, with the extent of overexpression correlating to transfection efficiency (red dotted line in Figure 3.2c; Figure 3.S1, Supplementary information).) Using the Ac-IEPD-pNA cleavage assay, we also verified that an S183A mutant of

GrB is catalytically inactive and can serve as a negative control in subsequent experiments (Figure 3.2b).

We next evaluated the sensitivity of SUMO-GrB to endogenous SENP1 expression levels found in different cell lines. The Ac-IEPD-pNA cleavage assay was performed on SUMO-GrB co-incubated with lysates from a panel of seven human cell lines (Jurkat, H9, Raji, HEK293T, PC-3, RWPE-1, and MCF7), and SENP1 protein levels in each cell line were separately quantified by western blot. The results indicated a strong linear correlation between SUMO-GrB activation and SENP1 expression levels, demonstrating a robust SENP1-dose dependent response (Figure 3.2c and Figure 3.S1, Supplementary Information). Strikingly, SUMO-GrB was sensitive to relatively modest fold-differences in SENP1 expression, highlighting its ability to quantitatively differentiate endogenous levels of SENP1 found in different cell types.

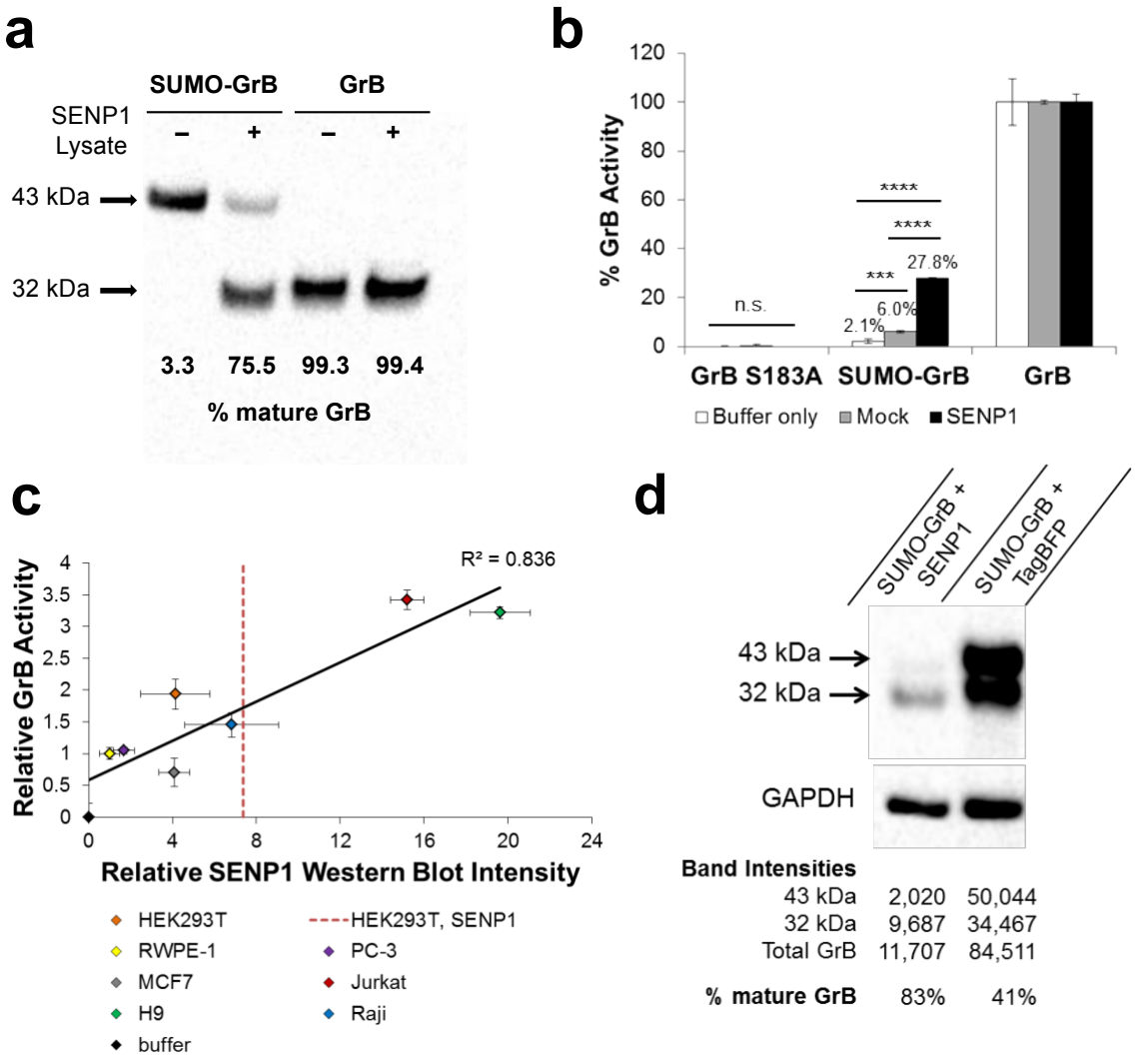
a
SUMO-GrB
GrB
SENP1 Lysate
–
+
–
+
43 kDa
32 kDa
3.3
75.5
99.3
99.4
% mature GrB
b
% GrB Activity
120
100
80
60
40
20
0
****
****
***
27.8%
6.0%
2.1%
n.s.
GrB S183A
SUMO-GrB
GrB
Buffer only
Mock
SENP1
c
R² = 0.836
Relative GrB Activity
Relative SENP1 Western Blot Intensity
HEK293T
HEK293T, SENP1
RWPE-1
PC-3
MCF7
Jurkat
H9
Raji
buffer
d
SUMO-GrB + SENP1
SUMO-GrB + TagBFP
43 kDa
32 kDa
GAPDH
Band Intensities
43 kDa 2,020 50,044
32 kDa 9,687 34,467
Total GrB 11,707 84,511
% mature GrB 83% 41%
e
Normalized GrB Activity (dOD405/dt/total GrB)
3.E-08
2.E-08
1.E-08
0.E+00
*
SUMO-GrB + SENP1
SUMO-GrB + TagBFP

Figure 3.2. SUMO-GrB is efficiently processed and activated by SENP1 in a dose-responsive manner. (a) Cleavage of purified SUMO-GrB following co-incubation with mock or SENP1-overexpressing HEK293T lysates. Percent mature GrB was calculated by normalizing the intensity of the 32-kDa mature GrB band by the total intensity of the 43-kDa SUMO-GrB and the mature GrB bands on the western blot. Purified mature GrB was included as a control, which was unaffected by the presence of SENP1. (b) Enzymatic activity of GrB molecules as quantified by Ac-IEPD-pNA cleavage. Purified SUMO-GrB was co-incubated with mock or SENP1-overexpressing HEK293T lysates as in (a). Percent GrB activity was calculated as the rate of Ac-IEPD-pNA cleavage normalized to the rate of cleavage by mature GrB. (c) SENP1 dose-responsive activation of purified SUMO-GrB following co-incubation with lysates from a panel of seven human cell lines. SENP1 protein level in each cell line was quantified via western blot, and GrB activity was quantified via the Ac-IEPD-pNA cleavage assay. GrB activity and SENP1 protein level for each sample were normalized to those of RWPE-1 to enable clear visualization of the data spread. The red dotted line indicates the SENP1 expression level of HEK293T cells transiently transfected with SENP1-encoding plasmids. Western blots corresponding to x-axis values are shown in Figure S1, Supporting Information. (d) Intracellular cleavage of SUMO-GrB by SENP1. HEK293T cells were transiently transfected with SUMO-GrB plus plasmids encoding either TagBFP-T2A-SENP1 or TagBFP alone. Cell lysates were collected 24 hours post transfection and probed for GrB by western blot. Total GrB refers to the sum of the 43-kDa SUMO-GrB and 32-kDa mature GrB bands, and % mature GrB was calculated as described in (a). (e) Enzymatic activity of SUMO-GrB–transfected cell lysates as quantified by Ac-IEPD-pNA cleavage. Twenty-five μg of the same cell lysates as shown in (d) were reacted with 200 μM Ac-IEPD-pNA. The rate of Ac-IEPD-pNA cleavage was normalized by the amount of total GrB in each lysate based on western blot results shown in (d). All plotted values indicate the mean of triplicate samples and error bars represent ±1 standard deviation (s.d.). * $p < 5E-3$; *** $p < 5E-5$; **** $p < 5E-12$.

To confirm that SENP1-mediated cleavage and activation of SUMO-GrB can also occur in the intracellular environment, we transfected HEK293T cells to express SUMO-GrB with and without SENP1. Western blot results indicate that cells transfected with SUMO-GrB alone contained significant amounts of both SUMO-GrB and mature GrB (Figure 3.2d), consistent with the fact that HEK293T cells express a basal level of endogenous SENP1[42] (Figure 3.2c). In contrast, the vast majority of GrB content in cells co-transfected with SUMO-GrB and SENP1 was in the mature form (Figure 3.2d), confirming SENP1-dependent cleavage of the SUMO peptide inside transfected cells. To verify that the cleaved GrB was functionally active, we performed Ac-IEPD-pNA cleavage assays using the same cell lysates as used in the western blots. We observed significantly higher enzymatic activity in cells that were transfected with SENP1, after normalizing by the amount of total GrB (SUMO-GrB plus mature GrB) present in each sample (Figure 3.2e). These results confirm SENP1-specific activation of SUMO-GrB in the intracellular

environment. It was noted that HEK293T cells co-transfected with SUMO-GrB and SENP1 contained significantly less total GrB compared to cells transfected with SUMO-GrB alone, suggesting that the activation of SUMO-GrB by SENP1 may have led to toxicities that compromised the cells' health and ability to produce transgenic proteins at high levels. This hypothesis is supported by the observation that HEK293T cells transfected with mature GrB yielded even lower levels of total GrB expression (Figure 3.S2, Supplementary Information). We next sought to confirm whether the presence of active GrB indeed results in cytotoxicity.

SUMO-GrB selectively triggers apoptosis of SENP1-overexpressing cells

The effect of GrB expression in HEK293T cells was first established using wild-type GrB as a positive control. Surprisingly, the results indicated a lack of overt cytotoxicity based on high transfection efficiency (i.e., no depletion of transfected cells due to toxicity of transgenic construct), as well as lack of staining by the viability dye 7-AAD and the apoptosis marker Annexin V (Figure 3.S3, Supplementary Information). Although GrB is the main cytotoxic molecule with which T cells trigger target-cell apoptosis, T cells typically release GrB together with other effector molecules such as perforin, a pore-forming protein, during degranulation[43]. The absence of these accessory proteins may account for the drastic reduction in cytotoxicity observed in cells transfected with GrB alone. Nevertheless, closer inspection of GrB-transfected cells revealed a marked change in cell physiology as evidenced by the appearance of a distinct cell population exhibiting low forward scatter (FSC), which is characteristic of late-apoptotic cells with reduced cell size[44,45] (Figure 3.3a and Figure 3.S4, Supplementary Information). Furthermore, we observed a loss of cell adherence resulting from GrB expression, suggesting compromised integrity of GrB-transfected cells (Figure S5a, Supporting Information).

Next, HEK293T cells were transiently transfected to express SUMO-GrB plus either the fluorescent protein TagBFP or SENP1 fused to TagBFP via a 2A peptide, and the physiology of transfected (TagBFP+) cells was analyzed by flow cytometry. SUMO-GrB–expressing cells

showed significant reduction in FSC only in the presence of SENP1 (Figure 3.3), indicating SENP1-induced apoptosis. Concurrent loss of cell attachment was also observed in SUMO-GrB–expressing cells in the presence of SENP1, albeit to a lesser extent compared to cells transfected with wild-type GrB (Figure 3.S5b, Supplementary Information). Importantly, control samples transfected with GrB S183A showed no change in FSC or cell-detachment patterns regardless of the presence of SENP1, confirming that SENP1 does not have any intrinsic toxicity (Figure 3.S5c, Supplementary Information). Taken together, these results indicate that SUMO-GrB selectively triggers cell apoptosis in a SENP1-specific manner.

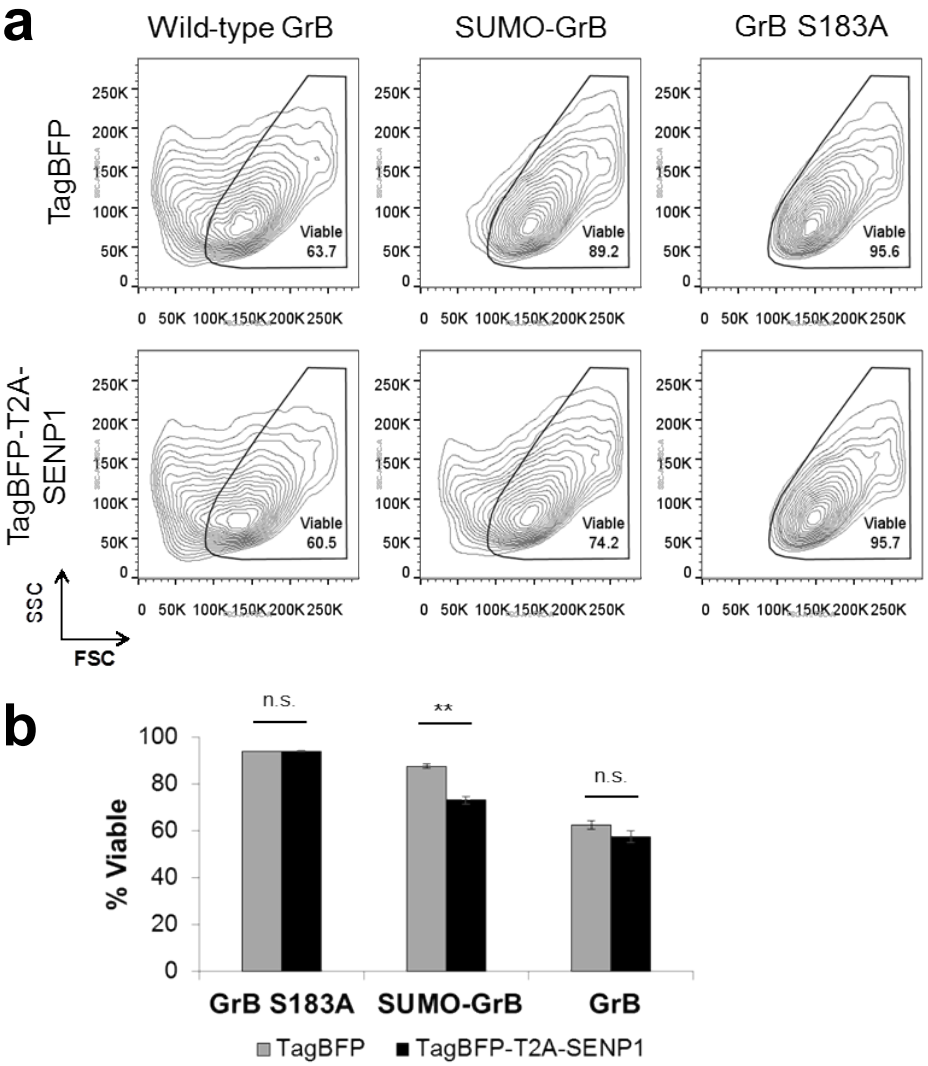

Figure 3.3. SUMO-GrB selectively triggers apoptosis of SENP1-overexpressing HEK293T cells. HEK293T cells were transiently transfected to co-express either TagBFP or TagBFP-T2A-SENP1 plus wild-type GrB, SUMO-GrB, or GrB S183A, which is an inactive GrB mutant. (a) Side scatter (SSC) vs. forward scatter (FSC) plot of transfected (TagBFP+) and 7-AAD– cell populations (see *Figure 3—supplementary figure 2* for gating strategy). Marked reduction in FSC was observed among cells expressing wild-type GrB regardless of SENP1 presence, as well as among cells expressing SUMO-GrB specifically in the presence of SENP1. Plots shown are representative of two independent experiments, each with triplicate samples. (b) Quantification of the % viability among samples shown in (a), $**p < 5E-4$. All plotted values indicate the mean of triplicate samples and error bars represent ±1 s.d.

The COVERT architecture is modular and compatible with diverse proteases

Given the evidence supporting the predicted mechanism of SUMO-GrB activation, we hypothesized that the basic COVERT architecture could be systematically adjusted to accommodate different N-terminal fusion partners and, consequently, different protease specificities. To explore the potential for extending the COVERT platform to additional protease targets, we designed COVERT molecules that are specifically activated by enterokinase (EK) and tobacco etch virus protease (TEVp). Since EK cleaves at the end of the Asp-Asp-Asp-Asp-Lys (DDDDK) motif, it is readily compatible with the COVERT architecture—i.e., a direct N-terminal fusion of DDDDK to Ile16 of GrB generates an EK-responsive GrB zymogen, termed DDDDK-GrB.

In contrast, TEVp cleaves its canonical recognition sequence Glu-Asn-Leu-Tyr-Phe-Gln-Gly (ENLYFQG) between the P1-Gln and P1'-Gly residues, such that an N-terminal fusion of the entire ENLYFQ↓G sequence would leave an N-terminal Gly residue attached to GrB upon cleavage by TEVp, thus rendering the wild-type TEVp cleavage sequence incompatible with COVERT activation. However, prior studies have demonstrated enzymatic promiscuity by TEVp, which can process sequences containing alternative, non-proline residues in the P1' position, albeit with reduced efficiency[46]. Therefore, we rationalized that fusing the first six residues of the TEVp cleavage sequence in front of Ile16 of GrB would constitute a ENLYFQ↓I cleavage site in

the resulting COVERT molecule, termed ENLYFQ-GrB, which enables activation in response to TEVp-mediated cleavage.

The conditional activation of DDDDK-GrB and ENLYFQ-GrB were characterized by quantifying their rates of Ac-IEPD-pNA cleavage before and after exposure to their cognate proteases. Secreted, His-tagged DDDDK-GrB and ENLYFQ-GrB were purified from the supernatant of transiently transfected HEK293T cells and co-incubated with increasing amounts of purified EK and purified TEVp, respectively. The results showed efficient, dose-dependent activation of DDDDK-GrB by EK, with a linear, 647-fold increase in GrB activity (R^2 = 0.994) over an 80-nM range of EK input concentrations (Figure 3.4a). As anticipated, ENLYFQ-GrB was also activated by TEVp in a dose-responsive manner, showing linear correlation between GrB activity and TEVp concentration up to 150 nM (R^2 = 0.944) (Figure 3.4b). However, the rates of activation, calculated as GrB activity per mole of target-protease input, indicate that EK is 7.52-fold more efficient than TEVp at activating its cognate COVERT molecule (Figure 3.4c). This finding is consistent with reports indicating reduced cleavage activity of TEVp against the non-canonical ENLYFQ↓I target sequence[46].

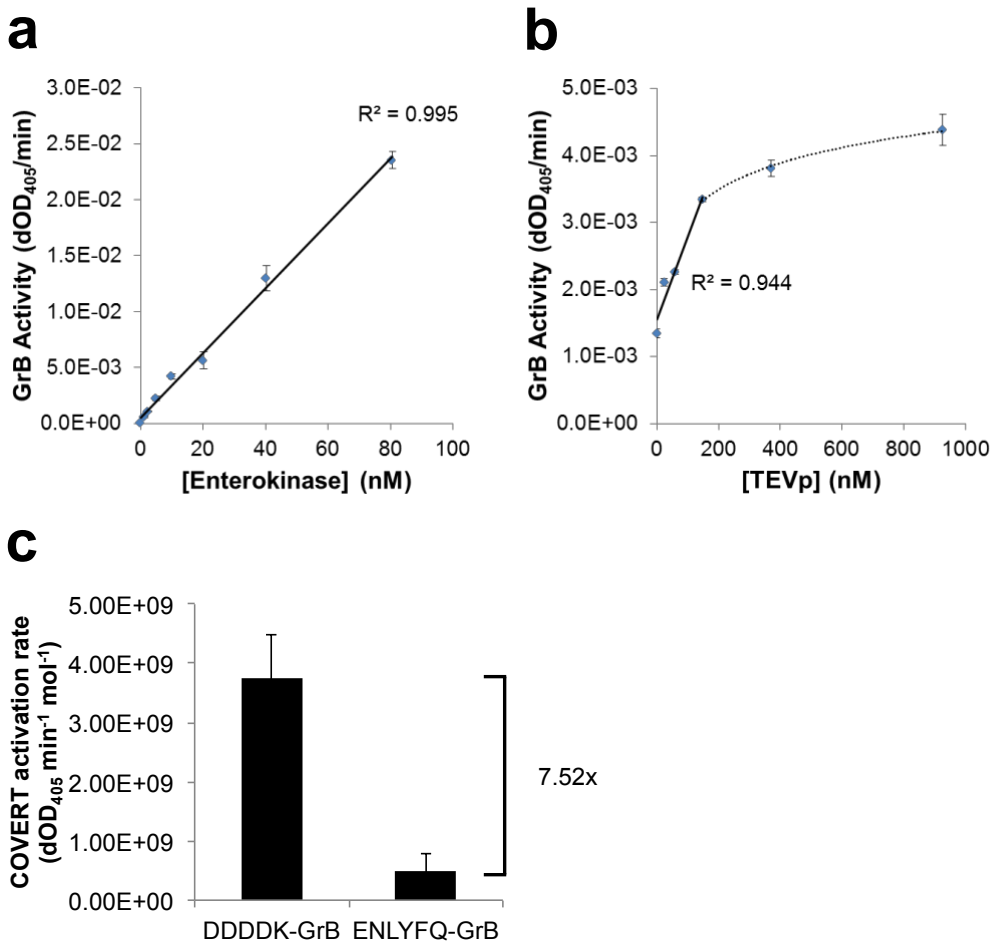

Figure 3.4. N-terminal fusion architecture can accommodate diverse inhibitory motifs to yield unique COVERT molecules that are specifically activated by cognate proteases. (a,b) DDDDK-GrB and ENLYFQ-GrB were purified from the supernatant of transiently transfected HEK293T cells and co-incubated with EK and TEVp, respectively. The resulting GrB activity of (a) DDDDK-GrB and (b) ENLYFQ-GrB against Ac-IEPD-pNA substrates was quantified by the rate of increase in absorbance at 405 nm. (c) GrB activity per mole of target protease (i.e. EK or TEVp) was calculated to compare the relative rate of COVERT activation. All values indicate the mean of triplicate samples and error bars represent ±1 s.d.

To further investigate the versatility of the COVERT platform, ENLYFQ-GrB was evaluated for its ability to selectively mediate cytotoxicity against HEK293T cells expressing TEVp. In contrast to SENP1, TEVp is not mammalian in origin, and its forced expression mimics a state of viral infection. Transient expression of GrB in HEK293T cells resulted in marked changes in cell physiology regardless of whether the cells co-expressed TEVp (Figure 3.5a). In contrast, ENLYFQ-GrB elicits the appearance of the low-FSC population only in the presence of TEVp

(Figure 3.5b). This population is again absent in cells transfected with GrB S183A (Figure 5c), indicating that the cytotoxicity in the ENLYFQ-GrB plus TEVp sample can be attributed to selective COVERT activation rather than any potential toxicity directly resulting from TEVp expression. Along with the SUMO-GrB data, these results support the modularity and versatility of the COVERT platform for targeting proteolytic markers of a variety of disease states.

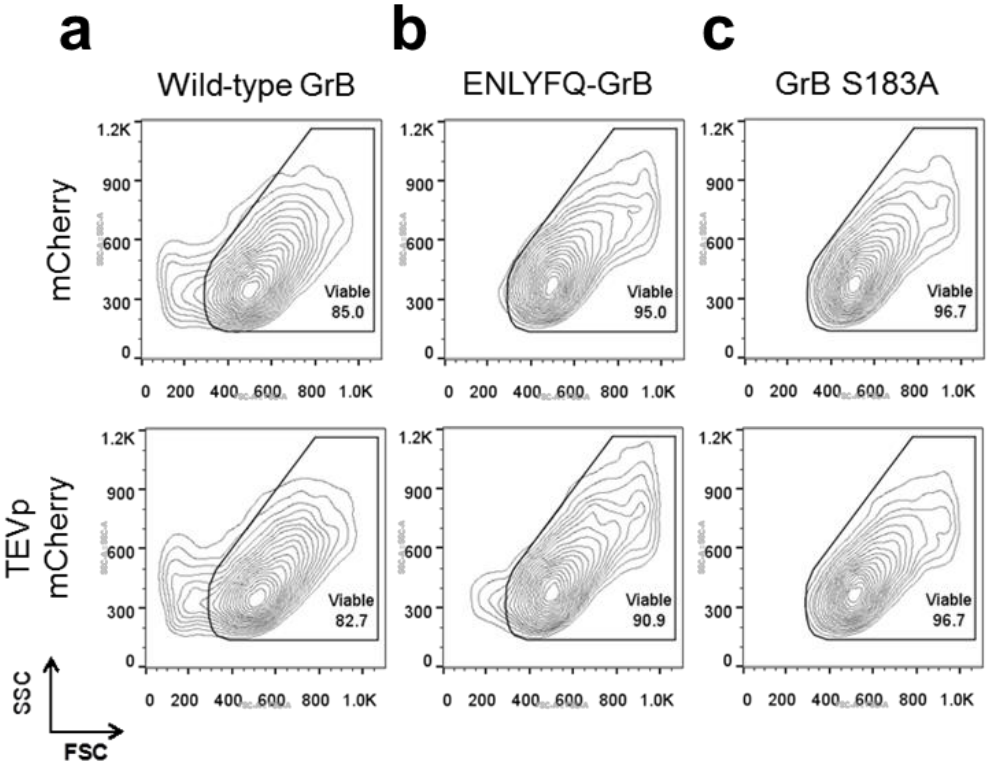

Figure 3.5. Selective induction of apoptosis in TEVp-overexpressing HEK293T cells by ENLYFQ-GrB. HEK293T cells were transiently transfected to co-express either mCherry or TEVp (each tagged with mCherry) plus (a) wild-type GrB, (b) ENLYFQ-GrB, or (c) GrB S183A. Co-expression of ENLYFQ-GrB and TEVp resulted in the appearance of a small, but significant, population of cells exhibiting decreased FSC, signifying the specific induction of GrB-mediated cytotoxicity. Contour plots show the SSC vs. FSC scatter of transfected (mCherry+) and DRAQ7– cell populations. Plots shown are representative of triplicate samples.

DISCUSSION

The lack of disease-exclusive surface targets has been a major obstacle to the development of safely targeted therapies, including adoptive T-cell therapy. In this study, we

developed a protein-based therapeutic platform that directly addresses this limitation by enabling the interrogation of intracellular antigen expression prior to unleashing cytotoxicity. By taking advantage of the zymogen behavior of wild-type GrB, we were able to apply an N-terminal fusion strategy to construct synthetic GrB zymogens, termed COVERT molecules, that can be activated by a variety of target proteases, including SENP1, EK, and TEVp. Each evaluated COVERT molecule displayed a robustly dose-dependent and protease-specific activation profile, confirming the modularity of the N-terminal fusion architecture. The ability to systematically engineer COVERT molecules responsive to researcher-specified inputs highlight the versatility to target a wide array of previously unexploited disease markers, including those found in cancers as well as viral infections.

In particular, dysregulation of SENP1 expression is frequently implicated in multiple cancers[34–36], and SENP1 overexpression is strongly correlated with poor prognosis of prostate cancer patients[47]. We demonstrated that SUMO-GrB molecules can be engineered to selectively trigger apoptotic phenotypes in human cells that overexpress SENP1. Importantly, basal SENP1 expression levels result in minimal activation and SUMO-GrB–mediated cytotoxicity, corroborating the promise of such engineered GrB molecules as safe, targeted therapeutics. In addition, we demonstrated that SUMO-GrB is remarkably sensitive to physiological differences in SENP1 expression among a panel of seven human cell lines, suggesting additional utility as a SENP1-detection agent during cancer-biomarker screening of patient samples. Standard screening protocols routinely involve RT-PCR or immunohistochemistry, both of which are labor-intensive and prone to variability in sample preparation or scoring[48,49]. SUMO-GrB enables rapid quantification of SENP1 levels directly from biological samples, potentially offering shorter turnaround times and increased detection accuracy.

The structural modularity of the COVERT platform suggests that novel diagnostic and therapeutic proteins can be systematically generated for a variety of protease targets. The only requirement for compatibility with the COVERT platform is an N-terminal peptide that can be

specifically cleaved by the target protease to reveal an N-terminal Ile16 residue for GrB. Each COVERT molecule we have evaluated thus far exhibits highly efficient production in human cells, suggesting robust protein folding of recombinant GrB. Nevertheless, protease cleavage efficiency is an important parameter to be considered, as it dictates the dynamic range of GrB activation. For example, we observed that the highly efficient EK could elicit a >600-fold induction in DDDDK-GrB activity, whereas TEVp could only achieve a 3.3-fold induction in ENLYFQ-GrB activity due to the limited cleavage efficiency of TEVp against the ENLYFQI motif. Despite this limited dynamic range detected by Ac-IEPD-pNA cleavage assays, we were still able to observe significant changes in cell physiology in the presence versus absence of TEVp, highlighting the importance of cell-based evaluations. The fact that proteases such as TEVp can recognize multiple target peptides with different efficiency levels provides a potential method by which to calibrate the sensitivity of COVERT molecules, a flexibility that may be critical in therapeutic applications.

The cytotoxic switch architecture developed in this study sets the foundation for a new class of protein-based therapeutics that complements exciting frontier technologies in targeted therapy. In addition to compatibility with T-cell therapy, the COVERT architecture can also be combined with a variety of C-terminal antibody conjugations previously reported to direct GrB molecules to specific cell types[27,28]. By including both N- and C-terminal fusions, one could engineer AND-gate molecules that perform the first step of target identification at the cell surface via antibody-mediated protein uptake, followed by a second interrogation step inside the target cell prior to activation of GrB's enzymatic activity. Such engineered GrB molecules would require both a surface-bound antigen and an intracellular protease to trigger target-cell apoptosis, thereby increasing targeting specificity and the safety profile of GrB-based therapeutics. By enabling biologics and cellular therapies to sense and respond to intracellular tumor antigens, the COVERT platform can serve to bridge the gap between omics-mediated biomarker discovery and the transformative promise of precision medicine.

ACKNOWLEDGEMENTS

The authors thank W. Clifford Boldridge and ZeNan L. Chang for technical assistance. This research was supported by the National Institutes of Health (5DP5OD012133; grant to YYC) and the National Science Foundation (1553767; grant to YYC). PH was supported by the Biotechnology Training in Biomedical Sciences and Engineering Program funded by the National Institutes of Health.

REFERENCES

1. Collins, D. C., Sundar, R., Lim, J. S. J. & Yap, T. A. Towards Precision Medicine in the Clinic: From Biomarker Discovery to Novel Therapeutics. *Trends Pharmacol. Sci.* **38,** 25–40 (2017).
2. Garraway, L. A. Genomics-driven oncology: framework for an emerging paradigm. *J. Clin. Oncol.* **31,** 1806–14 (2013).
3. Imai, K. & Takaoka, A. Comparing antibody and small-molecule therapies for cancer. *Nat. Rev. Cancer* **6,** 714–727 (2006).
4. Adams, G. P. & Weiner, L. M. Monoclonal antibody therapy of cancer. *Nat. Biotechnol.* **23,** 1147–1157 (2005).
5. Denmeade, S. R. & Isaacs, J. T. Engineering enzymatically activated 'molecular grenades' for cancer. *Oncotarget* **3,** 666–7 (2012).
6. Wu, A. M. & Senter, P. D. Arming antibodies: prospects and challenges for immunoconjugates. *Nat. Biotechnol.* **23,** 1137–1146 (2005).
7. Hinrichs, C. S. & Restifo, N. P. Reassessing target antigens for adoptive T-cell therapy. *Nat. Biotechnol.* **31,** 999–1008 (2013).
8. Rosenberg, S. A. Finding suitable targets is the major obstacle to cancer gene therapy. *Cancer Gene Ther.* **21,** 45–7 (2014).
9. Duong, C. P. M., Yong, C. S. M., Kershaw, M. H., Slaney, C. Y. & Darcy, P. K. Cancer immunotherapy utilizing gene-modified T cells: From the bench to the clinic. *Mol. Immunol.* **67,** 46–57 (2015).
10. Kochenderfer, J. N. *et al.* Chemotherapy-Refractory Diffuse Large B-Cell Lymphoma and Indolent B-Cell Malignancies Can Be Effectively Treated With Autologous T Cells Expressing an Anti-CD19 Chimeric Antigen Receptor. *J Clin Oncol* **33,** 540–549 (2015).
11. Davila, M. L. *et al.* Efficacy and Toxicity Management of 19-28z CAR T Cell Therapy in B Cell Acute Lymphoblastic Leukemia. *Sci. Transl. Med.* **6,** 224ra225 (2014).

12. Maude, S. L. *et al.* Chimeric Antigen Receptor T Cells for Sustained Remissions in Leukemia. *N. Engl. J. Med.* **371,** 1507–1517 (2014).
13. Wang, X. *et al.* Phase 1 studies of central memory–derived CD19 CAR T–cell therapy following autologous HSCT in patients with B-cell NHL. *Blood* **127,** 2980–2990 (2016).
14. Morgan, R. A. *et al.* Case report of a serious adverse event following the administration of T cells transduced with a chimeric antigen receptor recognizing ERBB2. *Mol. Ther.* **18,** 843–51 (2010).
15. Parkhurst, M. R. *et al.* T cells targeting carcinoembryonic antigen can mediate regression of metastatic colorectal cancer but induce severe transient colitis. *Mol. Ther.* **19,** 620–6 (2011).
16. Davies, H. *et al.* Mutations of the BRAF gene in human cancer. *Nature* **417,** 949–54 (2002).
17. Kranenburg, O. The KRAS oncogene: past, present, and future. *Biochim. Biophys. Acta* **1756,** 81–2 (2005).
18. Dang, C. V. MYC on the path to cancer. *Cell* **149,** 22–35 (2012).
19. Ochsenbein, A. F. Principles of tumor immunosurveillance and implications for immunotherapy. *Cancer Gene Ther.* **9,** 1043–55 (2002).
20. Kintzing, J. R., Filsinger Interrante, M. V. & Cochran, J. R. Emerging Strategies for Developing Next-Generation Protein Therapeutics for Cancer Treatment. *Trends Pharmacol. Sci.* **37,** 993–1008 (2016).
21. Zhang, J., Yang, P. L. & Gray, N. S. Targeting cancer with small molecule kinase inhibitors. *Nat. Rev. Cancer* **9,** 28–39 (2009).
22. Andrade, F. *et al.* Granzyme B Directly and Efficiently Cleaves Several Downstream Caspase Substrates: Implications for CTL-Induced Apoptosis. *Immunity* **8,** 451–460 (1998).
23. Pinkoski, M. J. *et al.* Entry and Trafficking of Granzyme B in Target Cells During

Granzyme B-Perforin–Mediated Apoptosis. *Blood* **92,** 1044–1054 (1998).

24. Smyth, M. J., McGuire, M. J. & Thia, K. Y. Expression of recombinant human granzyme B. A processing and activation role for dipeptidyl peptidase I. *J. Immunol.* **154,** 6299–305 (1995).

25. Trapani, J. A. Granzymes: a family of lymphocyte granule serine proteases. *Genome Biol.* **2,** REVIEWS3014 (2001).

26. Rotonda, J. *et al.* The three-dimensional structure of human granzyme B compared to caspase-3, key mediators of cell death with cleavage specificity for aspartic acid in P1. *Chem. Biol.* **8,** 357–68 (2001).

27. Rosenblum, M. G. & Barth, S. Development of novel, highly cytotoxic fusion constructs containing granzyme B: unique mechanisms and functions. *Curr. Pharm. Des.* **15,** 2676–92 (2009).

28. Dälken, B., Giesübel, U., Knauer, S. K. & Wels, W. S. Targeted induction of apoptosis by chimeric granzyme B fusion proteins carrying antibody and growth factor domains for cell recognition. *Cell Death Differ.* **13,** 576–85 (2006).

29. Bond, J. S. & Butler, P. E. Intracellular Proteases. *Ann. Rev. Biochem* **56,** 333–64 (1987).

30. Hickey, C. M., Wilson, N. R. & Hochstrasser, M. Function and regulation of SUMO proteases. *Nat. Rev. Mol. Cell Biol.* **13,** 755–766 (2012).

31. Flotho, A. & Melchior, F. Sumoylation: A Regulatory Protein Modification in Health and Disease. *Annu. Rev. Biochem.* **82,** 357–385 (2013).

32. Bawa-Khalfe, T. & Yeh, E. T. H. SUMO Losing Balance: SUMO Proteases Disrupt SUMO Homeostasis to Facilitate Cancer Development and Progression. *Genes Cancer* **1,** 748–752 (2010).

33. Mattoscio, D. & Chiocca, S. SUMO pathway components as possible cancer biomarkers. *Futur. Oncol.* **11,** 1599–1610 (2015).

34. Cheng, J., Bawa, T., Lee, P., Gong, L. & Yeh, E. T. H. Role of desumoylation in the

development of prostate cancer. *Neoplasia* **8,** 667–76 (2006).

35. Ma, C. *et al.* SUMO-specific protease 1 regulates pancreatic cancer cell proliferation and invasion by targeting MMP-9. *Tumour Biol.* **35,** 12729–35 (2014).

36. Jacques, C. *et al.* Two-Step Differential Expression Analysis Reveals a New Set of Genes Involved in Thyroid Oncocytic Tumors. *J. Clin. Endocrinol. Metab.* **90,** 2314–2320 (2005).

37. Yam, P. *et al.* Design of HIV Vectors for Efficient Gene Delivery into Human Hematopoietic Cells. *Mol. Ther.* **5,** 479–484 (2002).

38. Zah, E., Lin, M.-Y., Silva-Benedict, A., Jensen, M. C. & Chen, Y. Y. T cells expressing CD19/CD20 bi-specific chimeric antigen receptors prevent antigen escape by malignant B cells. *Cancer Immunol. Res.* **4,** 498–508 (2016).

39. Ewen, C. *et al.* A novel cytotoxicity assay to evaluate antigen-specific CTL responses using a colorimetric substrate for Granzyme B. *J. Immunol. Methods* **276,** 89–101 (2003).

40. Bailey, D. & O'Hare, P. Characterization of the localization and proteolytic activity of the SUMO-specific protease, SENP1. *J. Biol. Chem.* **279,** 692–703 (2004).

41. Trapani, J. A., Browne, K. A., Dawson, M. & Smyth, M. J. Immunopurification of Functional Asp-ase (Natural Killer Cell Granzyme B) Using a Monoclonal Antibody. *Biochem. Biophys. Res. Commun.* **195,** 910–920 (1993).

42. Kolli, N. *et al.* Distribution and paralogue specificity of mammalian deSUMOylating enzymes. *Biochem. J.* **430,** 335–44 (2010).

43. Voskoboinik, I., Dunstone, M. A., Baran, K., Whisstock, J. C. & Trapani, J. A. Perforin: structure, function, and role in human immunopathology. *Immunol. Rev.* **235,** 35–54 (2010).

44. Desjardins, L. M. & MacManus, J. P. An Adherent Cell Model to Study Different Stages of Apoptosis. *Exp. Cell Res.* **216,** 380–387 (1995).

45. Bortner, C. D. & Cidlowski, J. A. A necessary role for cell shrinkage in apoptosis.

Biochem. Pharmacol. **56,** 1549–1559 (1998).

46. Kapust, R. B., Tözsér, J., Copeland, T. D. & Waugh, D. S. The P1′ specificity of tobacco etch virus protease. *Biochem. Biophys. Res. Commun.* **294,** 949–955 (2002).

47. Li, T., Huang, S., Dong, M., Gui, Y. & Wu, D. Prognostic impact of SUMO-specific protease 1 (SENP1) in prostate cancer patients undergoing radical prostatectomy. *Urol. Oncol.* **31,** 1539–45 (2013).

48. Dall, P. *et al.* Comparison of immunohistochemistry and RT-PCR for detection of CD44v-expression, a new prognostic factor in human breast cancer. *Int. J. Cancer* **60,** 471–477 (1995).

49. Bernard, P. S. & Wittwer, C. T. Real-Time PCR Technology for Cancer Diagnostics. *Clin. Chem.* **48,** 1178–1185 (2002).

SUPPLEMENTARY INFORMATION

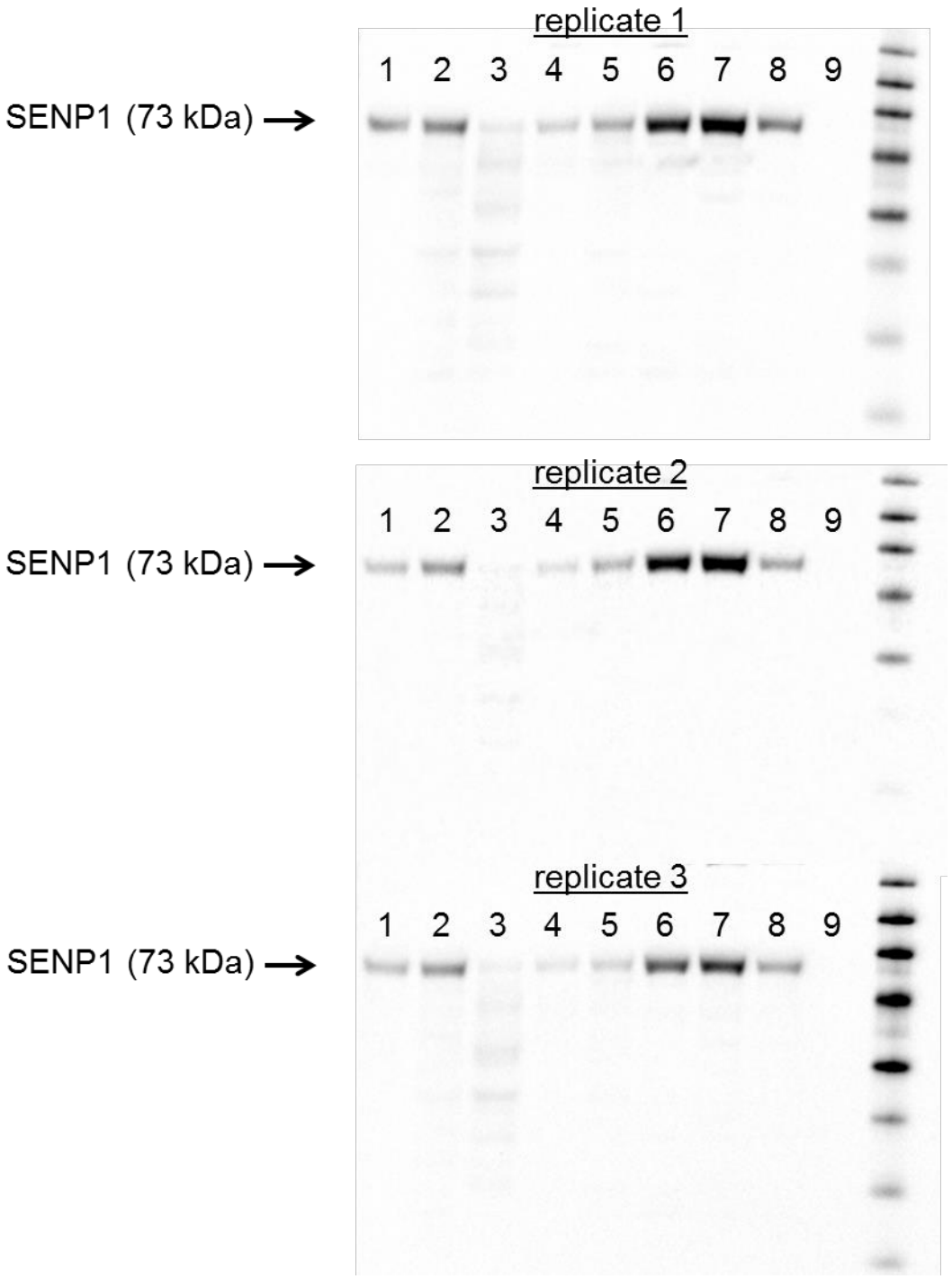

Figure 3.S1. Western blots of SENP1 expression in various cell lines. Triplicate western blots of SENP1 expression in HEK293T (lane 1), SENP1-transfected HEK293T (lane 2), RWPE-1 (lane 3), PC-3 (lane 4), MCF7 (lane 5), Jurkat (lane 6), H9 (lane 7), Raji (lane 8), lysis buffer only (lane 9). Quantified values are shown on the x-axis of Figure 2c.

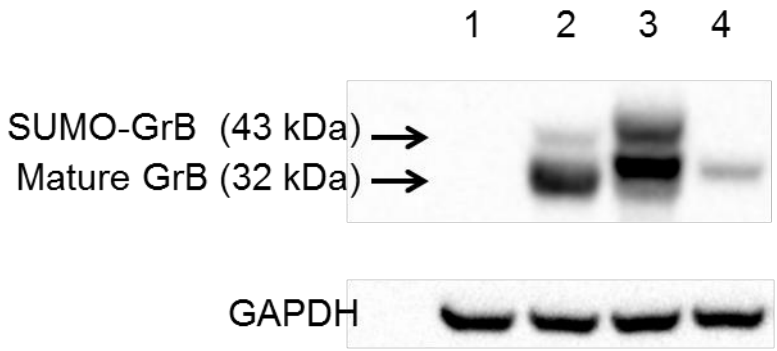

Figure 3.S2. SUMO-GrB is cleaved in a SENP1-specific manner in transfected HEK293T cells. HEK293T cells were either untransfected (lane 1) or transfected with SUMO-GrB + SENP1-T2A-TagBFP (lane 2), SUMO-GrB + TagBFP (lane 3), or mature GrB + SENP1-T2A-TagBFP (lane 4). A western blot of cell lysates was probed for GrB, and a duplicate blot was probed for GAPDH (which runs at approximately the same height as mature GrB and thus could not be probed on the same blot as GrB). Co-expression of SENP1 resulted in increased cleavage of SUMO-GrB into the mature GrB form. Expression of mature GrB as well as cleavage of SUMO-GrB into mature GrB resulted in noticeable decreases in the total GrB protein content, suggesting that toxicity triggered by active GrB reduced the ability of HEK293T cells to produce high levels of transgenic proteins.

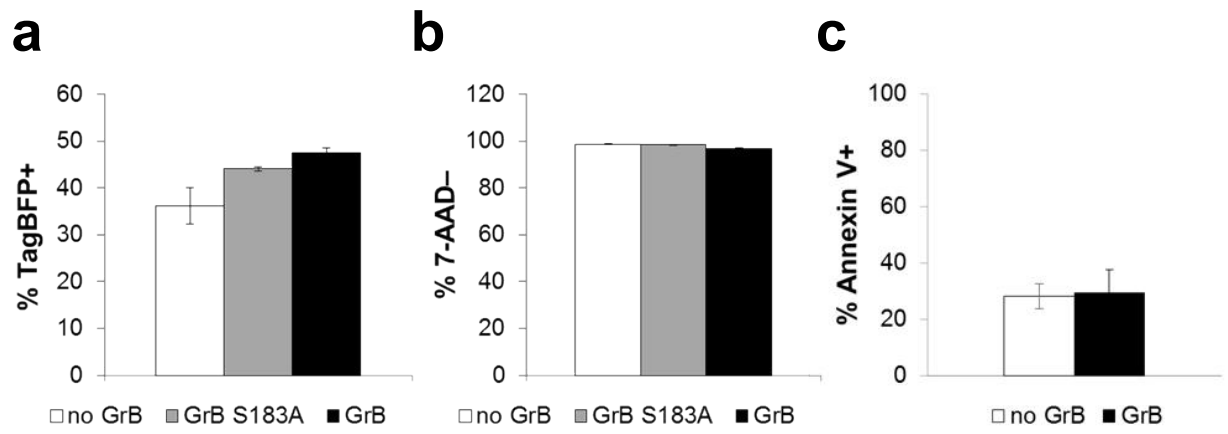

Figure 3.S3. Transient expression of GrB was not overtly toxic to HEK293T cells based on transfection efficiency and viability staining. (a) HEK293T cells co-transfected with GrB- and TagBFP-encoding plasmids did not result in the depletion of transfected (TagBFP+) cells, relative to cells transfected with plasmids encoding no GrB or the inactive GrB S183A mutant. (b) Cells transfected in the same manner as in (a) showed no difference in viability level based on 7-AAD staining. (c) Transient transfection with a mock plasmid or GrB also did not result in differences in Annexin V staining. All values indicate the mean of triplicate samples and error bars represent ±1 s.d.

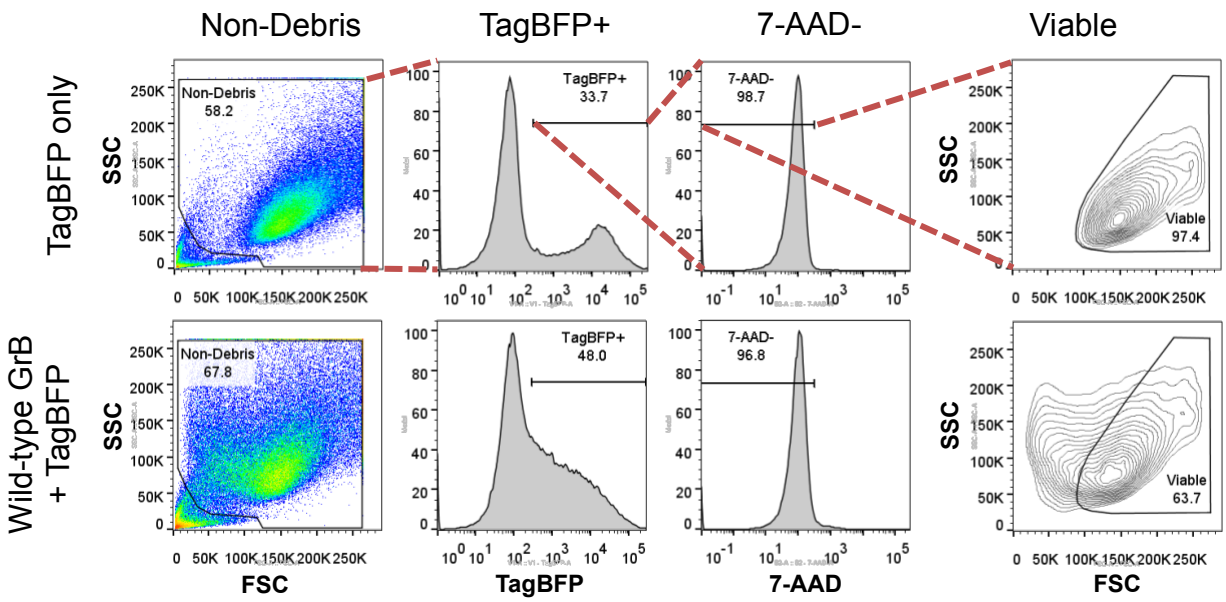

Figure 3.S4. Gating strategy for analysis of GrB-mediated cytotoxicity in transiently transfected HEK293T cells. The "Non-Debris" gate excludes autofluorescent debris. TagBFP marks the transfected population, and 7-AAD exclusion removes necrotic cells. The final SSC vs. FSC scatter allows visualization of physiologically healthy populations, which are defined as "viable." As noted in the text, the % TagBFP+ and % 7-AAD– are statistically indistinguishable between samples transfected with and without wild-type GrB.

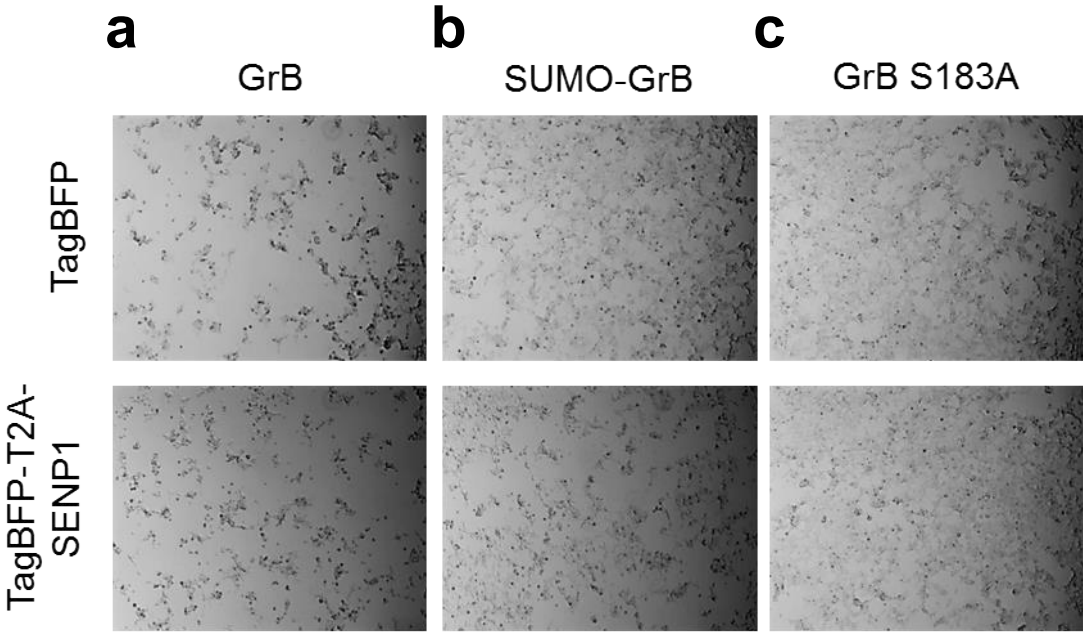

Figure 3.S5. Expression of GrB results in altered cell morphology and loss of adherence by HEK293T cells. HEK293T cells were transiently transfected to co-express either TagBFP or TagBFP-T2A-SENP1 plus (a) wild-type GrB, (b) SUMO-GrB, or (c) GrB S183A. Cells were imaged at 20x magnification 24 hours post-transfection. Cells expressing GrB exhibited compromised cell integrity and detached from the plate surface. Loss of cell adherence was also observed in cells co-expressing SUMO-GrB and SENP1, but not GrB S183A.

Text 3.S1. COVERT DNA sequences.

Kozak-Murine IgGκ leader-Hisx6-DDDDK-GrB:
GCCGCCACCATGGAGACAGACACACTCCTGCTATGGGTGCTGCTGCTCTGGGTTCCAGGT
TCCACAGGTCACCACCATCACCATCACGACGACGACGACAAGATCATCGGGGGACATGAG
GCCAAGCCCCACTCCCGCCCCTACATGGCTTATCTTATGATCTGGGATCAGAAGTCTCTGA
AGAGGTGCGGTGGCTTCCTGATACAAGACGACTTCGTGCTGACAGCTGCTCACTGTTGGG
GAAGCTCCATAAATGTCACCTTGGGGGCCCACAATATCAAGGAACAGGAGCCGACCCAGC
AGTTTATCCCTGTGAAAAGACCCATCCCCCATCCAGCCTATAATCCTAAGAACTTCTCCAAT
GACATCATGCTACTGCAGCTGGAGAGAAAGGCCAAGCGGACCAGAGCTGTGCAGCCCCT
CAGGCTACCTAGCAACAAGGCCCAGGTGAAGCCAGGGCAGACATGCAGTGTGGCCGGCT
GGGGGCAGACGGCCCCCCTGGGAAAACACTCACACACACTACAAGAGGTGAAGATGACA
GTGCAGGAAGATCGAAAGTGCGAATCTGACTTACGCCATTATTACGACAGTACCATTGAGT
TGTGCGTGGGGGACCCAGAGATTAAAAAGACTTCCTTTAAGGGGGACTCTGGAGGCCCTC
TTGTGTGTAACAAGGTGGCCCAGGGCATTGTCTCCTATGGACGAAACAATGGCATGCCTC
CACGAGCCTGCACCAAAGTCTCAAGCTTTGTACACTGGATAAAGAAAACCATGAAACGCTA
CTAA

Kozak-Murine IgGκ leader-Hisx6-DDDDK-GrB S183A:
GCCGCCACCATGGAGACAGACACACTCCTGCTATGGGTGCTGCTGCTCTGGGTTCCAGGT
TCCACAGGTCACCACCATCACCATCACGACGACGACGACAAGATCATCGGGGGACATGAG
GCCAAGCCCCACTCCCGCCCCTACATGGCTTATCTTATGATCTGGGATCAGAAGTCTCTGA
AGAGGTGCGGTGGCTTCCTGATACAAGACGACTTCGTGCTGACAGCTGCTCACTGTTGGG
GAAGCTCCATAAATGTCACCTTGGGGGCCCACAATATCAAGGAACAGGAGCCGACCCAGC
AGTTTATCCCTGTGAAAAGACCCATCCCCCATCCAGCCTATAATCCTAAGAACTTCTCCAAT
GACATCATGCTACTGCAGCTGGAGAGAAAGGCCAAGCGGACCAGAGCTGTGCAGCCCCT
CAGGCTACCTAGCAACAAGGCCCAGGTGAAGCCAGGGCAGACATGCAGTGTGGCCGGCT
GGGGGCAGACGGCCCCCCTGGGAAAACACTCACACACACTACAAGAGGTGAAGATGACA
GTGCAGGAAGATCGAAAGTGCGAATCTGACTTACGCCATTATTACGACAGTACCATTGAGT
TGTGCGTGGGGGACCCAGAGATCAAGAAAACTAGCTTCAAGGGAGATGCCGGAGGCCCT
CTTGTGTGTAACAAGGTGGCCCAGGGCATTGTCTCCTATGGACGAAACAATGGCATGCCT
CCACGAGCCTGCACCAAAGTCTCAAGCTTTGTACACTGGATAAAGAAAACCATGAAACGCT
ACTAA

Kozak-Murine IgGκ leader-Hisx6-SUMO-GrB:
GCCGCCACCATGGAGACAGACACACTCCTGCTATGGGTGCTGCTGCTCTGGGTTCCAGGT
TCCACAGGTCACCACCATCACCATCACTCCGATCAGGAGGCCAAACCATCAACCGAAGAT
CTCGGGGACAAGAAAGAGGGCGAATATATCAAGCTTAAGGTGATTGGCCAAGATAGTAGC
GAAATTCACTTCAAAGTGAAAATGACCACTCACCTGAAGAAACTGAAAGAGTCCTACTGTCA
GCGACAGGGCGTGCCAATGAACAGCCTGAGATTTCTGTTCGAGGGACAGCGAATCGCTGA
TAACCACACACCTAAGGAACTCGGAATGGAAGAAGAGGATGTAATAGAGGTTTACCAGGAA
CAGACCGGAGGGATCATCGGGGGACATGAGGCCAAGCCCCACTCCCGCCCCTACATGGC
TTATCTTATGATCTGGGATCAGAAGTCTCTGAAGAGGTGCGGTGGCTTCCTGATACAAGAC
GACTTCGTGCTGACAGCTGCTCACTGTTGGGGAAGCTCCATAAATGTCACCTTGGGGGCC
CACAATATCAAGGAACAGGAGCCGACCCAGCAGTTTATCCCTGTGAAAAGACCCATCCCC
CATCCAGCCTATAATCCTAAGAACTTCTCCAATGACATCATGCTACTGCAGCTGGAGAGAA
AGGCCAAGCGGACCAGAGCTGTGCAGCCCCTCAGGCTACCTAGCAACAAGGCCCAGGTG
AAGCCAGGGCAGACATGCAGTGTGGCCGGCTGGGGGCAGACGGCCCCCCTGGGAAAAC
ACTCACACACACTACAAGAGGTGAAGATGACAGTGCAGGAAGATCGAAAGTGCGAATCTG
ACTTACGCCATTATTACGACAGTACCATTGAGTTGTGCGTGGGGGACCCAGAGATTAAAAA
GACTTCCTTTAAGGGGGACTCTGGAGGCCCTCTTGTGTGTAACAAGGTGGCCCAGGGCAT

TGTCTCCTATGGACGAAACAATGGCATGCCTCCACGAGCCTGCACCAAAGTCTCAAGCTTT
GTACACTGGATAAAGAAAACCATGAAACGCTACTAA

Kozak-Murine IgGκ leader-Hisx6-ENLYFQ-GrB:
GCCGCCACCATGGAGACAGACACACTCCTGCTATGGGTGCTGCTGCTCTGGGTTCCAGGT
TCCACAGGTCACCACCATCACCATCACGAAAACCTGTACTTCCAAATCATCGGGGGACATG
AGGCCAAGCCCCACTCCCGCCCCTACATGGCTTATCTTATGATCTGGGATCAGAAGTCTCT
GAAGAGGTGCGGTGGCTTCCTGATACAAGACGACTTCGTGCTGACAGCTGCTCACTGTTG
GGGAAGCTCCATAAATGTCACCTTGGGGGCCCACAATATCAAGGAACAGGAGCCGACCCA
GCAGTTTATCCCTGTGAAAAGACCCATCCCCCATCCAGCCTATAATCCTAAGAACTTCTCCA
ATGACATCATGCTACTGCAGCTGGAGAGAAAGGCCAAGCGGACCAGAGCTGTGCAGCCCC
TCAGGCTACCTAGCAACAAGGCCCAGGTGAAGCCAGGGCAGACATGCAGTGTGGCCGGC
TGGGGGCAGACGGCCCCCCTGGGAAAACACTCACACACACTACAAGAGGTGAAGATGACA
GTGCAGGAAGATCGAAAGTGCGAATCTGACTTACGCCATTATTACGACAGTACCATTGAGT
TGTGCGTGGGGGACCCAGAGATTAAAAAGACTTCCTTTAAGGGGGACTCTGGAGGCCCTC
TTGTGTGTAACAAGGTGGCCCAGGGCATTGTCTCCTATGGACGAAACAATGGCATGCCTC
CACGAGCCTGCACCAAAGTCTCAAGCTTTGTACACTGGATAAAGAAAACCATGAAACGCTA
CTAA

Kozak-GrB leader-GrB:
GCCGCCACCATGCAGCCCATCCTGCTCCTTCTGGCCTTCCTGCTGCTGCCCAGGGCCGAC
GCCATCATCGGGGGACATGAGGCCAAGCCCCACTCCCGCCCCTACATGGCTTATCTTATG
ATCTGGGATCAGAAGTCTCTGAAGAGGTGCGGTGGCTTCCTGATACAAGACGACTTCGTG
CTGACAGCTGCTCACTGTTGGGGAAGCTCCATAAATGTCACCTTGGGGGCCCACAATATCA
AGGAACAGGAGCCGACCCAGCAGTTTATCCCTGTGAAAAGACCCATCCCCCATCCAGCCT
ATAATCCTAAGAACTTCTCCAATGACATCATGCTACTGCAGCTGGAGAGAAAGGCCAAGCG
GACCAGAGCTGTGCAGCCCCTCAGGCTACCTAGCAACAAGGCCCAGGTGAAGCCAGGGC
AGACATGCAGTGTGGCCGGCTGGGGGCAGACGGCCCCCCTGGGAAAACACTCACACACA
CTACAAGAGGTGAAGATGACAGTGCAGGAAGATCGAAAGTGCGAATCTGACTTACGCCATT
ATTACGACAGTACCATTGAGTTGTGCGTGGGGGACCCAGAGATTAAAAAGACTTCCTTTAA
GGGGGACTCTGGAGGCCCTCTTGTGTGTAACAAGGTGGCCCAGGGCATTGTCTCCTATGG
ACGAAACAATGGCATGCCTCCACGAGCCTGCACCAAAGTCTCAAGCTTTGTACACTGGATA
AAGAAAACCATGAAACGCTACTAA

Kozak-GrB leader-GrB S183A:
GCCGCCACCATGCAGCCCATCCTGCTCCTTCTGGCCTTCCTGCTGCTGCCCAGGGCCGAC
GCCATCATCGGGGGACATGAGGCCAAGCCCCACTCCCGCCCCTACATGGCTTATCTTATG
ATCTGGGATCAGAAGTCTCTGAAGAGGTGCGGTGGCTTCCTGATACAAGACGACTTCGTG
CTGACAGCTGCTCACTGTTGGGGAAGCTCCATAAATGTCACCTTGGGGGCCCACAATATCA
AGGAACAGGAGCCGACCCAGCAGTTTATCCCTGTGAAAAGACCCATCCCCCATCCAGCCT
ATAATCCTAAGAACTTCTCCAATGACATCATGCTACTGCAGCTGGAGAGAAAGGCCAAGCG
GACCAGAGCTGTGCAGCCCCTCAGGCTACCTAGCAACAAGGCCCAGGTGAAGCCAGGGC
AGACATGCAGTGTGGCCGGCTGGGGGCAGACGGCCCCCCTGGGAAAACACTCACACACA
CTACAAGAGGTGAAGATGACAGTGCAGGAAGATCGAAAGTGCGAATCTGACTTACGCCATT
ATTACGACAGTACCATTGAGTTGTGCGTGGGGGACCCAGAGATCAAGAAAACTAGCTTCAA
GGGAGATGCCGGAGGCCCTCTTGTGTGTAACAAGGTGGCCCAGGGCATTGTCTCCTATGG
ACGAAACAATGGCATGCCTCCACGAGCCTGCACCAAAGTCTCAAGCTTTGTACACTGGATA
AAGAAAACCATGAAACGCTACTAA

Kozak-GrB leader-SUMO-GrB:

GCCGCCACCATGCAGCCCATCCTGCTCCTTCTGGCCTTCCTGCTGCTGCCCAGGGCCGAC
GCCTCCGATCAGGAGGCCAAACCATCAACCGAAGATCTCGGGGACAAGAAAGAGGGCGA
ATATATCAAGCTTAAGGTGATTGGCCAAGATAGTAGCGAAATTCACTTCAAAGTGAAAATGA
CCACTCACCTGAAGAAACTGAAAGAGTCCTACTGTCAGCGACAGGGCGTGCCAATGAACA
GCCTGAGATTTCTGTTCGAGGGACAGCGAATCGCTGATAACCACACACCTAAGGAACTCG
GAATGGAAGAAGAGGATGTAATAGAGGTTTACCAGGAACAGACCGGAGGGATCATCGGGG
GACATGAGGCCAAGCCCCACTCCCGCCCCTACATGGCTTATCTTATGATCTGGGATCAGAA
GTCTCTGAAGAGGTGCGGTGGCTTCCTGATACAAGACGACTTCGTGCTGACAGCTGCTCA
CTGTTGGGGAAGCTCCATAAATGTCACCTTGGGGGCCCACAATATCAAGGAACAGGAGCC
GACCCAGCAGTTTATCCCTGTGAAAAGACCCATCCCCCATCCAGCCTATAATCCTAAGAAC
TTCTCCAATGACATCATGCTACTGCAGCTGGAGAGAAAGGCCAAGCGGACCAGAGCTGTG
CAGCCCCTCAGGCTACCTAGCAACAAGGCCCAGGTGAAGCCAGGGCAGACATGCAGTGT
GGCCGGCTGGGGGCAGACGGCCCCCCTGGGAAAACACTCACACACACTACAAGAGGTGA
AGATGACAGTGCAGGAAGATCGAAAGTGCGAATCTGACTTACGCCATTATTACGACAGTAC
CATTGAGTTGTGCGTGGGGGACCCAGAGATTAAAAAGACTTCCTTTAAGGGGGACTCTGG
AGGCCCTCTTGTGTGTAACAAGGTGGCCCAGGGCATTGTCTCCTATGGACGAAACAATGG
CATGCCTCCACGAGCCTGCACCAAAGTCTCAAGCTTTGTACACTGGATAAAGAAAACCATG
AAACGCTACTAA

Kozak-GrB leader-ENLYFQ-GrB:
GCCGCCACCATGCAGCCCATCCTGCTCCTTCTGGCCTTCCTGCTGCTGCCCAGGGCCGAC
GCCGAAAACCTGTACTTCCAAATCATCGGGGGACATGAGGCCAAGCCCCACTCCCGCCCC
TACATGGCTTATCTTATGATCTGGGATCAGAAGTCTCTGAAGAGGTGCGGTGGCTTCCTGA
TACAAGACGACTTCGTGCTGACAGCTGCTCACTGTTGGGGAAGCTCCATAAATGTCACCTT
GGGGGCCCACAATATCAAGGAACAGGAGCCGACCCAGCAGTTTATCCCTGTGAAAAGACC
CATCCCCCATCCAGCCTATAATCCTAAGAACTTCTCCAATGACATCATGCTACTGCAGCTG
GAGAGAAAGGCCAAGCGGACCAGAGCTGTGCAGCCCCTCAGGCTACCTAGCAACAAGGC
CCAGGTGAAGCCAGGGCAGACATGCAGTGTGGCCGGCTGGGGGCAGACGGCCCCCCTG
GGAAAACACTCACACACACTACAAGAGGTGAAGATGACAGTGCAGGAAGATCGAAAGTGC
GAATCTGACTTACGCCATTATTACGACAGTACCATTGAGTTGTGCGTGGGGGACCCAGAGA
TTAAAAAGACTTCCTTTAAGGGGGACTCTGGAGGCCCTCTTGTGTGTAACAAGGTGGCCCA
GGGCATTGTCTCCTATGGACGAAACAATGGCATGCCTCCACGAGCCTGCACCAAAGTCTC
AAGCTTTGTACACTGGATAAAGAAAACCATGAAACGCTACTAA

Kozak-GrB leader-GlyGlu propeptide-GrB-G4S-mCherry
GCCGCCACCATGCAGCCCATCCTGCTCCTTCTGGCCTTCCTGCTGCTGCCCAGGGCCGAC
GCCGGGGAGATCATCGGGGGACATGAGGCCAAGCCCCACTCCCGCCCCTACATGGCTTA
TCTTATGATCTGGGATCAGAAGTCTCTGAAGAGGTGCGGTGGCTTCCTGATACAAGACGAC
TTCGTGCTGACAGCTGCTCACTGTTGGGGAAGCTCCATAAATGTCACCTTGGGGGCCCAC
AATATCAAGGAACAGGAGCCGACCCAGCAGTTTATCCCTGTGAAAAGACCCATCCCCCATC
CAGCCTATAATCCTAAGAACTTCTCCAATGACATCATGCTACTGCAGCTGGAGAGAAAGGC
CAAGCGGACCAGAGCTGTGCAGCCCCTCAGGCTACCTAGCAACAAGGCCCAGGTGAAGC
CAGGGCAGACATGCAGTGTGGCCGGCTGGGGGCAGACGGCCCCCCTGGGAAAACACTCA
CACACACTACAAGAGGTGAAGATGACAGTGCAGGAAGATCGAAAGTGCGAATCTGACTTA
CGCCATTATTACGACAGTACCATTGAGTTGTGCGTGGGGGACCCAGAGATTAAAAAGACTT
CCTTTAAGGGGGACTCTGGAGGCCCTCTTGTGTGTAACAAGGTGGCCCAGGGCATTGTCT
CCTATGGACGAAACAATGGCATGCCTCCACGAGCCTGCACCAAAGTCTCAAGCTTTGTACA
CTGGATAAAGAAAACCATGAAACGCTACGGGGGTGGTGGGAGCATGGTGAGCAAGGGCG
AGGAGGATAACATGGCCATCATCAAGGAGTTCATGCGCTTCAAGGTGCACATGGAGGGCT

CCGTGAACGGCCACGAGTTCGAGATCGAGGGCGAGGGCGAGGGCCGCCCCTACGAGGG
CACCCAGACCGCCAAGCTGAAGGTGACCAAGGGTGGCCCCCTGCCCTTCGCCTGGGACA
TCCTGTCCCCTCAGTTCATGTACGGCTCCAAGGCCTACGTGAAGCACCCCGCCGACATCC
CCGACTACTTGAAGCTGTCCTTCCCCGAGGGCTTCAAGTGGGAGCGCGTGATGAACTTCG
AGGACGGCGGCGTGGTGACCGTGACCCAGGACTCCTCCTTGCAGGACGGCGAGTTCATC
TACAAGGTGAAGCTGCGCGGCACCAACTTCCCCTCCGACGGCCCCGTAATGCAGAAGAAG
ACCATGGGCTGGGAGGCCTCCTCCGAGCGGATGTACCCCGAGGACGGCGCCCTGAAGG
GCGAGATCAAGCAGAGGCTGAAGCTGAAGGACGGCGGCCACTACGACGCTGAGGTCAAG
ACCACCTACAAGGCCAAGAAGCCCGTGCAGCTACCCGGCGCCTACAACGTCAACATCAAG
TTGGACATCACCTCCCACAACGAGGACTACACCATCGTGGAACAGTACGAACGCGCCGAG
GGCCGCCACTCCACCGGCGGCATGGACGAGCTGTACAAGTAA

Chapter 4. Reprogramming T-cell Lytic Selectivity with Engineered Granzyme B Switches

ABSTRACT

Advances in genome-editing technologies are now enabling the design and implementation of increasingly sophisticated cell-based devices. While T cells engineered to express CD19-targeting chimeric antigen receptors (CARs) have yielded complete and durable responses in patients with relapsed B-cell cancers, the lack of tumor-exclusive candidate surface antigens poses an inherent risk for on-target, off-tumor toxicities. We propose to address this barrier to clinical translation by reprogramming T cells to sense and respond to intracellular disease signatures, thus expanding the repertoire of candidate antigens that can be targeted by adoptive T-cell therapy. Specifically, we are genetically replacing the endogenous and constitutively cytotoxic granzyme B (GrB) payload with a GrB-based switch, termed Cytoplasmic Oncoprotein VErifier and Response Trigger (COVERT), which induces target-cell apoptosis only when activated by interaction with an intracellular target antigen within diseased cells. However, the sheer amount of genetic manipulation required to disable wild-type GrB and introduce both COVERT and CAR expression represents a significant challenge for T-cell manufacture. Here, we systematically optimize the multiplexed delivery of CRISPR/Cas9 components and homology-directed repair templates (HDR-Ts) to develop a robust workflow for COVERT/CAR-T cell engineering. We demonstrate the feasibility and flexibility of COVERT/CAR-T cell manufacturing by simultaneously integrating a small ubiquitin-like modifier (SUMO)-GrB fusion into the GrB locus, and either a HER2 CAR or a CD19 CAR into the T-cell receptor alpha chain constant region (TRAC) locus, and provide the first demonstrations of selective T-cell–mediated cytotoxicity in response to MHC-independent intracellular antigen expression.

INTRODUCTION

The ability to efficiently generate defined genomic modifications in primary human cells has long been an outstanding goal for gene therapy and cellular therapeutics engineering. Programmable site-specific nucleases including zinc-finger nucleases (ZFNs), transcription activator-like effector nucleases (TALENs), and the clustered regularly interspaced short palindromic repeats (CRISPR)/CRISPR-associated protein 9 (Cas9) system are now enabling the perturbation of chromosomal elements for the systematic elucidation of novel genetic relationships, as well as the precise construction of next-generation mammalian cell-based devices[1,2]. In particular, engineered T cells have emerged as promising targets and instruments for therapeutic applications. For example, ZFN-mediated disruption of C-C chemokine receptor 5 (CCR5) or C-X-C chemokine receptor 4 (CXCR4) coreceptor expression confers immunity against human immunodeficiency virus (HIV) infection to edited $CD4^+$ T-cell populations[3], while CRISPR/Cas9-edited programmed cell death protein 1 (PD-1)–knockout T cells capable of resisting immunosuppression in the tumor microenvironment are currently under clinical evaluation[4]. As advances in bioinformatics reveal new opportunities for therapeutic intervention, the development of pioneering T-cell technologies requires increasingly efficient gene-editing strategies to support progressively sophisticated therapeutic designs.

Adoptive T-cell therapy—a paradigm in which disease-targeting T cells serve as the therapeutic modalities for the treatment of cancers, chronic viral infections, and autoimmune disorders—has demonstrated remarkable curative potential in patients with relapsing B-cell malignancies[5–8], but clinical translation has not been extended to most cancers. In particular, the lack of tumor-exclusive surface markers presents a fundamental challenge to adoptive T-cell therapy due to the inherent risk for 'on-target, off-tumor' toxicities[9–11]. To address this barrier, we propose to directly reprogram T cells to interrogate target cells for the expression of intracellular disease signatures with granzyme B (GrB)-based cytotoxic switches, termed Cytoplasmic Oncoprotein VErifier and Response Trigger (COVERT). These COVERT switches are delivered

into target cells in the same manner as wild-type GrB, but only initiate cytotoxic cascades upon encounter with intracellular target antigens, thus sparing misidentified normal cells. However, achieving COVERT-mediated regulation of T-cell lytic function hinges on the efficient disruption of endogenous, constitutively active cytotoxic payloads, particularly wild-type GrB. Meanwhile, additional genomic modifications are also necessary to stably impart COVERT and chimeric antigen receptor (CAR) expression. Thus, the sheer number of genetic modifications required poses a formidable engineering challenge, further complicated by the limited timeframe in which genetic manipulations are permissible in primary human T cells.

Unlike immortalized cell lines, primary cells can only be obtained from biopsied tissues and have finite capacities for self-renewal, contributing to limited cell yields and shorter life spans. Primary human T cells face additional engineering constraints as the transfer of exogenous nucleic acids and proteins is markedly inefficient for unstimulated cells, while repeated antigen stimulation renders T cells prone to T-cell exhaustion, with the irreversible loss of effector function[12,13]. This dichotomy between the impacts of cell activation severely restricts the amount of genetic manipulation that clinical T-cell products can withstand. Furthermore, clinical applications often require therapeutic cell-manufacturing processes to operate with very short turnaround times, in order to treat patients within the narrow treatment window between T-cell isolation and further disease progression[14]. As a result, there has been increasing interest in developing gene-transfer technologies and manufacturing workflows that can efficiently import multiple genetic operations into primary human T cells.

Traditional T-cell engineering processes have largely relied on viral and ‘Sleeping Beauty’ transposon-based delivery of stably integrating genetic elements[14,15]. The most prevalent gene-transfer vectors include lentiviral and retroviral systems derived from the HIV genome, each theoretically capable of packaging up to ~9 kilobase pairs (kb) of genetic material. While this is usually sufficient for the transduction of a single chimeric antigen receptor (CAR) spanning ~2 kb, the Chen lab has previously determined that the efficiency of gene transfer drops substantially

when two distinct CARs are packaged in tandem (~4-5 kb). Apart from construct packaging limitations, the randomly integrating nature of viral and transposon-based platforms preclude the targeted disruption of genetic elements, and also raise safety concerns over the risk for proto-oncogene activation[16]. Alternative strategies, such as mRNA electroporation, avoid complications that may arise from random gene integration, but only facilitate transient gene expression, mitigating the long-term benefits of adoptive T-cell therapy.

In contrast, site-specific genome-editing technologies mediate precise double-stranded breaks (DSBs) at pre-determined genomic loci. Since human cells commonly mend by non-homologous end-joining (NHEJ) with a high frequency of frame-shifting insertions or deletions (indels), targeted DSB formation thus enables a means to silence endogenous gene expression[17,18]. Alternatively, a homology-directed repair (HDR) template can be supplied to site-specifically integrate exogenous genes at the DSB, enabling greater control over transgene copy number, as well as greater predictability over the DNA footprint and its impact on therapeutic safety[19,20]. While earlier genome-editing tools such as ZFNs and TALENs feature nucleases tethered to individually optimized strings of DNA-binding protein domains, CRISPR single-guide RNAs (sgRNAs) direct Cas9 nuclease activity via Watson–Crick base-pairing with target DNA, yielding a system more conducive to rapid design and multiplexing for high-throughput applications[21,22]. To further streamline nuclease delivery, researchers recently developed protocols to directly electroporate pre-formed CRISPR/Cas9 ribonucleoprotein (RNP) complexes into cells, thereby eliminating the transcriptional, translational, and assembly burden for expressing each component individually[23]. Transient delivery of CRISPR/Cas9 RNPs via electroporation also limits T-cell exposure to nuclease activity, reducing the risk of off-target DNA cleavage and immunogenicity[23]. In the same vein, HDR templates are typically delivered transiently, as single- or double-stranded DNA oligonucleotides [23,24], or via packaging into non-integrating adeno-associated virus (AAV)[25,26]. Utilizing this approach, one recent study demonstrated that precise CAR integration into the T-cell receptor alpha chain constant region

(TRAC) locus enabled T cells to perform more robustly than virally generated counterparts in an *in vivo* model, possibly due to more uniform CAR expression amongst the engineered T-cell population[19].

The rapid progression of genome-editing technologies has opened the door for the design and implementation of sophisticated cell-based systems with vast therapeutic potential. Here, we present an optimized workflow for the manufacture of COVERT/CAR-T cells, as well as the first example of COVERT regulation over T-cell–mediated cytotoxicity specifically in response to intracellular tumor antigen expression.

METHODS

DNA Constructs. DNA was chemically synthesized as oligonucleotides or gBlocks by Integrated DNA Technologies (Coralville, IA) and assembled using standard molecular cloning techniques. Unless otherwise indicated, all constructs were cloned into the epHIV7 lentiviral expression vector[27]. The QPY variant of human GrB was used in this study, and SUMO1t-GrB was generated via isothermal DNA assembly, as described in Chapter 3. The CD19 CAR (short IgG4 hinge, 4-1BB costimulatory domain) was constructed as previously reported[28], and the HER2 CAR (long IgG4 hinge-CH2-CH3 spacer, CD28 costimulatory domain) was previously cloned by Eugenia Zah. For CRISPR/Cas9 experiments, the SpCas9 and SaCas9 sequences were obtained from the pX330 and pX602 vectors via Addgene (plasmids 42230 and 61593), respectively. The MSCV-IRES-EGFP retroviral vector and pHIT60 and RD114 retroviral packaging vectors were generous gifts from Dr. Steven Feldman (National Cancer Institute). Target-cell lines were generated by stable integration of mCherry-NLS or mCherry-NLS-T2A-SENP1, inserted downstream of the 5' LTR in a modified MSCV vector with a woodchuck hepatitis virus posttranscriptional regulatory element (WPRE) inserted at the ClaI site by restriction-ligation cloning. The pX602 AAV2 construct plasmid listed above also served as the

base vector for AAV6 constructs, and the pXX6 and pHelper AAV6 packaging vectors were kind gifts from Dr. David Schaffer (UC Berkeley).

Cell Lines. HEK293T, MCF7, Jurkat E6, and H9 cells were obtained from ATCC (Manassas, VA) in 2011, and ATCC verified the identity of each purchased cell line by short tandem repeat analysis prior to shipment. Parental K562 cells were a gift from Dr. Laurence Cooper in 2001, and Raji cells were a generous gift from Dr. Michael C. Jensen (Seattle Children's Research Institute); the cell line was originally obtained from ATCC in 2003 and both K562 and Raji cell lines were authenticated again by short tandem repeat profiling at the University of Arizona Genetics Core in 2015. Cells were cultured in DMEM (HEK293T and MCF7), or RPMI-1640 (Jurkat, H9, and K562) supplemented with 10% heat-inactivated FBS (HI-FBS). All mammalian cell cultures were maintained at 37°C and 5% CO_2.

Cell Transfection. HEK293T cells were seeded at 2.5 x 10^4 cells/0.25 mL/well in 48-well plates, 24 hours prior to transfection with 250 ng plasmid DNA and 15 nmol linear polyethylenimine (PEI, 25 kDa). DNA mixtures diluted in 150 mM NaCl were complexed with PEI, incubated at room temperature for 15 min, and then applied to seeded HEK293T cells. For IVT mRNA or purified protein nucleofection experiments, Jurkat or primary human T cells (5 x 10^6) were resuspended in 100 µL of Amaxa Cell Line Nucleofector™ V Solution (Lonza, Walkersville, MD) and electroporated with 3.1 pmol IVT mRNA (corresponding to 5 µg of Cas9-T2A-EGFP mRNA) or 300 pmol purified protein using Program X-001 (Jurkat) or Program T-017 (primary human T cells) of the Nucleofector™ 2b Device (Lonza), according to the manufacturer's protocol. Nucloefected cells were allowed to incubate at room temperature within the nucleofection cuvette for 10 minutes prior to transfer into complete T-cell media. Primary human T-cell cultures were also supplemented with 50 U/mL IL-2 (Life Technologies) and 1 ng/mL IL-15 (Peprotech).

Surveyor *In Vitro* Cleavage Assay. Genomic DNA was harvested from CRISPR/Cas9-treated cells 48 hours post-exposure via the Qiagen DNeasy Blood & Tissue kit, according to manufacturer's instructions. Oligos flanking the CRISPR/Cas9 cut site were used to PCR amplify a ~700 bp fragment, and 400 ng of purified PCR product from each sample was mixed with 400 ng of purified PCR product from wild-type genomic DNA in 20 µL of 1x NEB Taq Polymerase Buffer (New England Biolabs, Ipswich, MA). DNA mixtures were allowed to form duplexes in a thermocycler with the following program: 95°C for 10 min, 95°C to 85°C at -2°C/sec, 85°C for 1 min, 85°C to 75°C at -0.3°C/sec, 75°C for 1 min, 75°C to 65°C at -0.3°C/sec, 65°C for 1 min, 65°C to 55°C at -0.3°C/sec, 55°C for 1 min, 55°C to 45°C at -0.3°C/sec, 45°C for 1 min, 45°C to 35°C at -0.3°C/sec, 35°C for 1 min, 35°C to 25°C at -0.3°C/sec, 25°C for 1 min, hold at 12°C. Following duplex formation, 10 µL of the duplexed product was reacted with 1 µL of Surveyor Nuclease (IDT) supplemented with 1 µL of Surveyor Enhancer, 1.5 µL of 0.15 M $MgCl_2$, and 1.5 µL of 10x NEB Tag Polymerase Buffer. Reactions were incubated at 42°C for 30 min and terminated by addition of 1.67 µL of Stop Solution (supplied in kit), prior to loading into a 2% agarose gel. Untreated, duplexed DNA was also loaded to serve as an undigested control.

***In Vitro* Transcription.** Templates for IVT mRNA or IVT sgRNA were cloned with a T7 promoter immediately preceding the transcribed sequence. If the first base was not a G, a G was added to improve the efficiency of T7 polymerase activity. IVT mRNA was generated via the Ambion MEGAscript® T7 Transcription kit (ThermoFisher Scientific, Waltham, MA), with each 20 µL reaction supplemented by 1 µL of GTP, according to the manufacturer's protocol. IVT sgRNA was generated via the Ambion MegaShortscript™ T7 Transcription kit (ThermoFisher Scientific) with 300 ng of template PCR product, or the NEB HiScribe™ Quick High Yield RNA Synthesis kit (New England Biolabs) with 600 ng of template PCR product, according to manufacturer's protocols.

Cas9 Protein Purification. His-tagged, SV40 NLS-SpCas9-NP NLS was cloned into the Novagen pET28a vector (EMD Millipore, Burlington, MA) behind the T7 promoter and subsequently transformed into the BL21(DE3) *E. coli* expression strain. Each production batch was initiated by inoculating a single re-streaked colony into 300 mL of Luria-Bertani (LB) media supplemented with 35 µg/mL of kanamycin-sulfate and 1% glucose at 37°C and 190 rpm. At 16-18 hours post-inoculation, the starter culture was back-diluted 1:100 into 1 L of LB plus kanamycin in 2 L baffled shake flasks at 37°C and 190 rpm. Culture density was monitored until OD_{600} reached 0.5, at which point Cas9 expression was induced with 400 µM isopropyl β-D-1-thiogalactopyranoside (IPTG), and flasks were moved to shake at 18-25°C overnight. Cells were harvested by centrifugation at 2500 *x g* for 20 min and resuspended in 50 mL of binding buffer (500 mM NaCl, 20 mM Tris, pH 8.0) per 1 L of induction culture. Resuspended cells were aliquoted into 50 mL Falcon tubes along with 1 Protease Inhibitor Cocktail tablet (ThermoFisher Scientific) and placed in an ice-water bath, prior to sonication with the following program: 25 W amplitude for 7.5 x 20 sec “on”, 30 sec “off” pulses. Lysates were combined into PPCO centrifuge tubes and spun down at 16,000 *x g* for 20 min at 4°C, and supernatants were batch-bound to Ni-NTA resin (Life Technologies) in binding buffer for 1 hour prior to being washed three times with binding buffer supplemented with 20 mM imidazole (Fisher Scientific, Hampton, NH), and then eluted with binding buffer supplemented with 500 mM imidazole through a chromatography column. Eluted proteins were buffer-exchanged into Cas9 storage buffer (20 mM HEPES, 150 mM KCl, 1 mM TCEP, pH 7.5, 10% glycerol) by successive concentration and resuspension steps in Amicon centrifugal columns (10 kDa; EMD Millipore, Billierica, MA) following manufacturer’s recommendations. Protein concentration was determined via Bradford assay (Bio-Rad, Hercules, CA) and diluted to 10 mg/mL prior to aliquoting into 0.65 mL microfuge tubes and storage at -80°C.

CRISPR/Cas9 RNP *In Vitro* Cleavage Assay. IVT sgRNAs were pre-complexed with purified SpCas9 protein at the indicated sgRNA:Cas9 ratios prior to co-incubation with a PCR amplicon containing the target DNA sequence for 30 min at room temperature. *In vitro* cleavage assay reaction products were subsequently resolved on an agarose gel.

Primary Human T-cell Isolation and Culture. Primary human $CD8^+$ T cells were isolated from healthy donor blood samples obtained from the UCLA Blood & Platelet Center using the RosetteSep $CD8^+$ Human T-cell Enrichment Cocktail (Stemcell Technologies, Vancouver, Canada), according to the manufacturer's protocol, and subsequently cryopreserved at 25-50 x 10^6 cells/mL in complete T-cell media supplemented with 10% DMSO. Thawed T cells were seeded at 1 x 10^6 cells/mL in T-cell media (RPMI-1640 supplemented with 10% HI-FBS), and stimulated with anti-CD3/CD28 Dynabeads (Life Technologies, Carlsbad, CA) at 1:1 cell:bead ratio. Cultures were supplemented with 50 U/mL IL-2 (Life Technologies) and 1 ng/mL IL-15 (Peprotech, Rocky Hill, NJ) every 48 hours unless noted otherwise.

Lentivirus Production and Transduction. HEK293T cells were seeded at 3 x 10^6 cells/9 mL complete DMEM/10-cm dish 24 hours prior to transfection by the linear PEI method. Sixteen hours post-transfection, cells were washed with 10 mL of phosphate buffered saline (PBS) and cultured in DMEM plus 10% HI-FBS and 60 mM sodium butyrate. Viral supernatants were harvested on each of the two subsequent days post-media change, and cell debris was removed by centrifugation followed by filtration through a 0.45-µm low–protein-binding membrane. Viral supernatants collected at 24 hours post-media change was mixed with 40% polyethylene glycol 8000 (PEG 8000) and rotated overnight at 4°C. PEGylated lentivirus particles were pelleted by centrifugation at 2000 *x g* for 20 min at 4°C and resuspended in the viral supernatant harvested at 48 hours post-media change prior to ultracentrifugation at 24,500 rpm for 1 hour and 34 min at 4°C using a SureSpin 360 rotor in a WX Sorvall 90 Ultra ultracentrifuge (ThermoFisher Scientific).

After decanting the supernatant, viral pellets were dissolved in 200 µL of serum-free RPMI-1640 for 1 hour at 4°C and aliquoted for storage at -80°C.

CRISPR/Cas9 RNP Nucleofection. Chemically synthesized sgRNAs (Synthego, Menlo Park, CA) were ordered with 2'-O-methyl analogs and 3' phosphorothioate internucleotide linkages at the 3 bases on both 5' and 3' ends for GrB sgRNA#9 (G*C*C*AGGGCAGACAUGCAGUG) and TRAC sgRNA#1 (C*A*G*GGUUCUGGAUAUCUGU). Each sgRNA was resuspended to 100 µM in nuclease-free Tris-HCl pH 8.0 and aliquoted for storage at -20°C upon arrival. 3 µL of thawed sgRNA was diluted with 4.5 µL of nuclease-free H_2O in a 0.65 mL microfuge tube, while 5 µL of thawed in-house purified SpCas9 protein (10 mg/mL) was diluted with 2.5 µL of Cas9 storage buffer in a separate microfuge tube. CRISPR/Cas9 RNP complexes were assembled by adding diluted Cas9 to diluted sgRNA at 1:1 sgRNA:Cas9 ratio over a period of ~30 seconds, while swirling gently. Complexing reactions were allowed to incubate at room temperature for at least 10 minutes prior to nucleofection. 5 x 10^6 primary human $CD8^+$ T cells were washed 3 times with PBS (no FBS) via centrifugation at 100 *x g* for 10 min prior to resuspension in 100 µL of Ingenio® electroporation solution (Mirus Bio LLC, Madison, WI) and electroporated with the entire 300 pmol RNP complexing mixture using Program T-017 of the Nucleofector™ 2b Device (Lonza), according to the manufacturer's protocol. Nucloefected cells were allowed to incubate at room temperature within the nucleofection cuvette for 10 minutes prior to transfer into complete T-cell media supplemented with 50 U/mL IL-2 (Life Technologies) and 1 ng/mL IL-15 (Peprotech).

AAV6 Production and Transduction. HEK293T cells were seeded at 3 x 10^6 cells/9 mL complete DMEM/10-cm dish 24 hours prior to transfection by the linear PEI method. Three days post-transfection, cells were detached by scraping with a rubber policeman, resuspended in the original supernatant, and pelleted by centrifugation at 1620 *x g* for 2.5 min. After decanting the supernatant, cell pellets were resuspended in 0.8 mL of lysis buffer (50 mM Tris base, 150 mM

NaCl, pH 8.2) per 10-cm dish. Lysates were subjected to three cycles of freeze-thaw in liquid nitrogen and a 37°C water bath and treated with 10 U/mL Benzonase (EMD Millipore) at 37°C for 45 min. Supernatants were clarified by centrifugation at 13,200 *x g* for 10 min and combined into a 50 mL Falcon tube for storage at 4°C. AAV6 particles were layered on top of an iodixanol (Optiprep; Stemcell Technologies) density gradient (top to bottom: AAV6 lysate, 15% iodixanol, 25% iodixanol, 40% iodixanol, 54% iodixanol) and spun at 30,000 rpm for 18 hours in sealed polyallomer tubes using a SureSpin 360 rotor in a WX Sorvall 90 Ultra ultracentrifuge. Purified AAV6 particles were obtained by syringe needle puncture and extraction of the interfacial layer between the 40% iodixanol and 54% iodixanol layers, and subsequently buffer-exchanged into PBS + 0.001% Tween-20 by successive concentration and resuspension steps in Amicon centrifugal columns (10 kDa; EMD Millipore). For HDR template delivery, CRISPR/Cas9 RNP-nucleofected primary human T cells were seeded at 1 x 10^6 cells/500 µL complete T-cell media/well in a 48-well plate (assuming no cell death from the nucleofection), and incubated at 37°C for 10 minutes prior to addition of 50 µL of purified, buffer-exchanged AAV6 (per HDR target locus).

Flow Cytometry. For purified protein delivery experiments, cells were washed once in 1x PBS 1 hour post-nucleofection with SaCas9-G4S-sfGFP, prior to data acquisition on a MACSQuant VYB (Miltenyi Biotec, San Diego, CA). For genome-editing experiments involving the TRAC locus, cells were stained with a biotinylated antibody for TCRα/β (clone IP26; Biolegend, San Diego, CA) followed by a secondary streptavidin antibody conjugated to PE (Jackson ImmunoResearch, West Grove, PA). CAR expression was determined by antibody staining for FLAG-tag (clone L5; Biolegend). For intracellular staining experiments, cells were fixed with 1.5% formaldehyde in T-cell media for 15 min prior to permeabilization with ice-cold methanol for 30 min. Cells were subsequently stained with antibodies for GrB (clone GB11; Biolegend) or an isotype control (clone

MOPC-21; Biolegend). Compensation and data analysis were performed using FlowJo Data Analysis software (TreeStar, Ashland, OR).

Western Blot. Lysates were prepared by incubating cells in lysis buffer (150 mM NaCl, 20 mM Tris pH7.2, 1% (v/v) Triton-X) on ice for 45 min, and clarified of nuclear debris by centrifugation at 20,000 *x g* for 10 min. The protein concentration of the supernatant was determined via Bradford assay (Bio-Rad). Protein samples were resolved on 4-12% bis-tris SDS-PAGE gels, blotted onto nitrocellulose membranes, and probed with antibodies for GrB (clone 2C5; Santa Cruz Biotech, Dallas, TX) or SENP1 (clone C12; Santa Cruz Biotech), followed by staining with an anti-mouse secondary antibody conjugated to horseradish peroxidase (HRP; Jackson ImmunoResearch). Blots were visualized using SuperSignal West Pico Chemiluminescent Substrate (ThermoFisher Scientific).

TIDE Analysis. Genomic DNA was harvested via the Qiagen DNeasy Blood & Tissue kit, according to manufacturer's instructions. Oligos flanking the CRISPR/Cas9 cut site were used to PCR amplify a ~900 bp fragment for Sanger sequencing (Retrogen, San Diego, CA). Chromatograms were subsequently uploaded to the TIDE calculator web tool (www.tide.deskgen.com) for % indel analysis with the following parameters: left boundary, 200; decomposition window, 300-500; indel size range, 50.

FACS. Cells were washed and resuspended at 10-20 x 10^6 cells/mL in PBS + 2 % HI-FBS, and sorted on pre-sterilized FACSAriaI, FACSAriaII, or FACSAriaIII instruments at the UCLA Flow Cytometry Core Facility.

IncuCyte. MCF7 cells engineered to express NLS-tagged mCherry were seeded at 1 x 10^4 cells/well in a 96-well flat-bottom plate and co-incubated with CAR-expressing primary human

$CD8^+$ T cells at 1:1 E:T ratio in complete T-cell media, where E denotes the number of CAR^+ T cells. Images were acquired on the IncuCyte ZOOM Live Cell Imaging System (Essen Bioscience) every 2 hours. The number of $mCherry^+$ cells was normalized to the number of $mCherry^+$ cells seeded into each well at the time of the 1st challenge.

Repeated Antigen Challenge Assay. Engineered $CD19^+$ K562 target cells were seeded at 1 x 10^5 cells/well in a 48-well plate and co-incubated with CAR-expressing primary human $CD8^+$ T cells at 1:1 E:T ratio in complete T-cell media, where E denotes the number of CAR^+ T cells. Media color and culture density were routinely evaluated, and if necessary, half-media changes were performed to mitigate nutrient inhibition. Every 48 hours, 50 µL was harvested from resuspended samples to quantify the number of surviving $mCherry^+$ target cells and $mCherry^-$ T cells. Following sample harvest, 1 x 10^5 fresh target cells were added to each culture. Target-cell fold-survival and T-cell fold-expansion are normalized to the number of cells seeded at the time of the 1st challenge.

Statistics. Statistical significance was determined via two-tailed, homoscedastic Student's *t*-test with a *p*-value cutoff of 5E-2.

RESULTS

Packaging and expression limit lentiviral delivery of CRISPR/Cas9 to primary human T cells

Lentiviral vectors have become the workhorse gene-transfer technology for primary human T-cell engineering due to the stability and efficiency of gene transfer, as well as the relatively low toxicity to T cells. Since our prior study in Chapter 2 indicates that the COVERT platform may require complete disruption of endogenous GrB expression, we rationalized that

lentiviral integration may represent an ideal delivery platform to achieve prolonged exposure of CRISPR/Cas9 components targeting the GrB locus and guarantee eventual NHEJ-mediated knockout. We started by cloning a panel of sgRNAs targeting exon 2 of GrB into the pX330 CRISPR/Cas9 plasmid described in Cong *et al.*[29], and transfecting HEK293T cells to transiently express both the sgRNA and Cas9 protein (Figure 4.1a). Genomic DNA was harvested 48 hours post-transfection and the region spanning the expected CRISPR/Cas9 cut sites was amplified via polymerase chain reaction (PCR) prior to denaturing and re-hybridization with WT amplicons for evaluation of indel formation by a Surveyor nuclease *in vitro* cleavage assay (Figure 4.1b). The Surveyor nuclease recognizes and cleaves mismatched base pairs (bp) that result from annealing between DNA strand(s) altered during NHEJ-mediated repair, enabling agarose gel-based quantification of the fraction of mutated PCR-amplified genomic DNA. All on-target sgRNAs enabled cleavage of the GrB locus, with GrB sgRNA#2 exhibiting the greatest cleavage efficiency (Figure 4.1b).

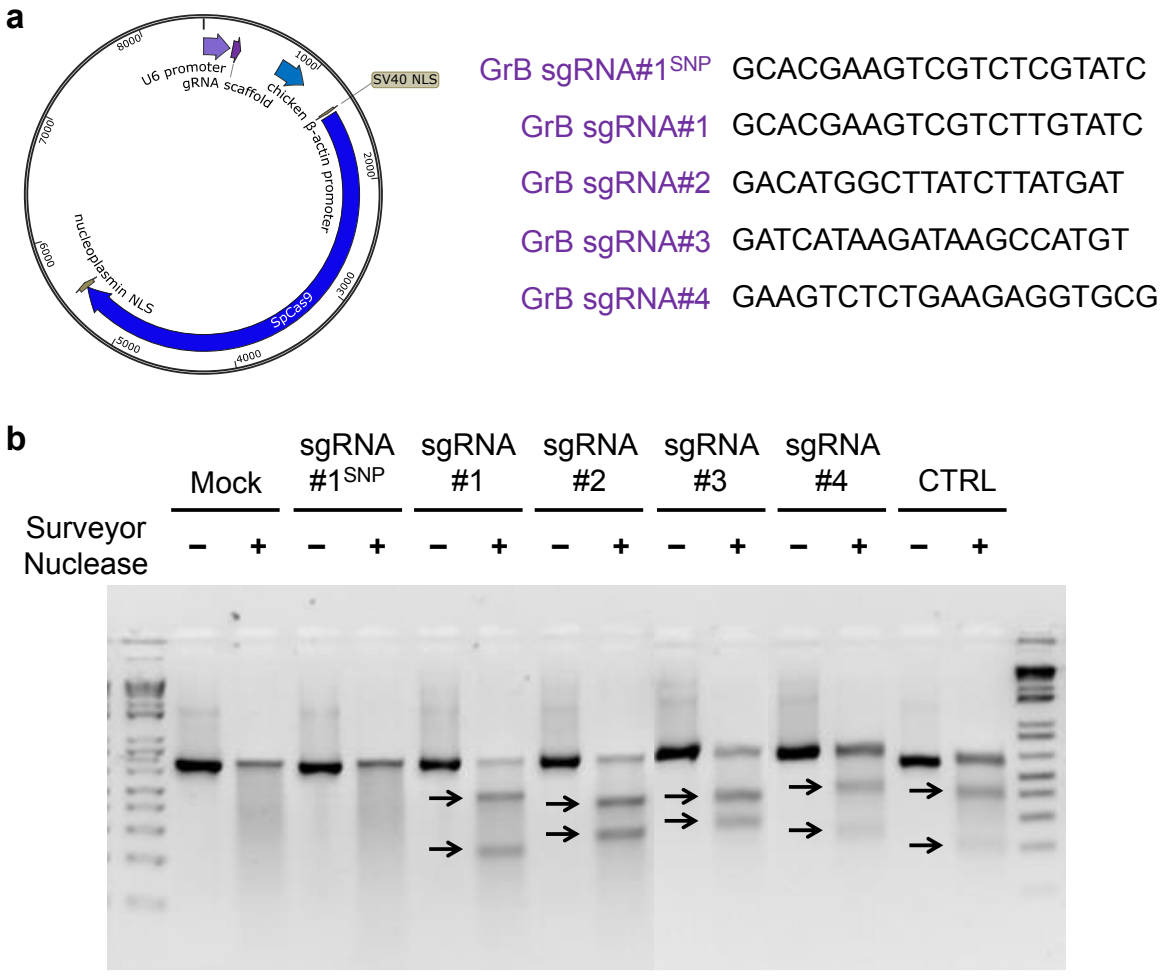

Figure 4.1. A panel of sgRNAs enables efficient indel formation at the GrB locus in transiently transfected HEK293T cells. (a) A panel of sgRNAs targeting DNA sequences located in exon 2 of GrB was cloned into the pX330 CRISPR/Cas9 vector (Addgene #42230) behind the U6 pol III promoter. GrB sgRNA#1^{SNP} differs from GrB sgRNA#1 by a single DNA base at a position known to contain a single-nucleotide polymorphism (SNP). (b) Genomic DNA was isolated from HEK293T cells 48 hours following transfection with the panel of GrB sgRNAs in the CRISPR/Cas9 plasmid. A 754-bp fragment spanning GrB exon 2 was PCR-amplified from the harvested genomic DNA and then denatured and re-hybridized with WT amplicons prior to evaluation of indel formation via a Surveyor nuclease cleavage assay. Genomic DNA was harvested from mock-transfected HEK293T cells as a negative control, while the positive cleavage control (CTRL) was supplied by the Surveyor assay kit. The arrows indicate the expected fragment size for successful mismatch generation at the respective CRISPR/Cas9 cut sites.

An 'all-in-one' CRISPR/Cas9 lentiviral vector was designed to encode a human U6 pol III promoter driving the expression of GrB sgRNA#2, along with a strong, constitutive EF1α promoter to drive the expression of a nuclear localization sequence (NLS)-tagged *S. pyogenes* Cas9 linked

to a fluorescent protein transduction marker via a 2A self-cleaving peptide (Figure 4.2a). Although the CRISPR/Cas9 lentivirus construct spanned only 8.5 kb between the long-terminal repeats (LTRs), and should therefore be within the lentivirus packaging limit, lentiviral titers were consistently an order-of-magnitude lower than the titers obtained for batches of various CAR-encoding lentiviruses prepared in the same virus production cycle (Figure 4.2a,b). Consistent with our results, other groups have demonstrated that the packaging efficiency of engineered lentiviral vectors strongly correlates with construct size, with log reductions in viral titers for every additional ~2 kb[30]. Unsurprisingly, less than 5% of lentivirus-treated primary human $CD4^+$ T cells stably integrated the CRISPR/Cas9 construct, while stable transduction was undetectable in primary human $CD8^+$ T cells (Figure 4.2c). To evaluate whether stable expression enabled CRISPR/Cas9-mediated disruption of the GrB locus, we isolated both the positively and negatively transduced $CD4^+$ populations via fluorescence-activated cell sorting (FACS) and probed for GrB expression by western blot. Interestingly, the degree of GrB disruption in lentivirus-transduced $CD4^+$ T cells was similar between populations sorted for $mCherry^+$ and $mCherry^-$ (Figure 4.2d), indicating that the duration of Cas9 expression did not necessarily correlate with a greater incidence of GrB knockout.

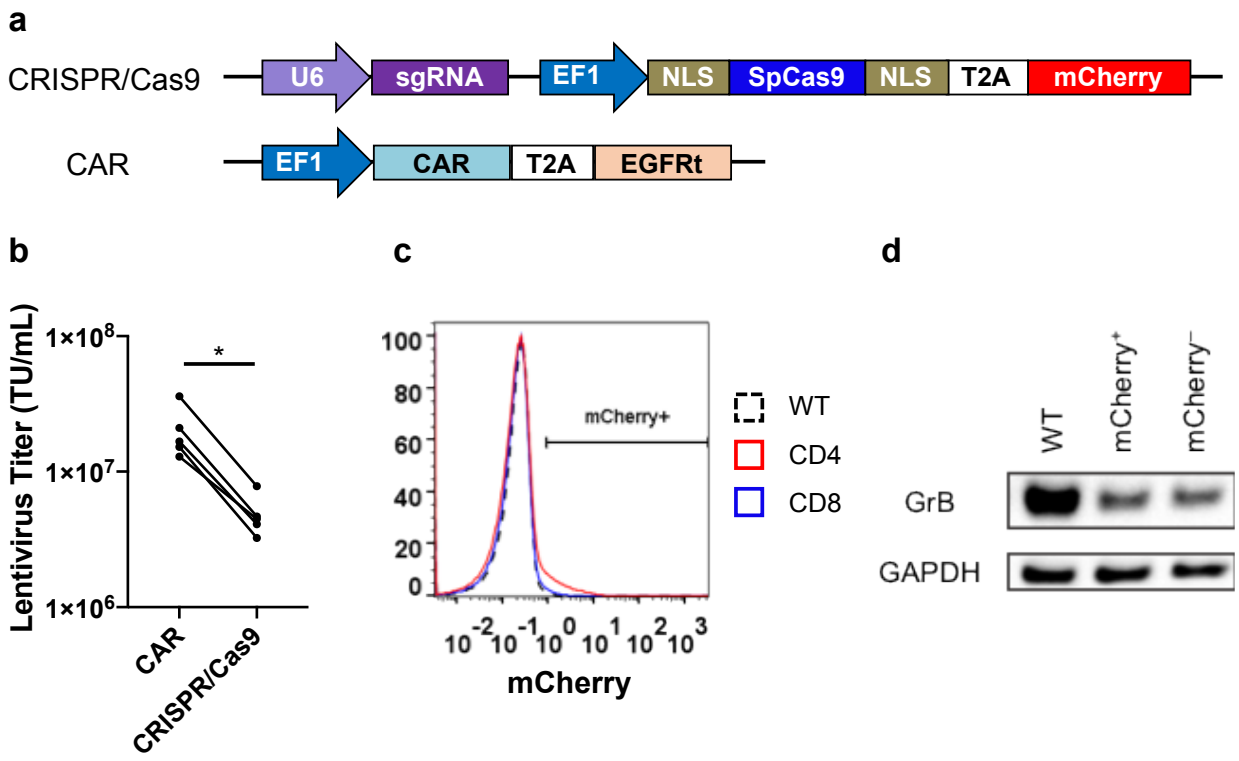

Figure 4.2. Poor lentivirus titers prevent efficient integration of CRISPR/Cas9 components into primary human T cells. (a) An 'all-in-one' CRISPR/Cas9 lentiviral construct was designed to encode GrB sgRNA#2 behind a human U6 promoter, as well as the strong EF1α promoter driving the expression of NLS-tagged SpCas9 fused to mCherry via a 2A self-cleaving viral peptide. The length of the CRISPR/Cas9 lentiviral construct spans 8.5 kb between the 5' and 3' LTRs, while typical CAR lentivirus constructs are only ~5.5 kb from LTR to LTR. (b) Lentivirus titers for the CRISPR/Cas9 construct are consistently an order of magnitude lower than titers obtained for various CAR constructs prepared during the same virus production cycle. Each pair of points represents batches of lentivirus prepared at the same time. (c) Stable transduction of primary human $CD4^+$ and $CD8^+$ T cells with the CRISPR/Cas9 lentivirus was quantified by the mCherry transduction marker. Transduction efficiencies were typically less than 5% for CD4s and undetectable for CD8s. (d) CRISPR/Cas9 lentivirus-transduced primary human $CD4^+$ T cells were sorted by FACS to isolate the population that stably integrated the CRISPR/Cas9 construct ($mCherry^+$). Cell lysates were then probed for GrB expression via western blot, with GAPDH serving as the protein-loading control. * $p < 5E\text{-}3$.

Despite the lack of stable Cas9 expression, the $mCherry^-$ $CD4^+$ T-cell population exhibited a loss of GrB expression relative to untransduced T cells (Figure 4.2d), suggesting that transient Cas9 expression may be sufficient to induce DSBs. Therefore, we designed *in vitro* transcription (IVT) templates encoding either Cas9-T2A-EGFP or EGFP alone (EGFP-only) and generated IVT mRNA for nucleofection into Jurkat human T cells (Figure 4.3a). Although an equal molar amount

of IVT mRNA was nucleofected, the resulting % EGFP$^+$ was noticeably lower for the Cas9-T2A-EGFP construct relative to EGFP-only, and the peak expression level of Cas9-T2A-EGFP yielded an MFI EGFP 23.1-fold lower than maximum expression for EGFP-only (Figure 4.3b). The duration of Cas9-T2A-EGFP expression was also relatively short-lived (Figure 4.3b), indicating that the translation efficiency of Cas9 may present a bottleneck for CRISPR/Cas9 expression and activity in human T cells. A similar trend was observed in primary human CD8$^+$ T cells, with extremely poor expression of Cas9-T2A-EGFP mRNA despite nearly 64.1% transfection efficiency of EGFP-only (Figure 4.S1, Supplementary Information).

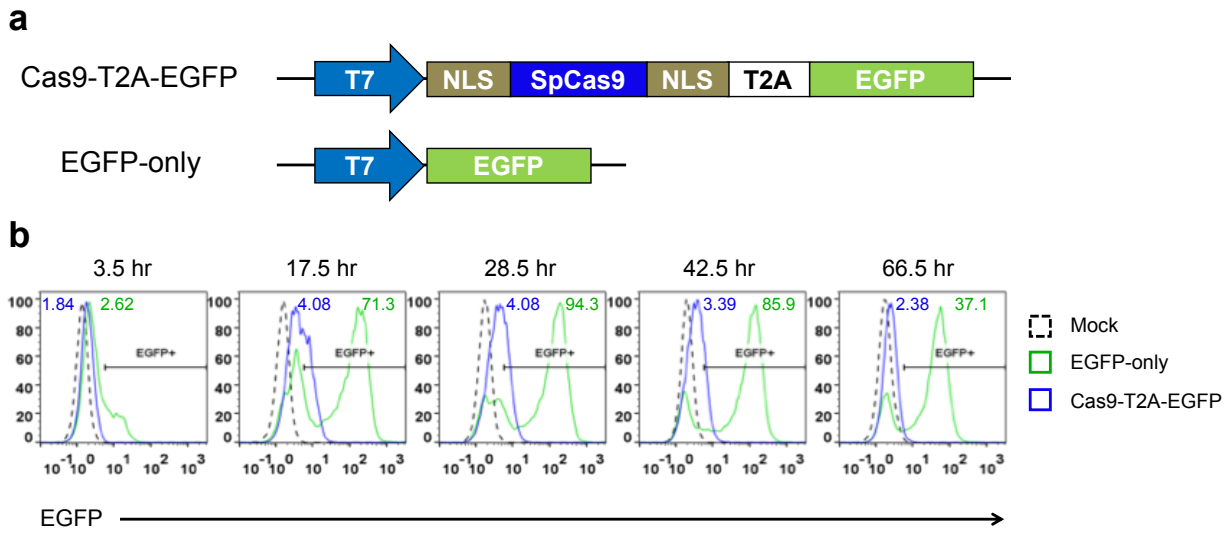

Figure 4.3. Nucleofected Cas9-T2A-EGFP IVT mRNA is poorly translated in Jurkat T cells. (a) An EGFP fluorescent protein tag was fused to NLS-tagged SpCas9 via a 2A self-cleaving viral peptide and the fusion construct was cloned behind a T7 promoter to enable IVT. (b) EGFP expression in Jurkat T cells nucleofected with Cas9-T2A-EGFP or EGFP-only IVT mRNA was quantified by flow cytometry every 12-24 hours. At 28.5 hours post-nucleofection, the peak expression level of the EGFP-only construct was 23.1-fold higher than for Cas9-T2A-EGFP. The values adjacent to each histogram peak indicate the MFI EGFP for each sample.

CRISPR/Cas9 RNPs mediate efficient gene disruption in primary human T cells

By relieving the transcriptional and translational burden of expressing individual CRISPR/Cas9 components from primary human T cells, the electroporation of pre-complexed

RNPs represents a more efficient method of CRISPR/Cas9 delivery[23]. To evaluate the efficacy of this approach, we purified His-tagged, NLS-tagged SpCas9 protein from transformed BL21(DE3) *E. coli* cells via Ni^{2+}-affinity chromatography and generated IVT sgRNAs from the original GrB sgRNA panel for *in vitro* RNP complexing (Figure 4.4a). PCR-amplified DNA containing the GrB target sequence was then co-incubated with CRISPR/Cas9 RNPs pre-complexed at 0.3:1, 1:1, or 3:1 sgRNA:Cas9 ratio, and subsequently analyzed via gel electrophoresis to quantify the DNA cleavage efficiency (Figure 4.4a,b). Once again, all on-target sgRNAs enabled robust cleavage of the target DNA, when RNP complexes were prepared at 1:1 or higher sgRNA:Cas9 complexing ratio (Figure 4.4b). However, nucleofection of pre-complexed CRISPR/Cas9 RNPs into primary human $CD4^+$ and $CD8^+$ T cells failed to elicit detectable indel formation at endogenous GrB loci, indicating that the *in vitro* cleavage efficiency observed under tightly controlled reaction conditions with readily accessible target DNA may not reflect the genome-editing efficiency in primary human T cells (Figure 4.4c,d).

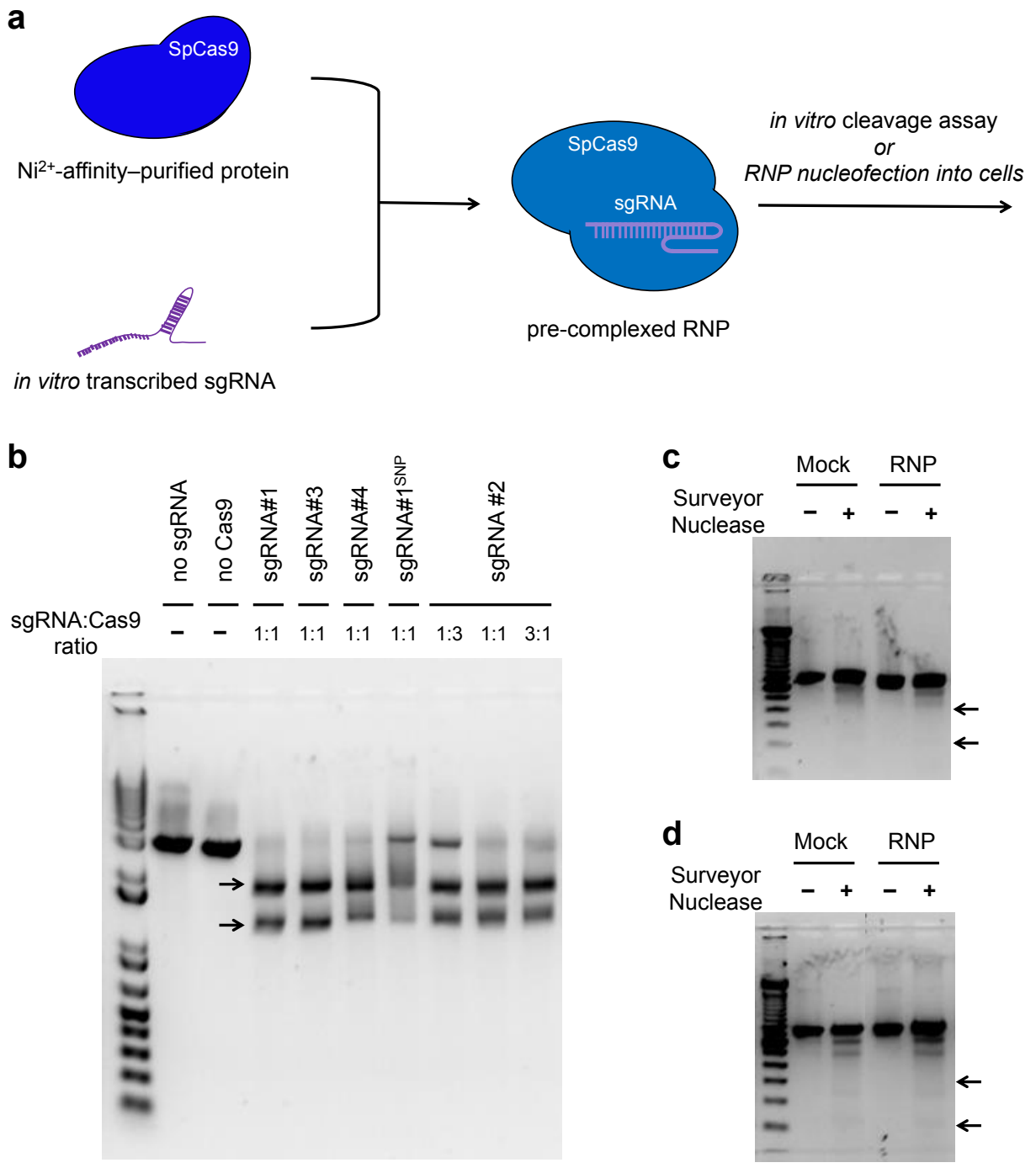

Figure 4.4. CRISPR/Cas9 RNPs pre-complexed by co-incubating Ni^{2+}-affinity purified Cas9 protein and IVT sgRNA mediate efficient cleavage of target DNA, but fail to elicit indel formation at the GrB locus in primary human T cells. (a) Schematic of CRISPR/Cas9 RNP complex assembly. (b) GrB-targeting IVT sgRNAs were pre-complexed with purified SpCas9 protein at 1:3, 1:1, or 3:1 sgRNA:Cas9 ratio prior to co-incubation with a PCR amplicon containing the GrB target DNA sequence. *In vitro* cleavage assay reaction products were subsequently resolved on an agarose gel, with arrows indicating the expected cleavage products for each sgRNA. (c,d) Primary human $CD4^+$ (c) and $CD8^+$ (d) T cells were nucleofected with pre-assembled

CRISPR/Cas9 RNPs containing GrB sgRNA#2 and genomic DNA was harvested 48 hours post-RNP delivery. Surveyor nuclease assays failed to reveal specific cleavage that would have resulted in the expected fragment lengths indicated by the arrows.

To determine if the lack of genome-editing may have been a consequence of inefficient RNP delivery into primary human T cells, we cloned and purified a His-tagged fusion construct consisting of *S. aureus* Cas9 (SaCas9) tethered to superfolder GFP (sfGFP) via a short, flexible linker (Figure 4.5a). SaCas9 differs from its SpCas9 ortholog by a substantially truncated recognition lobe (REC) domain, leaving SaCas9 with a molecular weight of 130 kDa, approximately 35 kDa smaller than SpCas9. Since the fusion of sfGFP to SpCas9 would have further enlarged an already sizeable protein and potentially hindered cytoplasmic entry during nucleofection, we instead fused sfGFP (27 kDa) to SaCas9 to generate a 157 kDa protein that could serve as a fluorescently tagged proxy for SpCas9 during the delivery process. Purified SaCas9-G4S-sfGFP was successfully taken up by nucleofected Jurkats and primary human $CD8^+$ T cells at protein concentrations equal to or lower than the normal RNP concentration (Figure 4.5b-d), suggesting that protein or RNP complex delivery may not have been the limiting factor to genome editing.

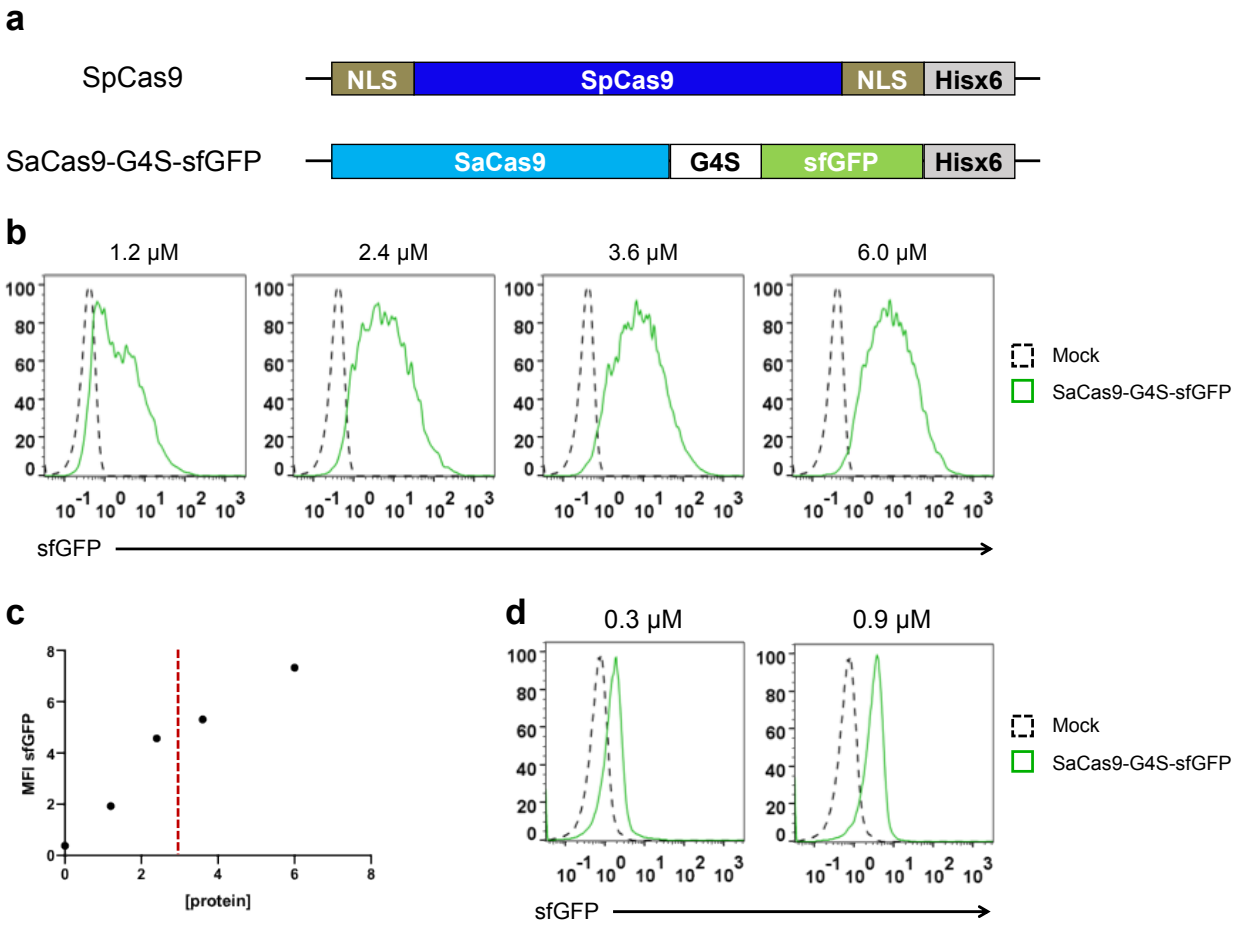

Figure 4.5. Nucleofection of purified sfGFP-tagged SaCas9 protein in Jurkats and primary human CD8$^+$ T cells indicate efficient protein uptake by both cell types. (a) Schematics of the NLS-tagged SpCas9 construct used to generate purified SpCas9 protein for RNP assembly and the SaCas9-G4S-sfGFP fusion used to evaluate the efficiency of protein delivery via nucleofection. Fusion of the 3.3 kb SaCas9 sequence with the 0.7 kb sfGFP sequence yields a 157 kDa protein to serve as a proxy of near-equal mass to the 165 kDa SpCas9 protein. (b) Nucleofection of Ni^{21}-affinity purified SaCas9-G4S-sfGFP protein into Jurkat T cells resulted in 97-100% transfection efficiency at all protein input concentrations tested. (c) MFI quantification of the results from (b), with the dashed red line indicating the protein input concentration used for CRISPR/Cas9 RNP nucleofection. (d) Nucleofection of purified SaCas9-G4S-sfGFP protein in primary human CD8$^+$ T cells at protein inputs 3- to 10-fold lower than the RNP input concentration still resulted in successful protein uptake in 59.0% and 81.1% of T cells, respectively, by Overton histogram subtraction.

Chemically Synthesized sgRNA Outperforms IVT sgRNA

Although there appears to be general agreement regarding the optimal electroporation programs for different transformed cell lines and primary cell types, we noticed considerable

variability between available *in vitro* RNP assembly protocols across the literature. In particular, while the sgRNA:Cas9 complexing ratio is often referenced as the most important parameter for optimizing RNP complexing and electroporation, the wide range of sgRNA:Cas9 complexing ratios selected across different research groups hints at underlying discrepancies in complex preparation[17,31–33]. We therefore speculated that the source and purity of sgRNA may greatly impact the efficiency of CRISPR/Cas9 RNP assembly, and consequently, nuclease activity. Most IVT sgRNA protocols simply purify sgRNA transcripts via commercially available RNA clean-up kits, which do not include steps for size-selection of full-length sgRNA products, thus allowing contaminating transcription products to interfere with productive complex assembly. While gel extraction methods enable the specific recovery of full-length IVT sgRNA, purified yields are often greatly reduced and remain subject to considerable batch-to-batch variability. Instead, we have found chemically synthesized sgRNA to disrupt endogenous gene expression with greater efficiency than IVT sgRNA (Figure 4.6a,b). The batch-to-batch consistency of chemically synthesized sgRNA also facilitates head-to-head comparison of different sgRNA sequences targeting the same gene with greater confidence (Figure 4.6c,d). While all of the GrB-targeting sgRNAs we tested exhibited similar performance when generated via IVT, the relative ranking of each sgRNA varied between experiments. In contrast, nucleofection of RNPs assembled with chemically synthesized sgRNAs has enabled more consistent characterization of relative genome-editing efficiencies, and led to the identification of an sgRNA (GrB sgRNA#9) that routinely mediates indel formation in exon 4 of GrB with 80-85% efficiency. Having demonstrated that chemically synthesized sgRNAs enable highly efficient CRISPR/Cas9-mediated knockout of GrB expression, we also optimized our RNP delivery protocol by titrating the RNP input to achieve maximal knockout efficiency in primary human $CD8^+$ T cells (Figure 4.S2, Supplementary Information).

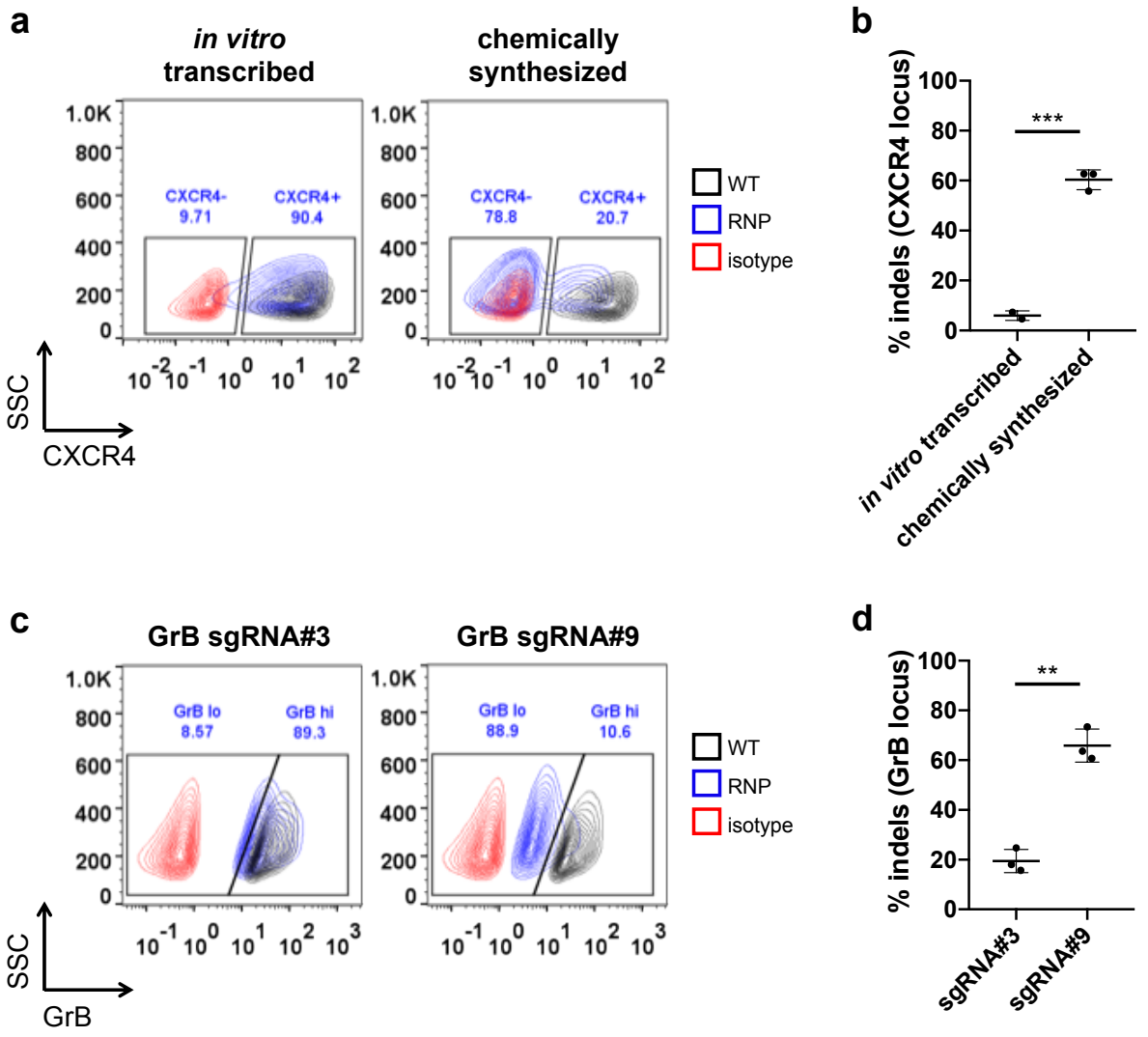

Figure 4.6. CRISPR/Cas9 RNPs assembled with chemically synthesized sgRNA outperform RNP complexes prepared with IVT sgRNA. (a) CRISPR/Cas9 RNPs targeting the CXCR4 locus were nucleofected into primary human CD8$^+$ T cells and CXCR4 surface expression was assessed via flow cytometry 4 days post-RNP delivery. (b) Genomic DNA was harvested from the samples in (a) and oligos flanking the expected CXCR4 cut site were used to PCR-amplify the target locus. The % indels were calculated by TIDE analysis. (c) Chemically synthesized GrB sgRNA#3 and GrB sgRNA#9 were used to assemble CRISPR/Cas9 RNP complexes for nucleofection into primary human CD8$^+$ T cells. Intracellular GrB protein levels were quantified by flow cytometry 4 days post-RNP delivery. (d) % indels calculated by TIDE analysis for the samples in (c). All population frequencies displayed correspond to the RNP-treated sample (blue). Each plotted data point represents an independent experiment with a different primary human T-cell donor and error bars represent ±1 s.d. ** p < 5E-3, *** p < 5E-4.

Multiplexed RNP Delivery Yields Simultaneous Gene Knockout at TRAC & GrB Loci

A major advantage for CRISPR/Cas9 over previous genome-editing platforms is the ease of nuclease targeting, with several powerful web tools specifically designed to assist sgRNA design. We exploited the abundance of available design aids to identify sgRNAs that efficiently target the TRAC locus (Figure 4.7a). Since T-cell receptors (TCRs) require heterodimerization between TCRα and TCRβ chains to form stable complexes at the cell surface, TRAC knockout effectively silences endogenous TCR expression, an important consideration for limiting graft-versus-host disease (GvHD) in clinical applications. The genetic ablation of TCR expression is now being explored for allogeneic CAR-T cell platforms that would streamline the T-cell manufacturing process and enable the production of 'off-the-shelf' therapies[34]. To evaluate the future feasibility of incorporating allogeneic manufacturing strategies into our developing COVERT platform, we took advantage of the capacity for CRISPR/Cas9 to simultaneously mediate multiple genetic edits by multiplexing the nucleofection of CRISPR/Cas9 RNPs targeting both the TRAC and GrB loci in primary human $CD8^+$ T cells. After 7 days, we stained for both TCR and intracellular GrB expression and observed nearly 70% of the viable T-cell population to be $TCR\alpha/\beta^-$ GrB^{lo}, with the knockout efficiency at each locus approximately equal to the knockout efficiency of that locus in isolation (Figure 4.7b). As described in Chapter 2, successful GrB knockout results in the disruption of GrB expression following CRISPR/Cas9-mediated indel generation, but pre-exisiting intracellular GrB protein can remain intact in the lytic granule compartment until degranulated or diluted between daughter cells during cell division. As a result, the GrB^{lo} population corresponds to cells that have undergone genetic GrB knockout, but still contain residual intracellular GrB stockpiles. Over the past several months, our lab has further expanded the range of genomic targets and successfully multiplexed the delivery of CRISPR/Cas9 RNPs targeting additional combinations of genes into specific subsets of primary human T cells, highlighting the robustness and versatility of the gene-editing platform.

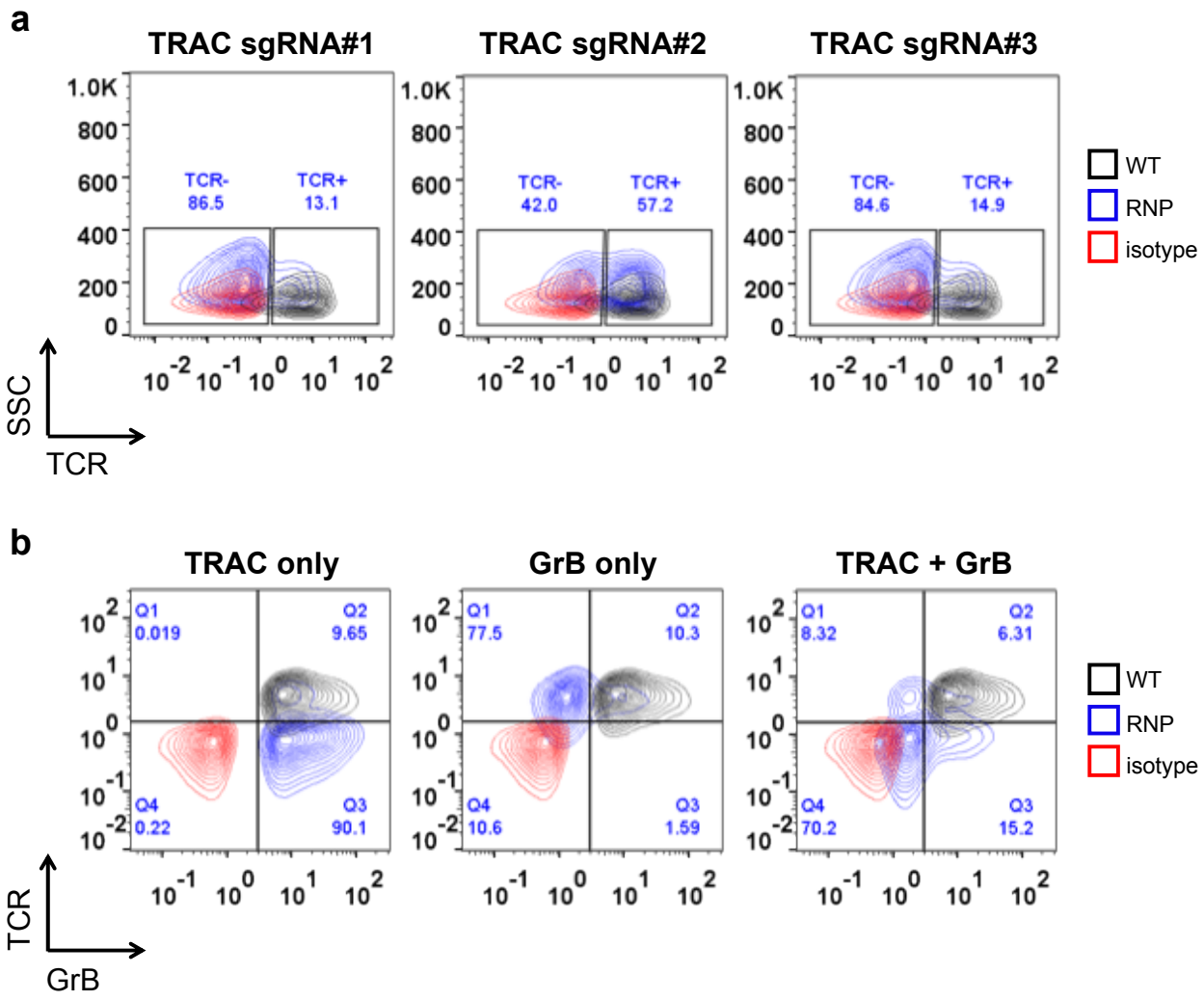

Figure 4.7. Multiplexed CRISPR/Cas9 RNP delivery enables efficient disruption of multiple endogenous loci. (a) A panel of sgRNAs targeting the TRAC locus were evaluated by comparing TCR surface expression in primary human CD8$^+$ T cells 7 days post-RNP nucleofection. (b) Knockout efficiency of TCR surface expression and GrB intracellular expression were assessed by flow cytometry 7 days following nucleofection of primary human CD8$^+$ T cells with CRISPR/Cas9 RNPs targeting the TRAC locus only, GrB locus only, or both loci. All population frequencies displayed correspond to the RNP-treated sample (blue).

AAV6 HDR-Ts mediate efficient site-specific gene insertion in primary human T cells

While our protocol for CRISPR/Cas9 RNP delivery routinely mediates GrB knockout with upwards of 80% efficiency, the residual GrB$^+$ T-cell population may still interfere with COVERT regulation of T-cell–mediated cytotoxicity. Unlike proteins expressed at the cell surface, endogenous GrB is stored within sealed lytic granule compartments and thereby inaccessible to

immunostaining agents that facilitate typical cell-isolation strategies such as fluorescence-activated cell sorting (FACS) or magnetic bead sorting. Therefore, we decided to mark GrB-edited cells via site-specific integration of an EGFP HDR marker with 500 bp homology arms on either end of the CRISPR/Cas9 cut site in exon 4 of the GrB locus ([GrB HDR]-EGFP) (Figure 4.8a). To facilitate optimizing the delivery of the HDR template (HDR-T), we first constructed an AAV serotype 6 (AAV6) vector encoding EGFP driven by an EF1α promoter (EF1α-EGFP) (Figure 4.8a). Although AAV6 production titers are generally lower than for more common serotypes, such as AAV1 and AAV2, AAV6 is the only known serotype that infects hematological cells with any appreciable efficiency[35]. We started by titrating the addition of in-house generated EF1α-EGFP AAV6 to activated primary human $CD8^+$ T cells at inputs ranging from 5 µL/10^6 cells to 200 µL/10^6 cells. Although transduction was observed at the lowest AAV6 input tested, primary human $CD8^+$ T cells required the EF1α-EGFP to be supplied between 50 µL/10^6 cells to 100 µL/10^6 cells to achieve near-complete transduction efficiency, a range we proceeded to use in all subsequent experiments (Figure 4.8b). Increasing the AAV6 input to 200 µL/10^6 cells resulted in a decrease in transduction efficiency, possibly due to toxicities associated with AAV6 transduction. We proceeded to incorporate AAV6 transduction of the [GrB HDR]-EGFP HDR template into our genome-editing workflow on Day 3, immediately following nucleofection with CRISPR/Cas9 RNPs (Figure 4.8c). When GrB RNP-treated primary human $CD8^+$ T cells were transduced with [GrB HDR]-EGFP AAV6, HDR was observed in 30-38% of treated cells across multiple electroporation platforms and programs (Figure 4.8d).

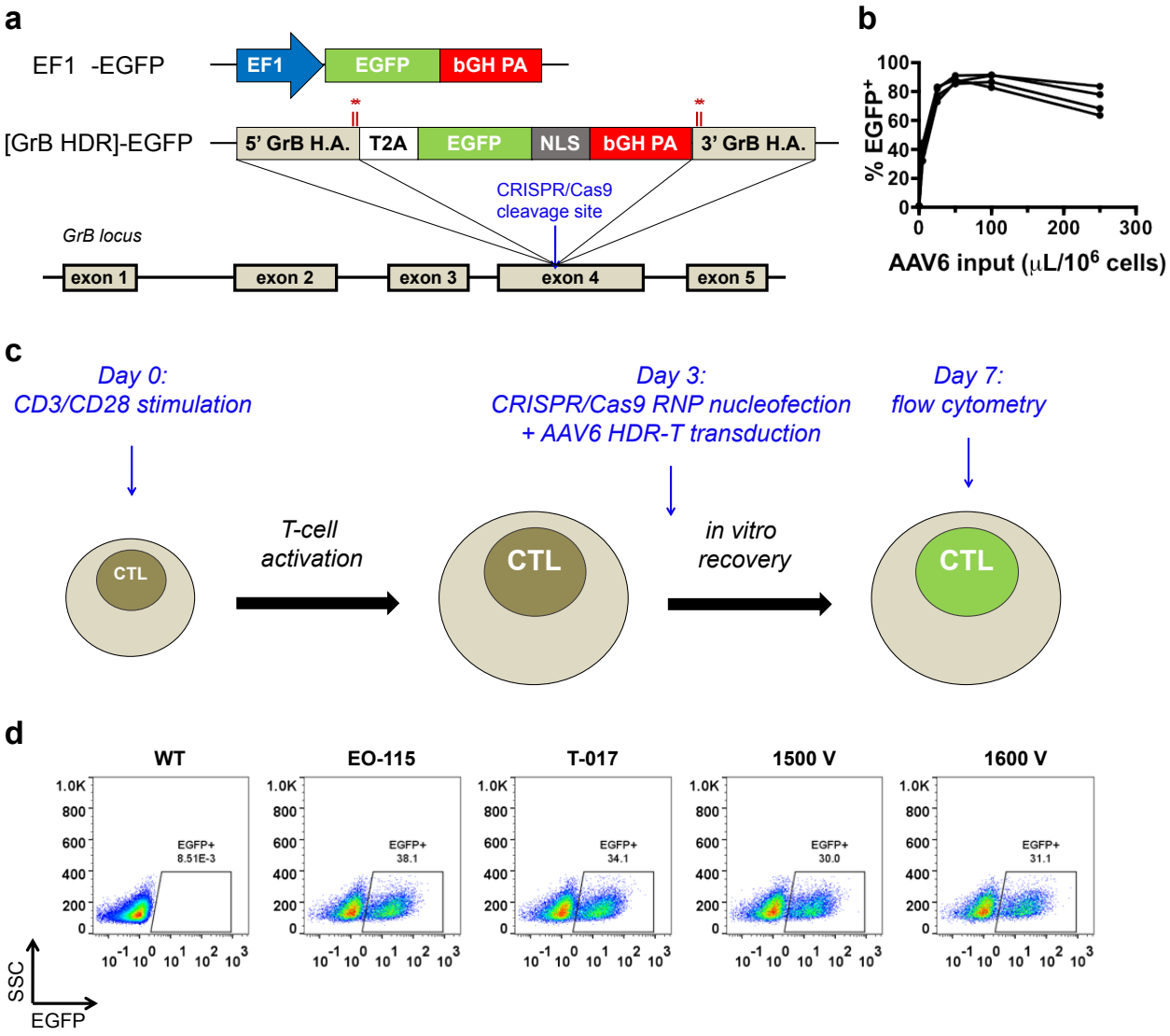

Figure 4.8. AAV6 transduction of HDR-Ts efficiently directs site-specific insertion of exogenous genes. (a) Schematic of AAV6 constructs encoding constitutive EGFP expression behind an EF1α promoter (EF1α-EGFP) or an HDR template to direct site-specific integration of EGFP at the CRISPR/Cas9 cut site in exon 4 of GrB ([GrB HDR-EGFP]). The HDR was designed to mediate the in-frame insertion of a T2A-EGFP-NLS fusion to enable translation of the EGFP HDR marker from mRNA transcripts expressed as a result of GrB promoter activity. The red asterisks indicate the location of point mutations intentionally introduced into the HDR template in order to prevent sgRNA annealing once HDR has been accomplished. H.A., homology arm; bGH pA, bovine growth hormone polyA termination sequence. (b) Primary human $CD8^+$ T cells transduced with EF1α-EGFP were analyzed by flow cytometry to determine the transduction efficiency 2 days post-transduction. Each set of connected data points represents a single transduction experiment involving one of two batches of AAV6 and one of two primary human T-cell donors. (c) Schematic of the T-cell engineering workflow involving CRISPR/Cas9 RNP nucleofection and AAV6 HDR-T transduction 3 days after T-cell activation with CD3/CD28 Dynabeads. (d) Efficiency of [GrB HDR]-EGFP insertion into the GrB locus of primary human $CD8^+$ T cells was analyzed via flow cytometry on Day 7 following T-cell activation. T cells electroporated by different electroporation

instruments and parameters (Nucleofector 4D program EO-115; Nucleofector 2b program T-017; Neon 1500 volts (V), 10 millisecond pulses, 3 pulses; Neon 1600 V, 10 ms, 3 pulses) all enabled HDR with 30-38% efficiency at the GrB locus.

Since the delivery of COVERT switches into target cells relies on surface receptor engagement of surface-bound antigens, we also developed AAV6 HDR templates to site-specifically insert a FLAG-tagged CD19 CAR, HER2 CAR, or CD20-CD19 bispecific CAR into the TRAC locus (Figure 4.9a). We have observed pre-HDR T-cell viability to be an important indicator of HDR efficiency, so the ability to integrate a CAR in the same engineering step as COVERT replacement of endogenous GrB streamlines the COVERT/CAR engineering process by minimizing the handling and stressing of T cell prior to Day 3. Similar to the EGFP insertion into the GrB locus, CAR integration into the TRAC locus efficiently replaced endogenous expression of the TRAC domain with CAR expression, thus simultaneously silencing endogenous TCR expression (Figure 4.9b). Although slight donor-dependent variability has been observed, CAR integration into the TRAC locus is routinely accomplished with 50-75% HDR efficiency, a range comparable to the expected transduction efficiencies for randomly inserting lentiviral or retroviral constructs. Interestingly, despite being integrated into the same target locus and theoretically being regulated via the same promoter, CAR surface expression varied among the three CAR constructs (Figure 4.9c,d), indicating that construct-dependent factors may contribute to differences in HDR marker expression.

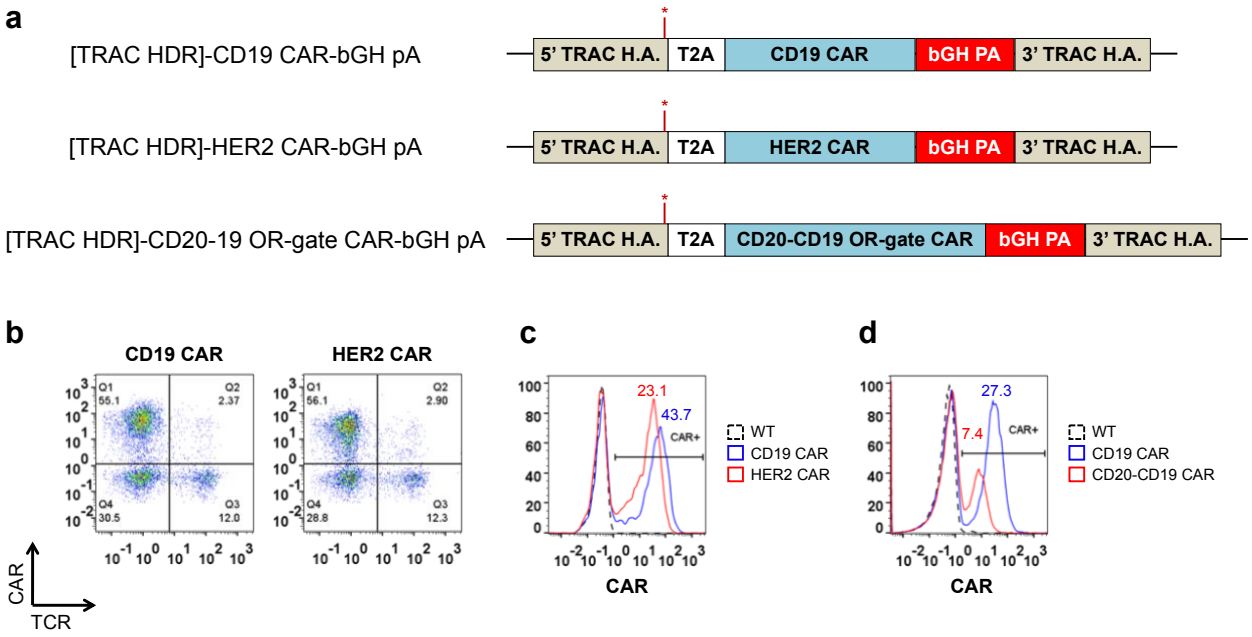

Figure 4.9. AAV6 transduction of HDR-Ts mediates efficient integration of CAR constructs into the TRAC locus. (a) Schematic of AAV6 HDR-Ts directing the insertion of a CD19 CAR, a HER2 CAR, or a CD20-CD19 bispecific CAR into the TRAC locus. The red asterisk indicates the position of an intentional point mutation in the protospacer adjacent motif (PAM) sequence in the HDR-T to prevent CRISPR/Cas9-mediated cleavage following HDR. H.A., homology arm; bGH pA, bovine growth hormone polyA termination sequence. (b) Efficiencies of CD19 CAR and HER2 CAR integration into the TRAC locus were analyzed by flow cytometry on Day 7 following T-cell activation. Near-complete disruption of TCR expression was observed in CAR^+ cells. (c,d) CAR expression levels of CD19 CAR vs. HER2 CAR and CD19 CAR vs. CD20-CD19 bispecific CAR following site-specific insertion into the TRAC locus. Values adjacent to the histogram peaks indicate the MFI CAR expression for each sample.

However, since the overall observed HDR efficiencies were far superior at the TRAC locus relative to the GrB locus, we reasoned that the discrepancy may also be the result of locus-specific features. For example, the induction of targeted DSBs and homology-driven repair both require the target locus to be readily accessible for the delivered nuclease and HDR template. We have previously shown that the upregulation of GrB expression is strongly tied to T-cell activation (Chapter 2), and it is not difficult to envision that the accessibility of the GrB locus may be strongly influenced by T-cell activation status. Thus, to optimize the HDR efficiency at the GrB locus, we systematically evaluated the impact of T-cell stimulation and HDR construct design.

IL-2 Signaling Enhances HDR Efficiency at the GrB Locus

Although strong CD3/CD28 stimulation is pre-requisite for CRISPR/Cas9 RNP delivery into the nucleus, we speculated that the accessibility of the GrB locus may be partially obstructed under high levels of RNA polymerase-driven transcriptional activity. Therefore, culturing conditions and cytokine feeding regimens that induce strong GrB transcription may hinder efficient gene-editing. While the Chen lab traditionally supplements T-cell culture media with 50 U/mL interleukin (IL)-2 and 1 ng/mL IL-15, the native GrB promoter region contains several response elements that are sensitive to the downstream effects of IL-2 signaling[36]. In order to elucidate the impact of IL-2 signaling on HDR efficiency at the GrB locus, we devised to culture primary human $CD8^+$ T cells in the presence or absence of IL-2. However, since the near-complete withholding of cytokine support may lead to deleterious effects on T-cell survival, T cells cultured in the absence of IL-2 were fed with 10 ng/mL IL-15, a growth- and memory-inducing cytokine that shares structural similarity with IL-2[37]. Following 72 hours of CD3/CD28 stimulation and cytokine exposure, cells were nucleofected with CRISPR/Cas9 RNPs targeting TRAC and GrB and subsequently transduced with AAV6 HDR templates directing the insertion of FLAG-tagged HER2 CAR into the TRAC locus and EGFP into the GrB locus. Surprisingly, the efficiency of EGFP integration into the GrB locus decreased in the absence of IL-2 (Figure 4.10a), indicating that active transcription at the target locus may not significantly impede CRISPR/Cas9-mediated cleavage and HDR. Importantly, HDR efficiency at the TRAC locus was unaltered by the lack of IL-2 signaling (Figure 4.10b).

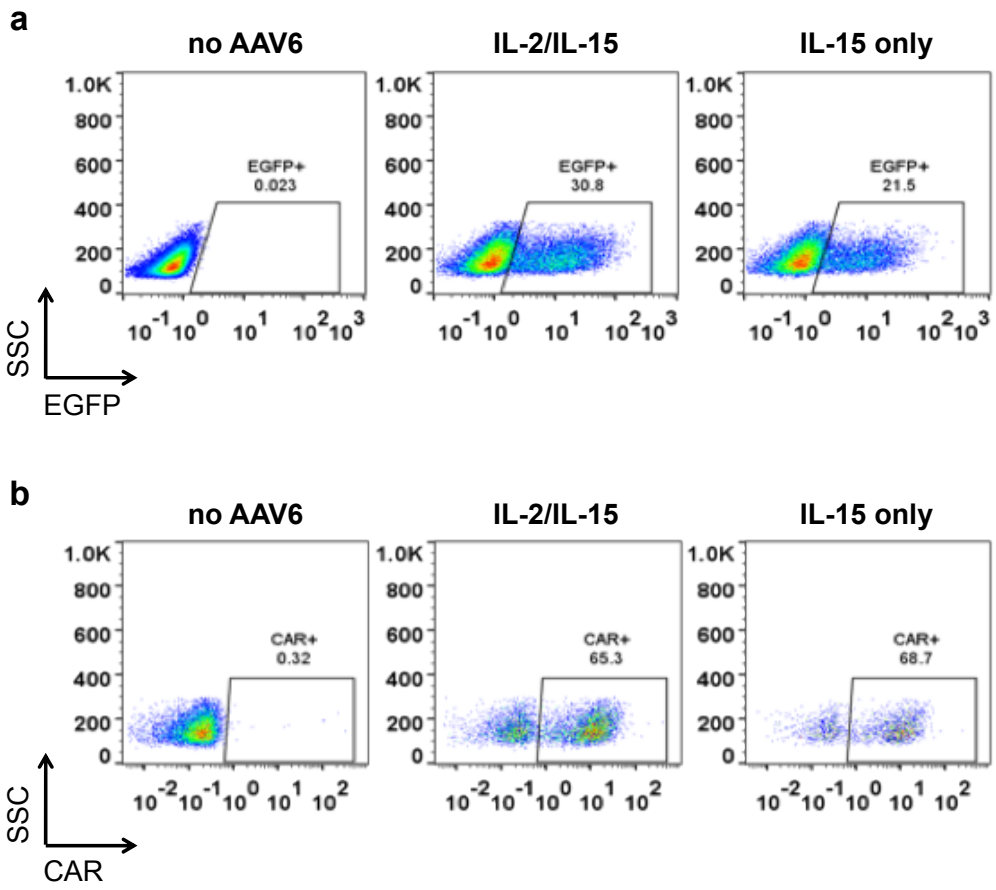

Figure 4.10. Cytokine feeding regimen influences HDR efficiency at the GrB locus, but not the TRAC locus of primary human CD8$^+$ T cells. (a) Primary human CD8$^+$ T cells were activated by CD3/CD28 Dynabeads and cultured in the presence of 50 U/mL IL-2 + 1 ng/mL IL-15 or 10 ng/IL-15 only. Cells were nucleofected with CRISPR/Cas9 RNPs targeting the GrB locus and transduced with [GrB HDR]-EGFP AAV6 on Day 3, and analyzed for HDR efficiency on Day 7 following T-cell activation. (b) HDR efficiency in human CD8$^+$ T cells engineered with TRAC-targeted RNP and [TRAC HDR]-HER2 CAR-bGH pA on Day 7 following T-cell activation.

Incorporation of an Exogenous Termination Sequence and Perfect Homology Arms Increases HDR Efficiency at the GrB Locus

In Chapter 3, we demonstrated the selective cytotoxic action of a small ubiquitin-like modifier (SUMO)-GrB fusion in response to proteolytic cleavage by sentrin-specific protease 1 (SENP1) following transient transfection in HEK293T cells. To facilitate the manufacture of COVERT-T cells targeting SENP1, we iteratively optimized the design of an AAV6 HDR template that inserts an EGFP HDR marker directly fused to codon-optimized SUMO-GrB via a self-

cleaving 2A peptide into the GrB locus (Figure 4.11a). The original template was designed with 500 bp homology arms on either side of the CRISPR/Cas9 cut site, along with intentional point mutations along the length of the sgRNA target sequence to prevent nuclease activity against the repaired DNA. Furthermore, since SUMO-GrB and endogenous GrB encode identical peptides from the cleavage location onward, the HDR template was designed such that the 4^{th} and 5^{th} exons of endogenous GrB would complete the SUMO-GrB sequence. Despite minimizing the length of the exogenous DNA insertion, the integration efficiency and expression level of the EGFP HDR marker in the SUMO-GrB construct were markedly reduced relative to EGFP alone (Figure 4.11b). One striking difference between the SUMO-GrB construct and EGFP-only construct is the incorporation of an exogenous bovine growth hormone (bGH pA) termination sequence into the latter (Figure 4.11a). Therefore, we re-designed the SUMO-GrB HDR template to include the entire GrB coding sequence, as well as the bGH pA signal (Figure 4.11a), changes that strongly enhanced the expression of the EGFP HDR marker (Figure 4.11b). Although the precise reason for the increased expression level remains under investigation, one possibility is that the exclusion of the endogenous GrB 3' untranslated region (3' UTR) and its microRNA (miRNA)-sensitive regulatory elements prevents post-transcriptional degradation of the transcribed mRNA[38]. An additional improvement in HDR efficiency was obtained by reverting the mutations in the GrB homology arms to match the native sequence, such that the homologous regions align flush with the CRISPR/Cas9 cleavage site (Figure 4.11a,b). Interestingly, while extension of the homology arms to a flush alignment enabled the HDR efficiency of the SUMO-GrB construct to approach the HDR efficiency of the EGFP-only construct, the same modification failed to improve the integration of EGFP-only, suggesting that we may have encountered an intrinsic limitation to HDR at the GrB locus.

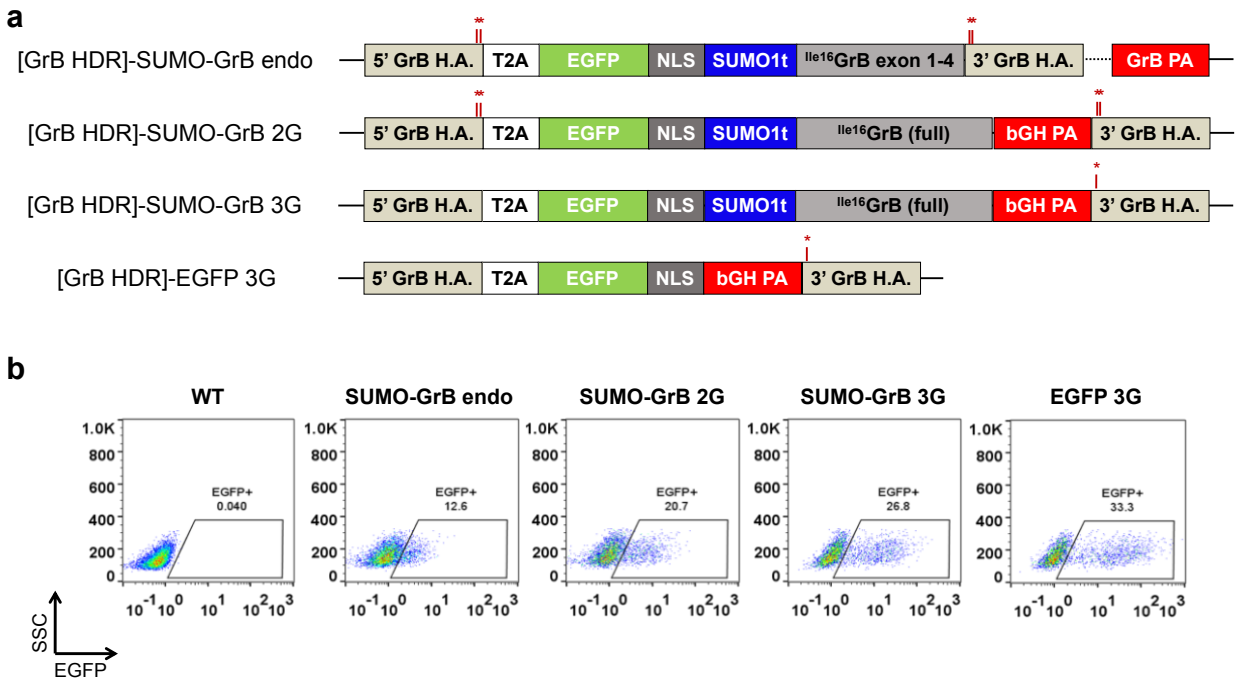

Figure 4.11. HDR-T construct optimization increased the efficiency of site-specific SUMO-GrB integration into the GrB locus by 3-fold. (a) Schematic of HDR-Ts directing HDR at the GrB locus. The original [GrB HDR]-SUMO-GrB endo construct only encoded the GrB sequence preceding the CRISPR/Cas9 cut site, with the remainder of exon 4 and all of exon 5 being provided by the endogenous GrB DNA. The mRNA transcript is eventually terminated by the endogenous GrB polyA termination sequence. The red asterisks indicate the position of intentional mutations in the HDR-Ts to prevent CRISPR/Cas9-mediated cleavage of repaired DNA. H.A., homology arm; GrB pA, human GrB polyA termination sequence; bGH pA, bovine growth hormone polyA termination sequence. (b) HDR efficiencies for each AAV6 HDR-T in primary human $CD8^+$ T cells were evaluated via flow cytometry on Day 7 following T-cell activation.

SUMO-GrB/CAR-T cells selectively lyse SENP1-overexpressing target cells

Having optimized the T-cell manufacturing process to site-specifically integrate SUMO-GrB into the GrB locus, we moved to evaluate the lytic selectivity of SUMO-GrB T cells against SENP1-overexpressing target cells. SUMO-GrB/HER2 CAR-T cells were generated by multiplexing the delivery of CRISPR/Cas9 RNPs and AAV6 HDR templates to simultaneously integrate a HER2 CAR into the TRAC locus and EGFP-T2A-SUMO-GrB into the GrB locus (Figure 4.12a). FLAG-CAR^+ $EGFP^+$ cells were isolated via fluorescence-activated cell sorting (FACS) and challenged at 1:1 effector:target (E:T) ratio with either naturally HER2-expressing wild-type MCF7 breast cancer cells or an analogous cell line previously engineered to overexpress SENP1 (Figure

4.12b and Figure 4.S3, Supplementary Information). Replacement of endogenous GrB expression with SUMO-GrB enabled partial protection of wild-type MCF7 targets expressing SENP1 at low, basal levels, while retaining a degree of lytic activity equal to HER2 CAR (WT GrB) control T cells against SENP1-overexpressing cells (Figure 4.12c). As discussed in Chapter 2, genetic disruption of endogenous GrB expression may not have been sufficient to completely eliminate GrB-mediated cytotoxicity in previously unchallenged T cells. Unfortunately, a lack of T-cell proliferation and rapid T-cell death following target-cell encounter precluded the opportunity to subject the engineered SUMO-GrB/HER2 CAR-T cells to successive MCF7 challenges.

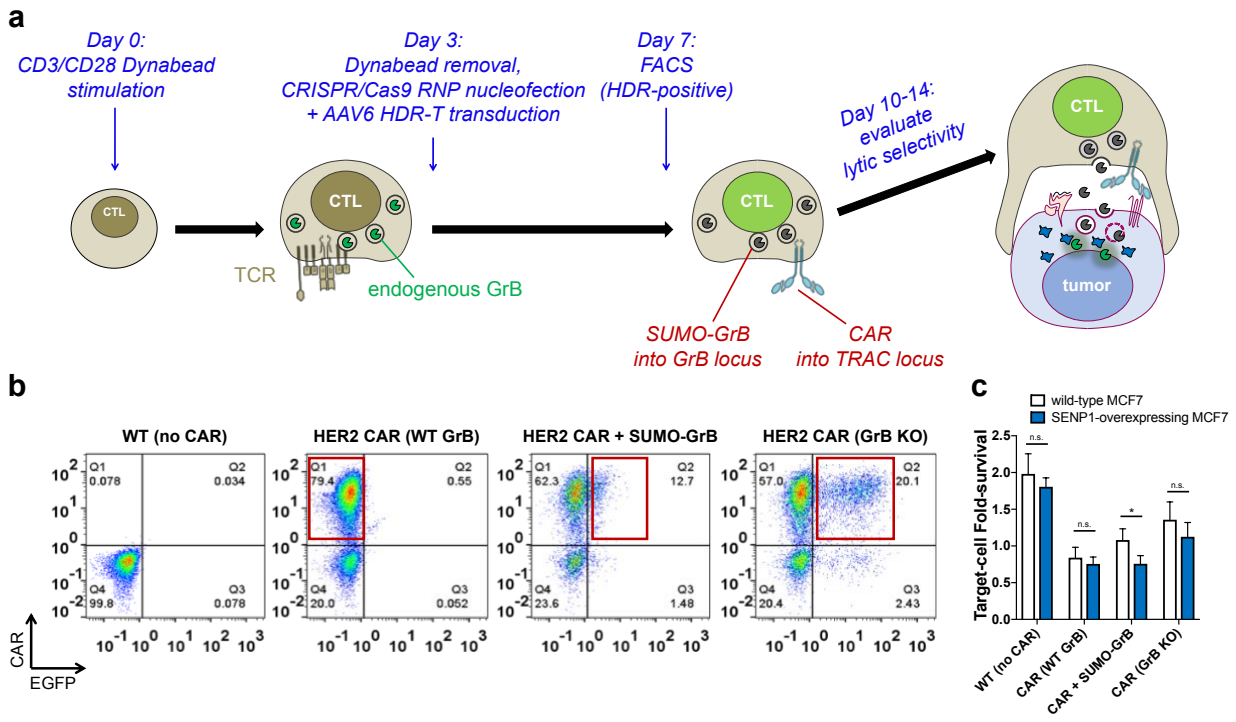

Figure 4.12. SUMO-GrB/HER2 CAR-T cells exhibit selective lytic potential against SENP1-overexpressing MCF7 cells. (a) Schematic of T-cell engineering workflow to site-specifically integrate SUMO-GrB into the GrB locus and a CAR into the TRAC locus. Cells were sorted via FACS on Day 7 following T-cell activation and expanded until co-culture with target cells between Days 10-14. (b) Pre-FACS HDR efficiencies for HER2 CAR insertion at the TRAC locus and an EGFP HDR marker at the GrB locus were analyzed by flow cytometry. Cell populations isolated by FACS are indicated by the red boxes. (c) SUMO-GrB/HER2 CAR-T cells selectively lysed SENP1-overexpressing MCF7 target cells relative to wild-type MCF7 control targets. Sorted HER2 CAR$^+$ T cells were co-cultured with MCF7 target cells at 1:1 E:T ratio, and target-cell survival was quantified by time-lapse microscopy via IncuCyte. Representative data from one of

two primary human T-cell donors are shown. All plotted data points indicate the mean of triplicate samples and error bars represent ±1 s.d. * p < 5E-2, n.s., not statistically significant.

Since other research groups have demonstrated that the antigen density on the target-cell surface required for T-cell–mediated cytotoxicity is lower than the requisite antigen density to stimulate T-cell expansion[39], we speculated that the HER2 surface-expression level of MCF7 cells may have been insufficient to trigger proliferation and long-term survival by HER2 CAR-expressing T cells (Figure 4.S4, Supplementary Information). Second-generation CD19 CARs containing either CD28 or 4-1BB costimulatory domains have demonstrated the most clinical success, and are considered to be the gold standards of CAR engineering, due to robust activation of T-cell effector functions and resistance to T-cell exhaustion[40]. We therefore repeated our SUMO-GrB/CAR-T cell manufacturing process with a CD19 CAR in place of the HER2 CAR (Figure 4.13a). To evaluate the lytic selectivity of SUMO-GrB/CD19 CAR-T cells, we also generated a panel of SENP1 knockout, SENP1 wild-type, and SENP1-overexpressing cell lines from K562 chronic myelogenous leukemia (CML) cells previously engineered to already express the extracellular domain of CD19 antigen (K19) (Figure 4.S5, Supplementary Information). Repeat challenges at 1:1 E:T ratio by each K562 target-cell line revealed the specific reduction of growth potential for SENP1-overexpressing cells co-cultured with SUMO-GrB/CD19 CAR-T cells, relative to EGFP/CD19 CAR-T and off-target CAR-T controls (Figure 4.13b). However, SUMO-GrB/CD19 CAR-T cells failed to completely clear SENP1-overexpressing targets, perhaps a consequence of the lack of T-cell proliferation (Figure 4.13c).

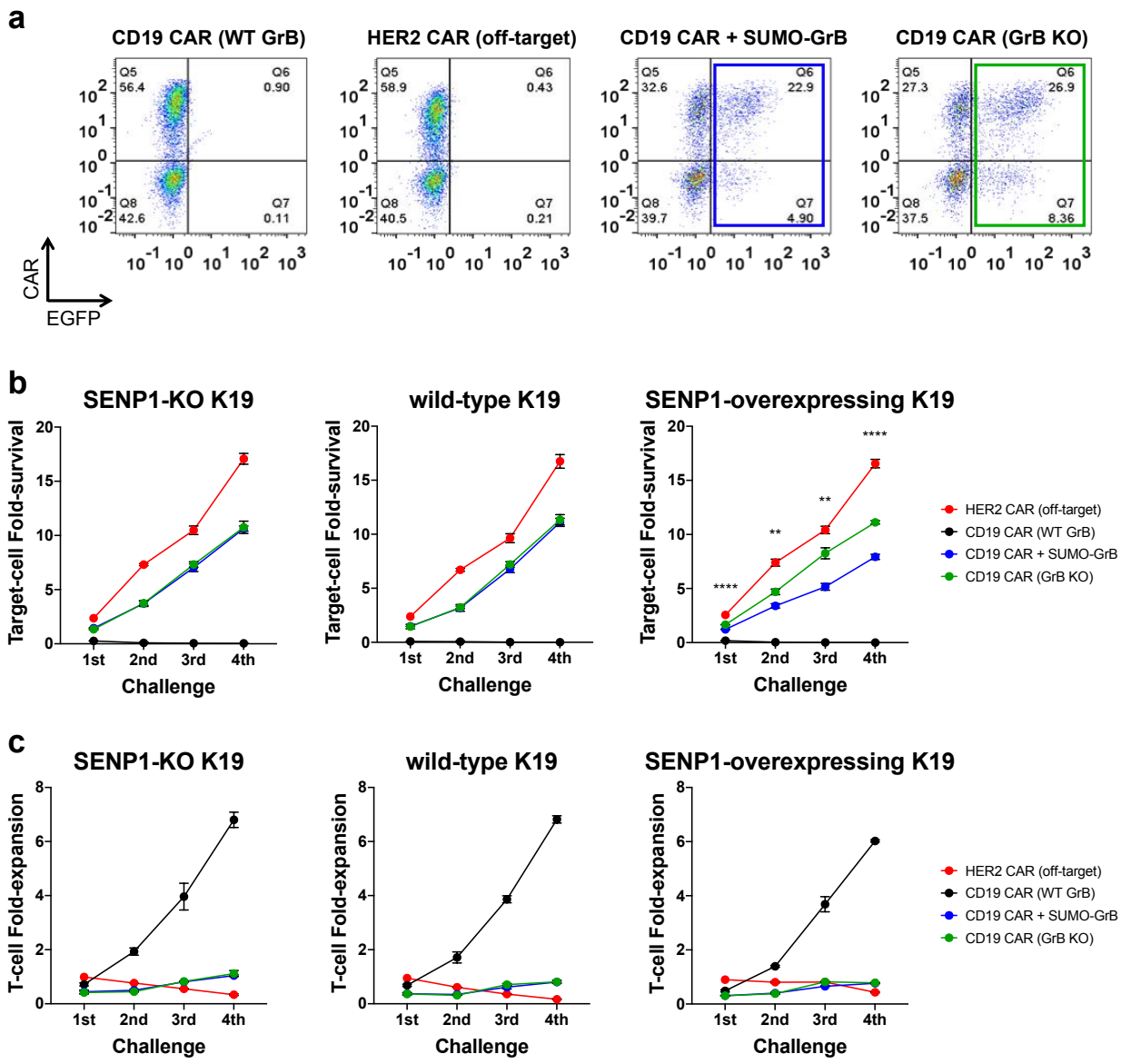

Figure 4.13. SUMO-GrB/CD19 CAR-T cells selectively reduce the proliferative potential of SENP1-overexpressing CD19$^+$ K562 cells. (a) Pre-FACS HDR efficiencies for CD19 CAR integration into the TRAC locus and SUMO-GrB integration into the GrB locus of primary human CD8$^+$ T cells. Blue and green boxes indicate the sorting gates during FACS to isolate EGFP$^+$ T cells. CD19 CAR (WT GrB) and HER2 CAR (off-target) samples were not stained nor sorted to prevent CAR activation from FLAG staining. (b,c) The % CAR$^+$ of sorted EGFP$^+$ CD19 CAR + SUMO-GrB and EGFP$^+$ CD19 CAR (GrB KO) T-cell populations and unsorted CD19 CAR (WT GrB) and HER2 CAR (off-target) samples were adjusted with Mock T cells to establish a 1:1 CAR$^+$ E:T ratio with CD19$^+$ K562 (K19) target cells. Target-cell survival (b) and T-cell expansion (c) were quantified every 2 days by flow cytometry prior to re-challenge by addition of fresh target cells. Asterisks denote statistical significance between the CD19 CAR + SUMO-GrB and CD19 CAR (GrB KO) samples. All plotted data points indicate the mean of triplicate samples and error bars represent ±1 s.d. ** p < 5E-3, **** p < 5E-5.

While the duration of T-cell survival was lengthened in the CD19 CAR/K19 model, both of the GrB RNP-treated T cell lines again exhibited limited proliferative potential (Figure 4.13c), hinting at possible T-cell exhaustion resulting from prolonged exposure to a combination of CD19 antigen stimulation, K562 defense mechanisms, and nutrient competition. Prior work in the Chen lab has demonstrated that K562 cells are innately more resistant to CAR-T cell–mediated lysis than most cell lines, and CD19 CAR (WT GrB) T cells generated from donor primary human $CD8^+$ T cells that appear to possess poor lytic potential have also been observed to exhibit a lower degree of CAR-T cell proliferation (Figure 4.S6, Supplementary Information). It remains to be seen whether the slow rate of SENP1-mediated SUMO-GrB activation, and the resulting impact on tumor-killing dynamics, may thus decrease proliferative potential or render SUMO-GrB T cells more prone to T-cell exhaustion when challenged with lysis-resistant tumor cells. While the use of more susceptible target-cell lines could aid in the elucidation of this phenomenon, we have observed most human cell lines to possess an inherent biological resistance to the manipulation of SENP1 levels, thereby restricting our ability to develop alternative CAR/target-cell models specifically for SUMO-GrB (Figure 4.S7-4.S9, Supplementary Information). Lastly, although we cannot discount with absolute certainty the possibility that the disruption of GrB expression may cause an intrinsic biological defect in T-cell survival, such a phenomenon would seem improbable given our findings in Chapter 2 (Figure 2.7d and Figure 2.8a-d).

DISCUSSION

Although the recent United States Food and Drug Administration (FDA)-approval of CD19 CAR-T cell therapies for patients with relapsing B-cell malignancies highlights the unprecedented anti-tumor potency of engineered T cells[41,42], a number of fundamental limitations have prevented the clinical translation of adoptive T-cell therapy for the vast majority of diseases. One challenge in particular stems from the lack of tumor-exclusive surface-bound antigens that are accessible

for targeting with engineered T-cell receptors, prompting the design of increasingly sophisticated cell-based therapies that can process more complex input signals to dictate safer therapeutic outcomes. For example, we devised a strategy to engineer T cells that can interrogate target cells for the expression of intracellular biomarkers prior to triggering target-cell apoptosis. In the preceding chapter, we described the development of a SUMO-GrB fusion that only initiates GrB activation upon intracellular encounter with SENP1. However, the need to completely disable endogenous cytotoxic payload(s) in engineered CTLs has presented a significant hurdle to the implementation of COVERT technology.

The ability to rewire the natural circuitry of mammalian cells has benefitted tremendously from the recent advent of powerful and robust genome-editing technologies. In this study, we explored the potential of CRISPR/Cas9 RNPs and AAV6 HDR-Ts to simultaneously replace endogenous GrB and TCR expression in primary human $CD8^+$ T cells with SUMO-GrB and a HER2 or CD19 CAR, respectively, thus enabling regulation over CTL lytic activity in response to SENP1-overexpression. Although lentiviruses and retroviruses have long been the standard gene transfer technologies for T-cell engineering, we demonstrated that the lentiviral packaging limit prevents efficient delivery of CRISPR/Cas9 components into primary human T cells. Furthermore, the transcriptional and translational burden of CRISPR/Cas9 expression appears to hinder efficient genome editing when T cells are required to express each component individually. In contrast, we harnessed an innovative technological breakthrough in CRISPR/Cas9 delivery involving pre-assembly of CRISPR sgRNA with Cas9 protein to yield RNP complexes that are immediately available for genome editing[23,25]. We examined the parameters that influence CRISPR/Cas9 RNP delivery and activity, and determined that the source and quality of sgRNA strongly influences genome-editing efficiency. After optimizing our protocol for CRISPR/Cas9 RNP assembly, we leveraged the capacity of multiplexed RNP delivery to efficiently mediate simultaneous knockout of both GrB and TCR expression, demonstrating the feasibility of

combining COVERT technology with other developing T-cell engineering strategies, such as the generation of allogeneic T cells for 'off-the-shelf' therapeutics.

By encoding HDR-Ts in AAV6 viral particles, we were able to achieve template delivery with greater than 90% efficiency into primary human T cells, enabling systematic optimization of T-cell culturing conditions and HDR-T construct design to maximize site-specific integration of SUMO-GrB at the GrB locus. Beyond increasing the efficiency of COVERT-T cell manufacturing, the finding that incorporation of a strong, exogenous bGH pA termination sequence into the HDR template boosted the expression level of an EGFP HDR marker points toward an opportunity to gain understanding of the impact of the 3' UTR on GrB expression. Several T-cell activation-induced genes are post-transcriptionally regulated by mechanisms which enables more rapid control over effector responses than would be possible with transcriptional modulation alone[43,44]. Although prior studies have already shown evidence of post-transcriptional regulation over GrB expression, the precise molecules and interactions that govern human GrB expression levels have yet to be completely elucidated. Thus, the genome-editing protocols outlined in this chapter, including CRISPR/Cas9 RNP nucleofection and AAV6 HDR-T transduction, may aid the elucidation of an important facet of GrB biology.

Given the efficiency of multiplexed genome editing, we proceeded to develop an optimized workflow for the manufacture of COVERT/CAR-T cells by site-specifically integrating SUMO-GrB into the GrB locus, and a CAR into the TRAC locus. When SUMO-GrB/CAR-T cells were challenged with on-target tumor cells, SUMO-GrB was able to specifically lyse or slow the proliferation of SENP1-overexpressing targets, offering the first demonstration of selective T-cell–mediated cytotoxicity in response to intracellular antigen expression. By simply exchanging the CAR in the AAV6 HDR-T targeting the TRAC locus, we were also able to generate SUMO-GrB/HER2 CAR-T cells and SUMO-GrB/CD19 CAR-T cells to target an MCF7 breast cancer cell line, as well as a K562 chronic myeloid leukemia cell line, respectively. The ability to pair COVERT

molecules with any surface receptor technology thus highlights the adaptability of the COVERT platform to enhance the therapeutic precision of engineered T cells against distinct diseases.

Although additional characterization of SUMO-GrB/CAR-T cell function may provide insights into opportunities to improve upon the selective lytic potential against SENP1-overexpressing cells, the work presented here represents a significant first step toward demonstrating proof-of-concept for the COVERT platform. The difficulty of manipulating SENP1 expression levels in most human cell lines, coupled with the slow activation kinetics of SUMO-GrB, may have restricted our present study to *in vitro* model systems that are sub-optimal for the evaluation of COVERT-regulated T-cell lytic activity. Therefore, the careful selection of target intracellular antigens and design of COVERT molecules exhibiting greater dynamic ranges of expression and activation, respectively, may be necessary to establish more dramatic differences in the control of tumor-cell outgrowth. Nevertheless, our results portend a promising strategy for the manufacture of T cells that can regulate lytic function in response to non-canonical input signals. We anticipate ongoing work to yield the progression of COVERT technology into a robust engineering platform that will substantially expand the pool of candidate disease signatures, thereby widening the breadth of diseases that can harness the remarkable curative potential of adoptive T-cell therapy.

ACKNOWLEDGEMENTS

The work presented in this chapter was supported by the National Institutes of Health (5DP5OD012133; grant to YYC) and the National Science Foundation (1553767; grant to YYC). PH was supported by the Biotechnology Training in Biomedical Sciences and Engineering Program funded by the National Institutes of Health. We also thank Dr. Caroline Kuo for her generosity in assisting our attempts to troubleshoot the development of our CRISPR/Cas9 RNP delivery protocol.

REFERENCES

1. Singer, M. *et al.* A Distinct Gene Module for Dysfunction Uncoupled from Activation in Tumor-Infiltrating T Cells. *Cell* **166,** 1500–1511.e9 (2016).
2. Simeonov, D. R. *et al.* Discovery of stimulation-responsive immune enhancers with CRISPR activation. *Nature* **549,** 111–115 (2017).
3. Didigu, C. A. *et al.* Simultaneous zinc-finger nuclease editing of the HIV coreceptors ccr5 and cxcr4 protects CD4+ T cells from HIV-1 infection. *Blood* **123,** 61–9 (2014).
4. Baylis, F. & McLeod, M. First-in-human Phase 1 CRISPR Gene Editing Cancer Trials: Are We Ready? *Curr. Gene Ther.* **17,** 309–319 (2017).
5. Kochenderfer, J. N. *et al.* Chemotherapy-Refractory Diffuse Large B-Cell Lymphoma and Indolent B-Cell Malignancies Can Be Effectively Treated With Autologous T Cells Expressing an Anti-CD19 Chimeric Antigen Receptor. *J Clin Oncol* **33,** 540–549 (2015).
6. Davila, M. L. *et al.* Efficacy and Toxicity Management of 19-28z CAR T Cell Therapy in B Cell Acute Lymphoblastic Leukemia. *Sci. Transl. Med.* **6,** 224ra225 (2014).
7. Maude, S. L. *et al.* Chimeric Antigen Receptor T Cells for Sustained Remissions in Leukemia. *N. Engl. J. Med.* **371,** 1507–1517 (2014).
8. Wang, X. *et al.* Phase 1 studies of central memory–derived CD19 CAR T–cell therapy following autologous HSCT in patients with B-cell NHL. *Blood* **127,** 2980–2990 (2016).
9. Rosenberg, S. A. Finding suitable targets is the major obstacle to cancer gene therapy. *Cancer Gene Ther.* **21,** 45–7 (2014).
10. Hinrichs, C. S. & Restifo, N. P. Reassessing target antigens for adoptive T-cell therapy. *Nat. Biotechnol.* **31,** 999–1008 (2013).
11. Fesnak, A. D., June, C. H. & Levine, B. L. Engineered T cells: the promise and challenges of cancer immunotherapy. *Nat. Publ. Gr.* **16,** (2016).
12. Wherry, E. J. & Kurachi, M. Molecular and cellular insights into T cell exhaustion. *Nat. Rev. Immunol.* **15,** 486–99 (2015).

13. Chen, Y. Y. Efficient Gene Editing in Primary Human T Cells. *Trends Immunol.* **36,** 667–669 (2015).

14. Sharpe, M. & Mount, N. Genetically modified T cells in cancer therapy: opportunities and challenges. *Dis. Model. Mech.* **8,** 337–50 (2015).

15. Jin, Z. *et al.* The hyperactive Sleeping Beauty transposase SB100X improves the genetic modification of T cells to express a chimeric antigen receptor. *Gene Ther.* **18,** 849–56 (2011).

16. Anson, D. S. The use of retroviral vectors for gene therapy-what are the risks? A review of retroviral pathogenesis and its relevance to retroviral vector-mediated gene delivery. *Genet. Vaccines Ther.* **2,** 9 (2004).

17. Kim, S., Kim, D., Cho, S. W., Kim, J.-S. J. & Kim, J.-S. J. Highly efficient RNA-guided genome editing in human cells via delivery of purified Cas9 ribonucleoproteins. *Genome Res.* **24,** 1012–9 (2014).

18. Ran, F. A. *et al.* In vivo genome editing using Staphylococcus aureus Cas9. *Nature* **520,** 186–91 (2015).

19. Eyquem, J. *et al.* Targeting a CAR to the TRAC locus with CRISPR/Cas9 enhances tumour rejection. *Nature* **543,** 113–117 (2017).

20. MacLeod, D. T. *et al.* Integration of a CD19 CAR into the TCR Alpha Chain Locus Streamlines Production of Allogeneic Gene-Edited CAR T Cells. *Mol. Ther.* **25,** 949–961 (2017).

21. Jinek, M. *et al.* A Programmable Dual-RNA-Guided DNA Endonuclease in Adaptive Bacterial Immunity. *Science (80-.).* **337,** 816–821 (2012).

22. Anders, C., Niewoehner, O., Duerst, A. & Jinek, M. Structural basis of PAM-dependent target DNA recognition by the Cas9 endonuclease. *Nature* **513,** 569–573 (2014).

23. Schumann, K. *et al.* Generation of knock-in primary human T cells using Cas9 ribonucleoproteins. *Proc. Natl. Acad. Sci.* **112,** 201512503 (2015).

24. Roth, T. L. *et al.* Reprogramming human T cell function and specificity with non-viral genome targeting. *bioRxiv* 183418 (2017).

25. Gaj, T. *et al.* Targeted gene knock-in by homology-directed genome editing using Cas9 ribonucleoprotein and AAV donor delivery. *Nucleic Acids Res.* **45,** e98–e98 (2017).

26. Maeder, M. L. & Gersbach, C. A. Genome-editing Technologies for Gene and Cell Therapy. *Mol. Ther.* **24,** 430–46 (2016).

27. Yam, P. *et al.* Design of HIV Vectors for Efficient Gene Delivery into Human Hematopoietic Cells. *Mol. Ther.* **5,** 479–484 (2002).

28. Zah, E., Lin, M.-Y., Silva-Benedict, A., Jensen, M. C. & Chen, Y. Y. T cells expressing CD19/CD20 bi-specific chimeric antigen receptors prevent antigen escape by malignant B cells. *Cancer Immunol. Res.* **4,** 498–508 (2016).

29. Cong, L. *et al.* Multiplex Genome Engineering Using CRISPR/Cas Systems. *Science (80-.).* **339,** 819–823 (2013).

30. Kumar, M., Keller, B., Makalou, N. & Sutton, R. E. Systematic Determination of the Packaging Limit of Lentiviral Vectors. *Hum. Gene Ther.* **12,** 1893–1905 (2001).

31. DeWitt, M. A. *et al.* Selection-free genome editing of the sickle mutation in human adult hematopoietic stem/progenitor cells. *Sci. Transl. Med.* **8,** (2016).

32. Hendel, A. *et al.* Chemically modified guide RNAs enhance CRISPR-Cas genome editing in human primary cells. *Nat. Biotechnol.* **33,** 985–989 (2015).

33. Lin, S., Staahl, B. T., Alla, R. K. & Doudna, J. A. Enhanced homology-directed human genome engineering by controlled timing of CRISPR/Cas9 delivery. *Elife* **3,** (2014).

34. Poirot, L. *et al.* Multiplex genome edited T-cell manufacturing platform for 'off-the-shelf' adoptive T-cell immunotherapies. *Cancer Res.* **75,** 3853–3864 (2015).

35. Ellis, B. L. *et al.* A survey of ex vivo/in vitro transduction efficiency of mammalian primary cells and cell lines with Nine natural adeno-associated virus (AAV1-9) and one engineered adeno-associated virus serotype. *Virol. J.* **10,** 74 (2013).

36. Wargnier, A. *et al. Identification of human granzyme B promoter regulatory elements interacting with activated T-cell-specific proteins: Implication of Ikaros and CBF binding sites in promoter activation*. *Immunology* **92,** (1995).

37. Sockolosky, J. T. *et al.* Selective targeting of engineered T cells using orthogonal IL-2 cytokine-receptor complexes. *Science* **359,** 1037–1042 (2018).

38. Trifari, S. *et al.* MicroRNA-directed program of cytotoxic CD8+ T-cell differentiation. *Proc. Natl. Acad. Sci. U. S. A.* **110,** 18608–13 (2013).

39. Watanabe, K. *et al.* Target antigen density governs the efficacy of anti-CD20-CD28-CD3 ζ chimeric antigen receptor-modified effector CD8+ T cells. *J. Immunol.* **194,** 911–20 (2015).

40. Long, A. H. *et al.* 4-1BB costimulation ameliorates T cell exhaustion induced by tonic signaling of chimeric antigen receptors. *Nat. Med.* **21,** 581–590 (2015).

41. Abid, M. B. The revving up of CARs. *Gene Ther.* **25,** 162–162 (2018).

42. Jain, M. D., Bachmeier, C. A., Phuoc, V. H. & Chavez, J. C. Axicabtagene ciloleucel (KTE-C19), an anti-CD19 CAR T therapy for the treatment of relapsed/refractory aggressive B-cell non-Hodgkin's lymphoma. *Ther. Clin. Risk Manag.* **14,** 1007–1017 (2018).

43. Millet, P., Vachharajani, V., McPhail, L., Yoza, B. & McCall, C. E. GAPDH Binding to TNF-α mRNA Contributes to Posttranscriptional Repression in Monocytes: A Novel Mechanism of Communication between Inflammation and Metabolism. *J. Immunol.* **196,** 2541–51 (2016).

44. Chang, C.-H. *et al.* Posttranscriptional control of T cell effector function by aerobic glycolysis. *Cell* **153,** 1239–51 (2013).

SUPPLEMENTARY INFORMATION

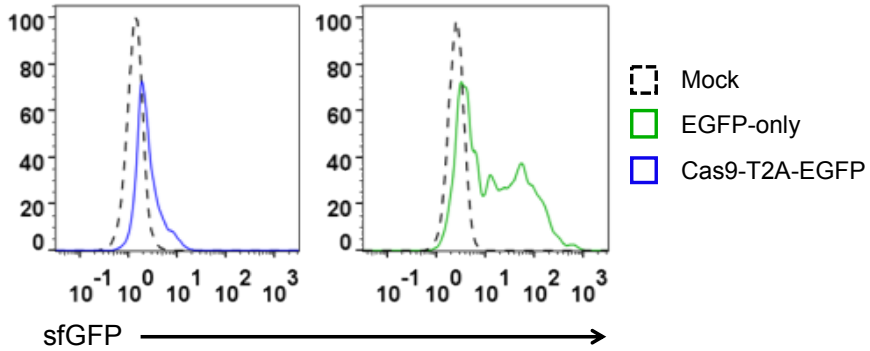

Figure 4.S1. Nucleofected Cas9-T2A-EGFP IVT mRNA is poorly translated in primary human CTLs. Primary human $CD8^+$ T cells were nucleofected with 3.1 pmol of Cas9-T2A-EGFP IVT mRNA or EGFP-only and EGFP expression was quantified via flow cytometry 20 hours post-nucleofection.

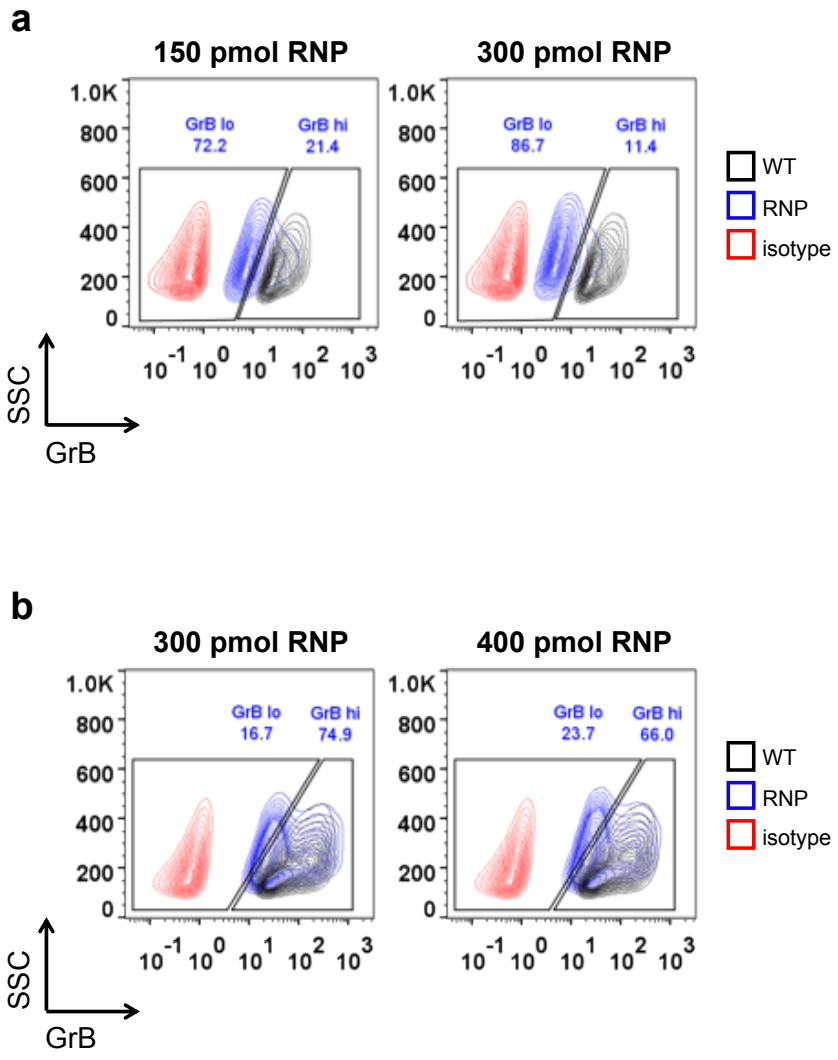

Figure 4.S2. Titration of RNP input for GrB knockout in primary human CTLs. (a,b) Knockout efficiency of GrB intracellular expression was assessed by flow cytometry 7 days following nucleofection of primary human $CD8^+$ T cells with GrB-targeted CRISPR/Cas9 RNPs at different RNP input levels. The samples in (a) and (b) are from different primary human T-cell donors. All population frequencies displayed correspond to the RNP-treated sample (blue).

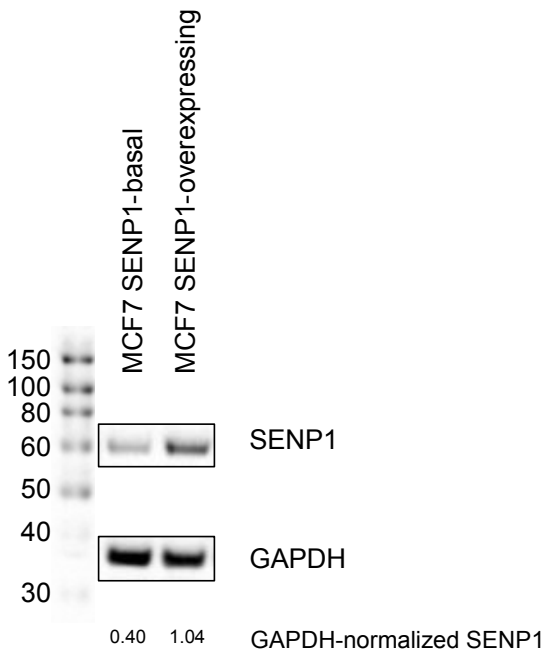

Figure 4.S3. Western blots of SENP1 expression in engineered MCF7 cell lines. MCF7 cells were retrovirally transduced to express either mCherry-SV40 NLS (MCF7 SENP1-basal) or SENP1-T2A-mCherry-SV40 NLS (MCF7 SENP1-overexpressing). Polyclonal populations were isolated via FACS for mCherry^{+} marker expression and allowed to proliferate in culture for at least 2 passages prior to harvesting lysates for western blot, probed with antibodies against SENP1 and GAPDH as a loading control. Western blot band intensities were quantified via ImageJ.

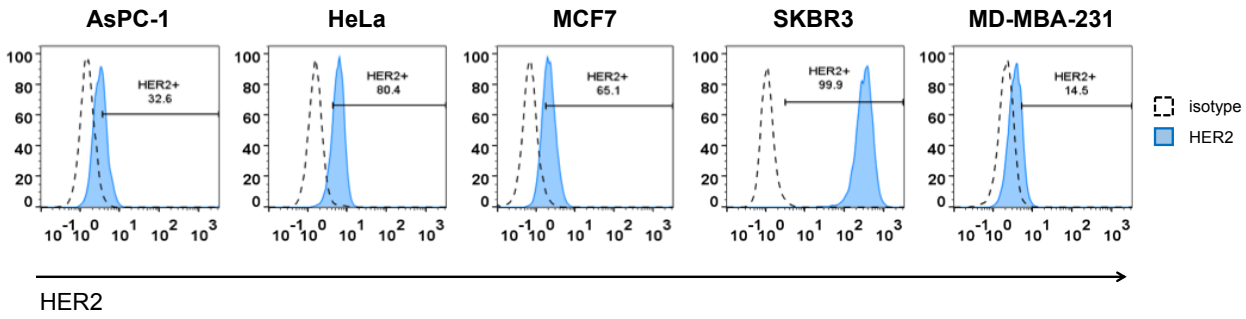

Figure 4.S4. Surface staining for HER2 expression in various human cell lines. The HER2 surface expression levels of AsPC-1 (pancreatic cancer), HeLa (cervical cancer), MCF7, SKBR3, and MD-MBA-231 (breast cancer) cells were quantified via flow cytometry. Among the lines tested, only SKBR3 exhibited strong HER2 surface expression. MCF7 was selected as the parental target cell line for SUMO-GrB experiments since SKBR3 cells exhibited altered cell morphology and reduced growth rate in *in vitro* cell culture when retrovirally transduced to overexpress SENP1.

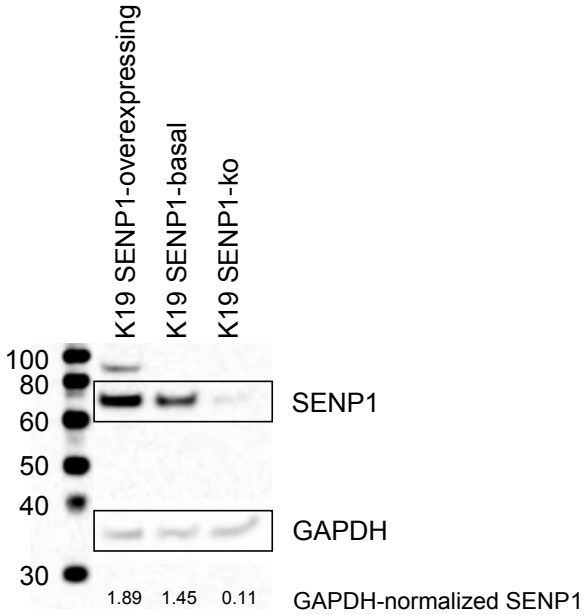

Figure 4.S5. Western blots of SENP1 expression in engineered CD19$^+$ K562 cell lines. K562 cells previously engineered to stably express the ectodomain of CD19 antigen were either retrovirally transduced to express mCherry-SV40 NLS (K19 SENP1-basal) or SENP1-T2A-mCherry-SV40 NLS (K19 SENP1-overexpressing), or treated with CRISPR/Cas9 RNPs targeting the SENP1 locus and AAV6 HDR templates directing T2A-mCherry-NLS integration at the CRISPR/Cas9 cut site (K19 SENP1-ko). Polyclonal populations were isolated via FACS for mCherry$^+$ marker expression and allowed to proliferate in culture for at least 2 passages prior to harvesting lysates for western blot, probed with antibodies against SENP1 and GAPDH as a loading control. The appearance of the higher (~90 kDa) band in the SENP1-overexpressing lysate has routinely been observed across several cell lines engineered to overexpress SENP1. Western blot band intensities were quantified via ImageJ.

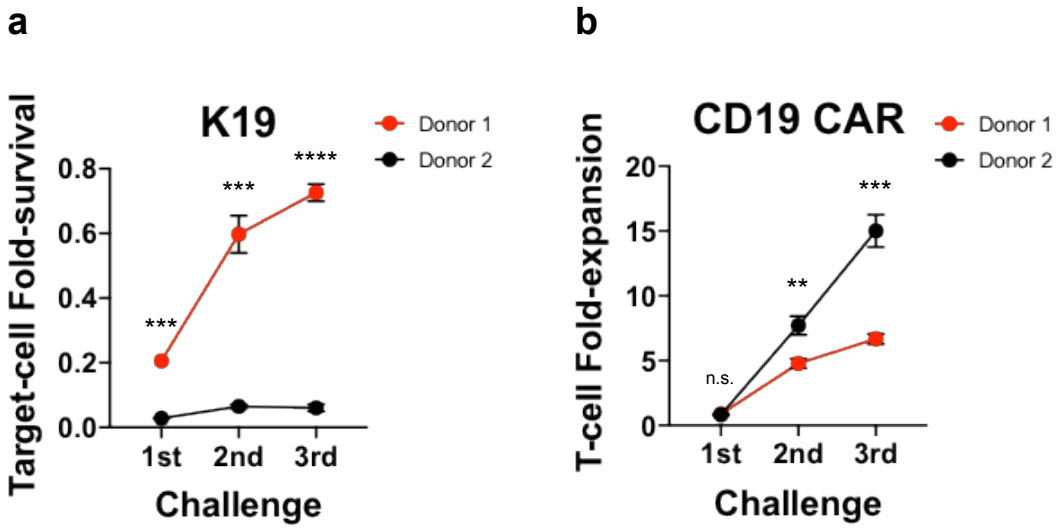

Figure 4.S6. CD19^{+} K562 target cells are resistant to T-cell–mediated cytotoxicity by select primary human CTL donors. (a,b) CD19 CAR-T cells were generated by knocking in a 2nd generation CD19 CAR with a 4-1BB costimulatory domain into the TRAC locus via CRISPR/Cas9 RNP nucleofection and AAV6 HDR-T transduction. Unsorted T cells were challenged with CD19^{+} K562 (K19) target cells at 1:1 E:T ratio, with fresh target-cell addition every 48 hours. Immediately prior to re-challenge, samples were resuspended and the number of surviving targets (a) and T cells (b) were both counted via flow cytometry. All plotted data points indicate the mean of triplicate samples and error bars represent ±1 s.d. ** p < 5E-3, *** p < 5E-4, **** p < 5E-5.

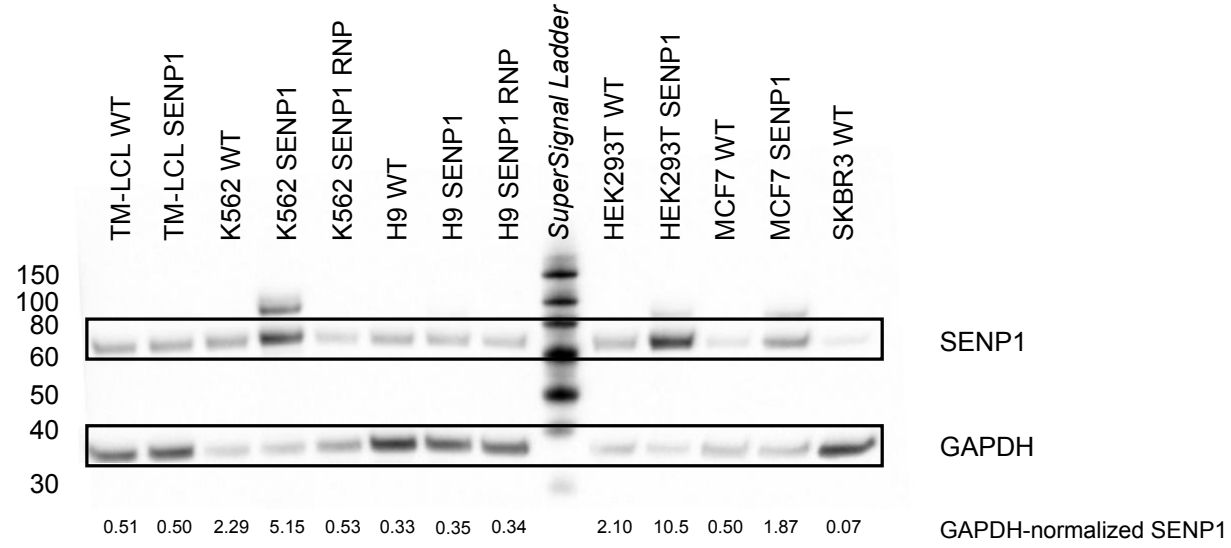

Figure 4.S7. Western blots of SENP1 expression in unsorted TM-LCL, H9, K562, HEK293T, and MCF7 cell lines**.** Cells were either transduced with retrovirus encoding mCherry-NLS (cell lines denoted "WT") or SENP1-T2A-mCherry-NLS (cell lines denoted "SENP1"), or treated with CRISPR/Cas9 RNPs targeting the SENP1 locus (cell lines denoted "SENP1 RNP"), and allowed to proliferate in culture for at least 2 passages. Lysates from unsorted cells were harvested for western blot and probed by antibodies for SENP1 and GAPDH as a protein loading control. Among the cell lines tested, only K562, HEK293T, and MCF7 exhibited differences in SENP1 expression between engineered SENP1 conditions. Transduction efficiencies for both retrovirus constructs ranged from 15-50% for each cell line. The appearance of the higher (~90 kDa) band in the SENP1-overexpressing lysate has routinely been observed across several cell lines engineered to overexpress SENP1. Western blot band intensities were quantified via ImageJ.

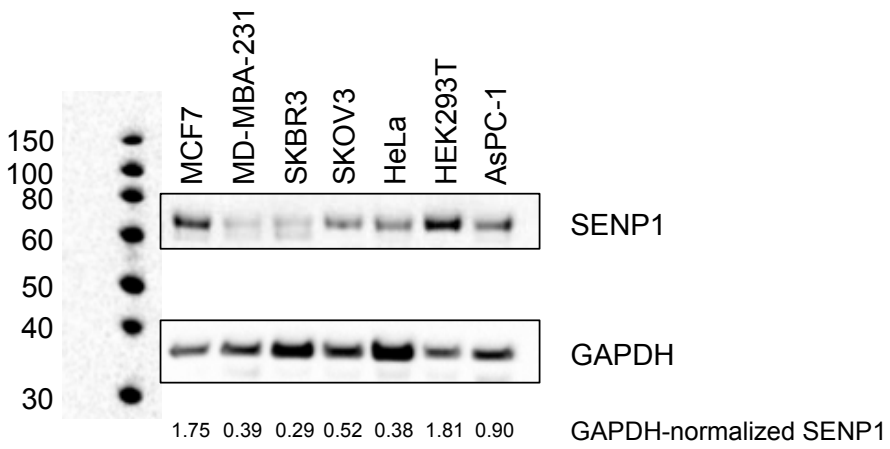

Figure 4.S8. Western blots of SENP1 expression in various HER2$^+$ wild-type human cell lines. Lysates were harvested from wild-type MCF7, MD-MBA-231, SKBR3, SKOV3, HeLa, HEK293T, and AsPC-1 cells for western blot, probed by antibodies for SENP1 and GAPDH as a loading control. Among the cell lines tested, SKBR3 cells naturally express SENP1 at relatively low levels, while MCF7 and HEK293T express SENP1 at relatively high levels. Interestingly, we were able retrovirally transduce MCF7 and HEK293T cells to stably overexpress SENP1, but attempts to do the same in SKBR3 resulted in altered cell morphology and reduced growth rate, suggesting that the SKBR3 cell line may be negatively impacted by strong perturbations in SENP1 expression. Western blot band intensities were quantified via ImageJ.

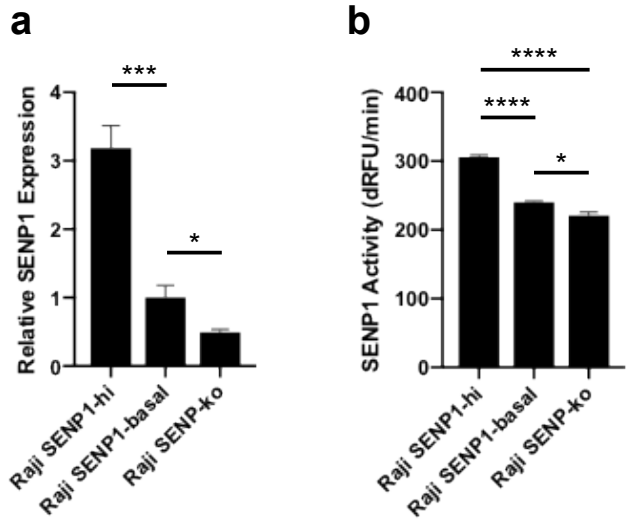

Figure 4.S9. Differences in SENP1 mRNA expression yield limited alterations to SENP1 activity levels in engineered Raji cell lines. (a) Raji cells were transduced with lentivirus to stably express mCherry-T2A-SENP1 (Raji SENP1-hi), mCherry (Raji SENP1-basal), or an 'all-in-one' CRISPR/Cas9 construct targeting the SENP1 locus with an mCherry transduction marker (Raji SENP1-ko). Polyclonal populations were isolated via FACS for mCherry^{+} marker expression and allowed to proliferate in culture for at least 2 passages prior to isolation of mRNA and subsequent cDNA preparation. SENP1 expression levels were quantified via qPCR with the cDNA serving as template, and normalized to the quantified expression level of human β-actin as a loading control. The Raji SENP1-hi cell line exhibited greater than 6-fold difference in SENP1 mRNA expression relative to the Raji SENP1-ko cell line. (b) Lysates were harvested from each cell line and SENP1 activity was measured via a fluorometric SUMO1-AMC substrate. Although statistically significant differences in SENP1 activity were observed, only a 1.39-fold difference in SENP1 activity levels separate the Raji SENP1-hi cell line from the Raji SENP1-ko cell line, despite a greater than 6-fold difference in relative SENP1 mRNA expression, indicating that there may be limitations to the functional overexpression of SENP1.

Chapter 5. Interrogating Non-proteolytic Intracellular Disease Signatures with Allosteric Granzyme B Switches

ABSTRACT

Although engineered T cells have demonstrated remarkable curative potential in the treatment of relapsed B-cell lymphomas, the widespread implementation of adoptive T-cell therapy remains limited by the lack of tumor-exclusive biomarkers available for targeting at the cell surface. We propose to expand the pool of disease signatures that can be targeted via adoptive T-cell therapy by reprogramming T cells to express granzyme B (GrB)-based Cytoplasmic Oncoprotein VErifier and Response Trigger (COVERT) molecules, which interrogate target cells for intracellular antigen expression prior to inducing target-cell apoptosis. Here, we describe initial efforts to construct an allosteric COVERT switch architecture by inserting a nanobody domain into the GrB host protein. We demonstrate the specific activation of an enhanced green fluorescent protein (EGFP)-binding COVERT in response to EGFP, and show that different nanobodies can be inserted at the same location to yield COVERT molecules targeting different ligands. Since the unpredictability of fusion protein structure and function presents a formidable challenge for rational protein engineering strategies, we also outline a retrovirus cytotoxicity assay (RVCA) screening methodology that enables characterization of the cytotoxic potential of each construct, as well as a transposition-mediated cloning strategy for the unbiased construction of a domain insertion COVERT library. Although the COVERT screening platform requires further optimization and validation, we anticipate that the development of a modular COVERT architecture to greatly enhance the therapeutic precision and application of adoptive T-cell therapy as a front-line cancer treatment option for a broader range of diseases.

INTRODUCTION

Protein allostery—the regulation of protein activities via distal interactions—is the foundational basis for much of the signaling dynamics that governs biological systems[1,2]. Over the past several decades, extensive progress in the study of structural protein biology has cast considerable light on the molecular origins of natural allosteric interactions and paved the way for the design of synthetic fusion proteins spanning a diverse array of applications in biotechnology and medicine[3,4]. For example, genetic fusion of maltose-binding protein (MBP) and β-lactamase enables modulation of ampicillin antibiotic resistance in response to maltose availability[4], while linking the hypoxia-inducible factor-1α (HIF-1α)–binding domain of human protein 300 (p300) to yeast cytosine deaminase (yCD) merges the unrelated functions of hypoxia sensing and prodrug activation[5]. This focus on rewiring protein-based circuitry has also coincided with the recent and rapid expansion of omics-driven biomarker discovery to yield an unprecedented scale of opportunity for therapeutic biosensor development. Most notably, the development of chimeric antigen receptors (CARs) that convert the detection of surface-bound antigens into downstream signaling to drive T-cell activation has jump-started an emerging paradigm centered on treating cancer patients with T cells engineered to specifically target tumors[6–8]. This therapeutic strategy, termed adoptive T-cell therapy, has proven to be extraordinarily effective at redirecting T-cell effector functions against malignant B cells in patients with relapsing leukemic disease[9–12]. However, the lack of tumor-exclusive candidate surface markers severely restricts the application of adoptive T-cell therapy to a few select diseases.

We propose to directly address this barrier to clinical translation by developing granzyme B (GrB)-based cytotoxic switches that specifically trigger target-cell apoptosis upon encounter with a defined intracellular disease signature. In Chapters 3 and 4, we detailed the design and implementation of cleavage-activated Cytoplasmic Oncoprotein VErifier and Response Trigger (COVERT) switches to selectively regulate T-cell–mediated cytotoxicity in response to intracellular tumor proteases. However, the nature of GrB activation strictly requires the

generation of an N-terminal Ile16 residue, thus limiting the pool of intracellular target antigens to the subset of proteases that recognize cleavage sites containing an Ile residue in the P1' position[13]. To expand the versatility of the COVERT platform toward non-proteolytic disease signatures, we aim to develop modular COVERT switch architectures that reversibly modulate GrB activity according to target ligand abundance. Advancements in antibody production techniques and recombinant protein technologies are now enabling the rapid identification of high-affinity proteins with exquisite specificity for custom targets[14]. Along with the robust conversion of antibodies into single-chain variable fragments (scFvs) that retain antigen-binding specificity, the recent discovery of variable domain heavy-chain (VHH) nanobodies further diversifies the nearly limitless portfolio of protein-binding moieties available for the design of allosteric protein switches[15–17].

The simplest method for linking protein activities involves fusing the C-terminus of one protein domain to the N-terminus of the next, often via peptide linkers that spatially segregate each domain to facilitate proper folding. While this strategy often minimizes perturbations to the structural integrity of each individual protein domain, a subset of proteins (e.g., GrB, perforin, etc.) are sensitive to the addition of exogenous amino acids at one or both termini. To enable the fusion of such proteins, researchers have developed a number of creative protein engineering strategies including circular permutation and domain insertion[18,19]. In circular permutation, the original protein termini are fused together, and the primary sequence is split in another location to generate a new pair of N- and C- termini which become available for protein fusion[18,20]. The related strategy of domain insertion leaves the N- and C-termini of the host protein intact, while both termini of the inserted protein are fused to internal residues within the host primary sequence[19,21]. While both approaches have yielded successful examples of engineered protein chimeras, the tertiary structure and biochemical activities of synthetic protein fusions remain challenging to predict from primary sequence information.

Despite substantial research investment into elucidating the molecular self-assembly patterns of natural and engineered proteins[22,23], the sheer complexity of protein-folding interactions continues to frustrate efforts toward developing algorithms for robust *de novo* protein structure predictions. As a result, rational engineering of protein allostery may fail to generate the desired biochemical behavior simply due to protein misfolding, leaving rational allosteric protein designs time-consuming to validate and unconducive to iterative optimization[19]. In contrast, the advent of next-generation sequencing (NGS) technologies has enabled high-throughput screens of protein construct libraries to rapidly interrogate a vast topological space, greatly increasing the likelihood of identifying influential structure-function relationships that may not be initially obvious. Although the selection of library generation and screening methodologies are both subject to protein-specific parameters that determine the library size and biochemical properties, the avoidance of sampling biases is essential to the robust and efficient identification of high-performing construct variants. An innovative strategy for unbiased domain insertion involves the random integration of modified transposon elements throughout the host protein sequence, followed by exchange of the transposon with the insertion domain of interest[24]. This approach has been successfully coupled with deep sequencing techniques to profile insertion hotspots in the programmable Cas9 nuclease for the insertion of ligand-binding domains that can reversibly regulate genome-editing activities in response to a target biomarker[24].

Another important consideration is the accurate functional characterization of protein activities, which may be impacted by the biological properties of the expression host organism. For example, the lack of glycosylation and the propensity for protein aggregation into inclusion bodies preclude the exogenous expression of active human GrB in *E. coli*[25]. Thus, while the high efficiency of gene transfer, ease of clonal isolation, and rapid growth rate often make prokaryotic hosts advantageous for high-throughput library screening applications, the COVERT platform requires the adaptation of alternative expression systems and screening methodologies.

In this chapter, we present exploratory approaches toward engineering allosteric COVERT switches via both rational design and high-throughput library screening. We show that domain insertion of a nanobody is permissible within select solvent-exposed loops of the GrB tertiary structure and demonstrate proof-of-concept for a cytotoxicity-driven COVERT screening platform in mammalian cells. We also report the unbiased construction of a nanobody domain insertion library via transposition and comment on the remaining challenges for platform validation. By integrating a structurally conserved nanobody with programmable antigen specificity to allosterically regulate GrB activity, our vision is to develop a modular COVERT architecture that enables the rapid design and optimization of customized COVERT switches for each and any target intracellular disease signature.

METHODS

DNA Constructs. DNA was chemically synthesized as oligonucleotides or gBlocks by Integrated DNA Technologies (Coralville, IA) and assembled using standard molecular cloning techniques. Unless otherwise indicated, all constructs were cloned into the epHIV7 lentiviral expression vector[26] or the MSCV retroviral expression vector. The plasmid for the engineered MuA-BsaI transposon was obtained from Addgene (plasmid 79769). The MSCV-IRES-EGFP retroviral vector and pHIT60 and RD114 retroviral packaging vectors were generous gifts from Dr. Steven Feldman (National Cancer Institute). COVERT constructs were inserted downstream of the 5' LTR in a modified MSCV vector with a woodchuck hepatitis virus posttranscriptional regulatory element (WPRE) inserted at the ClaI site by restriction-ligation cloning.

Cell Lines. HEK293T cells were obtained from ATCC (Manassas, VA) in 2011, and the identity of the cell line was verified by short tandem repeat analysis prior to shipment. Cells were cultured

in DMEM supplemented with 10% heat-inactivated FBS (HI-FBS). All mammalian cell cultures were maintained at 37°C and 5% CO_2.

Cell Transfection. HEK293T cells were seeded at 2.5 x 10^4 cells/0.25 mL/well in 48-well plates, 24 hours prior to transfection with 250 ng plasmid DNA and 15 nmol linear polyethylenimine (PEI, 25 kDa). DNA mixtures diluted in 150 mM NaCl were complexed with PEI, incubated at room temperature for 15 min, and then applied to seeded HEK293T cells.

MuA Transposition and Transformation. 200 ng of plasmid DNA containing the GrB host protein sequence was mixed with 400 ng of linearized MuA-BsaI transposon in MuA transposition buffer with 1 µL of 0.22 µg/µL MuA Transposase (ThermoFisher Scientific, Waltham, MA) and incubated in a thermocycler at 30°C for 1 hour. MuA Transposase was then inactivated by incubation at 75°C for 10 min. 2 µL of the reaction product was mixed with 20 µL of NEB® 10-beta electrocompetent *E. coli* (New England Biolabs, Ipswich, MA) in pre-chilled 1 mm gap electroporation cuvettes and immediately electroporated with Program 001 with a MicroPulser™ electroporator (Bio-Rad, Hercules, CA). Electroporated cells were immediately transferred to a microfuge tube with 900 µL of SOC media without antibiotics and allowed to recover at 37°C and 190 rpm for 1 hour. Following the recovery phase, 10 µL of cells were plated onto LB agar with 15 µg/mL chloramphenicol to assess transformation efficiency, while the remainder of the cells were inoculated into LB plus chloramphenicol liquid culture to propagate the transposition library.

Ni^{2+}-affinity Protein Purification. HEK293T cells were seeded at 15 x 10^6 cells/25 mL/flask in T-150 flasks and transfected via the linear PEI method. Culture media were changed to serum-free DMEM 16 hours post-transfection, and supernatants were harvested at 48 and 72 hours post-media change. Supernatants from different collection times were pooled, and His-tagged proteins were batch-bound to Ni-NTA resin (Life Technologies) in binding buffer (500 mM NaCl, 20 mM

Tris, pH 8.0) for 1 hour prior to being washed three times with binding buffer supplemented with 20 mM imidazole (Fisher Scientific, Hampton, NH), and then eluted with binding buffer supplemented with 500 mM imidazole through a chromatography column. Eluted proteins were buffer-exchanged into storage buffer (50 nM NaCl, 20 mM Tris pH7.4, 10% glycerol) by successive concentration and resuspension steps in Amicon centrifugal columns (10 kDa; EMD Millipore, Billierica, MA) following manufacturer's recommendations. Purified proteins were then aliquoted and frozen at -20°C.

Ac-IEPD-pNA Activity Assay. Ni^{2+}-affinity purified COVERT protein eluates were activated by co-incubation with purified enterokinase (EK, New England Biolabs) at room temperature overnight, according to manufacturer instructions. Protein concentrations were subsequently determined via Bradford Assay (Bio-Rad, Hercules, CA), according to manufacturer instructions. 2.5 pmol of purified COVERT protein was resuspended in 50 µL of lysis buffer prior to dilution with 50 µL of assay buffer (50 mM HEPES pH 7.5, 10% (w/v) sucrose, 0.05% (w/v) CHAPS, 5 mM DTT) containing 200 µM Ac-IEPD-pNA substrate (Enzo Life Sciences, Farmingdale, NY), as described by Ewen et al.[27]. In instances where protein concentrations were too low, 50 µL of EK-digested eluate was directly combined with 50 µL of assay buffer containing 200 µM Ac-IEPD-pNA substrate. Absorbance at 405 nm was measured every minute for 4 hours on an EONC microplate reader (BioTek, Winooski, VT). Activity was calculated by using the LINEST function in Excel to determine the line of best fit for the initial rate (dOD_{405}/min) by the least squares method.

Retrovirus Cytotoxicity Assay. HEK293T cells were seeded at 5.5 x 10^6 cells/9 mL/dish in 10-cm tissue-culture dishes and culture medium was replaced with fresh DMEM plus 10% HI-FBS immediately before transfection with 3.8 µg retroviral construct, 3.8 µg pHIT60, and 2.4 µg RD114 using linear PEI. Sixteen hours post-transfection, cells were washed with 5 mL of phosphate

buffered saline (PBS) and cultured in DMEM plus 10% HI-FBS, 20 mM HEPES, and 10 mM sodium butyrate for 8 hours before media change to DMEM plus 10% HI-FBS and 20 mM HEPES (no sodium butyrate). Viral supernatants were harvested on each of the two subsequent days post-media change, and filtered through a 0.45-μm low–protein-binding filter immediately prior to transduction. HEK293T cells were seeded for transduction at 3 x 10^6 cells/9 mL/dish in 10-cm tissue-culture dishes 24 hours prior to media change with filtered retroviral supernatant. Cells were allowed to continue proliferating for 2 days prior to analysis via flow cytometry or cell isolation via FACS. Genomic DNA was isolated from FACS-purified cell populations via the Qiagen DNeasy Blood & Tissue kit, and the COVERT sequence was PCR-amplified to generate NGS libraries.

Flow Cytometry. For GrB cytotoxicity experiments, transiently transfected HEK293T cells were harvested for analysis at 24 hours post-transfection. Culture media containing any dislodged cells were collected in centrifuge tubes before adherent cells were trypsinized and subsequently collected into the same tubes. The cells were washed twice with PBS prior to data acquisition on a MACSQuant VYB flow cytometer (Miltenyi Biotec, San Diego, CA). Compensation and data analysis were performed using FlowJo Data Analysis software (TreeStar, Ashland, OR).

FACS. Cells were washed and resuspended at 10-20 x 10^6 cells/mL in PBS + 2 % HI-FBS, and sorted on pre-sterilized FACSAriaI, FACSAriaII, or FACSAriaIII instruments at the UCLA Flow Cytometry Core Facility.

Statistics. Statistical significance was determined via two-tailed, homoscedastic Student's *t*-test with a *p*-value cutoff of 5E-2.

RESULTS

Identification of permissible nanobody insertion sites via rational design

Nanobodies are structurally conserved single-domain antibodies, and along with the technologies that enable generation of nanobodies with custom antigen specificity, represent an ideal ligand-binding moiety to incorporate into the development of modular allosteric COVERT molecules. However, as with most serine proteases, wild-type GrB is expressed as a zymogen with an N-terminal pro-peptide that must be cleaved off in order to allow conformational rearrangement and stabilization of the mature and active enzyme. In Chapters 2 and 3, we demonstrated the strict inhibition of GrB activity by natural and synthetic pro-domains which prevent N-terminal exposure of the Ile16 residue, thereby leaving the design of a GrB-based switch incompatible with an N-terminal fusion architecture. To overcome the limitations of this structural design rule, potential domain insertion sites were identified by analyzing the GrB crystal structure for solvent-exposed surface loops, such that the insertion of a nanobody would be less likely to distort the interior folding of GrB (Figure 5.1a).

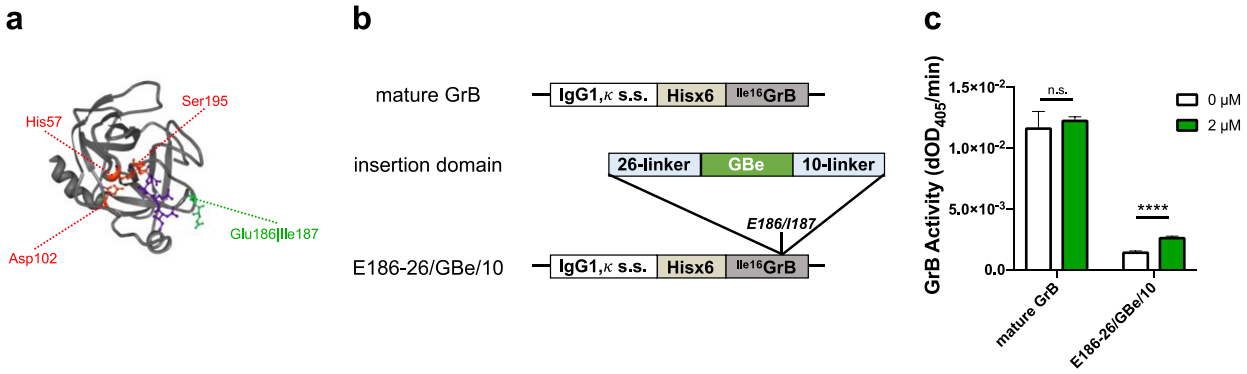

Figure 5.1. Rationally designed GBe nanobody domain insertion at the GrB Glu186/Ile187 site enables COVERT activation in response to EGFP. (a) Crystal structure of mature GrB (PDB #1IAU) indicating the catalytic triad (red), tetrapeptide substrate (purple), and the Glu186/Ile187 insertion site (green). (b) Schematic of DNA constructs for His-tagged, secreted mature GrB and the E186-26/GBe/10 COVERT with a GBe insertion into the Glu186/Ile187 site of GrB, flanked by 26- and 10-residue linkers on the N- and C-termini of the nanobody, respectively. (c) GrB activity of purified proteins were quantified in the presence or absence of EGFP via a chromogenic Ac-IEPD-pNA tetrapeptide substrate.

After identifying the Glu186/Ile187 site as the top candidate, we generated a green fluorescent protein (GFP)-binding COVERT by genetically fusing a fluorescence-enhancing variant of a GFP-binding nanobody (GBe) between the Glu186 and Ile187 residues with flexible 26- and 10-residue linkers on the N- and C-termini, respectively (E186-26/GBe/10) (Figure 5.1b). To facilitate biochemical characterization, a His-tagged, secreted version of E186-26/GBe/10 was collected from the supernatant of transiently transfected HEK293T cells and purified via Ni^{2+}-affinity chromatography. Following enterokinase-mediated His-tag removal, we measured GrB activity in the presence or absence of purified enhanced GFP (EGFP) protein using a chromogenic N-acetyl-Ile-Glu-Pro-Asp-paranitroanilide (Ac-IEPD-pNA) tetrapeptide substrate and observed a low low level of basal activity, along with a statistically significant 2.0-fold increase in GrB activity upon EGFP encounter (Figure 5.1c). Although this dynamic range of switch activity is too low for robust COVERT discrimination between $EGFP^+$ and $EGFP^-$ cells, the retention of GrB activity indicated that insertion of the GBe domain into the Glu186/Ile187 site is permissible for proper GrB folding. Buoyed by this knowledge, we speculated that the rigidity and length of the linker peptides connecting the nanobody to GrB may influence the orientation of the nanobody, as well as the allosteric shift between the bound and unbound states. Unfortunately, a panel of GBe insertions with different linkers to the Glu186/Ile187 site failed to improve the dynamic range of switch activity (data not shown).

While the Glu186/Ile187 site was originally chosen due to its distal positioning from the active site, we rationalized that alternative insertion sites closer to the substrate-binding cleft may be better suited for enabling greater conformational shifts and resulting switch dynamics. We further reasoned that relocating the nanobody–antigen binding interaction to a more proximal position could potentially introduce steric occlusion of the active site when the target antigen is bound. Therefore, the binding of a target antigen could serve to reduce COVERT activity and enable OFF-switch behavior, a format that can be leveraged to sense and respond to the loss of

intracellular markers that are instrumental for normal cell function. For instance, the absence of a tumor-suppressor gene could be a disease biomarker targeted by an OFF-switch COVERT molecule. To develop putative OFF-switch COVERT molecules, we generated a panel of constructs by fusing an mCherry-binding nanobody (LaM4) into alternative insertion sites (Figure 5.2a,b). We again attempted to purify each His-tagged COVERT via Ni^{2+}-affinity chromatography, but were unable to recover protein for 4 out of the 6 insertion sites. Among the two constructs that successfully yielded purified protein, K37-4/LaM4/5 exhibited basal GrB activity at a level 44.5-fold lower than E186-4/LaM4/5. Interestingly, despite the insertion of a different nanobody, the E186-4/LaM4/5 construct exhibited a similar level of basal activity relative to the E186-26/GBe/10, providing evidence that the permissible sites for domain insertion may be shared across different nanobodies. However, since K37-4/LaM4/5 was designed to be in the ON-state in the absence of the target antigen (i.e., mCherry), the basal level of GrB activity would be too low to provide the dynamic range necessary to trigger cytotoxicity selectively. Together with the lack of purified protein from the majority of rationally designed LaM4 insertions, the relatively low GrB activity of K37-4/LaM4/5 emphasizes the challenges associated with rational protein engineering.

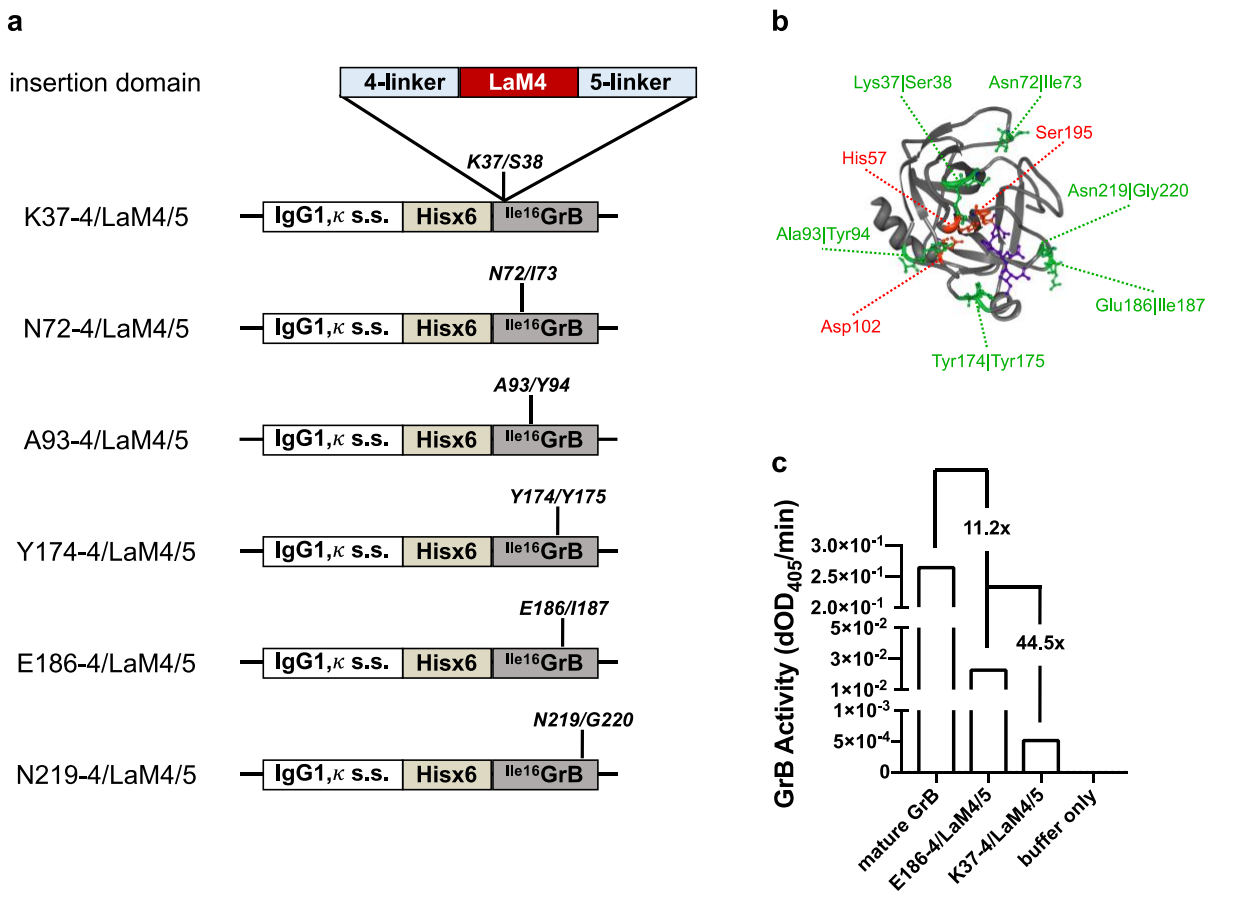

Figure 5.2. Rationally designed panel of LaM4 nanobody domain insertions at various alternative GrB surface loops fail to yield properly folded protein. (a) Schematic of DNA constructs for panel of His-tagged, secreted COVERT molecules with a LaM4 insertion into various site of GrB, flanked by 4- and 5-residue linkers on the N- and C-termini of the nanobody, respectively. The N-terminal His-tag prevents GrB activation during protein production, and is subsequently cleaved off following protein purification to enable evaluation of construct activity. (b) Crystal structure of mature GrB (PDB #1IAU) indicating the catalytic triad (red), tetrapeptide substrate (purple), and the selected sites from (a) for domain insertion (green). (c) GrB activity of E186-4/LaM4/5 and K37-4/LaM4/5 were quantified in the absence of target ligand via a chromogenic Ac-IEPD-pNA tetrapeptide substrate.

Development of a cytotoxicity-driven COVERT screening platform

To facilitate the simultaneous evaluation of greater numbers of putative COVERT switches, we devised a multi-stage screening methodology, termed retrovirus cytotoxicity assay (RVCA), in which retrovirus particles encoding a COVERT construct library are harvested from the supernatants of HEK293T retrovirus production cultures, and then applied to transduce freshly seeded HEK293T cells engineered to express the target antigen (Figure 5.3a). Control cells

lacking target antigen expression are also transduced with the same retrovirus library and all cells that stably integrate the COVERT transduction marker are isolated via fluorescence-activated cell sorting (FACS) prior to genomic DNA harvest and COVERT amplicon sequencing (Figure 5.3a). Since transient transfection and viral infection both enable expression of the construct library, cytotoxic sequences are preferentially depleted in two stages, first during the virus production phase, and again during viral transduction. In this manner, COVERT sequences that are selectively cytotoxic in the presence or absence of target antigen co-expression can be recovered and sub-cloned to iteratively enrich for high-performing ON- or OFF-switches, respectively.

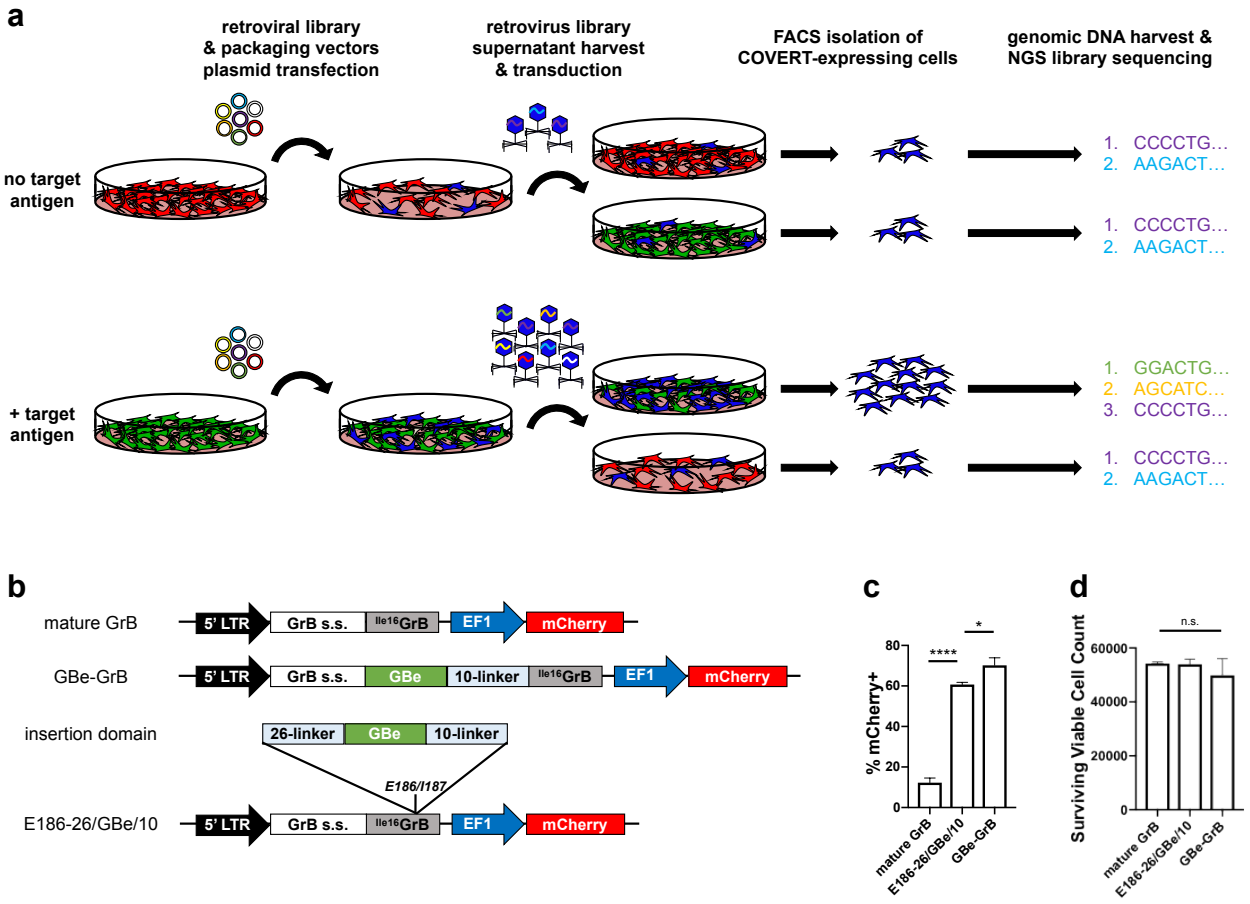

Figure 5.3. Cytotoxicity-driven retrovirus screening methodology (RVCA) successfully distinguishes mature GrB from inactive GrB constructs. (a) Schematic of RVCA platform. HEK293T cells engineered to co-express the target antigen (green) and off-target HEK293T cells (red) are each transiently transfected with a library of mTagBFP2-tagged COVERT constructs along with retroviral packaging vectors to generate retroviral particles encoding the COVERT

library. Transient expression of constructs with constitutive GrB activity by cells within the retrovirus production culture results in cell death and the depletion of cytotoxic variants from the retroviral library. Harvested retroviral particles are used to transduce both on- and off-target HEK293T cells prior to isolation of COVERT-expressing cells (blue) via FACS. Genomic DNA is harvested from sorted cell populations and sequenced by NGS platforms to enable comparison of fold-enrichment between library variants. Constructs that are active in the presence, and inactive in the absence, of the target antigen are putative ON-switches, while the reverse is true for putative OFF-switches. Sequences that are constitutively inactive are retained regardless of target antigen input. Surviving library sequences can be re-cloned into the retroviral construct vector to facilitate iterative screening and enrichment of high-performing switches. (b) Schematic of retroviral constructs used to validate the RVCA platform, with expression being driven by the promoter in the 5' long terminal repeat (LTR) region. Mature GrB is constitutively active, while the fusion of GBe to the N-terminus of GrB yields an inactive zymogen. The E186-26/GBe/10 construct served as an experimental construct known to possess a low level of basal GrB activity. GrB s.s., GrB signal sequence. (c,d) The transduction effiency (c) and surviving viable cell count (d) of HEK293T cells transduced with retrovirus produced by $EGFP^{-}$ cells was quantified via flow cytometry two days following retroviral transduction.

The E186-26/GBe/10 COVERT construct was re-cloned into a murine stem cell virus (MSCV)-based retroviral vector with a separately encoded mCherry transduction marker and subjected to the RVCA workflow, along with control constructs for constitutively cytotoxic mature GrB and an inactive N-terminal GBe fusion (Figure 5.3b). As anticipated, transduction of HEK293T cells resulted in a high % $mCherry^{+}$ for the inactive GBe-GrB construct, while only 10% of the mature GrB sample was transduced to express the mCherry fluorescent marker (Figure 5.3c). Meanwhile, the transduction efficiency of the E186-26/GBe/10 COVERT construct remained nearly as high as the inactive control, consistent with our prior observation that there is little basal activity of E186-26/GBe/10 in the absence of EGFP. Interestingly, there was little difference in the number of surviving cells between any of the transduced HEK293T cultures (Figure 5.3d), indicating that the poor transduction efficiency of mature GrB was primarily the consequence of a dramatic reduction in the number of viral particles generated by the production culture, most likely due to the cytotoxicity that accompanies mature GrB expression.

Having verified that the RVCA screening methodology can differentiate constructs based on GrB activity and cytotoxic potential, we generated a construct library of GBe insertions at the Leu146/Gly147 site, which we had previously identified as a permissible domain insertion site for

a StrepTagII peptide (Figure 5.4a,b). The N-terminal linker for the GBe insertion was varied by PCR amplification with oligos encoding Gly-Ser-NNK randomized codons, while the C-terminal linker was toggled between a 2-residue and 8-residue flexible linker comprised of Gly and Ser residues (Figure 5.4c). Following two rounds of RVCA screening in both $EGFP^+$ and $EGFP^-$ cells, the surviving COVERT sequences were identified by Illumina NGS, and fold-enrichment was determined by comparing the relative frequency of each sequence between the $EGFP^+$ and $EGFP^-$ pools (data not shown). Unfortunately, attempts to purify the top sequencing hits for biochemical validation failed to yield any protein, suggesting that the fold-enrichment scores calculated may have been the result of sampling biases introduced during either library generation or RVCA screening. One potential source of bias stems from the propensity for transiently transfected or retrovirally infected HEK293T cells to uptake multiple constructs simultaneously, potentially allowing a cytotoxic sequence to remove less cytotoxic sequences from the screened library by independently killing the producer cell. Therefore, we are currently exploring alternative strategies for construct gene transfer, such as site-specific integration into pre-defined 'landing pads'[28,29], which may better regulate construct copy number.

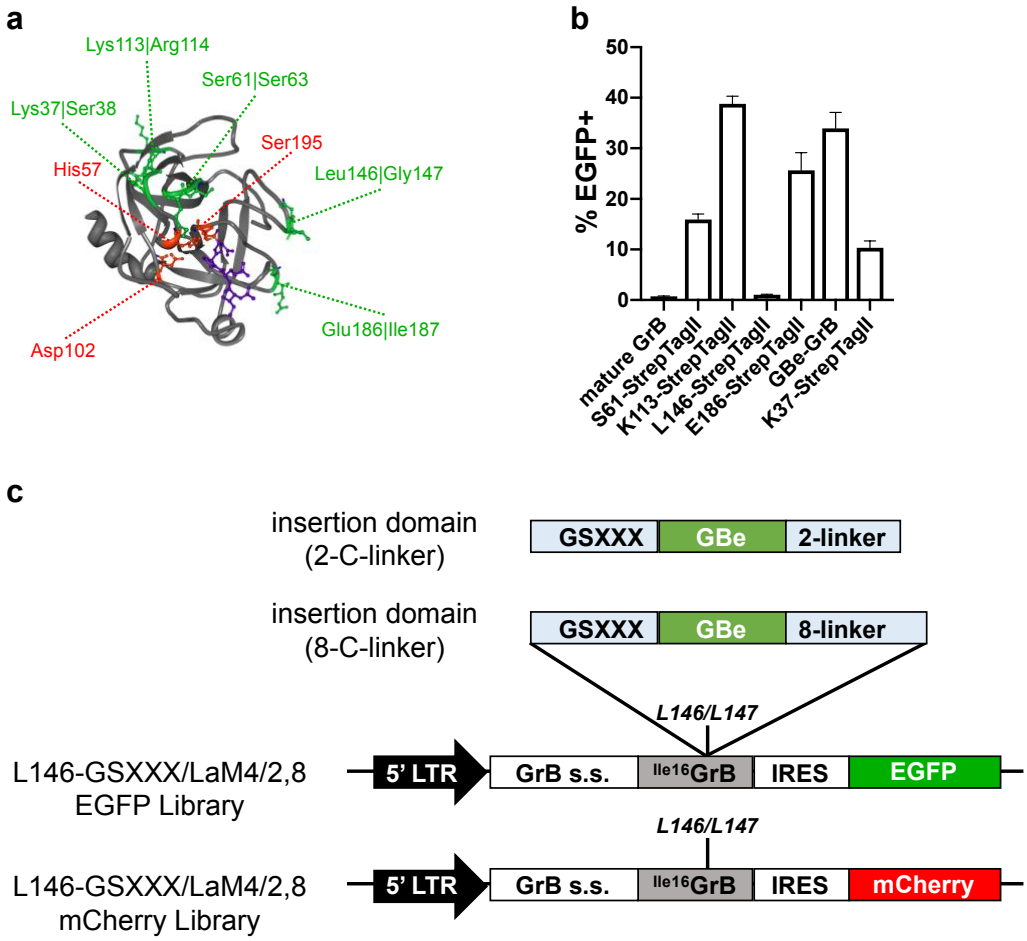

Figure 5.4. Generation of a linker library for GBe insertion into the Leu146/GLy147 site of GrB for RVCA screening. (a) Crystal structure of mature GrB (PDB #1IAU) indicating the catalytic triad (red), tetrapeptide substrate (purple), and selected sites for domain insertion of a StrepTagII peptide (green). Adapted from constructs and data generated by Laurence Chen. (b) Tranduction efficiencies following RVCA for StrepTagII peptide insertions into the sites indicated in (a). (c) A GBe COVERT library was cloned by inserting GBe into the Leu146/GLy147 site of GrB flanked by variable N- and C-terminal linkers. N-terminal linker diversity was generated by pooled oligos encoding randomized NNK codons at the three X residue positions, where N and K denote A/T/G/C bases and T/C bases, respectively. Library diversity was further increased by toggling the C-terminal linker between two fixed sequences, 2 and 8 residues in length, respectively. The library was cloned behind the 5' LTR in two separate retroviral expression vectors, one encoding the target EGFP antigen, and the other an irrelevant mCherry transduction marker behind an internal ribosome entry site (IRES). GrB s.s., GrB signal sequence.

Transposon-mediated generation of a nanobody insertion library

Although linker libraries may facilitate the fine-tuning of allosteric protein switch activities, the site of the domain insertion may have a greater impact on switch dynamic range. Therefore,

we adapted a transposition-based library cloning strategy to insert a GFP-binding nanobody variant (GB6), which recognizes a different epitope than GBe, into random sites throughout the GrB primary sequence (Figure 5.5). After gel electrophoresis-mediated selection for single-insertion clones, we verified that the GB6 nanobody was inserted in an unbiased manner, with 22.2% of the library consisting of productive clones with nanobody insertions in-frame and in the forward orientation (Figure 5.S1, Supplementary Information). Since the transposition does not preferentially integrate in any of the 3 reading frames, nor in either forward or reverse orientations, only 16.7% of the library was expected to contain productive insertions. However, the construct vector was designed such that only in-frame and forward oriented insertions would result in expression of a mTagBFP2 transduction marker, theoretically enabling selective enrichment of productive insertions during RVCA screening. Unfortunately, no enrichment in the fraction of productive insertions was observed following isolation of mTagBFP2^{+} cells (Figure 5.S1, Supplementary Information), again indicating that each sorted cell stably integrated multiple COVERT sequences prior to FACS.

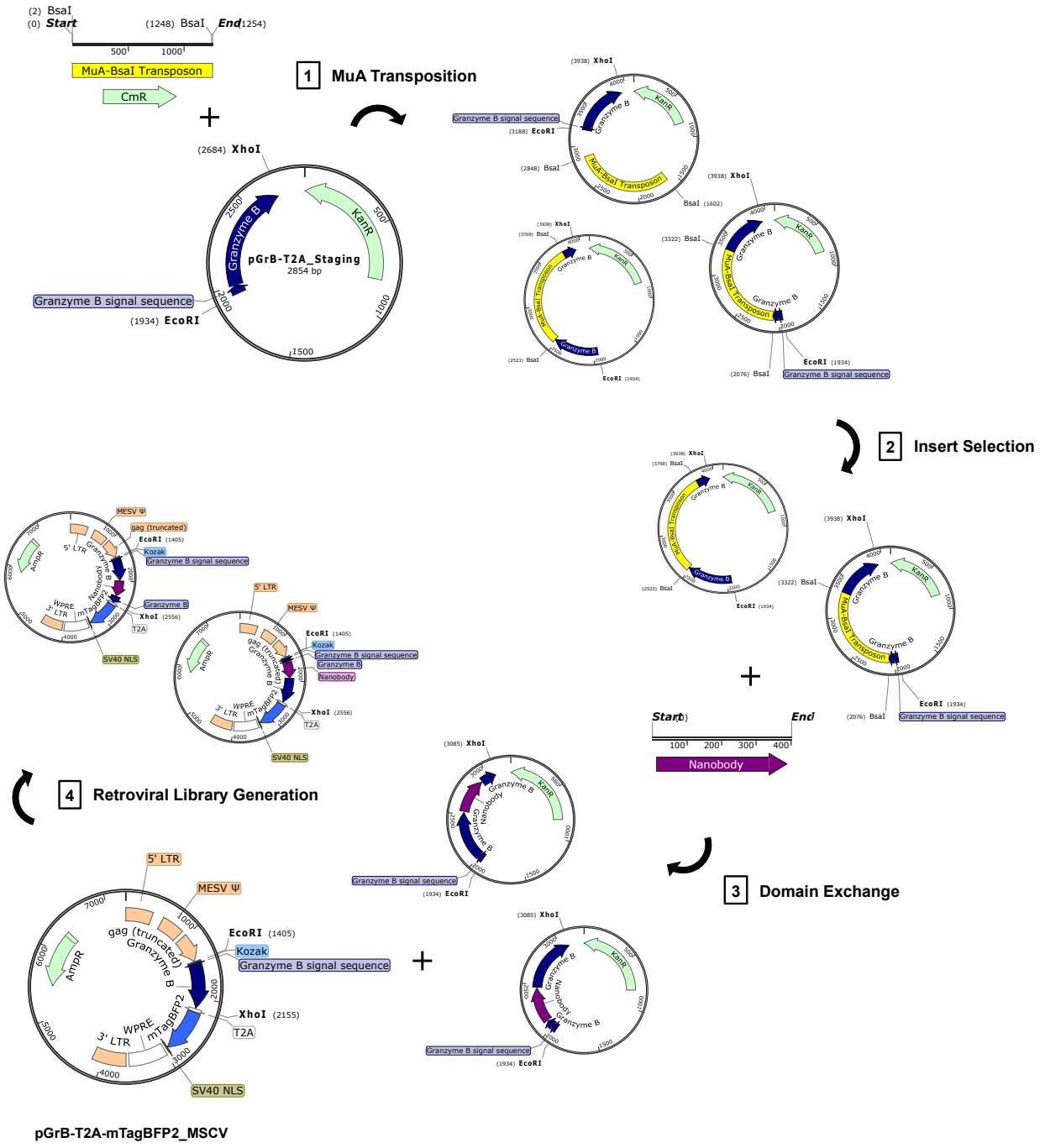

Figure 5.5. Schematic of transposition-mediated domain insertion for unbiased COVERT library generation. First, a modified MuA transposon (yellow) encoding chloramphenicol resistance and flanked by BsaI restriction sites is integrated into a staging vector containing the GrB (dark blue) host protein targeted for domain insertion. The clones resulting from successful transposition are selected by chloramphenicol, and clones in which transposition occurred within GrB are further selected by gel extraction of appropriately sized fragments (~700 GrB + ~1.25 kb transposon = ~2.1 kb) following digestion with restriction enzymes flanking the GrB sequence. After re-ligation of GrB sequences containing an internal transposon into the staging vector, the transposon is exchanged with a nanobody (purple) targeting the antigen of interest by Golden Gate assembly

with BsaI restriction-ligation. Lastly, GrB sequences bearing an inserted nanobody domain are transferred to a retroviral vector in-frame with a mTagBFP2 (blue) transduction marker separated by a 2A self-cleaving peptide. Since the transposition and subsequent nanobody domain exchange can occur in either forward or reverse orientations, the nanobody insert was designed to encode pre-mature stop codons if integrated in the reverse orientation, or if the original transposon was integrated such that the latter portion of GrB would be out-of-frame from the initial portion. Thus, only 1 out of 6 constructs, corresponding to those that retain the GrB reading are expected to allow successful translation of the mTagBFP2 transduction marker.

DISCUSSION

Despite regular demonstrations of complete and durable responses in patients with relapsed B-cell malignancies, the widespread implementation of adoptive T-cell therapy remains limited by the lack of tumor-exclusive biomarkers available for targeting at the cell surface. To overcome this barrier to clinical translation, we propose to reprogram T cells to sense and respond to intracellular antigens, thus expanding the number and diversity of disease signatures that can be targeted by adoptive T-cell therapy. In Chapter 3, we demonstrated that the N-terminal fusion of a truncated small ubiquitin-like modifier 1 (SUMO1) domain to mature GrB yields a cleavage-activated COVERT switch that selectively triggers cytotoxicity in human cells overexpressing sentrin-specific protease 1 (SENP1) (Figure 3.3). We also demonstrated the extension of the cleavage-activated COVERT architecture to enable recognition of alternative protease targets by swapping the SUMO1 domain with cognate proteolytic cleavage sequences. However, the repertoire of intracellular antigens that these cleavage-activated COVERTs can target is restricted to proteases that mediate flush cleavage to expose the Ile16 residue of mature GrB. To further expand the pool of candidate target disease signatures, we explored the design of allosteric COVERT switches that are activated or inhibited in response to ligand binding.

In this study, we focused on protein engineering strategies involving domain insertion of a nanobody into solvent-exposed surface loops in the GrB tertiary structure. The antigen-specificity of each nanobody is primarily determined by its complementarity determining regions (CDRs), with highly conserved, interspaced framework regions providing structural support[30]. Therefore,

we rationalized that the highly conserved, single-domain structure of nanobodies would be amenable to the development of a domain insertion architecture that can facilitate the modular construction of COVERT switches for alternative target epitopes or ligands. We demonstrate that insertion of GBe or LaM4 into the Glu186/Ile187 site of GrB allows the resulting COVERT to retain similar, low levels of basal GrB activity, providing evidence that once identified, the same site for domain insertion can tolerate different nanobodies targeting distinct antigens. To further expand the versatility of the COVERT platform, we proceeded to design a panel of domain insertion constructs intended to function as OFF-switches, which become inactive in the presence of a healthy biomarker, such as a tumor suppressor protein. However, our attempts to rationally design a nanobody insertion that retains high basal GrB activity frequently resulted in the lack of purifiable protein, indicative of protein misfolding, and highlighting the unpredictable nature of rational protein engineering.

To enable more rapid design and characterization of COVERT switches, we devised a cytotoxicity-driven, retrovirus-based screening methodology (RVCA), in which cytotoxic variants are depleted from a construct library by killing retrovirus-producing HEK293T cells, thereby enriching non-cytotoxic variants continuously packaged into retroviral particles. Application of harvested retrovirus to freshly seeded HEK293T cells enables a second phase of cytotoxicity-driven selection, and the enrichment of surviving COVERT sequences can be determined via NGS platforms. We demonstrated that poor retrovirus yield results in much-reduced transduction with highly cytotoxic mature GrB, relative to a non-cytotoxic control, indicating that the RVCA screen can separate constructs according to cytotoxic potential. However, the top variants from a linker library at the Leu146/Gly147 domain insertion site have proven difficult to validate by biochemical means, due to an inability to purify Leu146/Gly147 nanobody insertions with high efficiency.

This finding is surprising given that the Leu146/Gly147 site was originally identified to preserve GrB activity via the RVCA method. Although there is not enough evidence to conclude

a consistent explanation for the phenomena we have observed, this raises the concern that the RVCA may not predict GrB activity as robustly as initially believed. Since the RVCA method assumes a strong correlation between cytotoxic activity and reduced retrovirus production and transduction efficiency, the lack of transduction marker expression is taken to imply high levels of GrB activity. Unfortunately, the lack of transduction marker expression may also represent a general lack of protein expression or inefficient construct packaging, perhaps partly influenced by the diversion of cellular resources to support the unfolded protein response[31]. Another potential factor may be the propensity for transfected or transduced HEK293T cells to uptake multiple plasmids or retroviral particles, thus introducing multi-construct and multi-copy biases into the screening process. Although the initial RVCA validation experiments did not take any measures to prevent multi-copy transfection or transduction, each sample was only exposed to a single vector, such that any biases from the screening method would not have influenced the construct identity in the resulting readout. Thus, we are now exploring alternative strategies, including landing pad integration or retroviral transduction by limiting dilution to ensure single-construct expression.

At this time, it may also be beneficial to more precisely characterize the biological properties of COVERT expression in a non–T-cell context. While wild-type GrB is normally packaged into T-cell lytic granules, the absence of the lytic granule compartment leaves uncertainty as to where COVERT molecules are trafficked within HEK293T cells. The common structure most similar to lytic granules is the lysosome, but the repeated observation of specific GrB-mediated cytotoxicity in transiently transfected HEK293T cells (Figure 2.1, Figure 2.S1, Figure 3.3, Figure 3.5, and Figure 3.S5) is inconsistent with total GrB sequestration and inactivation in the acidic environment of lysosomes. Therefore, we are currently attempting to elucidate the patterns of GrB localization and cytotoxic action in HEK293T cells via microscopy. Toward this goal, we are also continuing efforts to design or implement fluorescent GrB reporters that are compatible with both microscopy and high-throughput screening.

Recognizing the value and importance of being able to generate and screen vast construct libraries, we established a cloning strategy for unbiased domain insertion of any ligand-binding domain into the host GrB sequence. We anticipate that the development of more robust screening methodologies will yield an optimized platform to enable the rapid construction and characterization of COVERT switches for a diverse array of disease signatures. By expanding the repertoire of candidate target antigens to include any ligand that can be bound by a nanobody, the maturation of the COVERT platform will enable adoptive T-cell therapy to target a plethora of previously inaccessible biomarkers, thereby enhancing therapeutic precision for a broader range of diseases.

ACKNOWLEDGEMENTS

The work presented in this chapter was supported by the National Institutes of Health (5DP5OD012133; grant to YYC) and the National Science Foundation (1553767; grant to YYC). PH was supported by the Biotechnology Training in Biomedical Sciences and Engineering Program funded by the National Institutes of Health. We thank William (Clifford) Boldridge for his insights and contributions toward the rational design and characterization of the E186-GBe constructs. We also thank Laurence Chen and Andrew Hou for their work on the RVCA screening methodology, as well as Sabah Rahman, Jaimie Chen, and Vinya Bhuvan for generating the initial transposition-mediated COVERT library. Lastly, we are indebted to Andrew and Laurence for continuing our explorations into optimizing the COVERT platform.

REFERENCES

1. Greener, J. G. & Sternberg, M. J. Structure-based prediction of protein allostery. *Curr. Opin. Struct. Biol.* **50,** 1–8 (2018).
2. Motlagh, H. N., Wrabl, J. O., Li, J. & Hilser, V. J. The ensemble nature of allostery. *Nature* **508,** 331–9 (2014).
3. Dueber, J. E., Yeh, B. J., Chak, K. & Lim, W. A. Reprogramming control of an allosteric signaling switch through modular recombination. *Science* **301,** 1904–8 (2003).
4. Guntas, G. & Ostermeier, M. Creation of an Allosteric Enzyme by Domain Insertion. *J. Mol. Biol.* **336,** 263–273 (2004).
5. Wright, C. M., Wright, R. C., Eshleman, J. R. & Ostermeier, M. A protein therapeutic modality founded on molecular regulation. *Proc. Natl. Acad. Sci. U. S. A.* **108,** 16206–16211 (2011).
6. Eshhar, Z., Waks, T., Gross, G. & Schindler, D. G. Specific activation and targeting of cytotoxic lymphocytes through chimeric single chains consisting of antibody-binding domains and the gamma or zeta subunits of the immunoglobulin and T-cell receptors. *Proc. Natl. Acad. Sci. U. S. A.* **90,** 720–4 (1993).
7. Porter, D. L., Levine, B. L., Kalos, M., Bagg, A. & June, C. H. Chimeric antigen receptor-modified T cells in chronic lymphoid leukemia. *N. Engl. J. Med.* **365,** 725–33 (2011).
8. Kalos, M. *et al.* T cells with chimeric antigen receptors have potent antitumor effects and can establish memory in patients with advanced leukemia. *Sci. Transl. Med.* **3,** 95ra73 (2011).
9. Kochenderfer, J. N. *et al.* Chemotherapy-Refractory Diffuse Large B-Cell Lymphoma and Indolent B-Cell Malignancies Can Be Effectively Treated With Autologous T Cells Expressing an Anti-CD19 Chimeric Antigen Receptor. *J Clin Oncol* **33,** 540–549 (2015).
10. Davila, M. L. *et al.* Efficacy and Toxicity Management of 19-28z CAR T Cell Therapy in B Cell Acute Lymphoblastic Leukemia. *Sci. Transl. Med.* **6,** 224ra225 (2014).

11. Maude, S. L. *et al.* Chimeric Antigen Receptor T Cells for Sustained Remissions in Leukemia. *N. Engl. J. Med.* **371,** 1507–1517 (2014).

12. Wang, X. *et al.* Phase 1 studies of central memory–derived CD19 CAR T–cell therapy following autologous HSCT in patients with B-cell NHL. *Blood* **127,** 2980–2990 (2016).

13. Smyth, M. J., McGuire, M. J. & Thia, K. Y. Expression of recombinant human granzyme B. A processing and activation role for dipeptidyl peptidase I. *J. Immunol.* **154,** 6299–305 (1995).

14. Kubala, M. H., Kovtun, O., Alexandrov, K. & Collins, B. M. Structural and thermodynamic analysis of the GFP:GFP-nanobody complex. *Protein Sci.* **19,** 2389–401 (2010).

15. Tang, J. C. *et al.* Detection and manipulation of live antigen-expressing cells using conditionally stable nanobodies. *Elife* **5,** 1154–1160 (2016).

16. Kirchhofer, A. *et al.* Modulation of protein properties in living cells using nanobodies. *Nat. Struct. Mol. Biol.* **17,** 133–8 (2010).

17. Vincke, C. *et al.* General Strategy to Humanize a Camelid Single-domain Antibody and Identification of a Universal Humanized Nanobody Scaffold. *J. Biol. Chem.* **284,** 3273–3284 (2008).

18. Baird, G. S., Zacharias, D. A. & Tsien, R. Y. Circular permutation and receptor insertion within green fluorescent proteins. *Proc. Natl. Acad. Sci. U. S. A.* **96,** 11241–6 (1999).

19. Nadler, D. C., Morgan, S.-A., Flamholz, A., Kortright, K. E. & Savage, D. F. Rapid construction of metabolite biosensors using domain-insertion profiling. *Nat. Commun.* **7,** 12266 (2016).

20. Guntas, G., Kanwar, M. & Ostermeier, M. Circular Permutation in the Ω-Loop of TEM-1 β-Lactamase Results in Improved Activity and Altered Substrate Specificity. *PLoS One* **7,** e35998 (2012).

21. Coyote-Maestas, W., He, Y., Myers, C. L. & Schmidt, D. Domain Insertion Permissibility is a Measure of Engineerable Allostery in Ion Channels. *bioRxiv* (2018).

22. Fleishman, S. J. & Baker, D. Role of the biomolecular energy gap in protein design, structure, and evolution. *Cell* **149,** 262–73 (2012).

23. Kuhlman, B., Baker, D., Wang, C. & Baker, D. Native protein sequences are close to optimal for their structures. *Proc. Natl. Acad. Sci. U. S. A.* **97,** 10383–8 (2000).

24. Oakes, B. L. *et al.* Profiling of engineering hotspots identifies an allosteric CRISPR-Cas9 switch. *Nat. Biotechnol.* **34,** 646–51 (2016).

25. Lorentsen, R. H., Fynbo, C. H., Thøgersen, H. C., Etzerodt, M. & Holtet, T. L. Expression, refolding, and purification of recombinant human granzyme B. *Protein Expr. Purif.* **39,** 18–26 (2005).

26. Yam, P. *et al.* Design of HIV Vectors for Efficient Gene Delivery into Human Hematopoietic Cells. *Mol. Ther.* **5,** 479–484 (2002).

27. Ewen, C. *et al.* A novel cytotoxicity assay to evaluate antigen-specific CTL responses using a colorimetric substrate for Granzyme B. *J. Immunol. Methods* **276,** 89–101 (2003).

28. Duportet, X. *et al.* A platform for rapid prototyping of synthetic gene networks in mammalian cells. *Nucleic Acids Res.* **42,** 13440–51 (2014).

29. Gaidukov, L. *et al.* A multi-landing pad DNA integration platform for mammalian cell engineering. *Nucleic Acids Res.* **46,** 4072–4086 (2018).

30. Bannas, P., Hambach, J. & Koch-Nolte, F. Nanobodies and Nanobody-Based Human Heavy Chain Antibodies As Antitumor Therapeutics. *Front. Immunol.* **8,** 1603 (2017).

31. Walter, P. & Ron, D. The Unfolded Protein Response: From Stress Pathway to Homeostatic Regulation. *Science (80-.).* **334,** 1081–1086 (2011).

SUPPLEMENTARY INFORMATION

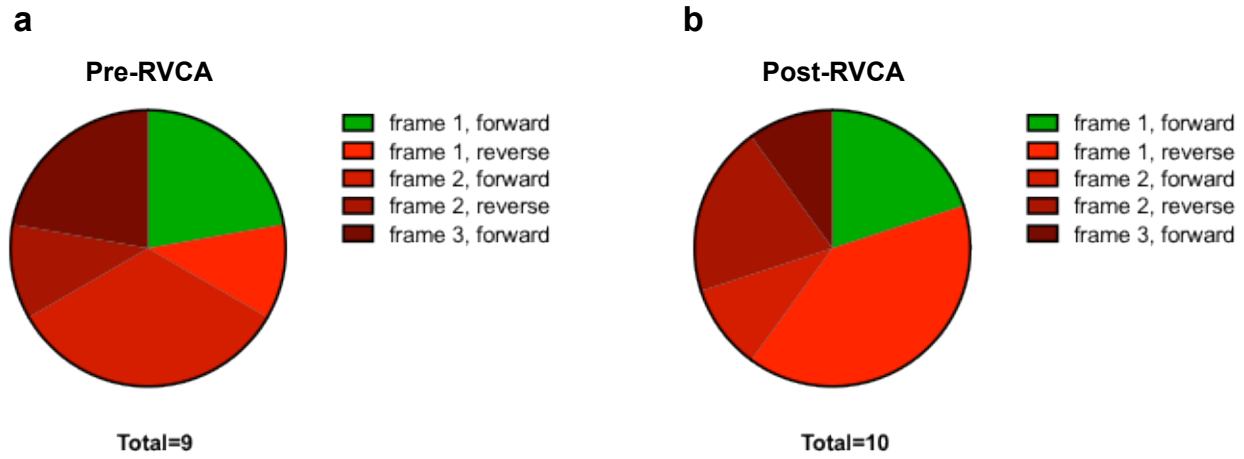

Figure 5.S1. Lack of enrichment for productive transposition-mediated nanobody insertions via RVCA screening. A transposition-mediated domain insertion library was generated by inserting a GB6 nanobody into the host GrB sequence. (a) Since the MuA transposase can mediate transposition in any of the 3 reading frames, and exchange of the nanobody with the transposon can occur in either forward or reverse orientations, there are 6 potential domain insertions between each codon. The COVERT retroviral expression vector was designed such that only 'productive' forward-oriented insertions in the 1st reading frame (green) would allow expression of an mTagBFP2 transduction marker. All other combinations of insertion position and orientation (different shades of red) terminate in pre-mature stop codon(s) within the nanobody sequence. Nine clones were submitted for Sanger sequencing following library construction, and results indicate that 2 out of 9 sequenced clones carry productive insertions, similar to the expected frequency of 1 out of 6. (b) However, following RVCA screening and FACS-mediated isolation of mTagBFP2^{+} cells (indicating COVERT expression from productive insertions), only 2 out of 10 sequenced clones carried forward-oriented insertions I the 1st reading frame, suggesting that the RVCA screen did not successfully enrich for productive sequences.

Chapter 6. Summary and Future Work

SUMMARY

Recent United States Food and Drug Administration (FDA) approvals highlight the remarkable curative potential of CD19 chimeric antigen receptor (CAR)-expressing T cells in patients with relapsing B-cell malignancies[1,2], but fundamental limitations currently prevent the widespread implementation of adoptive T-cell therapy as a front-line cancer treatment option. One challenge in particular stems from the lack of tumor-exclusive biomarkers that are accessible at the cell surface[3]. Since conventional strategies to redirect T-cell recognition rely on surface receptor–antigen interactions, normal cells that express the target antigen at low, basal levels are frequently at risk for 'on-target, off-tumor' toxicities[4]. Thus, the ability to reprogram T cells to interrogate target cells for the expression of well-characterized intracellular disease signatures represents a potentially transformative approach that can significantly enhance the therapeutic precision of adoptive T-cell therapy. Our strategy to 're-imagine' T-cell recognition revolves around the genetic replacement of cytotoxic T-cell effector payloads with conditionally active switch proteins, termed Cytoplasmic Oncoprotein VErifier and Response Trigger, which require encounter with an intracellular target antigen prior to initiating apoptosis.

In Chapter 2 of this thesis, we evaluated the cytotoxic contribution of human granzyme B (GrB), as well as the safe storage and delivery of recombinant GrB fusions to validate the suitability of GrB to serve as a molecular chassis for a T-cell–compatible cytotoxic switch. Since wild-type GrB is constitutively active and does not contribute to T-cell lytic specificity, we also demonstrated the successful depletion of wild-type GrB protein levels following repeated antigen stimulation. In Chapters 3 and 4, we detailed the design and implementation of a small ubiquitin-like modifier (SUMO)-GrB fusion to enable T cells to sense and respond to overexpression of sentrin-specific protease 1 (SENP1). In Chapter 3, we demonstrated that SUMO-GrB is

specifically activated by SENP1-mediated cleavage, and further showed selective cytotoxicity in HEK293T cells transiently transfected to co-express SENP1. The modularity of the N-terminal fusion architecture also enabled the design and construction of alternative COVERT switches to target different proteases by simple exchange of the SUMO domain with cognate cleavage sequences[5]. In Chapter 4, we systematically optimized the multiplexed delivery of CRISPR/Cas9 ribonucleoprotein (RNP) complexes and adeno-associated virus serotype 6 (AAV6) homology-directed repair templates (HDR-Ts) to streamline the COVERT/CAR-T cell manufacturing workflow. We then paired SUMO-GrB with either a HER2 CAR or a CD19 CAR and showed selective T-cell–mediated cytotoxicity by SUMO-GrB T cells against SENP1-overexpressing target cells, providing the first demonstrations of engineered T-cell lytic selectivity in response to intracellular antigen expression.

In Chapter 5, we outlined our preliminary work toward developing a modular, allosteric COVERT architecture by nanobody domain insertion. We devised a cytotoxicity-driven, retrovirus-based screening methodology, and validated a transposition-mediated cloning strategy to generate unbiased domain insertion libraries for rapid COVERT switch optimization. This work thus serves as the foundation for the development of the COVERT system into a platform technology that significantly expands the pool of candidate target antigens for adoptive T-cell therapy.

FUTURE WORK

Improving the Robustness of COVERT/CAR-T cell Performance

Although SUMO-GrB/HER2 CAR-T cells and SUMO-GrB/CD19 CAR-T cells exhibited the potential for selective lytic activity against SENP1-overexpressing versions of MCF7 and $CD19^+$ K562 cells, respectively, the lack of robust T-cell proliferation prevented the long-term evaluation of COVERT/CAR-T cell performance. This may have been partly due to intrinsic biological

properties of the SUMO-GrB/SENP1 system, as multiple human cell lines appeared to resist our attempts to perturb SENP1 expression levels, thereby restricting our selection of target-cell lines for an *in vitro* model. The mechanism of SUMO-GrB activation is also inflexible to protein engineering, and we were unable to improve upon the kinetics of SENP1-mediated cleavage. Since the induction of T-cell exhaustion normally results from prolonged antigen stimulation[6], the dynamics of tumor-cell killing may impact the preservation of T-cell effector functions. Therefore, thresholds may exist for the speed of activation and maximum attainable activity that enable robust COVERT performance.

Another critical factor in determining T-cell effector function is the balance of T-cell activating and inhibitory signaling. In this work, we primarily focused on optimizing COVERT/CAR-T cell manufacture via multiplexed delivery of CRISPR/Cas9 RNPs and AAV6 HDR-Ts due to the desire to minimize T-cell manipulation. However, we have noticed that CAR expression levels tend to be lower when site-specifically inserted at the TRAC locus, relative to random integration via lentiviral or retroviral vectors. While early studies involving CAR integration into the TRAC locus indicate potential benefits in the form of reduced T-cell exhaustion and better *in vivo* activity[7], differences in *in vitro* performance between HDR-integrated CARs and retrovirally integrated CARs have not been systematically evaluated over the time scales used in our studies. Differences in CAR expression levels may influence the degree of T-cell activation and the capacity for effector functions. Since retention of proliferative potential is a crucial feature of cell-based therapeutics, it is also paramount to elucidate the parameters that govern the robustness of non-cytotoxic effector functions, first *in vitro*, and eventually in pre-clinical models.

Expanding the Versatility of the COVERT Platform

The application of modular design principles to COVERT switch development captures a core aim of synthetic biology to facilitate the rapid design and tuning of construct behavior for different input signals[8]. An important advantage of our nanobody domain insertion strategy is the

ease in which different nanobodies can be obtained for the desired binding affinity for each target antigen. Building on the initial goal of reprogramming T cells to interrogate target cells for the presence of an intracellular tumor antigen, the generation of COVERT OFF-switches further enables T cells to sense and respond to the *absence* of a target biomarker, creating AND-NOT–gate logic when paired with a surface receptor. The design and implementation of protein-based circuits may eventually allow T cells to compute even more complex logic programs.

While our preliminary attempts to expand the versatility of the COVERT platform have focused on sensing the presence or absence of protein inputs, disease-specific signatures can be manifest in the form of other biomolecules, including microRNAs (miRNAs) or metabolites. The incorporation of RNA- or metabolite-binding domains may further extend the reach of COVERT technology to include entirely new classes of targets that are currently inaccessible to adoptive T-cell therapy.

Exploring T-cell–mediated Delivery of Alternative Biosensors and Payloads

Lastly, the development of COVERT technology has centered on the design of GrB-based switches that can induce target-cell apoptosis upon intracellular activation. Along the way, we have demonstrated the ability to knock out and deplete GrB expression with high efficiency, and we have further demonstrated that GrB knockout is sufficient to cause a substantial defect in target-cell lysis by primary human $CD8^+$ T cells. This creates the opportunity to utilize T cells as a general delivery vehicle for alternative payloads. Other groups are already exploring the repurposing of T cells to traffic and deliver nanoparticle-immunomodulatory drug formulations to tumor sites, enabling more potent immune responses[9]. While cytotoxic payloads must kill the majority of the diseased cell population in order to achieve therapeutic efficacy, immunomodulatory payloads have the potential to impart therapeutic benefit without recognition or delivery to every individual target cell. For example, work by other groups have demonstrated that the enhancer of zeste 2 polycomb repressive complex 2 subunit (EZH2) epigenetic regulator

is responsible for regulating the differentiation and function of various T-cell subsets, and inhibition of EZH2 reprograms tumor-infiltrating regulator T cells (TI-Tregs) to support pro-inflammatory functions[10]. An example of a potential non-cytotoxic payload may therefore involve the design and delivery of a protein-based EZH2 inhibitor by GrB knockout T cells to TI-Tregs, thus enhancing anti-cancer immunity.

REFERENCES

1. Abid, M. B. The revving up of CARs. *Gene Ther.* **25,** 162–162 (2018).
2. Jain, M. D., Bachmeier, C. A., Phuoc, V. H. & Chavez, J. C. Axicabtagene ciloleucel (KTE-C19), an anti-CD19 CAR T therapy for the treatment of relapsed/refractory aggressive B-cell non-Hodgkin's lymphoma. *Ther. Clin. Risk Manag.* **14,** 1007–1017 (2018).
3. Rosenberg, S. A. Finding suitable targets is the major obstacle to cancer gene therapy. *Cancer Gene Ther.* **21,** 45–7 (2014).
4. Hinrichs, C. S. & Restifo, N. P. Reassessing target antigens for adoptive T-cell therapy. *Nat. Biotechnol.* **31,** 999–1008 (2013).
5. Ho, P., Ede, C. & Chen, Y. Y. Modularly Constructed Synthetic Granzyme B Molecule Enables Interrogation of Intracellular Proteases for Targeted Cytotoxicity. *ACS Synth. Biol.* **6,** 1484–1495 (2017).
6. Wherry, E. J. & Kurachi, M. Molecular and cellular insights into T cell exhaustion. *Nat. Rev. Immunol.* **15,** 486–99 (2015).
7. Eyquem, J. *et al.* Targeting a CAR to the TRAC locus with CRISPR/Cas9 enhances tumour rejection. *Nature* **543,** 113–117 (2017).
8. Ho, P. & Chen, Y. Y. Mammalian synthetic biology in the age of genome editing and personalized medicine. *Current Opinion in Chemical Biology* **40,** 57–64 (2017).
9. Schmid, D. *et al.* T cell-targeting nanoparticles focus delivery of immunotherapy to improve antitumor immunity. *Nat. Commun.* **8,** 1747 (2017).
10. Wang, D. *et al.* Targeting EZH2 Reprograms Intratumoral Regulatory T Cells to Enhance Cancer Immunity. *Cell Rep.* **23,** 3262–3274 (2018).